Modulation of acid sphingomyelinase function in lipid-induced insulin resistance

Inaugural-Dissertation

zur Erlangung des Doktorgrades
der Mathematisch-Naturwissenschaftlichen Fakultät
der Heinrich-Heine-Universität Düsseldorf

vorgelegt von
Mona Katharina Hendlinger
aus Nastätten

Düsseldorf, Oktober 2025

aus dem Institut für Klinische Diabetologie
des Deutschen Diabetes-Zentrums (DDZ)
Leibniz-Zentrum für Diabetes-Forschung
An der Heinrich-Heine-Universität Düsseldorf

Gedruckt mit der Genehmigung der
Mathematisch-Naturwissenschaftlichen Fakultät der
Heinrich-Heine-Universität Düsseldorf

Berichterstatter:

1. Prof. Dr. Michael Roden
2. Prof. Dr. Hadi Al-Hasani

Tag der mündlichen Prüfung:
29.04.2026

Table of contents

I Summary

Type 2 diabetes (T2D) is characterized by systemic insulin resistance and closely linked to abnormalities of lipid metabolism and mitochondrial function in insulin-responsive tissues such as skeletal muscle and liver. Among bioactive lipid species, ceramides have been identified as one contributor to insulin resistance by interfering with insulin signaling and mitochondrial functionality. Acid sphingomyelinase (ASM), a lysosomal enzyme that hydrolyzes sphingomyelin into ceramide, is involved in apoptosis, autophagy and lipid regulation, but its effects in tissue-specific metabolic regulation, particularly in skeletal muscle and liver under insulin-resistant and exercising conditions, remain incompletely understood.

This thesis investigates the regulation and function of ASM in both skeletal muscle and liver, focusing on its role in ceramide metabolism, mitochondrial dynamics, and insulin signaling. It is hypothesized that ASM has tissue-specific effects: in skeletal muscle, ASM may support membrane remodeling and mitochondrial integrity, thereby improving insulin sensitivity, whereas in the liver, elevated ASM activity may exacerbate lipotoxicity and contribute to the development of metabolic dysfunction-associated steatotic liver disease (MASLD). Consequently, analyses of human skeletal muscle biopsies before and after a 12-week high-intensity interval training (HIIT) program in men with T2D were combined with *in vivo* studies of rodent models of diabetes and MASLD and *in vitro* experiments in HepG2 cells exposed to lipotoxic and glucotoxic conditions with or without siRNA-mediated ASM knockdown.

In skeletal muscle, ASM protein levels were reduced in individuals with T2D compared to glucose-tolerant individuals. HIIT significantly increased ASM activity across all groups, accompanied by increased levels of very-long-chain ceramides (e.g., C22:0, C24:0, C24:1), especially among insulin-resistant individuals. These adaptations were associated with improved aerobic capacity (VO_2max). Further, regression analyses suggesting a link between ASM activity and markers of mitochondrial quality control. In contrast, ASM expression and activity were elevated in the liver of obese mice and correlated positively with hepatic lipid accumulation and body weight, indicating a context-dependent, detrimental role of ASM under hepatic metabolic stress.

In HepG2 cells, palmitate (one of the most common saturated fatty acid in western diet) treatment increased ASM expression, induced lipid droplet formation, and reduced cell viability. Surprisingly, ASM knockdown attenuated lipid droplet accumulation and

sensitized cells to palmitate-induced cell death. Furthermore, ASM knockdown impaired insulin signaling under lipotoxic and glucotoxic conditions, as evidenced by reduced AKT phosphorylation and increased inhibitory IRS2 phosphorylation. These findings suggest that while ASM may promote lipid sequestration into droplets to buffer lipotoxicity, it is also essential for maintaining insulin responsiveness under metabolic stress conditions.

Taken together, this thesis identifies ASM as a metabolically regulated enzyme with tissue-specific roles: it supports mitochondrial adaptions in skeletal muscle, while in the liver, it also buffers lipotoxic stress and helps preserve proximal insulin signaling, although generally associated with steatosis and inflammation. These findings highlight ASM as a context-dependent regulator of lipid homeostasis and a potential target for therapeutic intervention in T2D and MASLD, particularly in combination with exercise interventions.

II Zusammenfassung

Typ-2-Diabetes (T2D) ist charakterisiert durch eine systemische Insulinresistenz und steht in engem Zusammenhang mit Störungen des Lipidstoffwechsels, sowie einer beeinträchtigten mitochondrialen Funktion in insulinempfindlichen Geweben wie dem Skelettmuskel und der Leber. Unter den bioaktiven Lipidmediatoren gelten Ceramide als wesentliche Mitverursacher der Insulinresistenz, da sie sowohl die Insulinsignaltransduktion als auch mitochondriale Prozesse negative beeinflussen können. Die acide Sphingomyelinase (ASM), ein lysosomales Enzym, das Sphingomyelin zu Ceramiden hydrolysiert, ist an Apoptose, Autophagie und Lipidregulation, beteiligt. Ihre Rolle in der gewebespezifischen metabolischen Regulation – insbesondere in Skelettmuskel und Leber unter Bedingungen der Insulinresistenz und körperlicher Aktivität – ist jedoch bislang nur unvollständig verstanden.

Die vorliegende Arbeit untersucht die Regulation und Funktion von ASM in Skelettmuskel und Leber mit besonderem Fokus auf den Ceramidstoffwechsel, mitochondriale Dynamik und die Insulinsignaltransduktion. Es wurde die Hypothese aufgestellt, dass ASM in diesen Geweben unterschiedliche Funktionen erfüllt: Im Skelettmuskel könnte ASM durch Modulation der Membranstruktur und Beeinflussung mitochondrialer Prozesse zur Erhaltung der Insulinsensitivität beitragen, wohingegen

eine erhöhte ASM-Aktivität in der Leber lipotoxische Prozesse verstärken und zur Progression der metabolisch-assoziierten Steatose (MASLD) beitragen könnte. Zur Prüfung dieser Hypothesen wurden Analysen von Muskelbiopsien von Männern mit T2D vor und nach einem 12-wöchigen Hoch-Intensitäts-Intervalltraining (HIIT) mit *in vivo*-Studien an Mausmodellen von Diabetes und MASLD, sowie *in vitro*-Experimente an HepG2-Zellen kombiniert, die unter lipotoxischen und glukotoxischen Bedingungen mit oder ohne siRNA-vermittelten ASM-Knockdown kultiviert wurden.

Im Skelettmuskel zeigte sich bei Personen mit T2D im Vergleich zu glukose-toleranten Individuen eine reduzierte ASM-Proteinexpression. HIIT führte in allen Gruppen zu einem signifikanten Anstieg der ASM-Aktivität, begleitet von erhöhten Konzentrationen sehr langkettiger Ceramide (z. B. C22:0, C24:0, C24:1), insbesondere bei insulinresistenten Individuen. Diese Veränderungen gingen mit einer verbesserten aeroben Kapazität (VO_2max) einher. Regressionsanalysen deuteten auf einen Zusammenhang zwischen ASM-Aktivität und Markern mitochondrialer Qualitätskontrolle hin. Im Gegensatz dazu zeigten Lebern adipösen diabetischen Mäusen eine erhöhte ASM-Proteinexpression und -Aktivität, die positiv mit hepatischer Lipidakkumulation und Körpergewicht korrelierten. Diese Ergebnisse sprechen für eine kontextabhängige Rolle von ASM in der Förderung lipotoxischer Prozesse unter metabolischem Stress.

In HepG2-Zellen induzierte eine Behandlung mit Palmitat (eine der am häufigsten vorkommende gesättigte Fettsäure in der westlichen Ernährung) ein Anstieg der ASM-Expression, eine vermehrte Lipidtröpfchenbildung sowie eine verminderte Zellviabilität. Überraschenderweise verringerte ein ASM-Knockdown die Lipidtröpfchenbildung und machte die Zellen anfälliger für palmitatinduzierte Lipotoxizität. Darüber hinaus resultierte der Knockdown von ASM, unter lipotoxischen und glukotoxischen Bedingungen, in einer Beeinträchtigung der Insulinsignalübertragung, belegt durch eine reduzierte AKT-Phosphorylierung und eine verstärkte inhibitorische Phosphorylierung von IRS2. Diese Daten deuten darauf hin, dass ASM sowohl zur Lipidsequestrierung in Tröpfchen beiträgt und dadurch lipotoxische Effekte abmildern kann, als auch essenziell für die Aufrechterhaltung der Insulinsignalübertragung unter metabolischem Stress ist.

Zusammenfassend identifiziert diese Dissertation ASM als ein metabolisch reguliertes Enzym mit gewebespezifischen Funktionen: Im Skelettmuskel unterstützt ASM mitochondriale Anpassungen, während es in der Leber, obwohl häufig mit Steatose

und Inflammation assoziiert, zugleich lipotoxischen Stress abmildert und die proximale Insulinsignalübertragung erhält. Diese Ergebnisse kennzeichnen ASM damit als kontextabhängigen Regulator der Lipidhomöostase machen es zu einem potenziellen Ziel zur therapeutischen Behandlung von T2D und MASLD, insbesondere im Kombination mit trainingsbasierten Lebensstilinterventionen.

1 Introduction

1.1 Overview of diabetes mellitus: classification and emerging subtypes

Diabetes mellitus (DM) encompasses a spectrum of metabolic disorders primarily characterized by chronic hyperglycemia due to defects in insulin secretion, insulin action, or both (IDF, 2025). The diagnosis of DM is established based on specific criteria, including fasting plasma glucose levels of ≥126 mg/dL (7.0 mmol/L), a 2 h plasma glucose level of ≥200 mg/dL (11.1 mmol/L) following an oral glucose tolerance test (OGTT), a glycated hemoglobin (HbA1C) value of ≥6.5%, or random plasma glucose levels ≥200 mg/dL (11.1 mmol/L) accompanied by symptoms of hyperglycemia (IDF, 2025). Globally, the prevalence of DM continues to rise, presenting a significant public health challenge. According to most recent edition of IDF atlas more than 580 million people worldwide were living with DM in 2025 (IDF, 2025). DM is traditionally classified into four major types: type 1 diabetes mellitus (T1D), type 2 diabetes mellitus (T2D), gestational diabetes, and diabetes due to specific causes, such as monogenic diabetes or diseases of the exocrine pancreas (ADA, 2024). T1D is typically driven by immune-mediated pancreatic β-cells destruction, leading to a lack of insulin secretion, whereas T2D arises primarily from a combination of insulin resistance and relative insulin insufficiency (Roden and Shulman, 2019). In recent years, efforts to refine the classification of DM have led to the introduction of new subtypes. Analyses of the German Diabetes Study (GDS) of the German Diabetes Center (DDZ) has validated the concept of five distinct subtypes of DM based on phenotypic features introduced in a Scandinavian cohort (Ahlqvist et al., 2018). These subtypes exhibit distinct profiles in terms of whole-body insulin sensitivity, adipose tissue insulin resistance, and hepatic lipid content: mild age-related diabetes (MARD), mild obesity-related diabetes (MOD), severe autoimmune diabetes (SAID), severe insulin-resistant diabetes (SIRD), and severe insulin-deficient diabetes (SIDD) (Zaharia et al., 2019).

This idea of a new classification offers a more nuanced approach to understanding the heterogeneity of diabetes, particularly in distinguishing between the metabolic profiles and associated risks of complications across subtypes. For instance, individuals with SIRD exhibit severe insulin resistance, particularly in adipose tissue, and are at higher

risk of developing metabolic dysfunction-associated steatotic liver disease (MASLD), due to high hepatic lipid content (Zaharia et al., 2019).

1.2 Mechanisms and risk factors of type 2 diabetes mellitus

T2D is characterized by a progressive decline in insulin sensitivity, particularly in skeletal muscle, liver, and adipose tissue, coupled with an inadequate compensatory insulin secretion by pancreatic β-cells. Insulin resistance is defined by a shift in the insulin concentration-effect curve, requiring higher levels of insulin for cells to respond appropriately. As a result, insulin-sensitive tissues become less effective in glucose uptake, leading to increased blood glucose levels due to inadequate glucose disposal, reduced suppression of glucose production in the liver, and impaired lipid metabolism. In response, β-cells secrete more insulin to counteract this resistance, resulting in an initial state of hyperinsulinemia. However, persistent demand eventually compromises β-cell function, culminating in chronic hyperglycemia (Roden and Shulman, 2019). The pathogenesis of T2D is driven by a complex interplay of genetic predisposition, environmental factors, and lifestyle choices. Obesity, physical inactivity, and poor dietary habits are significant risk factors that exacerbate insulin resistance and promote the progression of T2D (Roden and Shulman, 2019). The number of individuals diagnosed with T2D is expected to rise significantly in the coming decades and the economic burden of T2D is substantial, with direct medical costs and indirect costs related to disability and loss of productivity, significantly straining healthcare systems globally (Butt et al., 2024). Effective prevention and management strategies, including lifestyle monitoring and adapted modifications, targeted pharmacological interventions, are crucial to addressing this growing global health concern (Crawford and Laiteerapong, 2024; Davies et al., 2022; IDF, 2025). Furthermore T2D as chronic metabolic disorder poses a significant public health challenge due to its associated concordant comorbidities, such as cardiovascular disease, nephropathy, retinopathy, but also discordant diseases like depression, rheumatologic diseases, chronic lung disease and malignant diseases (Eilat-Tsanani et al., 2021; Pearson-Stuttard et al., 2022).

1.3 The interplay between type 2 diabetes mellitus and steatotic liver disease: a growing global concern

The recent renaming of stigmatized non-alcoholic fatty liver disease (NAFLD) as MASLD reflects the growing understanding of the shared pathophysiological pathways between T2D and liver disease (Rinella et al., 2023; Roeb et al., 2024). MASLD is estimated to affect approximately 30% of the global adult population (Chan et al., 2023), with prevalence notably higher among individuals with T2D, reaching 65% according to a recent meta-analysis of 156 studies (En Li Cho et al., 2023). MASLD encompasses various stages, ranging from simple steatosis, now referred to as metabolic dysfunction-associated steatotic liver (MASL), to more advanced forms such as metabolic dysfunction-associated steatohepatitis (MASH) (Cusi et al., 2024). MASH is histologically defined by the presence of lobular inflammation and hepatocyte ballooning, which may lead to progressive fibrosis, cirrhosis, and even hepatocellular carcinoma (Dewidar et al., 2020). Individuals with advanced liver fibrosis face a significantly higher risk of liver-related mortality, with the risk rising exponentially with the severity of fibrosis (Arab et al., 2018). The progression of MASLD from simple steatosis to steatohepatitis and advanced fibrosis is closely tied to metabolic disturbances inherent in T2D, potentially exacerbating the progression of the other (Barrera et al., 2024), such as dysregulated lipid metabolism, alterations in mitochondrial function, and inflammation (Friedman et al., 2018; Hodson and Gunn, 2019; Mashek, 2021). Lipid accumulation within the liver in MASLD arises from several sources, including non-esterified fatty acids (NEFAs) derived from adipose tissue, increased *de novo* lipogenesis (DNL), and dietary fats (Chen et al., 2020). The two major metabolic fates of hepatic fatty acids are mitochondrial fatty acid oxidation (FAO) and esterification to form triglycerides (TAGs). The increased influx of fatty acids induces overloaded FAO and subsequent mitochondrial stress (Chen et al., 2020). Nevertheless hepatic mitochondria exhibit a dynamic plasticity in MASLD: FAO capacity is often upregulated in early MASL as a compensatory adaption to lipid overload (Koliaki et al., 2015; Sunny et al., 2011), but this mitochondrial adaption may diminish with disease progression, as oxidative function tends to decline when MASL progresses to MASH (Moore et al., 2022). These observations suggest that these flexible mitochondrial responses in the liver may act as compensatory mechanisms to mitigate lipid overload and protect against lipotoxicity during onset of MASL (Fromenty

and Roden, 2023), even though results across studies remain inconsistent (Pedersen et al., 2022; Petersen et al., 2016a).

Altered metabolism of various lipid species, including TAGs, diacylglycerols (DAGs), ceramides, and cholesterol, is a hallmark of MASLD (Syed-Abdul, 2023). In individuals with MASLD, DNL is generally higher than in healthy individuals, contributing to excessive lipid accumulation within the liver (Syed-Abdul, 2023). Elevated levels of TAGs and DAGs within the liver are indicative of disrupted lipid homeostasis and are frequently used as biomarkers for the severity of steatosis (Gorden et al., 2015). Ceramides, a class of sphingolipids, have been also implicated in the progression of insulin resistance and steatotic liver diseases, as their accumulation can promote inflammatory signaling pathways and hepatocellular damage (Syed-Abdul, 2023; Zhu et al., 2023). Similarly, cholesterol metabolism is adversely affected, contributing to the development of hepatic inflammation and fibrosis (Syed-Abdul, 2023; Zhu et al., 2023). In individuals with histologically-confirmed MASH, DNL is significantly lower as in those with MASL and is comparable to levels observed in healthy individuals (Syed-Abdul, 2023). This reduction in DNL is likely attributed to the reduced ability of fibrotic tissue to synthesize fatty acids. Additionally, as the disease advances from MASL to MASH, mitochondrial adaptation/plasticity declines further (Fromenty and Roden, 2023). *In vivo* studies using ^{31}P-magnetic resonance spectroscopy demonstrated that hepatic ATP-synthase flux is reduced in individuals with T2D compared with healthy controls (Szendroedi et al., 2009), indicating impaired hepatic energy metabolism in T2D. Measurements from human liver biopsies revealed that obese individuals with or without MASL exhibit higher mitochondrial respiratory capacity than lean individuals (Koliaki et al., 2015). However, obese individuals with MASH showed increased mitochondrial mass but lower maximal respiration compared with obese individuals without MASH (Koliaki et al., 2015).These findings are supported by a murine MASL models, which demonstrated an initial increase in mitochondrial respiratory capacity at the early stage of MASL, followed by a decline during disease progression to the advanced stage (Jelenik et al., 2017). Moreover, Gancheva et al. reported an increased hepatic oxidative capacity in MASH compared with healthy controls, whereas this adaptive response was lost in individuals with concomitant MASH and T2D, who showed a decline in oxidative capacity, particularly when fibrosis exceeded stage 1 (Gancheva et al., 2022). Together, these findings indicate that hepatic mitochondrial adaptation is preserved in obesity and early MASL, but progressively

deteriorates with the transition to MASH, especially when accompanied by T2D or hepatic fibrosis.

1.4 Insulin signaling and mechanisms of insulin resistance

1.4.1 Overview of insulin signaling pathway

Insulin signaling is initiated when insulin binds to its receptor (insulin receptor; InsR), a transmembrane protein, classified within the tyrosine kinase family. Upon insulin binding, the receptor undergoes a conformational change that activates its intrinsic kinase activity, leading to autophosphorylation and thereby creating docking sites for downstream signaling molecules (Boucher et al., 2014). This triggers the activation of the insulin receptor substrate (IRS) proteins, IRS1 (major role in skeletal muscle) and IRS2 (important in liver and skeletal muscle) (Previs et al., 2000; Sun et al., 1993; Wu et al., 2008). Phosphorylation of IRS proteins on tyrosine residues recruit phosphoinositide 3-kinase (PI3K), which converts phosphatidylinositol-4,5-bisphosphate (PIP2) to phosphatidylinositol-3,4,5-trisphosphate (PIP3), leading to the activation of protein kinase B (AKT). AKT is activated via phosphorylation at Thr308 by phosphoinositide-dependent kinase 1 (PDK1), and at Ser473 by mechanistic target of rapamycin complex 2 (mTORC2), which fully activates AKT (Hanke and Mann, 2009). In skeletal muscle and adipose tissue, AKT promotes the trafficking of glucose transporter type 4 (GLUT4) from intracellular storage vesicles to the plasma membrane, where it mediates glucose uptake (Chadt and Al-Hasani, 2020; Kahn, 2019). Additionally, activated AKT enhances glycogen synthesis in skeletal muscle by suppressing glycogenolysis (Roden and Shulman, 2019). In the liver, activated AKT inhibits glucose production and enhances glycogen synthesis and lipogenesis through key transcriptional regulators like forkhead box O1 (FOXO1) and sterol regulatory element-binding protein 1c (SREBP-1c) (Roden and Shulman, 2019). Through these mechanisms, AKT plays a central role in maintaining glucose homeostasis.

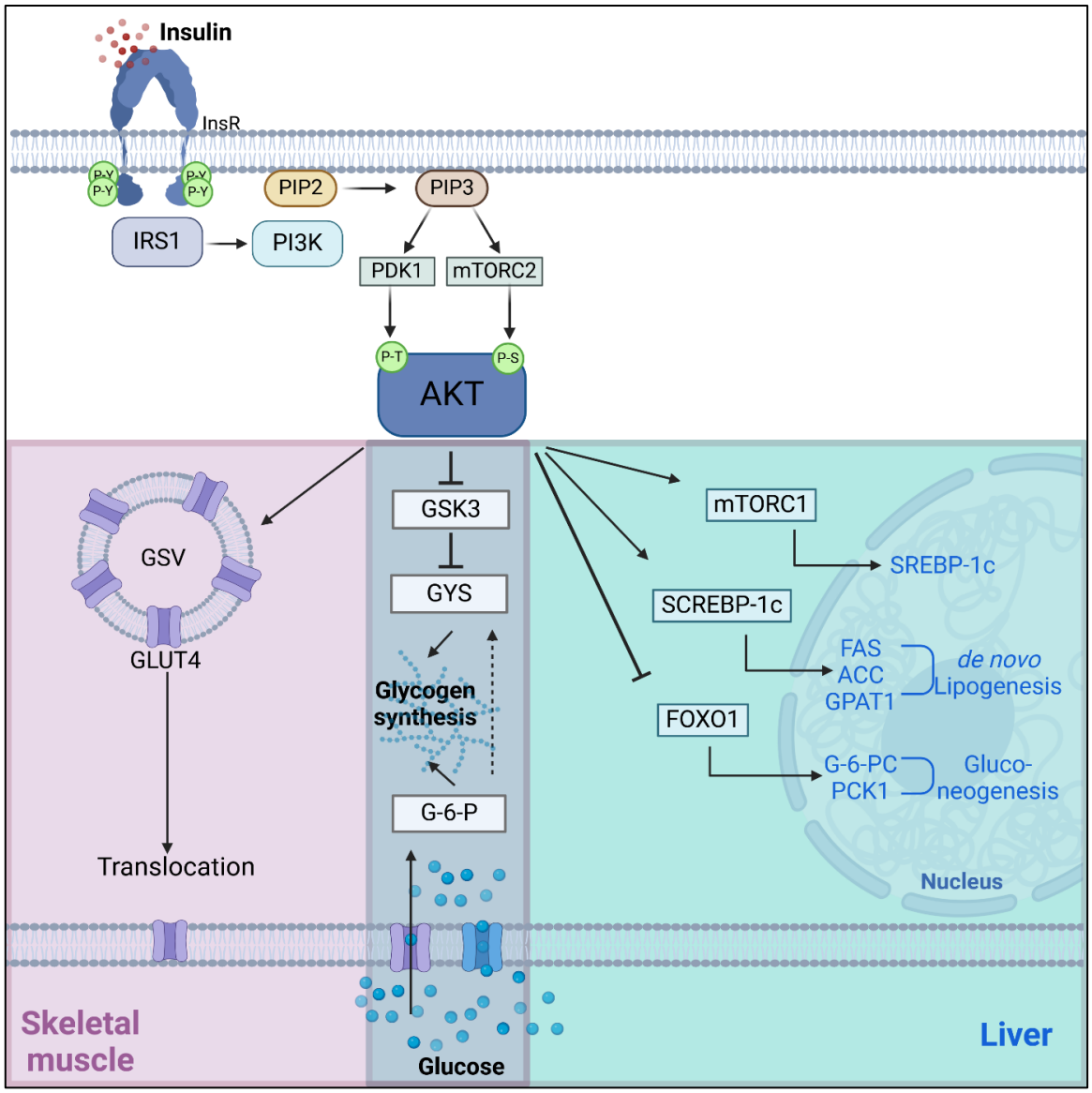

Figure 1: Insulin signaling and it´s metabolic effects in skeletal muscle and liver.

Upon insulin binding to its receptor (InsR), downstream signaling is initiated through insulin receptor substrate 1 (IRS1) followed by phosphoinositide 3-kinase (PI3K), leading to the conversion of phosphatidylinositol-4,5-bisphosphate (PIP2) into phosphatidylinositol-3,4,5-trisphosphate (PIP3). This activates protein kinase B (AKT) via phosphorylation by phosphoinositide-dependent kinase 1 (PDK1) and mechanistic target of rapamycin complex 2 (mTORC2). In skeletal muscle, AKT facilitates glucose uptake by promoting GLUT4 translocation from GLUT4 storage vesicles (GSV) to the plasma membrane. Additionally, AKT enhances glycogen synthesis by inhibiting glycogen synthase kinase 3 (GSK3), which leads to the activation of glycogen synthase (GYS). Glucose-6-phosphate (G-6-P) serves as an essential intermediate in both glycolysis and glycogen synthesis, which follows the same pathway in the liver. In the liver, AKT inhibits gluconeogenesis via forkhead box O1 (FOXO1) suppression and promotes *de novo* lipogenesis (DNL) via fatty acid synthase (FAS), acetyl-CoA carboxylase (ACC), and glycerol-3-phosphate acyltransferase 1 (GPAT1) through sterol regulatory element-binding protein 1c (SREBP-1c). Figure created with BioRender.com.

Insulin signaling is tightly regulated to prevent metabolic disturbances that could lead to insulin resistance. Serine/threonine protein phosphatases, such as protein phosphatase 2A (PP2A), play a critical role by dephosphorylating AKT and thereby attenuating the insulin signal. Similarly, lipid phosphatases, like phosphatase and

tensin homolog (PTEN), counteract PI3K signaling by dephosphorylating PIP3. Additionally, kinases including c-Jun N-terminal kinase (JNK), inhibitor of κB kinase (IKK), and both atypical and novel protein kinase Cs (PKCs) inhibit insulin signaling through increased serine/threonine phosphorylation and reduced tyrosine phosphorylation of IRS proteins. (Roden and Shulman, 2019) .

1.4.2 Molecular mechanisms underlying insulin resistance

Insulin resistance, a central characteristic of metabolic disorders such as obesity and T2D, arises from diminished insulin responsiveness of target tissues to insulin. In a healthy state, insulin regulates glucose homeostasis by promoting the uptake of plasma glucose into cells, inhibiting gluconeogenesis in the liver, suppressing lipolysis in adipose tissue, and facilitating glycogen synthesis as energy storage during fasting periods. However, these regulatory effects are compromised in insulin-resistant states, leading to hyperglycemia and dyslipidemia (Roden and Shulman, 2019).

1.4.2.1 Alterations of mitochondrial function

Alterations of mitochondrial function are characterized by decreased oxidative capacity (i.e., the ability of mitochondria to utilize oxygen for ATP production), impaired mitochondrial respiration (actual oxygen consumption during energy generation), altered mitochondrial dynamics (fusion and fission events), and increased reactive oxygen species (ROS) production, is a hallmark of metabolic diseases, including obesity and T2D (Fromenty and Roden, 2023).

In white adipose tissue (WAT) of obese, insulin-resistant, or T2D individuals, mitochondrial content and the expression of key genes involved in mitochondrial function are significantly downregulated (Dahlman et al., 2006; Krishnan et al., 2012). This is accompanied by decreased oxygen consumption and ATP production (Bogacka et al., 2005), along with reduced citrate synthase activity (CSA), a marker of mitochondrial content (Christe et al., 2013). Additionally, reduced mitochondrial respiration in the visceral compartment of WAT has been associated with diminished insulin sensitivity in obese individuals (Pafili et al., 2022b).

In skeletal muscle, mitochondrial respiration is similarly impaired, as individuals with T2D exhibit lower CSA and electron transport chain (ETC) activity compared to healthy individuals (Ritov et al., 2005). Moreover, T2D individuals demonstrate reduced submaximal ADP-stimulated oxidative phosphorylation, highlighting an overall decline

in mitochondrial efficiency (Phielix et al., 2008). This is associated with diminished expression of proliferator-activated receptor γ coactivator 1α (PGC-1α), a key regulator of mitochondrial biogenesis and oxidative metabolism (Mootha et al., 2003) and nuclear respiratory factor 1 (NRF-1), crucial for the expression of mitochondrial genes (Patti et al., 2003). Mitochondrial content is frequently lower in T2D individuals, contributing to the observed decline in mitochondrial respiration (Szendroedi et al., 2011).

Alterations of mitochondrial function in the liver, is also evident in obese and insulin-resistant individuals, especially those with MASH (Koliaki et al., 2015). Despite increased mitochondrial content (Gancheva et al., 2022), these individuals demonstrate reduced mitochondrial respiration caused by heightened proton leak via increased uncoupling, possibly reflecting an adaptation to manage elevated lipid levels and reduce lipotoxicity in early obesity stages with or without MASL (Koliaki et al., 2015). In advanced stages of MASL, altered mitochondrial function appears to arise from an accumulation of damaged mitochondria rather than increased biogenesis, further impairing mitochondrial function and contributing to mitochondrial inefficiency as MASH progresses (Koliaki et al., 2015). These impairments, including reduced ATP content and turnover, are evident in the livers of T2D individuals and highlight broader alteration in mitochondrial function in these conditions (Schmid et al., 2011; Szendroedi et al., 2009). Some studies report increased expression of genes associated with components of the oxidative phosphorylation machinery (e.g., *NDUFA6* [Complex I], *SDHC* [Complex II], *UQCRB* [Complex III], *COX4i1* [Complex IV], and *ATP5B* [Complex V]) in overweight individuals with T2D relative to lean controls (Misu et al., 2007), whereas others observed no differences in hepatic oxidative phosphorylation capacity or CSA across lean, obese, and T2D individuals (Lund et al., 2016). However, the changes of mitochondrial number and size, impaired oxidative phosphorylation, and increased ROS production are consistently linked to the development of MASLD, which frequently coexists with T2D (Younossi et al., 2019).

Mitochondrial dynamics, particularly the balance between fusion and fission events, play a crucial role in mitochondrial quality control by facilitating the exchange of mitochondrial content and the selective removal of damaged segments via mitophagy (Chan, 2020). Nutrient overload in conditions like obesity, T2D and MASLD shifts the balance toward fragmented mitochondria (Yoon et al., 2011). Reduced expression or altered activity of fusion proteins such as mitofusin 1 (MFN1), MFN2, and optic atrophy

1 (OPA1) as well as increased levels of the fission protein dynamin related protein 1 (DRP1) in adipose and muscle tissue correlates with obesity and T2D (Bach et al., 2005; Galloway et al., 2014; García-Peña et al., 2024; Hernández-Alvarez et al., 2010; Mancini et al., 2019; Zorzano et al., 2010). While initially thought to be pathological, mitochondrial fragmentation may also serve as an adaptive response to enhance FAO (Ngo et al., 2023).

Similarly high-fat-diet (HFD) mouse models show a shift toward mitochondrial fragmentation in adipose tissue (Mancini et al., 2019). Indeed, 12-week HFD reduces MFN1 and MFN2 mRNA levels and increases DRP1 expression, promoting mitochondrial fragmentation. Moreover, mice with adipose-specific MFN2 deletion exhibit increased adiposity, elevated plasma leptin, higher blood glucose levels, and insulin resistance, independent of diet (Mancini et al., 2019). This increased fat mass and reduction in MFN2 expression are associated with higher peroxisome proliferator-activated receptor γ (PPAR-γ) expression, a key regulator of adipogenesis and lipid metabolism (Mancini et al., 2019). Similarly, insulin sensitivity is enhanced in skeletal muscle of mice overexpressing MFN2, possibly through the activation of AMP-activated protein kinase (AMPK) which promotes GLUT4 translocation (Kong et al., 2013). Murine models of liver-specific depletion of MFN2 are also characterized by mitochondrial fragmentation, impaired glucose and insulin tolerance, and increased ROS production, which exacerbates endoplasmic reticulum (ER) stress and impair insulin signaling via JNK activation (Sebastián et al., 2012). In line, liver-specific MFN2 overexpression enhances insulin signaling, partly by decreasing the activity of suppressor of cytokine signaling 3 (SOCS3), a known inhibitor of insulin signaling (Gan et al., 2013; Rui et al., 2002). This shows that, reduced mitochondrial fusion and excessive fragmentation, especially without corresponding mitophagy, leads to alterations in mitochondrial function (Pinti et al., 2019; Sprenger and Langer, 2019).

Mitophagy, the process of selectively removing damaged mitochondria, is crucial for maintaining cellular and metabolic health (Ning et al., 2022). In obesity and T2D, an imbalance between mitochondrial biogenesis and the removal of damaged mitochondria disrupts metabolic function (Van Huynh et al., 2023). Genetic mutations in mitophagy-related genes such as *PINK1*, *Parkin*, *PDX1*, and *CLEC16A,* have been linked to both T1D and T2D in humans (Jin et al., 2014; Qu et al., 2011; Soleimanpour et al., 2015; Soleimanpour et al., 2014). In mice, deletion of the mitophagy receptor FUN14 domain-containing protein 1 (FUNDC1) in adipose tissue leads to macrophage

infiltration and increased inflammation after HFD, exacerbating obesity and insulin resistance (Wu et al., 2019a). AMPK ablation in adipose tissue, another regulator of mitophagy, similarly induces whole-body insulin resistance and MASLD (Desjardins and Steinberg, 2018). In contrast, increased expression of mitophagy markers (PTEN-induced kinase 1 (PINK1), E3 ubiquitin-protein ligase (Parkin), and Sequestosome 1 (SQSTM1)) was found in visceral WAT of T2D individuals with MASL compared to non-diabetic controls (He et al., 2021a). Studies in rodent skeletal muscle demonstrate that activation of heat-shock protein (HSP) 72 regulates PINK1-Parkin-mediated mitophagy, improving glucose tolerance and enhancing mitochondrial content and oxidative capacity (Drew et al., 2014; Henstridge et al., 2014). Evidence specific to liver mitophagy in T2D remains limited, apart from a study by Gancheva et al., which reported reduced levels of Parkin and phosphorylated Parkin in individuals with MASH, with or without T2D, compared to healthy controls. Notably, these differences disappeared when calculating the phos-Parkin/Parkin ratio (Gancheva et al., 2022). Nevertheless data from MASLD studies suggest general downregulation of mitophagy, contributing to alterations in mitochondrial function, oxidative stress, and inflammation, worsening MASLD progression (Edmunds et al., 2019; Undamatla et al., 2023; Yamada et al., 2018). For instance, reduced Parkin expression and increased levels of macrophage stimulating 1 (MST1), which inhibits AMPK and Parkin-mediated mitophagy, drive mitochondrial apoptosis and liver injury in MASLD mice model (Zhou et al., 2019). Notably, T2D individuals display impaired mitophagy flux and decreased expression of mitophagy genes, unlike pre-diabetic individuals with mild hyperglycemia who exhibit an increase in the expression levels of different mitophagy-related genes, such as *PINK1*, *Parkin* and *NIX* (encoding BNIP3-like protein X (NIX)) (Bhansali et al., 2017). Interestingly, dysregulated mitophagy in T2D individuals is associated with accumulated mitochondria with functional alterations and increased ROS in peripheral blood mononuclear cells (Bhansali et al., 2017). Of note, modulating mitophagy has gained interest as a therapeutic approach for insulin resistance (Ning et al., 2022).

In states of overnutrition, such as obesity, an excess of nutrients like carbohydrates and neutral lipids increases substrate flux into the mitochondria, accelerating electron flow through the ETC. This increased activity can lead to electron leakage, producing superoxide (O2•−) as a byproduct. Superoxide is then converted into hydrogen peroxide (H_2O_2), which, in excessive amounts, directly interferes with insulin signaling

pathways, contributing to insulin resistance (Akl et al., 2017; Fazakerley et al., 2018). While physiological levels of oxidative stress are essential for normal cellular signaling, excessive oxidative stress can cause DNA damage, protein oxidation, and lipid peroxidation, underlying conditions like neurodegeneration, cancer, insulin resistance and T2D (Lennicke and Cochemé, 2021).

In adipose tissue, chronic overnutrition induces mitochondrial ROS production and alters mitochondrial respiration, which contributes to local insulin resistance (Ahmed et al., 2021; Politis-Barber et al., 2020). These processes stimulate macrophage infiltration and the release of pro-inflammatory cytokines like tumor necrosis factor-α (TNF-α) and interleukin-6 (IL-6), which not only drive local inflammation but also promote systemic inflammation affecting multiple organs (Zatterale et al., 2019). Both TNF-α and IL-6 have been shown to associate with insulin resistance and can inhibit tyrosine phosphorylation of IRS1 (Feng et al., 2020). In visceral but not subcutaneous adipose tissue of obese individuals, inflammation is linked to reduced expression of lipogenic markers and decreased mitochondrial respiration (Harman-Boehm et al., 2007; Okamoto et al., 2007; Pafili et al., 2022a; Poulain-Godefroy et al., 2008).

In skeletal muscle, substantial evidence implicates ROS in the development of insulin resistance. A study by Anderson et al. demonstrated that obese individuals had higher mitochondrial H_2O_2 production in skeletal muscle compared to lean individuals, and excess fat intake significantly increased mitochondrial H_2O_2 emission, leading to insulin resistance in both rodents and humans (Anderson et al., 2009). Furthermore, in cardiomyocytes, ROS activates JNK, which subsequently activates nuclear factor kappa B (NF-κB) and p38 mitogen-activated protein kinase (p38 MAPK), triggering a cellular stress response (Tsai et al., 2012). This response is driven by increased metabolic flux and decreased expression of antioxidant enzymes, resulting in uncontrolled ROS production (Singh et al., 2022), that damages mitochondria and impairs their ability to meet cellular energy demands (Sangwung et al., 2020). Additionally, ROS-induced modifications of intracellular signaling molecules, such as protein tyrosine phosphatases (PTPs), further diminish insulin sensitivity (Meng et al., 2002). In the liver, mitochondrial ROS play a critical role in promoting insulin resistance and contributing to liver fibrogenesis in T2D. Mitochondrial ROS in hepatocytes increase serine phosphorylation of IRS1 and decrease insulin-stimulated tyrosine phosphorylation of IRS1, leading to insulin resistance (Nishikawa and Araki, 2007).

ROS further exacerbate liver pathology by activating hepatic myofibroblasts, which contributes to fibrotic changes in the liver (Bocca et al., 2022).

1.4.2.2 Endoplasmic reticulum stress

The relationship between ER stress and oxidative stress plays a key role in cellular homeostasis and metabolic function. The close connection between mitochondria and the ER, particularly at their membrane contact sites, allows the exchange of calcium, lipids, and metabolites to maintain balance (Sassano et al., 2017). However, oxidative stress in one organelle often affects the other, creating a vicious cycle of altered function. For instance, calcium released from ER-stores is taken up by mitochondria, disrupting the ETC and increasing ROS production and further exacerbates calcium imbalance, leading to ER stress and altered mitochondrial function (Görlach et al., 2015). However, initially ER stress occurs when the ER protein-folding capacity is exceeded, leading to unfolded protein accumulation and activation of the unfolded protein response (UPR), controlled by inositol-requiring enzyme 1 (IRE1), protein kinase R (PKR)-like endoplasmic reticulum kinase (PERK), and activating transcription factor 6 (ATF6) (Görlach et al., 2015). While transient UPR activation is adaptive, chronic activation in obesity and T2D has been linked to insulin resistance and metabolic dysfunction (Ma et al., 2024; Xu et al., 2023).

In adipose tissue, obesity-associated hypertrophy, hypoxia, and lipid overload activate UPR markers, including 78-kDa glucose-regulated protein (GRP78/BiP), phosphorylated IRE1α, and PERK (Sharma et al., 2008). Human and murine studies further show that C/EBP homologous protein (CHOP) expression and JNK activation are elevated in obese adipose tissue, correlating with increased secretion of pro-inflammatory cytokines (TNF-α, IL-6, monocyte chemoattractant protein-1 (MCP-1)) and reduced adiponectin levels, thereby exacerbating insulin resistance (Kern et al., 2001; Trayhurn, 2013; Xu et al., 2023). Additionally, ER stress activates JNK and NF-κB, leading to IRS1 serine phosphorylation, which inhibits insulin receptor signaling (Brown et al., 2020). Importantly, weight loss interventions have been shown to reverse ER stress markers, suggesting that obesity-induced ER stress is reversible (Gregor et al., 2009).

In skeletal muscle, biopsies from obese and T2D individuals reveal elevated UPR markers, such as spliced X-box binding protein 1 (XBP1) and GRP78, alongside increased expression of tribbles pseudokinase-3 (TRB3), a PERK-ATF4 target that

interferes with insulin signaling by blocking AKT phosphorylation (Koh et al., 2013). TRB3 has been recognized as a negative regulator of insulin signaling, as treating myotubes or mouse muscle with chemical ER stressors, such as tunicamycin or thapsigargin, increased TRB3 expression and caused insulin resistance, whereas muscles from TRB3-knockout mice were protected from HFD-induced insulin resistance (Koh et al., 2013). ER stress impacts skeletal muscle insulin responsiveness through multiple pathways. The IRE1-JNK pathway can operate in myocytes, leading to inhibitory phosphorylation of IRS1 and reduced GLUT4 translocation, thereby lowering glucose uptake (D'Alessandris et al., 2007; Petersen and Shulman, 2018). Moreover, ER-resident chaperones have recently been implicated in skeletal muscle insulin resistance, particularly protein disulfide isomerase A4 (PDIA4). PDIA4 expression is increased in human insulin-resistant muscle, palmitate-treated muscle cells and obese mice, who also show elevated IL-6 and TNF-α levels (Lee et al., 2022). Notably, knocking down PDIA4 in muscle cells reduces JNK activation, cytokine production, and insulin resistance, highlighting ER stress as a central factor in skeletal muscle dysfunction (Lee et al., 2022).

In the liver, ER stress contributes significantly to the development of hepatic insulin resistance and MASLD, especially in obesity and T2D. Liver biopsies from insulin-resistant individuals consistently show elevated GRP78, phosphorylated PERK, and IRE1α, indicating an active UPR compared to insulin-sensitive livers (Vesković et al., 2023). Such findings mirror animal models: mice or rats fed HFD or high-calorie diets exhibit hepatic UPR activation alongside worsening insulin resistance (Nasiri-Ansari et al., 2021; Wu et al., 2019b). Chronic UPR activation has been shown to induce XBP1, which subsequently upregulates SREBP-1c, a key driver of hepatic lipogenesis and TAG accumulation (Lee and Glimcher, 2009). Chronic ER stress therefore often correlates with heightened SREBP-1c activity and DNL in hepatocytes, promoting steatosis (Ferré and Foufelle, 2010; Gong et al., 2023). This lipid overload in hepatocytes further exacerbates ER stress, creating a feedback mechanism that sustains both steatosis and UPR activation (Baiceanu et al., 2016). Beyond lipid metabolism, sustained ER stress promotes hepatic inflammation and apoptosis. CHOP is upregulated in response to PERK-ATF4 pathway activation and plays a crucial role in hepatocyte apoptosis, contributing significantly to the progression of steatohepatitis (Rozpedek et al., 2016; Willy et al., 2015). Consistently, CHOP-knockout mouse models show reduced liver injury and improved insulin sensitivity following HFD

exposure (Mansour et al., 2022). Pharmacological interventions targeting ER stress pathways have shown therapeutic potential, with chemical chaperones or PERK–eIF2α–CHOP inhibitors (e.g., celastrol) demonstrating protective effects against ER stress and insulin resistance in obese mouse models (Tian et al., 2022). However, it is worth noting that the relationship between ER stress and hepatic metabolism is complex; a certain baseline UPR activity is necessary for normal lipid metabolism, and complete inhibition of UPR components can worsen metabolic outcomes. For instance, liver-specific IRE1α knockout mice develop more severe hepatic steatosis under HFD conditions, highlighting the complexity of ER stress in hepatic metabolism (Mansour et al., 2022; Wang et al., 2018). In line with this complexity, Dewidar et al. reported that GRP78 was downregulated in livers from murine models of obesity, diabetes and MASH, whereas CHOP downregulation was observed only in the obesity- and MASH-models. This pattern suggests a loss of adaptive UPR signaling that may differ across disease stages (Dewidar et al., 2023).

1.4.2.3 Abnormal lipid metabolism

1.4.2.3.1 Diacylglycerols and ceramides

The disruption of adipose tissue function, driven by excessive ROS production, ER stress, and altered mitochondrial function, compromises its role as a key energy storage site and endocrine organ. This impairment leads to elevated circulating levels of NEFAs due to increased lipolysis (Wondmkun, 2020), although a recent study indicate that the rise in plasma NEFAs observed in individuals with T2D is more likely a result of impaired lipid storage rather than enhanced lipolysis (Pereira et al., 2016).
However, pioneering human intervention studies in humans have demonstrated that acute increases in circulating NEFA impair insulin action. Infusion of TAG/heparin emulsions to elevate plasma NEFA levels produced a dose-dependent reduction of insulin-stimulated whole-body glucose uptake, mainly by suppressing glycogen synthesis and, to a lesser extent, carbohydrate oxidation (Boden et al., 1994). Using *in vivo* nuclear magnetic resonance spectroscopy, Roden et al. showed that lipid infusion in healthy individuals rapidly blunts intramuscular glucose-6-phosphate (G-6-P) accumulation, indicating an early inhibition of glucose transport/phosphorylation that precedes the decline in muscle glycogen synthesis and oxidative glucose metabolism (Roden et al., 1999; Roden et al., 1996). More recently, a single oral challenge with palm oil, a saturated fat, decreased whole-body, hepatic and adipose tissue insulin

sensitivity in lean humans, increased hepatic TAG and ATP content, enhanced gluconeogenesis and was accompanied by transcriptional regulation of innate immune and metabolic pathways, which may be implicated in MASLD progression (Hernández et al., 2017).

In line with these mechanistic data, elevated plasma NEFAs and lipid intermediates such DAGs and ceramides correlate with the severity of insulin resistance in obese individuals with T2D (Haus et al., 2009; Razquin et al., 2018). These lipids accumulate ectopically in skeletal muscle and liver, significantly contributing to lipotoxicity (Cheon and Cho, 2014; Mantzaris et al., 2011), marked by cellular stress and apoptosis, which underscores the detrimental effects of disrupted lipid metabolism on cellular function and viability (Chavez and Summers, 2010).

Early studies report that DAG accumulation is associated with the translocation of PKCθ in skeletal muscle and PKCε in the liver of insulin-resistant and T2D individuals (Roden and Shulman, 2019). Indeed obese and T2D individuals showed an overall increase in DAG content and PCKθ activation in skeletal muscle (Szendroedi et al., 2014). Specifically, total and cytosolic DAG can activate PKCθ in skeletal muscle, as shown in humans upon an acute lipid infusion. Activation of PKCθ results in phosphorylation of IRS1 at Ser1101, suppression of insulin-induced IRS1 tyrosine phosphorylation and AKT phosphorylation (Szendroedi et al., 2014). In contrast, another study showed that only membrane DAG was related to PKCε, but not PKCθ activation, and decreased insulin sensitivity in skeletal muscle of obese and T2D individuals, whereas, cytosolic DAG was inversely related to insulin resistance and PKCε activation (Bergman et al., 2012). These results indicate that the compartmentalization of DAG in skeletal muscle plays a role in modulating insulin sensitivity rather than total intramuscular DAG concentration, and suggests the possibility of PKC-independent pathways for DAG action on insulin signaling.

Early studies showed that hepatic DAG content of obese individuals with MASLD is negatively correlated with hepatic insulin sensitivity, mainly via activation of PKCε (Kumashiro et al., 2011; Magkos et al., 2012). Specifically, analysis of the cellular compartmentalization of DAG in rodent liver revealed that DAG increase in the membrane fraction of HFD mice, leading to PKCε activation and hepatic insulin resistance (Cantley et al., 2013). However, in mice with knockdown of comparative gene identification 58 (CGI-58), a lipid droplet (LD)-associated protein, that promotes TAG hydrolysis, DAG increase in LD or lipid-associated ER rather than the membrane,

preventing PKCε translocation to the plasma membrane and induction of insulin resistance (Cantley et al., 2013). Initial investigations revealed that a 3-day HFD in rats induced hepatic steatosis and insulin resistance, specifically activating PKCε without affecting other PKC isoforms (Samuel et al., 2007). Subsequent studies indicated that this activation of PKCε inhibits insulin-stimulated tyrosine phosphorylation of InsR, thereby linking elevated sn-1,2-DAG levels to the downregulation of insulin signaling (Petersen et al., 2016b). Furthermore, knockdown of lipin-1 or lipin-2, enzymes involved in DAG production, resulted in decreased hepatic DAG and TAG levels in HFD mice and improved glucose tolerance (Ryu et al., 2009; Ryu et al., 2011). Moreover, liver-specific overexpression of diacylglycerol-O-acyltransferase 2 (DGAT2), one of the two rate-limiting enzymes in the conversion of DAG to TAG, led to significantly reduced insulin sensitivity and a nearly 12-fold increase in hepatic DAG content (Jornayvaz et al., 2011).

In addition to the interference posed by DAG accumulation on insulin signaling, elevated ceramide levels have also been implicated in insulin resistance. Ceramides are bioactive membrane sphingolipids that play specialized regulatory roles in cellular metabolism, depending on their characteristic fatty acyl chain lengths and subcellular distribution.

In skeletal muscle, the role of ceramides in insulin resistance is more controversial and remains to be fully elucidated. Some studies have reported that higher total ceramide content correlates with lower insulin sensitivity in obese individuals with insulin resistance (Adams et al., 2004; Coen et al., 2010; Coen et al., 2013). However, other studies found no association between total ceramide content and insulin sensitivity in individuals with impaired glucose tolerance, obesity, or T2D (Skovbro et al., 2008). In contrast, healthy or endurance-trained individuals often display lower ceramide levels and higher insulin sensitivity, suggesting that the inverse relationship between ceramides and insulin action may not hold across all populations (Bergman et al., 2016b; Skovbro et al., 2008; Szendroedi et al., 2014). Notably, ceramide species C18:0 was elevated in individuals with T2D compared to athletes, and this increase was inversely correlated with insulin sensitivity, even in sedentary individuals without T2D (Bergman et al., 2016a; Tonks et al., 2016). Moreover, C18:0 was the predominant species induced from HFD in mouse skeletal muscle (Frangioudakis et al., 2010; Turpin-Nolan et al., 2019) and correlated positively with the expression of

ceramide synthase 1 (CerS1), enzyme responsible for C18:0 ceramide synthesis (Turpin-Nolan et al., 2019). In line, CerS1 deficiency or its pharmacological inhibition, protect against diet-induced obesity and insulin resistance but also increases the levels of other ceramide species (C22:0, C22:1, C24:0, C24:1) (Turner et al., 2018; Turpin-Nolan et al., 2019).

In addition to the overall content of ceramides, their intracellular localization in muscle appears to influence the onset of insulin resistance. Although there were no significant differences in total ceramide levels within the cytosolic and mitochondrial/ER fractions between individuals with T2D and athletes, ceramide content was elevated in the sarcolemmal and nuclear fractions of T2D individuals compared to athletes, lean and obese individuals (Perreault et al., 2018). The content of C18:0 ceramide in the sarcolemma, mitochondrial/ER, and nuclear fractions, but not in the cytosolic fraction, showed a significant inverse relationship with insulin sensitivity (Perreault et al., 2018). Both C16:0 and C18:0 muscle ceramides are associated with insulin resistance and their levels may reflect the severity of the metabolic dysfunction (Chung et al., 2017; Reidy et al., 2018). Different studies have provided insight into the role of ceramides, especially C18:0, in different signaling pathways. Of note, C18:0 acts as an inhibitor of PP2A, resulting in the inhibition of AKT phosphorylation in response to insulin (Mukhopadhyay et al., 2009). Furthermore, ceramide accumulation triggers the translocation of atypical PKCζ from the cytosol to caveolin-enriched microdomains within the plasma membrane, where it promotes the dephosphorylation of AKT by activating PP2A through a distinct pathway (Blouin et al., 2010; Stratford et al., 2004). Sustained ceramide action in cultured myocytes triggers JNK-dependent inhibitory phosphorylation of IRS1 and may modify InsR translocation into membrane lipid microdomains, thereby affecting insulin sensitivity (Hage Hassan et al., 2016).

Elevated hepatic ceramide levels, particularly species such as C16:0 and C18:0, are observed in rodents and humans with MASLD (Longato et al., 2012; Luukkonen et al., 2016). In line with this, Apostolopoulou et al. reported that individuals with MASH displayed markedly higher hepatic ceramide (C24:0) and dihydroceramide (C16:0, C22:0, C24:1) species compared with non-MASH obese individuals. However, this study also showed that total ceramide concentrations in liver and serum did not correlate with hepatic or whole-body insulin sensitivity (Apostolopoulou et al., 2018), underscoring that the profile and localization of individual ceramide species rather than the total ceramide pool may drive metabolic dysfunction. Likewise, another study

showed that hepatic inflammation is associated with altered total ceramide levels and concomitant upregulation of the same ceramide species (C16:0, C22:0, and C24:1) in MASH compared to livers without hepatic inflammation (Luukkonen et al., 2016). Studies using hepatic knockout mouse models have demonstrated that disrupting ceramide synthesis, specifically targeting C16:0 ceramide produced by CerS6, improves insulin sensitivity, reduces hepatic steatosis, and mitigates mitochondrial fragmentation (Hammerschmidt et al., 2019; Turpin et al., 2014). Therefore, compounds that reduce specific hepatic ceramides, show promise in mitigating obesity-related metabolic impairments (Hammerschmidt and Brüning, 2022; Raichur et al., 2019). Conversely, ceramide species such as C18:1 and C24:1 may exert protective effects by reducing body weight gain, enhancing glucose tolerance, and potentially alleviating liver inflammation and fibrosis under certain dietary conditions (Fox et al., 2011; Keppley et al., 2020; Wang et al., 2020). These findings highlight the nuanced and context-dependent roles of different ceramide species in liver metabolism and their implications for metabolic disease progression.

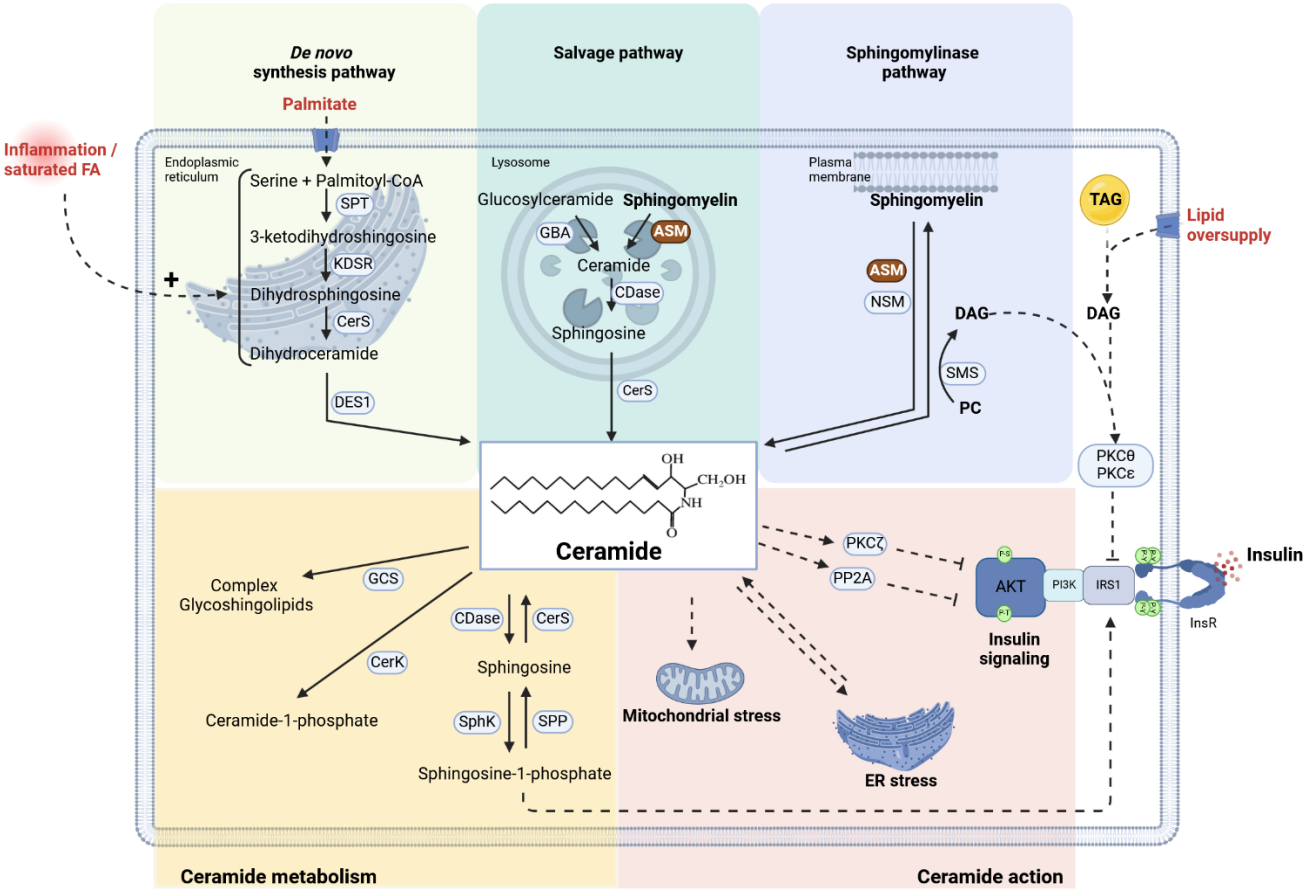

Figure 2: The role of ceramide and DAG synthesis and metabolism in insulin resistance.

Ceramide synthesis occurs through three major pathways: *de novo* synthesis, the salvage pathway, and the sphingomyelinase pathway. *De novo* synthesis begins in the endoplasmic reticulum (ER), where

serine and palmitoyl-CoA are condensed by serine palmitoyltransferase (SPT) to form 3-ketodihydrosphingosine. Subsequent reactions catalyzed by 3-ketodihydrosphingosine reductase (KDSR), ceramide synthase (CerS), and dihydroceramide desaturase (DES1) lead to the formation of ceramide. The salvage pathway involves the lysosomal breakdown of complex sphingolipids such as glucosylceramides and sphingomyelins into ceramide via glucocerebrosidase (GBA) and acid sphingomyelinase (ASM) respectively, or conversion into sphingosine, which can be recycled back into ceramide by CerS. The sphingomyelinase pathway involves hydrolysis of sphingomyelin at the plasma membrane by neutral sphingomyelinase (NSM) or ASM, generating ceramide.

Ceramides serve as precursors for complex glycosphingolipids and ceramide-1-phosphate (yellow panel). Ceramide is converted into glycosphingolipids via glucosylceramide synthase (GCS) or into ceramide-1-phosphate by ceramide kinase (CerK). Further metabolism involves ceramidase (CDase) hydrolyzing ceramide into sphingosine, which can be phosphorylated by sphingosine kinase (SphK) to generate sphingosine-1-phosphate (S1P), a signaling lipid. S1P can be dephosphorylated back into sphingosine by S1P phosphatase (SPP). In the context of insulin resistance, ceramide accumulation contributes to mitochondrial and ER stress (red panel). Ceramides inhibit insulin signaling through protein phosphatase 2A (PP2A)-mediated dephosphorylation of AKT and activation of atypical protein kinase C (PKCζ), impairing glucose uptake and insulin action. Additionally, diacylglycerols (DAGs), generated through lipid oversupply, triacylglycerol (TAG) hydrolysis, or the conversion of phosphatidylcholine (PC) into sphingomyelin, activate PKCθ in skeletal muscle and PKCε in the liver. This activation leads to the inhibitory phosphorylation of insulin receptor substrate 1 (IRS1), suppressing AKT activation and further exacerbating insulin resistance. Figure created with BioRender.com.

1.4.2.3.2 Membrane phospholipids

Phosphatidylcholine (PC) and phosphatidylethanolamine (PE) are fundamental components of cellular membranes, playing crucial roles in maintaining membrane integrity, fluidity, and the functional organization of membrane proteins (van der Veen et al., 2017). In mammalian plasma membranes, PC is primarily localized in the outer leaflet, while PE is enriched in the inner leaflet (Devaux, 1991). The distribution and amount of PC and PE within cellular membranes are of significant importance in the context of insulin resistance. The relative abundance and ratio of these phospholipids (PC:PE) have been shown to markedly influence membrane properties and insulin sensitivity in skeletal muscle and liver tissues (Chang et al., 2019).

In skeletal muscle, an inverse relationship between PC:PE ratio and insulin sensitivity was observed in endurance-trained athletes, obese sedentary individuals, and those with T2D. (Newsom et al., 2016). Similarly, in both normoglycemic and overweight dysglycemic men, basal PC:PE ratio negatively correlated with insulin sensitivity (Lee et al., 2018). Studies in mice with skeletal muscle-specific disruptions in genes encoding choline/ethanolamine phosphotransferase 1 (CEPT1) or fatty acid synthase (FAS), critical for phospholipid synthesis, reveal that imbalances in PC and PE synthesis can impair insulin sensitivity by affecting calcium homeostasis (Funai et al., 2016; Funai et al., 2013). The molar PC:PE ratio in the sarcoplasmic reticulum (SR) directly impacts the activity of sarcoplasmic/endoplasmic reticulum calcium ATPase (SERCA), responsible for translocation of calcium ions into SR for muscle contraction

(Funai et al., 2016; Funai et al., 2013). Reduced PE levels in the SR inhibit SERCA, thus impairing muscle function and decreasing insulin sensitivity (Gustavsson et al., 2011).

Individuals with MASLD exhibit lower hepatic and erythrocyte PC:PE ratios compared to healthy individuals (Arendt et al., 2013). Knockout mouse models of phosphatidylethanolamine N-methyltransferase (PEMT), lacking the ability to convert PE to PC in the liver, and deprived of dietary choline, showed reductions in the PC:PE ratio which results into steatosis, steatohepatitis, and ultimately, liver failure (Li et al., 2006; Walkey et al., 1998). PC may regulate liver steatosis through its feedback control on SREBP-1c. Low cellular levels of PC activate SREBP-1c, promoting its nuclear localization and the activation of lipogenic gene expression, resulting in LD formation within the liver (Walker et al., 2011). Conversely, obese mice exhibited increased hepatic ER membrane ratios of PC:PE compared to lean mice, associated with ER stress and steatosis. Correcting this ratio, via PEMT inhibition, results in reduced ER stress and improved glucose homeostasis (Fu et al., 2011). Thus, it seems that imbalance in PC:PE ratio, can have adverse consequences.

1.5 Acid sphingomyelinase: a key regulator in cellular lipid metabolism

1.5.1 Distinct isoforms, localization and activation mechanisms of acid sphingomyelinase

Acid sphingomyelinase (ASM) is a ubiquitously expressed enzyme responsible for the hydrolysis of sphingomyelin, a sphingolipid found in cell membranes, into ceramide and phosphorylcholine, a precursor of PC. In humans, two distinct forms of ASM are derived from a single *SMPD1* gene due to different posttranslational modifications and trafficking processes (Kornhuber et al., 2015). One form is localized to the lysosomal compartment (L-ASM), while the other form is secreted extracellularly (S-ASM) and requires exogenous Zn^{2+} ions for activation. S-ASM exhibit a significantly longer half-life and greater stability once secreted compared to L-ASM. This difference can be attributed to their distinct glycosylation patterns, resulting in different molecular weights (Jenkins et al., 2010; Kornhuber et al., 2015). However, an earlier study demonstrated that ASM resides in secretory lysosomes, which are mobilized upon stimulation to fuse

with the cell membrane (Perrotta et al., 2010). Similarly, several studies have observed that stimulation by various external stimuli, such as UV radiation, Fas ligand activation, and pathogenic factors like pore-forming bacterial toxins (Listeriolysin O, Pneumolysin), can trigger vesicles containing ASM to translocate to the plasma membrane, releasing the enzyme either to the outer leaflet or into the extracellular space. Additionally, oxidative stress inducers like H_2O_2, as well as mechanical stress through membrane wounding or inflammatory cytokines such as TNF-α and IL-1β, have been shown to induce ASM secretion. This ASM species is referred to as L-ASM by some researchers (Defour et al., 2014; Li et al., 2012), as S-ASM by others (Rotolo et al., 2005), while some studies do not specify its classification (Grassmé et al., 1997; Verdurmen et al., 2010), which complicates the distinction between different forms of ASM. However, ASM-1 is the only catalytically active isoform among the seven known isoforms, some of the inactive isoform (5-7) exert a dominant negative effect on L-ASM activity and thereby can affect cellular processes (Rhein et al., 2012). ASM not only catalyzes the hydrolysis of sphingomyelin to generate ceramide but also exhibits phospholipase C activity, cleaving 27 distinct sphingo- and glycerophospholipids, including those leading to the formation of DAG. However, ASM demonstrates a preferential hydrolysis of sphingolipids (Breiden and Sandhoff, 2021). Due to its broad substrate spectrum, inherited ASM deficiency, as seen in Niemann-Pick disease types A and B, results in the progressive accumulation of sphingomyelin. This primary lipid accumulation subsequently induces secondary accumulations of other lipids, such as cholesterol, glucosylceramide, and ganglioside GD3, predominantly within late endosomes and lysosomes (Rodriguez-Lafrasse et al., 1994; Vanier, 2013).

1.5.2 The role of acid sphingomyelinase in cellular homeostasis

ASM is implicated in various cellular processes, including apoptosis, ferroptosis, lysosomal membrane permeabilization (LMP), autophagy, and ER stress. In addition to its established role in bacterial and viral host defense (Schuchman, 2010), ASM is pivotal in both non-receptor and receptor-mediated apoptosis. One of the most well-studied non-receptor mediated apoptosis pathways involves UV light. UV-C irradiation, in particular, has been shown to result in redox-dependent activation and translocation of ASM to the outer leaflet of the plasma membrane, where it activates JNK (Charruyer et al., 2005) or to the mitochondrial membrane, where it induces Bcl-2-associated X protein (BAX) activation through ceramide generation, leading to apoptosis (Kashkar

et al., 2005; Zhang et al., 2001). Interestingly, overexpression of PKCζ protects against UV-C-induced apoptosis by preventing ASM translocation to the plasma membrane and subsequent ceramide production (Charruyer et al., 2007). ASM is also crucial for the activation of death receptors such as CD95 (Fas/Apo-1), TNF-α, and TNF-related apoptosis-inducing ligand (TRAIL), via forming ceramide platforms within plasma membranes ultimately leading to cell apoptosis (Stephan et al., 2017). Hepatocytes from ASM-deficient mice and wild-type hepatocytes with inhibited ASM activity showed resistance to TNF-α-induced cell death (García-Ruiz et al., 2003), demonstrating that ASM absence prevents ganglioside GD3 targeting to mitochondria, inhibiting TNF-α-mediated cell death (Colell et al., 2002; García-Ruiz et al., 2003). Additionally, ASM-generated ceramides activate cathepsin D (CTSD) in lysosomes, which in turn triggers pro-apoptotic proteins like BH3 interacting domain death agonist (Bid), caspase-9, and caspase-3, leading to mitochondria-mediated cell death (Heinrich et al., 2004).

Recent studies have implicated ASM in the activation of ferroptosis through ceramide production and the induction of autophagy, which subsequently leads to the accumulation of ROS and a decrease in glutathione peroxidase 4 (GPX4) levels (Ajoolabady et al., 2021) in human fibrosarcoma (HT-1080) cells (Thayyullathil et al., 2021), human osteoblasts (hFob1.19), and a T2D osteoporosis rat model (Du et al., 2023). ASM is also implicated in LMP, which leads to cytosolic acidification and the release of lysosomal proteases, subsequently impacting other organelles like mitochondria and ultimately inducing apoptosis (Li et al., 2008). For instance, palmitic acid (PA), one of the most prevalent saturated fatty acids in Western diets, induces LMP in hepatocytes, altering mitochondrial function, triggering cytochrome c release, and cell death (Li et al., 2008). However, ASM deficiency provides resistance to PA-induced lipotoxicity in primary mouse hepatocytes. Consistent with this resistance, hepatocytes from ASM-deficient mice are also resistant to cell death induced by amphiphilic lysosomotropic detergents, a protection attributed to increased lysosomal cholesterol level (Fucho et al., 2014).

ASM is also essential for autophagy induction, as arterial smooth muscle cells from ASM-deficient mice display defects in autophagosome-lysosome fusion due to impaired lysosomal function (Li et al., 2014). Furthermore ASM upregulates autophagy protein 5 (Atg5) expression in HepG2 cells (Park et al., 2008) and suppresses autophagy when knocked down in leukemia HL-60 cells (Taniguchi et al., 2012).

Despite ASM deficiency leads to defective autophagic flux, hepatocytes from ASM-deficient mice exhibit resistance to HFD-induced steatosis, indicating a complex interaction between autophagy and lipid metabolism (Fucho et al., 2014). Notably, suppression of autophagy with chloroquine/brefeldin induces ER stress in primary hepatocytes from wild-type mice, but not in ASM-deficient mice, suggesting that ASM is crucial for autophagy suppression-mediated ER stress (Fucho et al., 2014)

ASM also triggers ER stress through ceramide production and subsequent disruption of calcium signaling. Exogenous ASM treatment in hepatocytes disrupts ER calcium homeostasis, causing ER stress due to ceramide-induced calcium release to the cytosol, which interferes with the ability of the chaperone GRP78/BiP to bind UPR transducers (Fernandez et al., 2013). ASM-generated ceramide facilitates lysosomal fusion, regulates cytoskeleton and microtubule assembly, enhances autophagosome trafficking, and interacts with microtubule-associated protein 1A/1B-light chain (LC3I) to target lysosomes to autophagosomes (Varela et al., 2024).

Conversely, in lung cells, downregulation of ASM activity modifies lysosomal nutrient-sensing signaling, leading to increased autophagy and decreased levels of sphingosine and sphingosine-1-phosphate (S1P) (Justice et al., 2018), indicating tissue-specific effects of ASM.

1.5.3 Impact of acid sphingomyelinase in metabolic diseases

Niemann-Pick disease (NPD) types A and B, caused by ASM deficiency, lead to the accumulation of sphingomyelin in lysosomes (Vanier, 2013). In type A, the complete lack of ASM results in severe neurological impairments, hepatosplenomegaly, and early mortality. Type B, with partial ASM activity, presents with milder symptoms, including organ enlargement and pulmonary dysfunction (Vanier, 2013).

1.5.3.1 Function of acid sphingomyelinase in muscle regeneration and its implications for type 2 diabetes mellitus

Mouse models of ASM deficiency, mimicking NPD types A and B, exhibit shortened lifespans, ataxia, tremors, and reduced calcium release from the SR. These mice fatigue more quickly and exhibit impaired sarcolemma repair, particularly after skeletal muscle injury, which leads to an exaggerated loss of muscle force during recovery (Michailowsky et al., 2019b), underscoring the critical role of ASM in muscle repair. ASM facilitates this repair by its calcium-dependent release to the plasma membrane,

a process facilitated by its interaction with dysferlin, a protein involved in vesicle trafficking and fusion, to promote lesion internalization through ceramide production (Defour et al., 2014; Tam et al., 2010). Additionally, a recent study has shown that liver-derived ASM enhances muscle repair, improving overall muscle quality and health in animal models of muscle dystrophy (Bittel et al., 2022). Its involvement in maintaining muscle health makes it particularly relevant in the context of T2D, where muscle regeneration is often compromised (Espino-Gonzalez et al., 2024) and complicated by factors such as comorbidities, nutrition, genetics, physical activity, aging, and variations in fat and muscle distribution (Wolfe, 2006). Preclinical studies using HFD models of T2D, consistently demonstrate muscle deficits, including reduced lean mass, strength, and exercise capacity (Espino-Gonzalez et al., 2024), which are associated with factors such as lipid deposition, muscle fiber atrophy, impaired mitochondrial function, and increased ROS production (Lopez-Pedrosa et al., 2024).

While direct evidence of muscle ASM activity in T2D individuals is lacking, insights from related prediabetic rodent studies suggest a complex role. Increased ASM activity has been observed in heart muscle of HFD-induced diabetic mice, leading to ceramide accumulation (Liu et al., 2023). Notably, this study demonstrated that high glucose, PA, or ceramide treatment also increased ASM activity in H9c2 cells, a heart-derived cell line (Liu et al., 2023). Conversely, PA-treated C2C12 mouse myotubes showed decreased mRNA expression of the *SMPD1* gene (Park et al., 2016), but exogenous ASM treatment led to increased ceramide production (Ferreira et al., 2010). However, streptozotocin (STZ)-treated mice, which show β-cell failure and insulin deficiency, show either a slight reduction or no change in ASM activity across various muscle types, including the soleus, red gastrocnemius, and white gastrocnemius (Górska et al., 2004). This is accompanied by an increase in total ceramide content and a reduction in sphingomyelin content, largely driven by increased neutral sphingomyelinase (NSM) activity at the plasma membrane (Górska et al., 2004). Another study on prolonged STZ- or heparin-induced diabetes in rats confirmed these findings, showing increased ceramide content and decreased ASM activity in all three muscle types (Błachnio-Zabielska et al., 2010). Given that ASM activity is reduced in the skeletal muscles of T2D mouse models, this reduction could exacerbate impairments in muscle repair, particularly during exercise when muscle fibers are subjected to stress and damage. The decreased ASM activity may hinder essential repair mechanisms that depend on ceramide production and plasma membrane

resealing, processes critical for muscle recovery post-injury or exercise (Andrews et al., 2014; Draeger et al., 2014; Gakis et al., 2023). Interestingly, ASM phospholipase activity plays a key role in altering membrane composition by cleaving phosphorylcholin residues from both sphingomyelin and PC (Breiden and Sandhoff, 2021). This activity is modulated by lipid metabolites such as DAGs, ceramide, free fatty acids, and cholesterol, which promote sphingomyelin hydrolysis but inhibit PC cleavage (Oninla et al., 2014). In skeletal muscle, ASM-mediated sphingomyelin hydrolysis reorganizes plasma membrane lipid domains and receptor complexes, facilitating membrane resealing and modulating damage-induced inflammatory signaling-processes that critically influence muscle regeneration. Muscle injury is characterized by infiltration of pro-inflammatory M1 macrophages, which are gradually replaced by M2 macrophages which respond to anti-inflammatory signaling. M2 macrophages enhance the differentiation of muscle stem cells (satellite cells) and their fusion into myotubes, thus contributing to muscle repair (Tidball, 2011). Interestingly the study by Roux-Biejat et al. demonstrates that ASM-deficient mice show faster muscle repair after injury due to a reduction in early inflammation (Roux-Biejat et al., 2021). Following cardiotoxin-induced muscle damage, ASM-deficient mice exhibit lower levels of pro-inflammatory cytokines and an altered macrophage phenotype. In particular, these mice show a shift from pro-inflammatory M1 macrophages to anti-inflammatory M2 macrophages, which support tissue repair. While these findings suggest that ASM deficiency may benefit early repair (Roux-Biejat et al., 2021), its role in initiating the inflammatory response may still be crucial for the overall repair process, particularly under chronic metabolic stress. The role of ASM in muscle regeneration and function is complex and debated (1.6.3.1).

1.5.3.2 The role of acid sphingomyelinase in MASLD and insulin resistance

In the liver, ASM is involved in the development of steatosis and fibrosis. Elevated ASM mRNA levels have been observed in individuals with MASH (Moles et al., 2010b). In line, HFD-fed mice showed significantly increased hepatic ASM mRNA expression and ceramide content compared to littermates fed a normal diet. In contrast, ASM-deficient mice showed only a slight increase in ceramide content under HFD conditions, were resistant to HFD-induced steatosis (Fucho et al., 2014), and displayed reduced expression of lipogenic genes such as *Srebp1c, Dgat2*, *Fas* and *Acc* compared to wild-type mice (Fucho et al., 2014). The methionine-choline-deficient (MCD) diet typically

induces steatosis by impairing hepatic PC synthesis, which reduces very low-density lipoprotein (VLDL) secretion and leads to TAG accumulation in the liver (Haberl et al., 2020). ASM-deficient mice show resistance to steatosis induced by a MCD diet (Fucho et al., 2014), but maintained higher liver PC levels compared to wild-type mice (Prinetti et al., 2011). This conflicting results suggests that ASM contributes to steatosis progression but also protect the cell against VLDL accumulation, which leads to steatosis in the absence of methionine and choline (Prinetti et al., 2011). Another study showed that ASM is also implicated in fibrosis through CTSD activation, which promotes hepatic stellate cell proliferation (Moles et al., 2010b). Consistently, functional inhibition of ASM with the cationic amitriptyline, which induces detachment of ASM from the inner lysosomal membrane and its subsequent degradation, has been shown to reduce hepatic fibrosis in a carbon tetrachloride-induced fibrosis mouse model (Quillin et al., 2015).

In regard to insulin signaling, pharmacological inhibition of ASM normalizes HFD-induced hyperglycemia and improves both glucose tolerance and insulin sensitivity in mice (Fucho et al., 2014). Similarly, genetic deletion of ASM in low density lipoprotein (LDL) receptor-deficient (*Ldlr* $^{-/-}$) mice, which are predisposed to metabolic disease under HFD conditions, prevents diet-induced obesity and hyperglycemia as well as insulin resistance (Deevska et al., 2009). These mice also exhibit a decrease in hepatic TAG content along with increased levels of sphingomyelin, PE and interestingly also increased levels of PC, as well as ceramide content (Deevska et al., 2009). In contrast, hepatocytes isolated from ASM-deficient mice exhibit impaired glucose uptake and glycogen storage and LD formation upon high glucose treatment, likely due to enhanced AMPK phosphorylation and reduced GLUT2 expression (Osawa et al., 2011).

Conversely, hepatic overexpression of ASM via adenoviral delivery in both wild-type and diabetic *db/db* mice leads to improved glucose tolerance *in vivo*. In support of these *in vivo* findings, primary hepatocytes isolated from wild-type mice and transduced with adenoviral ASM showed elevated ceramide levels. However, the ceramide increase was relatively modest compared to the extent of sphingomyelin degradation, indicating that a substantial portion of the generated ceramide was further metabolized to S1P. This suggests that ASM exerts insulin-like effects primarily through S1P-mediated AKT activation. The balance between ASM-generated

ceramide and its conversion to S1P appears to be critical for these metabolic processes (Osawa et al., 2011).

In summary, ASM is an important regulator of sphingolipid metabolism with potential implications for hepatic steatosis, fibrosis, and insulin resistance. Current evidence from animal and cell models suggests that changes in ASM activity can affect ceramide and S1P metabolism however, the precise mechanisms and their relevance in humans remain to be elucidated.

1.6 The integrative role of physical activity in metabolic health

1.6.1 Impact of exercise training on metabolic pathways

Physical activity plays a crucial role in metabolic health, influencing various physiological processes that directly impact the development and progression of metabolic disorders such as T2D. Lifestyle interventions, incorporating both dietary modifications and regular exercise, remain the primary strategies for managing T2D (Kanaley et al., 2022; Röhling et al., 2016). However, variations in the type and structure of exercise programs can lead to different metabolic outcomes in human studies. Generally, exercise regimens are categorized into two primary forms: resistance (or strength) and endurance (or aerobic) training. Resistance training, characterized by the contraction of specific muscle groups at low frequency, such as during weightlifting, primarily aims to increase muscle hypertrophy, strength, and power. In contrast, endurance exercise, which involves high-frequency contraction of multiple muscle groups as seen in activities like running, predominantly enhances skeletal muscle oxidative capacity and overall endurance.

Exercise interventions can also vary in the duration, intensity, and frequency of sessions. Standard programs designed to improve glycemic control often prescribe moderate-intensity exercises, such as daily running sessions lasting approximately 60 minutes over several weeks (Nishida et al., 2004). However, the time commitment required for these interventions can be a barrier for participants. High-intensity interval training (HIIT) has emerged as a more time-efficient alternative, consisting of short bursts of high-intensity effort followed by low-intensity intervals or rest. These programs typically reduce the training frequency to three sessions per week (Jung et al., 2014; Madsen et al., 2015), as recommended for individuals with T2D (ADA, 2022).

1.6.2 Effects of acute and chronic exercise on metabolism

Acute exercise refers to a single session of physical activity that elicits immediate physiological responses, including enhanced glucose uptake and subsequent glycogen synthesis in skeletal muscle, as well as improved insulin sensitivity, which can persist for up to 48 h post-exercise (Hawley and Lessard, 2008; Perseghin et al., 1996). These acute metabolic effects are largely driven by the activation of key signaling pathways, such as AMPK, which facilitates the translocation of GLUT4 to the plasma membrane and promotes FAO in an insulin-independent manner (Hawley and Lessard, 2008). Human studies demonstrate that even a single bout of exercise increases plasma membrane GLUT4 content in both healthy individuals and those with T2D (Kennedy et al. 1999). The extent of glucose uptake by muscle during exercise is contingent on the intensity and duration of the activity. During prolonged exercise, especially when muscle glycogen stores are depleted, blood glucose plays a more prominent role in oxidative metabolism (Richter and Hargreaves, 2013). Intramyocellular lipid (IMCL) content, which is closely linked to insulin resistance (Krssak et al., 1999; Perseghin et al., 1999), can also be modulated by both acute and prolonged exercise, with more pronounced IMCL utilization occurring during longer exercise bouts, reflecting an increased reliance on lipid oxidation as glycogen becomes limited (Krssak et al., 2000; Rico-Sanz et al., 2000).

In contrast, chronic exercise, characterized by sustained and repeated physical activity over an extended period, induces long-term physiological adaptations in skeletal muscle, liver, and adipose tissue, which collectively enhance insulin sensitivity (Ashcroft et al., 2024). These adaptations encompass increased GLUT4 content and glycogen depletion as well as alterations in IMCL content, augmented mitochondrial biogenesis, increased oxidative capacity, and hypertrophy of muscle tissue, which have been observed in both healthy and insulin-resistant individuals (Dubé et al., 2008; Kanaley et al., 2022; Larsen et al., 2014). Various forms of exercise training - including aerobic, resistance, and HIIT - demonstrate significant benefits, particularly when sustained for periods exceeding 12 weeks, with each form showing positive effects in T2D individuals (Thomas et al., 2006). Both aerobic and resistance training have been shown to improve glycemic control, as evidenced by reductions in HbA1c and fasting blood glucose levels (Röhling et al., 2016). Meta-analyses indicate that combined aerobic and resistance exercise results in more substantial reductions in HbA1c compared to either modality alone (Röhling et al., 2016; Schwingshackl et al., 2014).

Furthermore, HIIT is increasingly recognized as the most effective exercise mode for reducing HbA1c and fasting blood glucose, as well as improving cardiorespiratory fitness, particularly in individuals with T2D (Francois and Little, 2015; Jelleyman et al., 2015). These distinct molecular effects of various exercise types underscore the complexity of exercise-induced adaptations in skeletal muscle, with each modality offering unique benefits in optimizing metabolic health, particularly for individuals with T2D.

1.6.3 Molecular adaptations induced by exercise in skeletal muscle

Skeletal muscle is the primary site for molecular adaptations induced by exercise, driven by contractile activity during physical activity. These adaptations include repartitioning of IMCL as well as increased glucose uptake and mitochondrial content.

1.6.3.1 Intramyocellular lipid dynamics and sphingolipid metabolism adaptations

IMCL, comprising TAGs, DAGs, and ceramides, play pivotal roles in skeletal muscle metabolism, with their content being dynamically regulated by exercise. Noninvasive ^{1}H NMR work in healthy, non-obese participants first demonstrated that higher IMCL correlates with whole-body insulin sensitivity (M-value), a finding extended to lean, nondiabetic first-degree relatives of individuals with T2D (Jacob et al., 1999). Elevated IMCL are also associated with insulin resistance in obesity and T2D (Goodpaster et al., 2000), yet also correlate with enhanced oxidative capacity and metabolic health in athletes - a phenomenon known as the "athlete's paradox" (Goodpaster et al., 2001).
In terms of acute regulation, a single bout of prolonged treadmill running to exhaustion decreases IMCL content in the active muscle (e.g. soleus) and shifts substrate use towards lipid oxidation as glycogen becomes limited. In contrast, the non-exercised muscle does not exhibit an increase in IMCL during exercise, but instead shows a decline during early recovery, likely reflecting substrate mobilization to support glycogen resynthesis in the previous active muscle groups (Krssak et al., 2000). Most studies report IMCL decreases after a single endurance training bout in athletes and lean individuals but not in obese individuals with or without T2D (Bergman et al., 1999; Bergman et al., 2018; Creer et al., 2005). However, acute resistance exercise reduces IMCL also in obese individuals (Creer et al., 2005; Harber et al., 2008), although IMCL return to baseline levels typically within 2 h of recovery (Harber et al., 2008; Koopman

et al., 2006). Acute exercise itself does not immediately impact intramyocellular triglycerides (IMTG), but IMTG utilization is influenced by initial concentrations (Creer et al., 2005) and occurs predominantly during the recovery period (3 to 18 h post-exercise), after which IMTG levels return to baseline (Kiens and Richter, 1998). Notably, IMTG stores and their utilization vary by sex, with women typically having higher stores and greater utilization during exercise than men (Steffensen et al., 2002). There are limited data on changes in muscle DAG in response to acute exercise. Bergman et al found that a bout of exercise did not change total cell DAG concentration in athletes and obese individuals with and without T2D (Bergman et al., 2018), but it transiently increases muscle sphingolipids, including ceramides, sphingosine, S1P, dihydroceramides, and glycosylceramides, in both trained and untrained individuals, which return to baseline values or even less within 2 h post-exercise (Bergman et al., 2016a; Helge et al., 2004). These changes may lead to improvement of insulin sensitivity (Aerts et al., 2007). Notably, sphingomyelin levels rise after acute exercise in trained but not untrained individuals, suggesting that sphingomyelin degradation is not a primary source of exercise-induced ceramide accumulation (Helge et al., 2004). Studies have shown increased levels of S1P in skeletal muscle across various exercise models in both humans and animals (Baranowski et al., 2015; Bergman et al., 2016b; Błachnio-Zabielska et al., 2008). One study found elevated mRNA levels of alkaline ceramidase, which hydrolyzes ceramide into sphingosine, and sphingosine kinase 1 (SphK1), which phosphorylates sphingosine to form S1P, in human muscle biopsies taken immediately after exercise and following a 2 h recovery period, suggesting that exercise stimulates the breakdown of ceramide to sphingosine and its subsequent conversion to S1P (Bergman et al., 2016b). This process, combined with increased extracellular S1P availability, may delay muscle fatigue (Cordeiro et al., 2019) and support muscle repair through activation of satellite cells (Calise et al., 2012; Donati et al., 2013). Interestingly, acute exercise increases ASM protein levels in rodent models, suggesting enhanced sphingomyelin degradation and ceramide production (Lee and Leem, 2019). Notably, ASM inhibition has been shown to reduce muscle damage, leading to the hypothesis that inhibiting ASM may lower ceramide levels via the sphingomyelin pathway, thereby mitigating myofiber cell death following muscle-damaging exercise (Lee and Leem, 2019). This is in contrasts with ASM role in sarcolemma repair, which is critical for maintaining muscle integrity (Michailowsky et al., 2019a).

Chronic aerobic exercise demonstrates various effects on IMTG content in individuals with obesity and T2D, reporting increases (Dubé et al., 2008), decreases (Bruce et al., 2004), or no change (Bruce et al., 2006), depending on study conditions. Chronic resistance exercise is often linked to increased IMTG levels in sedentary healthy individuals (Shepherd et al., 2014). Interestingly, IMTG accumulation does not directly cause insulin resistance but instead reflects an adaptation to exercise training, enhancing fuel supply and energy capacity (Dubé et al., 2008; Goodpaster et al., 2001). However, in sedentary individuals or those with T2D, the relationship between IMTG and insulin resistance depends on muscle fiber type and lipid droplet localization (Coen et al., 2010). For instance, in T2D, lipids are stored in larger droplets near the sarcolemma in type II fibers, whereas athletes store smaller droplets within intramyofibrillar regions of type I fibers. These smaller droplets exhibit higher turnover due to elevated Perilipin 5 (PLIN5) expression and interactions with mitochondria, enabling more efficient IMTG utilization (Gemmink et al., 2020). Chronic exercise, particularly when combined with weight loss, has been shown to reduce lipid intermediates like DAGs and ceramides, thereby improving insulin sensitivity in overweight and obese individuals (Bruce et al., 2006; Coen et al., 2015; Dubé et al., 2008; Dubé et al., 2011). However, these effects remain inconsistent, likely due to the advanced state of insulin resistance in some individuals (Petersen and Jurczak, 2016; Shepherd et al., 2017; Summers and Goodpaster, 2016). These data indicate that, chronic endurance exercise training can decrease whole cell DAG and ceramide concentration and composition, although these changes are not required for enhanced insulin sensitivity. This also suggests that alterations in specific ceramide species within distinct subcellular compartments may be more relevant in insulin desensitization than the overall amount of muscle ceramides. Notably, only the accumulation of specific ceramide species, such as C18:0 in the mitochondrial/ER subsarcolemmal fraction, is consistently linked to reduced insulin sensitivity (Bergman et al., 2016a; Perreault et al., 2018). The role of ASM in exercise, particularly in relation to ceramide synthesis, remains complex and somewhat contradictory. ASM activity has been shown to gradually decrease with the duration of exercise in rodents (Błachnio-Zabielska et al., 2011). However, a 5-week aerobic exercise program in rats demonstrated increased ASM activity (Błachnio-Zabielska et al., 2008). Yet, as ASM is critical for sarcolemma membrane repair, its observed increase may reflect the heightened need for membrane repair post-exercise (Michailowsky et al., 2019a).

Interestingly other sphingolipids like sphingosine and S1P remain unchanged in trained compared with untrained individuals (Bergman et al., 2016a), as well as following exercise training with or without weight loss (Coen et al., 2015; Dubé et al., 2011). Long-term (≥12 weeks) exercise has been associated with increases in PC and PE levels and a reduced PC:PE ratio in normoglycemic and prediabetic individuals, improvements linked to enhanced insulin sensitivity (Lee et al., 2018). The resulting changes in membrane composition, including a reduced PC:PE ratio, may enhance muscle function and calcium homeostasis by modifying membrane integrity, fluidity, and lipid raft organization. These adaptations support InsR kinetics, improving insulin signaling and facilitating glucose uptake (Lee et al., 2018).

1.6.3.2 Mitochondrial adaptations

Mitochondria are highly dynamic organelles that continuously adapt to the metabolic demands of skeletal muscle, particularly during exercise. These adaptations occur through coordinated changes in mitochondrial respiration, biogenesis, dynamics, and mitophagy, collectively working to optimize energy homeostasis and maintain mitochondrial quality. Exercise is a powerful stimulus for mitochondrial remodeling, yet the magnitude and nature of these adaptations differ between healthy individuals and those with metabolic disorders such as T2D.

Acute exercise enhances mitochondrial respiration primarily through the activation of key signaling pathways, including calcium/calmodulin-dependent protein kinase (CaMK) in response to elevated intracellular Ca^{2+} levels (Ojuka et al., 2003), p38 MAPK via ROS-mediated signaling (Irrcher et al., 2009; Puigserver et al., 2001) and AMPK due to the increased AMP:ATP ratio caused by muscle contractions (Winder et al., 2000). These mechanisms have been elucidated using rodent models as well as rodent and human myotubes. Additionally, phosphoproteomic analyses of human muscle biopsies of healthy young men following endurance, sprint, and resistance exercise have identified exercise-induced activation of mTOR and protein kinase A (PKA), further affecting mitochondrial function (Blazev et al., 2022). These pathways converge on peroxisome PGC-1α, a master regulator of mitochondrial respiration and oxidative metabolism (Handschin and Spiegelman, 2008; Puigserver and Spiegelman, 2003), resulting in enhanced mitochondrial respiration in healthy individuals (Hernández-Alvarez et al., 2010). However, the upregulation of PGC-1α expression in

skeletal muscle of individuals with T2D in response to acute endurance exercise appears to be blunted, suggesting an impaired mitochondrial regulatory response (Hernández-Alvarez et al., 2010).

Chronic exercise training, such as 6-weeks of endurance or low volume HIT, enhances mitochondrial respiration by increasing oxidative capacity, ATP production, and mitochondrial efficiency, contributing to improved metabolic health in normoglycemic individuals (Gibala et al., 2012). Complementary evidence from rodent models has provided mechanistic insights into these adaptations, demonstrating that chronic endurance exercise leads to elevated expression of PGC-1α and enhanced mitochondrial lipid metabolism (Mozaffaritabar et al., 2024). These adaptations in rodents are associated with upregulation of key proteins involved in energy sensing, lipid mobilization, and mitochondrial dynamics, including AMPK-α, mTOR, hormone-sensitive lipase (HSL), adipose triglyceride lipase (ATGL), G protein-coupled receptor 41 (GPR41), phosphatidylcholine cytidylyltransferase 2 (PCYT2), and MFN1 (Mozaffaritabar et al., 2024). Rodent studies further show that 4-weeks of voluntary wheel running, which reflect endurance training, markedly increase mitochondrial content in skeletal muscle, as evidenced by elevated levels of mitochondrial enzymes such as citrate synthase and cytochrome c oxidase (Drake et al., 2016). These molecular adaptations are consistent with human data, where several months of regular exercise - particularly combined endurance and resistance training - have been shown to increase mitochondrial content by approximately 20–50% in skeletal muscle of both individuals with T2D and normoglycemic controls (Phielix et al., 2010). Importantly, resistance exercise and HIIT can complement endurance training in promoting mitochondrial adaptions. In a 9-month intervention study involving individuals with T2D, combined endurance and resistance training elicited greater increases in mitochondrial content than endurance training alone, which showed only modest effects (Sparks et al., 2013). Moreover repeated bouts of endurance and interval training over a 4-week period have been shown to upregulate NRF-1 and NRF-2 as well as mitochondrial transcription factor A (TFAM), thereby promoting mitochondrial DNA replication and the transcription of oxidative phosphorylation genes (Islam et al., 2020), mechanisms central to mitochondrial biogenesis. Finally, regular exercise can partially restore mitochondrial function in individuals with T2D, who show impaired mitochondrial biogenesis at baseline (Bonen, 2009; Larsen et al., 2014). Some reports indicate that alternative pathways, such as AMPK activation, may

compensate for the blunted PGC-1α response, allowing mitochondrial improvements even in insulin-resistant muscle (Kjøbsted et al., 2018; Nishida et al., 2020; Viollet et al., 2009)

Mitochondrial dynamics, including fusion and fission, also play a crucial role in the adaptive response to exercise, potentially modulating mitochondrial respiration (Chen et al., 2023). A single bout of exercise induces rapid changes in mitochondrial dynamics, though findings on specific protein responses are inconsistent. Some human studies show that *MFN1/2* mRNA levels remain unchanged within the first 2-4 h post-exercise, along with stable MFN2 protein levels (Cartoni et al., 2005; Perry et al., 2010). However, other studies report an immediate post-exercise increase in *MFN2* mRNA expression without changes in *OPA1*, *FIS1*, or *DNM1L* (encoding DRP1) mRNA (Kruse et al., 2017). Interestingly, MFN2 protein levels acutely increase in healthy individuals but remain unchanged in T2D subjects, indicating a potentially impaired fusion response in diabetic muscle (Kruse et al., 2017). Despite this, activating phosphorylation side of DRP1 at Ser^{616} was elevated in both groups (Kruse et al., 2017), suggesting that acute exercise induces mitochondrial fragmentation to facilitate the removal of damaged mitochondria. Notably, an early-onset T2D cohort failed to upregulate MFN2 gene expression post-exercise, reinforcing the notion that mitochondrial fusion capacity is compromised in T2D muscle (Hernández-Alvarez et al., 2010). This reduced capacity for mitochondrial fusion may underlie the impaired mitochondrial adaptations observed in T2D individuals, contributing to metabolic inflexibility and reduced insulin sensitivity (Jheng et al., 2012).

Chronic exercise significantly remodels mitochondrial dynamics by promoting fusion and reducing excessive fission in skeletal muscles. For instance, a 12-week aerobic training in sedentary adults did not increase MFN1 or MFN2 expression but led to significant reductions in FIS1 and Parkin, suggesting a decline in both mitochondrial fission and mitophagy (Axelrod et al., 2019). Conversely, prolonged training tend to increase MFN1, MFN2, and OPA1 levels, leading to a more interconnected mitochondrial network (Arribat et al., 2019; Balan et al., 2019) and attenuates mitochondrial fission signaling in healthy individuals. Similarly, a 12-week aerobic training intervention showed a trend toward increased MFN1 and MFN2, and importantly, a reduction in DRP1 phosphorylation in obese insulin-resistant adults, which correlated with improved insulin sensitivity and fat oxidation (Fealy et al., 2014). Training for more than 8-weeks restores also a more balanced fission/fusion dynamic

in diabetic muscle, by elongating mitochondrial network (Axelrod et al., 2019; Hood et al., 2019), a critical change since diabetes is often associated with lower MFN2 and smaller mitochondria (Kelley et al., 2002) as compared to healthy individuals, and by increasing MFN content and mitochondrial size, which contribute to enhanced insulin sensitivity (Genders et al., 2020). However, other studies suggest that individuals with obesity or T2D exhibit a diminished ability to enhance mitochondrial fusion capacity. For instance, in some cases exercise failed to induce MFN2 protein upregulation in T2D individuals, suggesting an attenuated mitochondrial plasticity in metabolic disorders (Hernández-Alvarez et al., 2010). This impaired fusion response, coupled with the upregulation of DRP1-mediated fission in T2D muscle, leads to fragmented, less efficient mitochondria, further exacerbating insulin resistance and metabolic dysfunction (Jheng et al., 2012). Finally trained athletes exhibit higher basal levels of FIS1 and OPA1 compared to individuals with T2D, even though T2D muscle displays increased mitochondrial fragmentation. This underscores the complexity of mitochondrial dynamics, as it extends beyond fusion and fission to include inner mitochondrial membrane remodeling and cristae organization (Djalalvandi and Scorrano, 2022; Houzelle et al., 2021).

Beyond mitochondrial fusion and fission, mitophagy - the selective degradation of damaged mitochondria via autophagy - plays a central role in exercise-induced mitochondrial quality control and cellular homeostasis (Pickles et al., 2018). However, exercise-induced mitophagy adaptations also appear to be muscle-specific. For instance, acute exercise increases mitophagy markers, such as Parkin and LC3b-II, in soleus muscle, whereas no such changes are observed in the myocardium, gastric muscle, or abdominal muscle (Yoo et al., 2019). This muscle-specific induction of mitophagy likely reflects differential mitochondrial stress exposure during exercise. During muscular contractions, mitochondria are exposed to increased energetic and oxidative stress, which may lead to mitochondrial depolarization and the accumulation of dysfunctional organelles (Oliveira and Hood, 2019) that require selective removal. In response, the loss of mitochondrial membrane potential stabilizes PINK1, which accumulates on the outer mitochondrial membrane and subsequently activates Parkin. Parkin ubiquitinates mitochondrial proteins, triggering their recruitment into autophagosomes and subsequent degradation via the lysosomal system (Pickles et al., 2018). In healthy individuals, a single exercise session induces transient increases in mitophagy, characterized by the lipidation of LC3 proteins, which promotes

autophagosome formation. However, the mechanism underlying exercise-induced mitophagy has not been fully elucidated. A rodent study showed that acute exercise-induced mitophagy was preceded by increased AMPK and unc-51 like autophagy activating kinase 1 (ULK1) activity (Laker et al., 2017). AMPK phosphorylates ULK1 at Ser^{555} initiating autophagosome formation. Simultaneously, AMPK phosphorylates mitochondrial fission factor (MFF), facilitating DRP1 recruitment to fragment mitochondria and mark them for degradation (Laker et al., 2017). Human studies of young non-obese healthy males indicated that exercise activates phosphorylation of ULK1 primarily through AMPK and mTOR in skeletal muscle (Møller et al., 2015; Schwalm et al., 2015). In T2D, the mitophagy response to acute exercise appears to remain intact, as indicated by increased ULK1 phosphorylation (Ser^{555}) and reduced inhibitory phosphorylation (Ser^{757}), alongside elevated SQSTM1 and activation of the transcription factor FoxO3a, which promotes autophagy gene expression (Kruse et al., 2017). Chronic exercise also enhances the muscle mitophagy machinery as part of its long-term quality control improvements. Endurance-trained individuals exhibit higher basal expression of mitophagy proteins compared to untrained counterparts. For instance, one study comparing physically active and sedentary men, found that regular exercise was associated with an ~80% higher protein content of FIS1 and significantly elevated Parkin levels, particularly in older trained individuals (Balan et al., 2019). However, the extent to which chronic exercise improves mitophagy in T2D remains uncertain. In a 12-week endurance exercise study, mitochondrial complex II increased without significant changes in mitophagy markers in T2D muscle (Brinkmann et al., 2017).

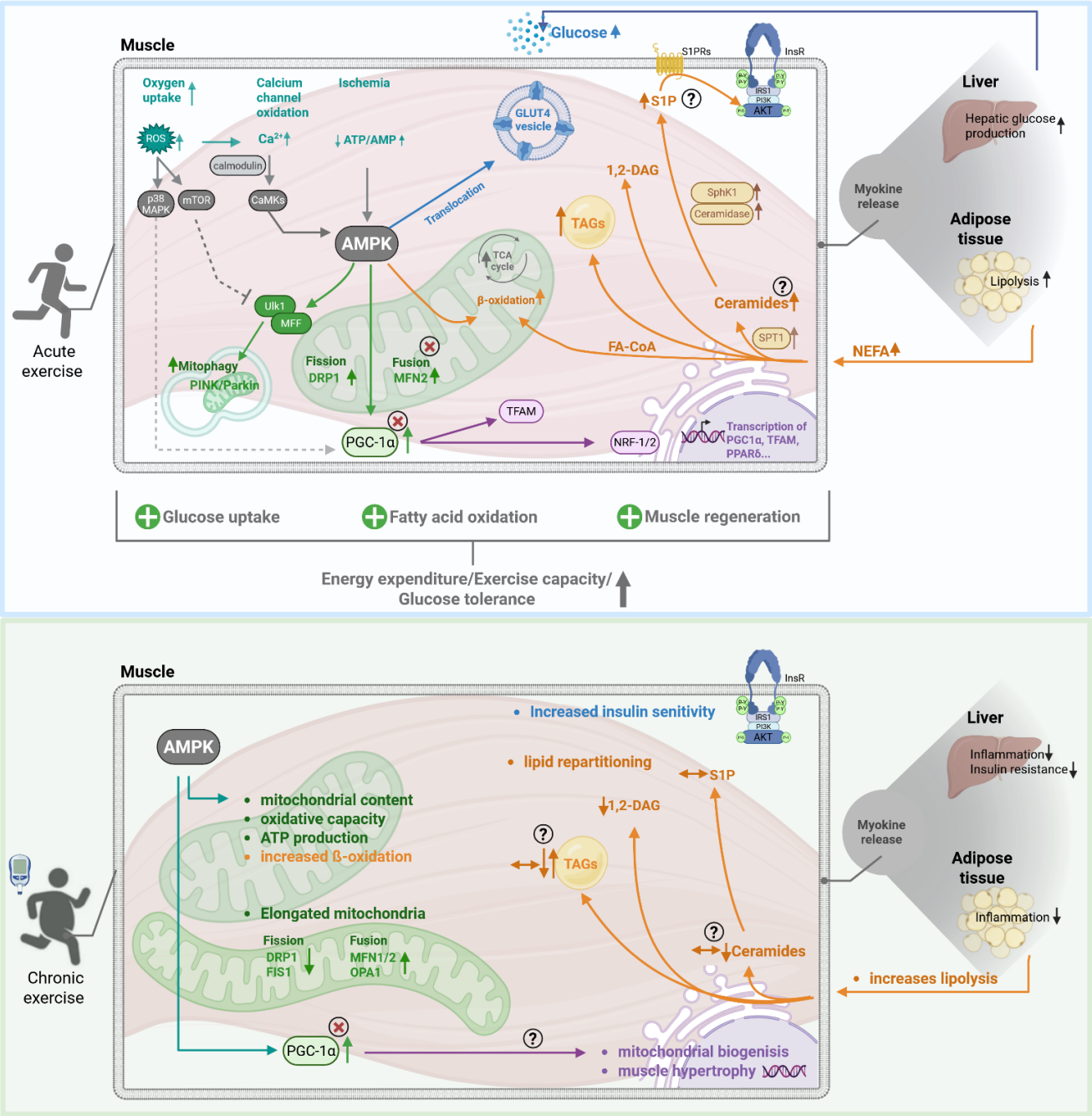

Figure 3: Acute and chronic exercise-induced adaptions in skeletal muscle and systemic metabolism in the context of T2D.

Acute exercise (top panel, blue background) increases reactive oxygen species (ROS), cytosolic calcium (Ca^{2+}), and the ATP/AMP ratio, thereby activating upstream kinases including p38 mitogen-activated protein kinase (p38 MAPK), the mechanistic target of rapamycin (mTOR), and calcium/calmodulin-dependent protein kinases (CaMKs), which converge on AMP-activated protein kinase (AMPK). AMPK orchestrates key adaptive processes by promoting mitophagy through mitochondrial fission factor (MFF) and unc-51-like autophagy activating kinase 1 (ULK1) along with the PTEN-induced kinase 1 (PINK1)/Parkin pathway. It further induces mitochondrial biogenesis via peroxisome proliferator-activated receptor gamma coactivator 1-alpha (PGC-1α), nuclear respiratory factors 1 and 2 (NRF-1/2), and mitochondrial transcription factor A (TFAM), and enhances glucose uptake through glucose transporter type 4 (GLUT4) translocation. Myokine release stimulates hepatic glucose production and adipose tissue lipolysis, raising circulating non-esterified fatty acids (NEFAs) and promoting intramyocellular lipid (IMCL) utilization, including triacylglycerols (TAGs), diacylglycerols (DAGs), and ceramides, the latter synthesized via serine palmitoyltransferase 1 (SPT1). Ceramide breakdown through ceramidase and SphK1 yields sphingosine-1-phosphate (S1P), which may improve

insulin sensitivity via sphingosine-1-phosphate receptor (S1PR) activation. Upward arrows indicate increased gene or protein expression, whereas red circled Xs mark blunted responses in T2D.

Chronic exercise (bottom panel, green background) leads to sustained metabolic improvements in individuals with T2D, including enhanced mitochondrial content, increased fatty acid oxidation (FAO), improved lipid repartitioning, and elevated insulin sensitivity. These adaptations, largely driven by persistent AMPK signaling, promote mitochondrial fusion (via mitofusin 1/2 [MFN1/2] and optic atrophy protein 1 [OPA1]), attenuate mitochondrial fission (via dynamin-related protein 1 [DRP1] and fission 1 protein [FIS1]), and result in an elongated and functionally efficient mitochondrial network. Chronic training also reduces the accumulation of lipotoxic lipid intermediates, thereby supporting systemic metabolic health in T2D. Circled question marks indicate mechanisms or responses for which the current literature presents conflicting or inconclusive findings. Figure created with BioRender.com.

Mitochondrial adaptations to exercise are essential for maintaining skeletal muscle energy homeostasis and overall metabolic health. While these responses are robust in normoglycemic individuals, those with T2D show more variable and often attenuated adaptations. The regulation of mitochondrial biogenesis, fusion, fission, and mitophagy is intricately linked to metabolic flexibility, and understanding these mechanisms may help optimize exercise interventions to improve metabolic health in both healthy individuals and those with T2D.

1.7 Hypotheses and objectives

Since ASM is involved in membrane remodeling and cellular stress responses, particularly in apoptosis, autophagy, and lipid metabolism, this dissertation explores its potential tissue-specific roles in skeletal muscle and liver. The first part focuses on skeletal muscle, aiming to investigate the regulation of ASM and its relationship to mitochondrial adaptations in response to a supervised HIIT program in individuals with varying degrees of insulin resistance and glucose tolerance. The second part addresses the liver, motivated by evidence that elevated ASM expression is associated with MASH in humans, while experimental downregulation in murine models reduces steatosis development during HFD. Building on this, the dissertation investigates the effects of ASM on hepatocellular viability and LD formation under conditions of metabolic stress, and further examines its consequences for insulin signaling.

The hypotheses tested in the first part of this dissertation are:

(i) Exercise increases ASM activity in skeletal muscle, influencing lipid metabolism, mitochondrial function, and insulin sensitivity.

(ii) ASM promotes plasma membrane remodeling in skeletal muscle, thereby supporting membrane repair and facilitating insulin signaling.

The hypotheses tested regarding the second part of this dissertation are:

(iii) Inhibition of ASM reduces the harmful effects of PA-induced lipotoxicity, thereby improving cell viability.

(iv) Inhibition of ASM preserves insulin signaling under PA-induced stress.

2 Material and Methods

2.1 Materials

2.1.1 Consumables and equipment

Table 1: Consumables

Name	Company
0.2 µm filter	Sartorius Lab instrument GmbH & Co. KG, Goettingen, Germany
Cell culture flasks (25 cm^2, 75 cm^2)	Sarstedt, Nümbrecht, Germany
Cell culture plates (6-; 12-; 24-; 96-wells)	Sarstedt, Nümbrecht, Germany
Centrifuge tubes (15 ml; 50 ml)	Greiner Bio-One, Kremsmünster, Austria
Immobilon-P Polyvinylidene difluoride (PVDF) Transfer Membrane	Millipore, Burlington, USA
MicroAmp Fast Optical 96-well Reaction Plate (qRT-PCR)	Applied Biosystems Inc, Waltham, Massachusetts, USA
MicroAmp Optical Adhesive Film (qRT-PCR)	Applied Biosystems Inc, Waltham, Massachusetts, USA
Mini-PROTEAN TGX Stain-Free Gels	BioRad Laboratories Inc., Hercules, California, USA
Pipette tips (10 µl; 20 µl; 100 µl; 200 µl; 1 ml)	Eppendorf, Hamburg, Germany Greiner Bio-One, Kremsmünster, Austria
Reaction tubes (0.5 ml; 1.5 ml; 2 ml; 5 ml)	Eppendorf, Hamburg, Germany
Serological pipets (5 ml; 10 ml, 25 ml; 50 ml)	Sarstedt, Nümbrecht, Germany
Syringe (1 ml; 5 ml; 10 ml)	B. Braun SE, Melsungen, Germany
Whatman paper	GE Healthcare Life Science, Chicago, USA

Table 2: Equipment

Name	Company
BBD 6220 incubator	Thermo Fisher Scientific, Waltham, Massachusetts, USA
Benchtop Centrifuge Z216 MK	Hermle Labortechnik, Wehingen, Germany
ChemiDoc XRS+ Imaging System	BioRad Laboratories Inc., Hercules, California, USA

Cytation™ 5 Cell Imaging Multi-Mode Reader	Agilent Technologies, Santa Clara, California, USA
Heating cabinet	Binder Labortechnik, Hebertshausen, Germany
HeraSafe KS 15 biological safety cabinet	Thermo Fisher Scientific, Waltham, USA
Infinite 200 Pro microplate reader	Tecan, Maennedorf, Switzerland
Megafuge ST4 Plus centrifuge	Thermo Fisher Scientific, Waltham, Massachusetts, USA
Mini-Protean Tetra System Gel Tank	BioRad Laboratories Inc., Hercules, California, USA
Neubauer chamber	Paul Marienfeld GmbH & Co. KG, Lauda-Königshofen, Germany
pH-Meter	Hanna Instruments Woonsocket, Rhode Island, USA
Pipets research plus	Eppendorf, Hamburg, Germany
PowerPac Basic Power supply	BioRad Laboratories Inc., Hercules, California, USA
Primovert microscope	Carl Zeiss AG, Oberkochen, Germany
Rocker 2D basic rocking shaker	IKA, Staufen, Germany
Stainless Steel Beads 5 mm	Qiagen, Hilden, Germany
SW 22 water bath	Julabo, Seelbach, Germany
Thermomixer compact	Eppendorf, Hamburg, Germany
TissueLyser II	Qiagen, Hilden, Germany
Trans-Blot Turbo Transfer System	BioRad Laboratories Inc., Hercules, California, USA
Vortex-Shaker VTX-3000L	Lab unlimited, Dublin, Ireland

2.1.2 Reagents and solutions

Table 3: Reagents and solutions

Name	Company
0,25% Trypsin EDTA (1x)	Gibco, Carlsbad, California
10x Tris/Glycine buffer (Transfer Buffer)	BioRad Laboratories Inc., Hercules, California, USA
10x Tris/Glycine/SDS buffer (Running Buffer)	BioRad Laboratories Inc., Hercules, California, USA

16% Formaldehyde (w/v), Methanol-free (PFA)	Thermo Fisher Scientific, Waltham, Massachusetts, USA
4x Laemmli sample buffer	BioRad Laboratories Inc., Hercules, California, USA
Albumin fraction V (pH 7.0)	AppliChem, Darmstadt, Germany
Blue Prestained Protein Standard, Broad Range (11-250 kDa)	New England BioLabs, Ipswich, USA
BODIPY™ 493/503 (4,4-Difluoro-1,3,5,7,8-Pentamethyl-4-Bora-3a,4a-Diaza-s-Indacen) Invitrogen™	Thermo Fisher Scientific, Waltham, Massachusetts, USA
Bovine Serum Albumin (BSA) Control for BSA-Fatty Acid Complexes (5 mM)	Cayman Chemical, Ann Arbor, Michigan, USA
BSA-Palmitate Saturated Fatty Acid Complex (5 mM)	Cayman Chemical, Ann Arbor, Michigan, USA
cOmplete-protease-inhibitor cocktail	Roche, Basel, Switzerland
D-(+)-Glucose	Sigma-Aldrich, St. Louis, Missouri, USA
Dimethylsulfoxid (DMSO)	Sigma-Aldrich, St. Louis, Missouri, USA
D-Mannitol	Sigma-Aldrich, St. Louis, Missouri, USA
Di-Phosphate-Buffered Saline (DPBS) (1x)	Gibco, Carlsbad, California
Eagle's Minimum Essential Medium (EMEM)	ATCC, Manassas, Virginia, USA
Ethanol absolute	VWR, Radnor PA, USA
Ethylenediaminetetraacetic acid (EDTA)	Sigma-Aldrich, St. Louis, Missouri, USA
Fetal Bovine Serum (FBS)	Merck, Darmstadt, Germany
HCl	Sigma-Aldrich, St. Louis, Missouri, USA
Hoechst Nucleic Acid Stains Invitrogen™	Thermo Fisher Scientific, Waltham, Massachusetts, USA
Immobilon Western Chemiluminescent HRP Substrate	Millipore, Burlington, USA
Insulin from bovine pancreas	Sigma-Aldrich, St. Louis, Missouri, USA
Isopropanol (2-Propanol)	Merck KGaA, Darmstadt, Germany
METAFECTENE® PRO	Biontex Laboratories GmbH, München, Germany
Methanol	Merck KGaA, Darmstadt, Germany
NaCl	Sigma-Aldrich, St. Louis, Missouri, USA
Nonidet® P40 (NP-40)	AppliChem, Darmstadt, Germany
Penicillin-Streptomycin (10.000 U/mL)	Gibco, Carlsbad, California

PhosStop phosphatase inhibitor cocktail	Roche, Basel, Switzerland
Powdered milk	Roth, Karlsruhe, Germany
Thiazolyl blue tetrazolium bromide (MTT), membrane-permeable dye	Abcam, Cambridge, UK
Tris ultrapure	AppliChem, Darmstadt, Germany
Tween20	Sigma-Aldrich, St. Louis, Missouri, USA
β-Mercaptoethanol	Sigma-Aldrich, St. Louis, USA

2.1.3 Buffers

Table 4: Buffers

Name	Component	Concentration
ASM activity assay buffer	NaCl Tris-HCl (pH 7.4) Triton X-100 protease inhibitor cocktail	150 mM 50 mM 0.6 % 1:25
Protein loading buffer	4x Laemmli Sample Buffer ß-Mercaptoethanol	90 % 10 %
Tris buffered saline Tween 20 (TBST)	Tris (pH 7.5) NaCl Tween20	20 mM 150 mM 0.1 %
Radioimmunoprecipitation assay (RIPA)-buffer	Tris-HCl (pH 7.4) NaCl EDTA NP-40 PhosStop phosphatase inhibitor cocktail cOmplete-protease-inhibitor cocktail	25 mM 150 mM 1 mM 0.2 % 1:10 1:25
SDS running buffer	10x Tris/Glycine/SDS buffer ddH_20	10 % 90 %
Western-Blot transfer buffer	10x Tris/Glycine buffer Methanol ddH_20	10 % 20 % 70 %

2.1.4 Protein standard and antibodies

Table 5: Protein standard for Western blot analysis

Name	Bands in kDa	Company
Blue Prestained Protein Standard, Broad Range (11-250 kDa)	250, 180, 130, 95, 72, 55, 43, 34, 26, 17, 11	New England BioLabs, Ipswich, USA

Table 6: Primary and secondary antibodies for Western blot analysis

Name	Dilution	Company
Anti-Akt rabbit #9272	1:1000 in 5 % BSA solution	Cell Signaling Technology, Danvers, USA
Anti-Phospho-Akt (Ser473) rabbit #9271	1:1000 in 5 % BSA solution	Cell Signaling Technology, Danvers, USA
Anti-IRS-2 rabbit #4502	1:1000 in 5 % BSA solution	Cell Signaling Technology, Danvers, USA
Anti-Phospho-IRS-2 (Ser388) rabbit 07-1517	1:500 in 5 % BSA solution	Merck KGaA, Darmstadt, Germany
Anti-Acid sphingomyelinase antibody [EPR23090-181] rabbit ab272729	1:1000 in 5 % milk solution	Abcam, Cambridge, UK
Secondary Anti-rabbit IgG, HRP-linked Antibody #7074	1:20000 in 5 % milk solution	Cell Signaling Technology, Danvers, USA

2.1.5 Primers and small interfering RNA (siRNA)

All primers were obtained from Qiagen (QuantiTect Primer Assays, 249900), with the corresponding GeneGlobe identification numbers listed in the table:

Table 7: Primers for qRT-PCR

Name	Company
B2M mouse (QT01149547)	Qiagen, Hilden, Germany
PPIA mouse (QT00247709)	Qiagen, Hilden, Germany
HPRT1 mouse (QT00166768)	Qiagen, Hilden, Germany
SMPD1 (ASM) mouse (QT00111041)	Qiagen, Hilden, Germany
ACTB2 human (QT01680476)	Qiagen, Hilden, Germany
SMPD1 (ASM) human (QT00111041)	Qiagen, Hilden, Germany

Table 8: siRNA for gene silencing

Name, Target	Sequenze	Company
Ambion™ Silencer™ Select Validated siRNA SMPD1 human (4427038)	5´->3´ Sense CUACCUACAUCGGCCUUAAtt Antisense UUAAGGCCGAUGUAGGUAGtt	Life Technologies, Carlsbad, California, USA

2.1.6 Kits

Table 9: Kits

Name	Company
Acid Sphingomyelinase Activity Assay Kit	Echelon Biosciences Inc. Salt Lake City, USA
MycoStrip™ 100 Mycoplasma Detection Kit	InvivoGen, Toulouse, France
Pierce™ BCA Protein Assay Kit	Thermo Fisher Scientific, Waltham, Massachusetts, USA
QuantiTect Reverse Transcription Kit	Qiagen, Hilden, Germany
QuantiTect SYBR Green PCR Kit	Qiagen, Hilden, Germany
RNeasy Mini Kit	Qiagen, Hilden, Germany

2.1.7 Cell lines and media

HepG2

Human hepatocellular carcinoma cells HepG2 [HB-8065 ™] were obtained from ATCC (Manassas, Virginia, USA).

Growth medium

Eagle's Minimum Essential Medium (EMEM) containing Earle's Balanced Salt Solution, non-essential amino acids, 2 mM L-glutamine, 1 mM sodium pyruvate, and 1500 mg/L sodium bicarbonate and supplemented with 10% (v/v) FBS and 1 % penicillin/streptomycin (P/S) was used to keep the cells in culture.

Starvation medium

Growth medium without FBS was used as starvation medium.

2.2 Methods

2.2.1 Mouse tissue sample acquisition

Mouse tissue samples used in this study were obtained from a separate study conducted previously by our group. Detailed methods regarding the acquisition, preparation, and initial processing of these samples are described before (Dewidar et al., 2023). In brief, diabetes was induced in male C57BL/6j mice by administering STZ, a compound known for its selective toxicity towards pancreatic β-cells, followed by 12-weeks of a regular chow (DIAB) or HFD (MASH), the latter causing diabetes-related MASH. The study included also mice fed only a regular chow (CON) or a HFD (OBES). For the purposes of this dissertation, these samples were used directly as provided.

2.2.2 Cell biological methods

2.2.2.1 Cultivation of the HepG2 cell line

From human hepatoblastoma cell line HepG2, cells were thawed from long-term storage following the recommended procedure of ATCC (Manassas, Virginia, USA). Cells were cultured in growth media in an incubator set at 5% CO_2 and 37 °C. Upon reaching approximately 80% confluency, cells were washed twice with prewarmed phosphate buffered saline (PBS), detached using 0.25% Trypsin EDTA, neutralized with growth medium, and transferred into new culture flasks at a 1:6 ratio. Prior to experiments, the cells underwent three passages. To prevent contamination, regular mycoplasma tests were conducted according to manufacturer's protocol (InvivoGen, Toulouse, France). Cryopreservation of HepG2 cell line was carried out using EMEM medium containing 20% FBS, 1 % P/S and 10% DMSO, (v/v).

2.2.2.2 Gene silencing with siRNA transfection of HepG2 cells

SMPD1 (ASM) gene silencing was achieved using siRNA (Life Technologies, Carlsbad, California, USA). METAFECTENE® PRO (Biontex Laboratories GmbH, München, Germany) was used as transfection reagent for the delivery of the siRNA into HepG2 cells, following manufacturer´s instructions. Various experimental approaches were tested and among those, the reverse transfection gave the highest knock-down rate. The transfection complex, consisting of transfection reagent and siRNA mixed in a ratio of 3:1 in growth media to achieve a final siRNA concentration

of 10 nm, was incubated at room temperature for 20 min before being added to the HepG2 cell suspension. The cells were then plated in dishes and 12 h later, the medium containing the transfection mixture was replaced with fresh growth medium. Samples were collected or assayed 72-96 h after transfection. The efficiency of gene knockdown was confirmed through western blot analysis and ASM enzymatic activity assay.

2.2.2.3 Treatment of HepG2

Cells were seeded in dishes with or without siRNA, and 12 h prior cell treatment, the medium was replaced by fresh starvation medium. Subsequently, either high-lipid or high-glucose load was simulated. PA, a common long-chain saturated fatty acid (C16:0) in Western diet (Burlingame et al., 2009), was complexed with bovine serum albumin (BSA) to create aqueous solutions for cell treatment. In this study, a commercially available 5 mM PA already coupled with BSA in NaCl was used, at a molar ratio of 6:1 which falls within the physiological condition range (Alsabeeh et al., 2018). The uncomplexed 5 mM BSA (Cayman Chemicals, Ann Arbor, Michigan, USA) was used as control. For high-glucose load, 1 M D-6-Glucose and 1 M Mannitol as osmotic control, both prepared in PBS, were utilized. The mentioned solutions were filtered using a 0.2 µM filter and prepared at the indicated concentrations in starvation media. The treatment solutions were added to the previously seeded HepG2 cells for indicated time periods. To assess insulin signaling, cells were stimulated with 10 nM insulin for 10 min following each treatment condition.

2.2.2.4 Assessment of cell viability

2.2.2.4.1 MTT assay

MTT cell viability assay was used to assess cell viability and proliferation, indirectly reflecting cell toxicity, following glucose treatment. HepG2 cells were plated in 96-well plates at a density of 1×10^4 cells/well and incubated in growth medium for 12 h. Subsequently, the medium was discarded and the cells received the treatments described in section 2.2.2.3 for different durations. At designated time points, the cells were rinsed with PBS once and then exposed to starvation medium containing 0.5 mg/mL MTT for 3 h. Following this incubation period, the medium was aspirated from each well and replaced with 100 µl DMSO. The plates were agitated on an orbital shaker for complete dissolution of the purple MTT formazan (1-(4,5-Dimethylthiazol-2-

yl)-3 ,5-diphenylformazan) and absorbance was measured at a wavelength of 590 nm in a plate reader system (Tecan infinite200Pro Software i-control). To obtain technical replicates and ensure reproducibility, each treatment condition was applied to three wells.

2.2.2.5 Cell staining with Hoechst and BODIPY

To investigate the impact of PA or high-glucose treatment on HepG2 cell metabolism, cell count and LD formation were evaluated by using Hoechst and BODIPY staining, respectively. Hoechst staining utilizes blue fluorescent dyes that become highly fluorescent when bound to DNA and that exhibit low toxicity in most types of cells. BODIPY (4,4-difluoro-1,3,5,7,8-pentamethyl-4-bora-3a,4a-diaza-s-indacene) was utilized for microscopy-based quantification of neutral lipid content. Following siRNA transfection (2.2.2.2) and/or experimental treatment (2.2.2.3), HepG2 cells were washed with warm PBS before applying a mixture containing Hoechst at a ratio of 1:5000 (4 µM) and BODIPY at a ratio of 1:2500 (2 µM) for 15 min in the dark at room temperature (RT). Subsequently staining solution was removed and the cells were fixed as described below. Analysis of cell count and LD formation was conducted with the Cytation™ 5 Cell Imaging Multi-Mode Reader, as described in the following section.

2.2.2.6 Fixation of HepG2 cells with paraformaldehyde

HepG2 cells were fixed to preserve their cytoskeleton and physiological state using 4 % warm paraformaldehyde (PFA). Following removal of the medium, the cells underwent two washes with warm PBS before being treated with pre-warmed 4 % PFA for a 20 min at RT. The PFA was then removed and the cells were washed three times with PBS.

2.2.2.7 Validation of cell count and lipid droplet formation

Fixed cells were captured using a 10 x objective lens of a Cytation™ 5 Cell Imaging Multi-Mode Reader, equipped with DAPI (377/447) and GFP (469/525) light cubes. The images, which include cell nuclei stained with Hoechst and LDs stained with BODIPY, underwent preprocessing and analysis, which involved generating primary and secondary masks to detect individual cell nuclei and calculate the average green fluorescence intensity surrounding each cell.

2.2.3 Biochemical methods

2.2.3.1 Protein concentration with bicinchoninic acid protein assay

The Pierce bicinchoninic acid (BCA) protein assay kit was used to assess protein concentration. Following the manufacturer's guidelines, protein concentrations were calculated using a standard curve of BSA. The absorbance of a series of known BSA solutions was plotted against their concentrations, and the concentration of each unknown sample was determined based on this standard curve.

2.2.3.2 Lysis of HepG2 cells

After removing cell media from cells and washing them with cold PBS, the cells were scraped and collected in centrifuge tubes followed by centrifugation at 2.000 x g for 5 min. After discarding the supernatant, radioimmunoprecipitation assay (RIPA) lysis buffer or ASM activity assay buffer was added to the pellet. Subsequently cells were placed on ice for 30 min and vortexed every 10 min. Finally, the cells suspension was centrifuged at 16.000 x g for 15 min at 4 °C, and the supernatant was transferred to a new tube for assessment of protein concentration. The lysate was then stored at -80 °C till further analysis.

2.2.3.3 Lysis of tissue

Tissue lysis requires vigorous mechanical homogenization. The frozen tissue was placed in a reaction tube and a 5 mm stainless bead was added together with RIPA buffer (approximately 300 µl of RIPA buffer for 20-30 mg of liver or skeletal muscle tissue). Tissues were homogenized with a TissueLyser 2 times 1 min at 25 Hz or until the tissue was disrupted. The resulting homogenate was centrifugated at 16.000 x g at 4 °C for 15 min. Next, the supernatant was transferred to a new tube and the protein concentration was determined using a BCA protein assay kit. Finally, the lysate was stored at -80°C for further analysis.

2.2.3.4 SDS-PAGE and Western blot analysis

Expression of proteins of interest was assessed by SDS-PAGE and Western-Blot.
For the separation of proteins extracted from HepG2 or tissues, protein lysate was heated at 95 °C for 5 min before being loaded onto 4–20 % gradient Mini-PROTEAN TGX Stain-Free precast gels. The gel was electrophoresed in a pre-made SDS running buffer (2.1.3) until the dye reached the bottom. For visualizing total protein, Mini-

PROTEAN TGX Stain-Free precast gels were activated using a ChemiDoc™ imager. Using a semi-dry blotting and Tris-glycine-methanol transfer buffer (2.1.3), proteins were transferred from the SDS-PAGE gel to a methanol activated polyvinylidene difluoride (PVDF) membrane via Trans-Blot Turbo Transfer System. After transfer, the membranes were UV activated for 1 min, allowing the visualization of total protein content on the membrane. Membranes were then blocked with 5 % milk in Tris buffered saline Tween 20 (TBST), followed by an incubation with primary antibody at 4 °C over night and with horseradish peroxidase (HRP)-conjugated secondary antibodies for 2 h at RT. The protein of interest was visualized with Bio-Rad ChemiDocTM MP Imaging System through chemiluminescence produced by the peroxide reagent and Luminol enhancer reagent. Finally, densitometric analysis was performed with the software ImageLab 6.0.1 (Bio-Rad 199 Laboratories). Protein expression was normalized to GAPDH or total protein, and an inter-run calibrator (IRC) was included on each gel to correct for run-to-run variation.

2.2.3.5 ASM activity assay

ASM enzymatic activity was measured using the ASM activity assay kit (Echelon Bioscience, Salt Lake City, UT) in accordance with the manufacturer's instructions. Frozen skeletal muscle tissue samples (15-25 mg) were homogenized in eight times their volume of cold ASM activity assay buffer (2.1.3). For thorough lysis, 2 mm glass beads (Sigma-Aldrich) were employed in conjunction with a Tissue Lyser (3 times 1 min at 20 Hz). For HepG2 cells, the cells were scraped in cold PBS and transferred to a reaction tube. Following centrifugation at 600 x g, the PBS was removed and the resulting cell pellet was dissolved in ASM activity assay buffer (2.1.3), approximately 20-50 µl depending on the size of the cell pellet. Tissue and cell lysate were centrifuged at 10.000 x g for 10 min at 4 °C to remove debris, and 15-20 µg of total protein was used to assess ASM activity according to the manufacturer's protocol. Fluorescence was measured using a fluorescence plate reader (Tecan Infinite 200Pro, Software i-control) at 360 nm excitation and 460 nm emission. ASM activity was normalized to total protein content, which was quantified using the BCA protein assay kit (2.2.3.1).

2.2.4 Molecular biological methods

2.2.4.1 RNA isolation

The Qiagen RNeasy Mini Kit was utilized to extract total RNA from HepG2 cells and animal tissues, according to the manufacturer's instructions. Briefly, samples were lysed and homogenized in a denaturing guanidine-thiocyanate–containing buffer to deactivate RNAses for intact RNA purification. Ethanol was added for proper binding conditions, and then the sample was applied to a RNeasy Mini spin column where total RNA binds to the membrane while contaminants are washed away efficiently. The high-quality RNA was eluted in RNase-free water. The concentration of isolated RNA was measured using a Tecan Plate reader and NanoQuant Plate™ at 260 nm with a 280 nm ratio allowing to determine RNA quality. Finally, the isolated RNA was stored at -80 °C until further use.

2.2.4.2 cDNA synthesis

The cDNA QuantiTect Reverse Transcription Kit was utilized to convert RNA to cDNA following the manufacturer's guidelines. After removal of genomic DNA, the RNA sample undergoes reverse transcription using a mix containing Quantiscript Reverse Transcriptase, Quantiscript RT Buffer, and RT Primer Mix. The process occurs at 42°C, followed by an inactivation step at 95°C. This yields complementary DNA (cDNA) from an RNA template through reverse transcription, which can then be directly used as template for quantitative Real-Time Polymerase Chain Reaction (qRT-PCR).

2.2.4.3 Quantitative qRT-PCR

The obtained cDNA (2.2.4.2) was employed to assess the efficiency of ASM silencing in HepG2 cells and to examine *SMPD1*/*ASM* transcription levels in mouse skeletal muscle and liver using qRT-PCR. The amount of cDNA present in the samples, which undergoes exponential amplification via RT-PCR, was measured through fluorescence signal. To achieve this, the QuantiTect SYBR Green PCR Kit (Qiagen, Hilden, Germany) were utilized, following the manufacturer`s protocol. The reactions were performed in triplicates for each sample, and three reference genes (housekeeping genes) were used for tissue analysis, whereas one housekeeping gene was used for HepG2 cell analysis. Additionally, an inter-run calibrator (IRC) was present on each plate and afterwards used as calibrator. For qRT-PCR, a 10 µl total volume reaction mixture was prepared as follows:

Table 10: qRT-PCR reaction mix

Substance	µl
SYBR Green	5
Primer mix (Qiagen)	1
cDNA (5ng/µl)	1-3
Nuclease-free H_2O	Add x µl
∑	10

The individual phases of the qRT-PCR cycle, which occur at different times and temperatures in the thermocycler, are listed in the following table.

Table 11: qRT-PCR cycling conditions

Temperature	Time	
95 °C	15:00 min	
94 °C	00:15 min	40 times
55 °C	00:30 min	
72 °C	00:30 min	
95 °C	00:15 min	
55 °C	01:00 min	
+0,3 °C until 95 °C		

2.2.4.4 Relative analysis of mRNA levels

The qRT-PCR data were evaluated using the double delta Ct analysis (ΔΔCt) (Livak and Schmittgen, 2001; Schmittgen and Livak, 2008). After normalization of Ct values of the gene of interest with the reference genes, the normalized results were scaled to the IRC, to obtain the expression fold change of each sample relative to the IRC, as described below:

- ΔCt = Ct(gene of interest)- Ct(geometric mean of all reference genes)
- ΔΔCt = ΔCt(sample) - ΔCt(IRC)
- 2-ΔΔCt

Calibrated normalized relative quantities (CNRQ values) were used for statistical analysis.

2.2.5 Statistical analysis and programs

Statistical analyses for the published clinical study embedded in this thesis (chapter 3.1) were conducted in collaboration with a professional statistician to ensure

methodological robustness. The statistical methods applied in that section are detailed within the respective publication and its figure legends.

For the experimental studies conducted within this thesis, statistical analyses were performed using GraphPad Prism (version 10.4.1). The statistical approaches used for the unpublished experimental data presented in this thesis were independently reviewed by a professional statistician to verify the appropriateness of the selected statistical models and tests. The analyses themselves, however, were conducted exclusively by the author of this thesis. Data are presented as mean ± standard deviation (SD). Comparisons between two groups were conducted using unpaired two-tailed Student's t-tests. For experiments involving multiple groups or repeated measures (e.g., time points or treatment conditions), one-way or two-way ANOVA was applied, followed by Tukey's, Dunnett's or Šidák's multiple comparison tests as appropriate. Correlation analyses were conducted using Pearson's correlation coefficient. A p-value <0.05 was considered statistically significant. All *in vitro* experiments were independently replicated at least three times unless otherwise noted. Heatmaps were generated in R-Studio (version 2024.12.1+563). During the final editing phase, language-editing software (ChatGPT, OpenAI, GPT-5 version) was used only for minor grammatical adjustments. The author takes full and sole responsibility for all unpublished data analyses, interpretations, and the entire written content of this thesis.

3 Results

This thesis integrates findings from two complementary experimental approaches to elucidate the role of ASM in metabolic regulation. The first part presents data from a clinical study investigating ASM protein and activity levels and its associations with mitochondrial quality control in human skeletal muscle following exercise training in men with T2D. The second part comprises mechanistic experiments in murine and cellular models designed to explore the tissue-specific function of ASM under metabolic stress conditions.

3.1 Publication: "Exercise training increases skeletal muscle sphingomyelinases and affects mitochondrial quality control in men with type 2 diabetes"

(Hendlinger et al., 2025)

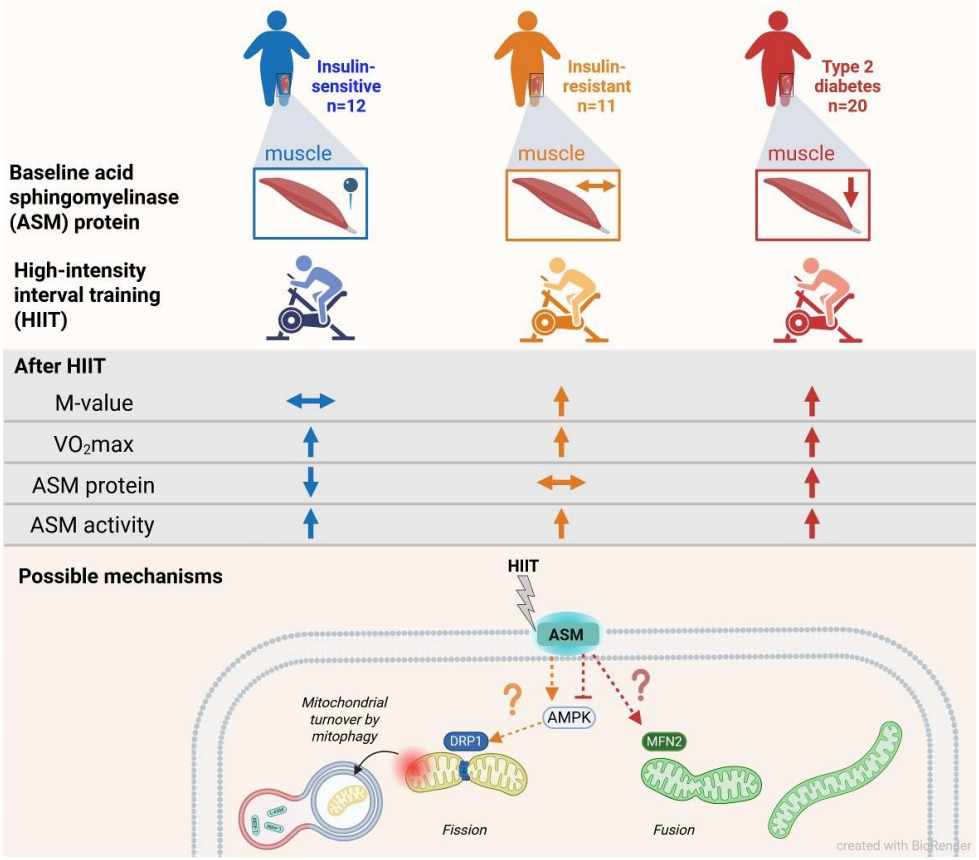

Graphical abstract of published data from the first part of this thesis.

Metabolism 172 (2025) 156361

Contents lists available at ScienceDirect

Metabolism

journal homepage: www.journals.elsevier.com/metabolism

Exercise training increases skeletal muscle sphingomyelinases and affects mitochondrial quality control in men with type 2 diabetes

Mona Hendlinger [a], Lucia Mastrototaro [a,b], Marten Exterkate [g], Maria Apostolopoulou [a,c], Yanislava Karusheva [a,b], Geronimo Heilmann [a,b], Polina Lipaeva [a,b,c,d], Klaus Straßburger [b,e], Sofiya Gancheva [a,c,f], Sabine Kahl [a,b,c], Michael Roden [c,a,b,*]

[a] Institute for Clinical Diabetology, German Diabetes Center, Leibniz Center for Diabetes Research at Heinrich Heine University Düsseldorf, Germany
[b] German Center for Diabetes Research, Partner Düsseldorf, München-Neuherberg, Germany
[c] Department of Endocrinology and Diabetology, Medical Faculty and University Hospital Düsseldorf, Heinrich Heine University Düsseldorf, Düsseldorf, Germany
[d] Institute for Medical Biometry and Bioinformatics, Medical Faculty and University Hospital, Heinrich Heine University, Düsseldorf, Germany
[e] Institute for Biometrics and Epidemiology, German Diabetes Center, Leibniz Center for Diabetes Research at Heinrich Heine University Düsseldorf, Düsseldorf, Germany
[f] Departamento de Nutrición, Diabetes y Metabolismo, Escuela de Medicina, Pontificia Universidad Católica, Santiago, Chile
[g] Department of Membrane Biogenesis and Lipidomics, Institute of Biochemistry, Heinrich Heine University Düsseldorf, Düsseldorf, Germany

ARTICLE INFO

Keywords:
Type 2 diabetes
Insulin resistance
High-intensity interval training
Sphingomyelinases
Ceramides
Mitochondrial quality control

ABSTRACT

Lipotoxic ceramides (CERs) are implicated in the development of insulin resistance, type 2 diabetes (T2D) and related complications. Exercise training improves insulin sensitivity, potentially via reducing intracellular lipids or enhancing mitochondrial oxidation. Acid sphingomyelinase (ASM), which hydrolyzes sphingomyelin (SM) to CERs, is crucial for muscle repair and development, yet its role in insulin-resistant states and response to exercise remain unclear.

We assessed ASM protein and activity, neutral sphingomyelinase (NSM) and sphingolipid species in skeletal muscle of insulin-sensitive (IS, $n = 12$), insulin-resistant (IR, $n = 11$) and T2D men ($n = 20$), before and after a 12-week high-intensity interval training (HIIT). Comprehensive phenotyping comprised hyperinsulinemic-euglycemic clamps, spiroergometry, targeted lipidomics and assessment of markers of mitochondrial quality control.

ASM protein was lower at baseline and increased after HIIT only in T2D ($p < 0.05$), while ASM activity rose across all groups (IS $p < 0.01$; IR and T2D $p < 0.001$). HIIT also increased NSM protein in all groups ($p < 0.05$). Despite lower baseline SM levels in T2D, HIIT led to elevated CERs species in T2D (C16:0, C20:0, C22:0, C24:1, C24:0) and in IR (C16:0, C20:0) (all $p < 0.05$). Regression analysis suggested that changes in ASM protein and activity relate to changes in mitochondrial fusion and fission as well as AMP-activated protein kinase (AMPK)-mediated mitophagy.

In conclusion, HIIT induces expression of both ASM and NSM and alters CER profiles in insulin-resistant skeletal muscle, independently of changes in insulin sensitivity. ASM could therefore rather contribute to exercise-induced mitochondrial remodeling than driving lipotoxicity, warranting further investigation of ASM as a potential target for exercise mimetic therapies.

1. Introduction

According to the most recent edition of the IDF atlas, type 2 diabetes mellitus (T2D), affects more than 580 million people worldwide and its prevalence continues to rise, mainly due to hypercaloric sedentary lifestyle [1]. Insulin resistance is a typical feature of T2D, which results from adipose tissue dysfunction, altered lipid handling and ectopic accumulation of bioactive lipid species, such as diacylglycerols (DAGs) and ceramides (CERs), in insulin-responsive tissues including liver and skeletal muscle [2]. CERs accumulation has been observed in some [3,4], but not in other studies of insulin-resistant muscle [5,6], raising the question of the role of certain CER species in muscle [7]. CERs are generated via (i) de novo synthesis from saturated fatty acids, (ii) lysosomal salvage catalyzed by acid sphingomyelinase (ASM), also termed sphingomyelin phosphodiesterase 1 (SMPD1) and

* Corresponding author at: German Diabetes Center at Heinrich Heine University Düsseldorf, Auf`m Hennekamp 65, 40225 Düsseldorf, Germany.
E-mail address: michael.roden@ddz.de (M. Roden).

https://doi.org/10.1016/j.metabol.2025.156361
Received 29 December 2024; Accepted 30 July 2025
Available online 5 August 2025
0026-0495/

Abbreviations

ASM	acid sphingomylinase
AMPK	AMP-activated protein kinase
BMI	body mass index
BSL	baseline
CER	ceramide
DAG	diacylglycerol
DRP1	dynamin-related protein 1
HbA1c	hemoglobin A1c
HIIT	high-intensity interval training
IRS1	insulin receptor substrate 1
IS	insulin-sensitive
IR	insulin-resistant
LD	lipid droplet
MFN	mitofusin
NSM	neutral sphingomyelinase
OPA1	optic atrophy 1
PKB/AKT	protein kinase B
PINK	PTEN-induced kinase
ROS	reactive oxygen species
SM	sphingomyelin
SMPD	sphingomyelin phosphodiesterase
T2D	Type 2 diabetes mellitus
VDAC	voltage-dependent anion channel

predominantly via the sphingomyelin (SM) pathway catalyzed by ASM and neutral sphingomyelinase (NSM; *SMPD3/4*) [8].

ASM protein content was found to be lower in skeletal muscle of sedentary insulin-resistant individuals [9], possibly reflecting impaired membrane remodeling, while elevated ASM activity could drive CER buildup [4,10]. In line, animal models showed divergent ASM patterns with increased activity in cardiac muscle during high-fat diet [10], but unchanged or reduced activity in diabetic skeletal muscle [11]. NSM activity was also found to be elevated in skeletal muscle of insulin-resistant humans, which leads to lower SM content [4,12]. These enzymatic alterations may enhance accumulation of CERs, which has been linked to mitochondrial stress, reflected by impaired oxidative phosphorylation along with increased reactive oxygen species (ROS) production and mitochondrial fragmentation [7]. This further suggests abnormal mitochondrial quality control, which comprises mitochondrial fusion, fission, biogenesis and mitophagy and relates to insulin resistance and T2D [13].

Exercise training represents one important strategy for the management of T2D [14,15], by increasing skeletal muscle glucose uptake and mitochondrial biogenesis, repartitioning intramyocellular lipids and ultimately improving insulin resistance [16–19]. Exercise training decreases both DAGs and CERs in skeletal muscle of insulin-resistant individuals [20–22], although individual CERs species show heterogeneous and compartment-specific responses depending on exercise mode [23,24]. Skeletal muscle SMs also respond differently to exercise with lower baseline, but higher post-exercise levels in trained individuals [25] and variable levels in sedentary prediabetic and T2D individuals after endurance training [12,26]. Exercise training may also affect sphingolipid-metabolizing enzymes. While data from humans are limited, rodent studies suggest acute exercise increases in ASM protein [27] and variable effects on ASM activity [28,29]. Finally, elevated NSM transcript and activity levels remain unchanged in athletes and sedentary humans [25,30]. Of note, modifications in lipid composition will likely affect mitochondrial functionality and quality control, which are improved by acute and chronic exercise, as demonstrated by increased mitofusin (MFN) expression, autophagy markers and mitophagy-related signaling pathways in skeletal muscle [31–33].

However, the effects of supervised effective exercise programs on skeletal muscle ASM, NSM, sphingolipids and their relationship to mitochondria in human with different degrees of insulin resistance and glucose tolerance are yet unknown. We hypothesized that (i) ASM expression differs among individuals with and without T2D and increases upon high-intensity interval training (HIIT) and that (ii) any ASM-mediated changes in CERs species would depend on muscle mitochondrial oxidative capacity. Thus, we investigated skeletal muscle ASM protein levels and activity as well as CER contents in persons without and with T2D, at baseline and after 12-week HIIT, the currently most efficient exercise mode to improve cardiorespiratory fitness (VO_2max), whole-body insulin sensitivity, body composition and mitochondrial function [34–36].

2. Material and methods

2.1. Study participants

The screening procedure, inclusion and exclusion criteria for the clinical study have been reported in detail before [36,37]. Of the 116 individuals initially screened, 67 were excluded due to predefined criteria. Individuals were excluded if they engaged in regular endurance training exceeding 60 min weekly, had known cardiovascular, renal or hepatic disease, were taking insulin-sensitizing agents or beta-blockers, consumed more than 30 g of alcohol per day or were current smokers. Additional 6 individuals were excluded due to time constraints for study completion. The study recruited only Caucasian men aged 50–60 years, of whom most featured overweight or class I obesity, although body mass index (BMI) was not a predefined matching criterion [37]. An a priori sample size calculation was performed based on data from a previous study of our research group [38], aiming to detect a 20 % relative change in M-value with a statistical power of 80 % and a cut off of $p < 0.05$. To account for multiple comparisons, the significance threshold was adjusted to $p < 0.025$ using the Bonferroni correction. Thus, the final cohort comprised 20 T2D and 23 glucose-tolerant men, the latter were subdivided into insulin-sensitive (IS, $n = 12$) and insulin-resistant (IR, $n = 11$) individuals (Table S1), based on clamp-derived whole-body insulin sensitivity (M-value), with values <5.5 mg kg^{-1} min^{-1} indicating insulin resistance [36,37]. The original individual data on M-values at baseline and after HIIT have been already reported [36]. Additionally, IS and IR participants showed no evidence of impaired fasting glucose or impaired glucose tolerance during the 75-g oral glucose tolerance test (oGTT), and none reported a family history of T2D. Among participants with T2D, 3 were drug-naive, while 9 were on metformin, 2 on sulfonylureas, 5 on metformin/DPP-4 inhibitor combination and 1 on a metformin/basal insulin combination therapy. They all refrained from drug intake for 3 days prior to metabolic tests to exclude their acute effects [39]. All participants gave written informed consent prior inclusion into the clinical study, which was approved by the institutional review board of the Medical Faculty of Heinrich Heine University Düsseldorf and registered on ClinicalTrials.gov with registration number NCT02039934. This study is a secondary analysis based on the previously published observations of changes in both insulin sensitivity and mitochondrial functionality and quality control [36,37].

2.2. Study protocol

The supervised HIIT protocol clinical study was performed at the German Diabetes Center (Deutsches Diabetes-Zentrum, DDZ) on a cycle ergometer, 3 times weekly, but not on consecutive days, for a total of 12 weeks as described [36]. Briefly, each supervised HIIT training session

lasted 35 min, comprising four 4-minute high-intensity intervals at 90 % of participants' baseline spiroergometry-determined maximal heart rate prior to inclusion in the study (HRm). These were alternated with three 3-minute intervals at 70 % of participants' HRm. Body weight stability was confirmed by monthly monitoring. Before (at baseline, BSL) and after 12 weeks of HIIT (HIIT), all participants underwent blood sampling, skeletal muscle biopsies (m. vastus lateralis), cardiometabolic tests and quantification of liver lipid content by ^{1}H-magnetic resonance spectroscopy [36]. Hyperinsulinemic-normoglycemic clamp tests were performed at 72 h after the final HIIT session to exclude acute effects of HIIT. Any glucose-lowering medication was discontinued for 72 h prior to the studies to exclude their acute metabolic effects.

2.3. Cardiometabolic tests

Spiroergometry was performed to obtain maximal oxygen uptake (VO_2max) by using an electronically-braked ergometer (Ergoline ergometrics 900, Bitz, Germany) [36]. Two-step hyperinsulinemic [insulin dose: 20 mU and 40 mU/(m^2 body surface area*min)]-euglycemic (target blood glucose: 5 mmol/l) clamp tests were performed to measure M-values [36].

2.4. Skeletal muscle biopsy

On the day of the clamp test, biopsies were obtained from the m. vastus lateralis directly prior to the initiation of the insulin infusion [5]. Briefly, the respective thigh region was anaesthetized (Lidocain 2 %, B. Braun, Melsungen, Germany) and 100–500 mg of muscle tissue were taken with a Bergstrom needle, immediately snap frozen in liquid nitrogen, split into ~50 mg aliquots and stored at −80 °C until further analysis.

2.5. Targeted sphingolipid analysis

Skeletal muscle biopsies (30–50 mg) were homogenized and fractionated into lipid droplet, cytosolic, and crude membrane fractions for separate analyses of CERs and SMs. CER concentrations were quantified by liquid chromatography with tandem mass spectrometry (LC-MS/MS) as described [40]. In an independent set of homogenized and fractionated muscle samples (30–50 mg), SMs were extracted using *n*-butanol-based phase separation and redissolved in 250 µl of methanol. Subsequent analysis quantified by LC-MS/MS was based on a previously developed method [41] with the following changes. Separation of the compounds was achieved by a changing gradient of eluent A (5 mM ammonium formate in water/acetonitrile 40:60, *v*/v) and eluent B (5 mM ammonium formate in acetonitrile/2-propanol, 10:90, v/v). The following linear gradient was applied: (i) 51 % eluent B for 3.0 min, (ii) a gradient from 51 % to 90 % eluent B over 16.0 min, (iii) holding for 3 min, (iv) returning to 51 % eluent B in 0.5 min, (v) and holding for 7.5 min. The column effluent was injected directly into a Thermo Q Exactive Plus (Thermo Fisher Scientific, Waltham, MA, USA) operating in positive ion mode: Spray Voltage: 3.20 kV, Capillary temperature: 230 °C, S-lens RF level: 50.0, sheath gas flow: 30, auxiliary gas flow: 5. Spectral data constituting total ion counts were analyzed using the MacCoss Lab Software Skyline (open-source MacCoss Lab, University of Washington, Seattle, WA, USA). The following transition settings were used: Scan range: 133.4–2000 *m/z*, MS1 filtering: Orbitrap, resolving power 70,000 at *m/z* 400. Total ion counts for extracted lipid species: SM_16:0 (*m/z* 703.575 $[M + H]^+$), SM_18:0 (*m/z* 731.606 $[M + H]^+$), SM_18:1 (*m/z* 729.591 $[M + H]^+$), SM_20:0 (*m/z* 759.638 $[M + H]^+$), SM_22:0 (*m/z* 787.669 $[M + H]^+$), SM_24:0 (*m/z* 815.700 $[M + H]^+$), SM_24:1 (*m/z* 813.684 $[M + H]^+$), were normalized for the internal standard DDM (*m/z* 528.338 $[M + NH_4]^+$), tissue wet weight (*Ww*), and quantified via the SPLASH™ LIPIDOMIX™ Mass Spec Standard Avanti Polar Lipids (Avanti Research, Alabaster, AL, USA). Total CER and SM contents were calculated as the sum of all detected species across subcellular fractions.

2.6. Western blotting

Skeletal muscle expression levels of proteins of interest were assessed by Western blotting as described [36]. Freshly lysed samples (25–50 mg snap-frozen tissue) were homogenized in 10 times (*w/v*) (250–500 µl per sample) of lysis buffer [25 mM Tris-HCl, 1 mM EDTA, 150 mM NaCl, and 0.20 % NP-40] supplemented with protease (cOmplete Tablets, EASYpack, Roche Diagnostics) and phosphatase (PhosSTOP, EASYpack, Roche Diagnostics) inhibitors to extract total soluble proteins. Homogenization was performed using a Tissue Lyzer (20 Hz, 1 min, three cycles), followed by centrifugation (13.000 rpm, 15 min, 4 °C) to remove insoluble material, including nuclei and unbroken cellular membranes. Proteins were transferred on polyvinylidene difluoride (PVDF) membranes from Millipore (Burlington, MA, USA), which were incubated overnight at 4 °C with freshly prepared primary antibodies diluted in Tris-buffered saline with Tween 20 (TBST) containing 5 % (*w/v*) non fat dry milk or bovine serum albumin (BSA), as recommended by the supplier (Table S2). Following incubation with primary antibodies, membranes were incubated for 2 h at room temperature with secondary antibodies freshly diluted in 5 % non-fat dry milk in TBST (Table S2), followed by protein detection with Immobilon Western Chemiluminescent horseradish peroxidase (HRP) Substrate (Millipore, Burlington, MA, USA) by using a Bio-Rad ChemiDocTM MP Imaging System in combination with the software ImageLab 6.0.1 (Bio-Rad Laboratories, Hercules, CA, USA) for densitometric analysis. Data are expressed in arbitrary units (A.U.) and normalized either to glyceraldehyde-3-phosphate dehydrogenase (GAPDH) or total protein content. To confirm the suitability of GAPDH for normalization, we verified that the protein abundance of GAPDH does not differ significantly between IS, IR and T2D groups at BSL or HIIT. For analysis and comparison of the protein expression on different gels, an inter-run calibrator (IRC) was loaded as reference sample on each gel to correct for run-to-run variation [42].

2.7. Acid sphingomyelinase (ASM) activity

ASM activity was measured by using the Echelon Bioscience assay kit (Salt Lake City, UT, USA) according to the manufacturer's instructions. An aliquot of 15–25 mg of frozen skeletal muscle tissue was homogenized 3-times for 1 min each at 20 Hz in 8-times the volume of cold lysis buffer (150 mM NaCl; 50 mM Tris-HCl (pH 7,4); 0,6 % Triton X-100; 1:25 protease inhibitor cocktail (cOmplete Tablets, EASYpack, Roche Diagnostics, Basel, Switzerland) with a Tissue Lyzer II (Qiagen, Hilden, Germany). Following debris removal by centrifugation (10.000*g*, 10 min, 4 °C), 15–20 µg of total protein were used to assess ASM activity. Immediately following sample preparation, the samples (BSL, HIIT) were processed using kits with the same lot number and analyzed simultaneously, using 96-well plates included in the kits, alongside with the provided standards. Fluorescence was measured in technical duplicates by fluorescence plate reader (Tecan infinite 200Pro Software i-control; Männedorf, Switzerland) at 360/460 nm excitation/emission. Data on ASM activity was normalized to protein content (µg), which was quantified using the bicinchoninic acid assay kit (Thermo Fisher Scientific, Waltham, MA, USA). Intra-assay CVs was less than 10 % for BSL and HIIT samples.

2.8. Statistical analysis

Data are given as mean and standard deviation (SD) or median (1st and 3rd quartile), as appropriate. All variables except age, BMI and hemoglobin A1c (HbA1c) were log-transformed before analysis. Mixed models for repeated measurements stratified by groups were applied in order to investigate changes between BSL and HIIT. To analyze between-group differences, generalized ANOVA was performed where residual variances were separately modelled in each group. We used linear regression analysis stratified by groups to investigate associations

between changes in ASM protein and ASM enzymatic activity as well as NSM protein with various metabolic and molecular parameters. These included changes in liver lipid content, M-value, VO_2max and biomarkers of insulin signaling, mitochondrial dynamics and mitophagy markers as well as sphingolipids (SMs and CERs). *P*-values from two-sided tests <5 % were considered to indicate significant differences. No formal correction for multiple comparisons was applied due to the biological interdependence of variables. Therefore, findings should be interpreted as exploratory and hypothesis-generating. All analysis were performed using SAS version 9.4 (SAS Institute, Cary, NC, USA) and graphs were plotted using GraphPad Prism 9.2 (GraphPad Software Inc., La Jolla, CA, USA). R package ComplexHeatmap version 2.16.0 was used to build heatmaps.

3. Results

3.1. Participants' characteristics at baseline and after HIIT

The anthropometric and clinical laboratory data have been previously reported [36,37]. Briefly, IS had comparable age, slightly lower BMI, but higher M-value than IR and T2D groups at BSL (Table S1). As expected, HbA1c was higher in T2D than in IR and IS groups. VO_2max was lower only in T2D compared to IS. Upon HIIT, VO_2max increased uniformly across all groups, while M-value increased only in IR and T2D (Table S1) [36,37]. For the present analyses, we calculated the exercise-induced changes within each group and compared the differences (Δ-values) between HIIT and BSL. The change of M-value from BSL to HIIT (ΔM-value) was higher in both insulin-resistant groups (IR and T2D) than in the IS group (Fig. 1A). VO_2max increased in 98 % of participants following HIIT, with greater changes (ΔVO_2max) in T2D compared to IR (Fig. 1B). These results indicate that insulin-resistant individuals may benefit more from HIIT in terms of cardiometabolic variables than insulin-sensitive individuals.

3.2. ASM activity and NSM protein rise after HIIT independently of insulin sensitivity

We next examined skeletal muscle ASM protein and activity as well as NSM protein in IS, IR and T2D group. At BSL, ASM protein levels (in arbitrary units, A.U.) were higher in both IS (1.08 ± 0.6) and IR (1.37 ± 1.1) participants than in T2D (0.62 ± 0.53, for both $p < 0.01$) (Fig. 1C). Following HIIT, ASM protein levels increased in T2D (1.07 ± 0.92; $p < 0.05$) but decreased in IS (0.71 ± 0.42; $p < 0.05$), the latter showing also lower ASM protein levels than IR (1.3 ± 1.3) (Fig. 1C). In line, ΔASM protein was higher in T2D than in IS (Fig. 1D). In contrast, ASM activity rose by 3.5–4.7 fold across all groups (Fig. 1E) without differences between groups (Fig. 1F). Interestingly, NSM protein levels (in A.U.) were lower in IR (0.33 ± 0.33) than in IS (0.81 ± 0.74; $p < 0.05$) and T2D (0.83 ± 0.57; $p < 0.01$) at BSL, but increased in all groups about 1.6–4.2 fold upon HIIT, with the most pronounced change in IR ($p < 0.001$) (Fig. 1G), also reflected by higher ΔNSM protein in IR than in T2D (Fig. 1H). These findings suggest that HIIT increases ASM activity and NSM protein in skeletal muscle independently of insulin sensitivity.

3.3. Despite lower total sphingomyelin at baseline, certain long-chain ceramides increase upon HIIT in T2D

To further explore whether increased ASM activity and NSM protein levels contribute to CER accumulation via the SM pathway, we quantified total sphingomyelin (T-SM) and ceramide (T-CER) content as well as their species (SM C/CER C) in skeletal muscle of representative subgroups (T2D, $n = 8$; IR, $n = 8$; IS, $n = 5$–6) at BSL and after HIIT. At BSL, T-SM content (in nmol/g *Ww*) was lower in T2D (8.68 ± 1.68) than in IS and IR (11.95 ± 1.37, $p < 0.001$ and 13.74 ± 3.72, $p < 0.05$) (Fig. 2A). Following HIIT, T-SM remained lower in T2D than in IR. T-CER levels were comparable among all groups at BSL (in nmol/g *Ww*: 16.7 ± 3.28 in IS, 16.1 ± 2.9 in IR, 15.12 ± 3.78 in T2D) and after HIIT (in nmol/g *Ww*: 17.59 ± 2.58 in IS, 18.17 ± 1.44 in IR, 18.07 ± 3.34 in T2D) (Fig. 2B). At BSL, all SM species were higher in IS than in T2D, except of C18:1 and C18:0 (Fig. 2C). Neither SM species (Fig. 2C) nor CER species changed upon HIIT in IS (Fig. 2D). Notably CER C22:0 was higher in IS than in IR after HIIT (Fig. 2D). In IR individuals, all SM species were elevated at BSL compared to T2D, except for C18:1. HIIT induced a rise in SM C16:0 and C22:0 and a reduction in C18:0. Notably, SM species remained elevated in IR compared to T2D also after HIIT, with the exception of C18:1 and C22:0 (Fig. 2E). Furthermore CER C16:0 and C20:0 were increased in IR after HIIT (Fig. 2F). In contrast individuals with T2D showed no changes in SM species following HIIT (Fig. 2G). However, all CER species, except of C18:1 and C18:0, were increased exclusively in T2D after HIIT (Fig. 2H). Notably, CERs C22:0 and C24:1 were also higher in T2D than in IR after HIIT (Fig. 2H). These results indicate that HIIT induces distinct alterations in SM and CER species in skeletal muscle of insulin-resistant individuals, suggesting a possible dissociation between SM catabolism and CER production.

3.4. Membrane sphingomyelin species are reduced in T2D, while HIIT increases specific sphingomyelin species in muscle lipid droplet of IS

Lipid species were additionally analyzed in three subcellular compartments: cytosol, membrane, and lipid droplets (LDs). No differences in cytosolic- and LD-SM species were observed between the groups, except for lower SM C18:0 in both fractions of IS compared to IR after HIIT. Conversely, almost all membrane-SM species were higher in both glucose-tolerant groups compared to T2D individuals, except for C18:1 (Fig. 3A, B). In IS, none of the cytosolic- nor membrane-SM species changed, while all LD-SM species significantly – except for C20:0 by trend ($p = 0.07$) – increased (Fig. 3A). Upon HIIT, no significant changes were observed in any of the 3 fractions in IR and T2D individuals (Fig. 3B, C). These data demonstrate that HIIT selectively increases SM species in LDs of insulin-sensitive individuals, while membrane and cytosolic SM levels remain unchanged across all groups.

3.5. Membrane long-chain ceramides increase in T2D individuals upon HIIT

In IS, cytosolic- and membrane-CER C22:0 were elevated compared to IR at BSL, and HIIT did not alter CER species in any subcellular fraction. However, cytosolic-CER C18:1 was lower in IS than in IR following HIIT (Fig. 4A). In IR, HIIT increases cytosolic-CER C18:1 and membrane-CER C16:0 and C20:0, as well as LD-CER C22:0 (Fig. 4B). Notably, T2D exhibited higher membrane-CER C24:0 than IR group at BSL. Following HIIT, T2D showed increases in cytosolic-CER C22:0 and C24:0, membrane-CER C20:0, C22:0, C24:1, C24:0 and LD-CER C24:0 (Fig. 4C). Overall, these results indicate that HIIT affects CER content within the subcellular compartments only in insulin-resistant participants.

3.6. Association of changes in protein expression and activity of muscle sphingomyelinases with changes of mitochondrial dynamics and sphingolipids

CERs influence mitochondrial dynamics by promoting fission and the release of cytochrome *c* [43], potentially affecting cardiorespiratory fitness and insulin resistance [44,45]. Thus, we next investigated whether changes (Δ-values) in ASM protein and activity, NSM protein as well as changes in SMs or CERs might drive the changes in insulin sensitivity and mitochondrial dynamics and quality control [37].

Regression analysis of Δ-values did not reveal an association between muscle ASM protein or activity level and T-CER, but a negative relationship of ΔASM activity with ΔCER C16:0, C24:1, C24:0 and ΔLD-SM C22:0 and C24:0 in T2D (Fig. 5A). However, ΔASM activity was positively associated with all measured LD-SM species in IR and by trend

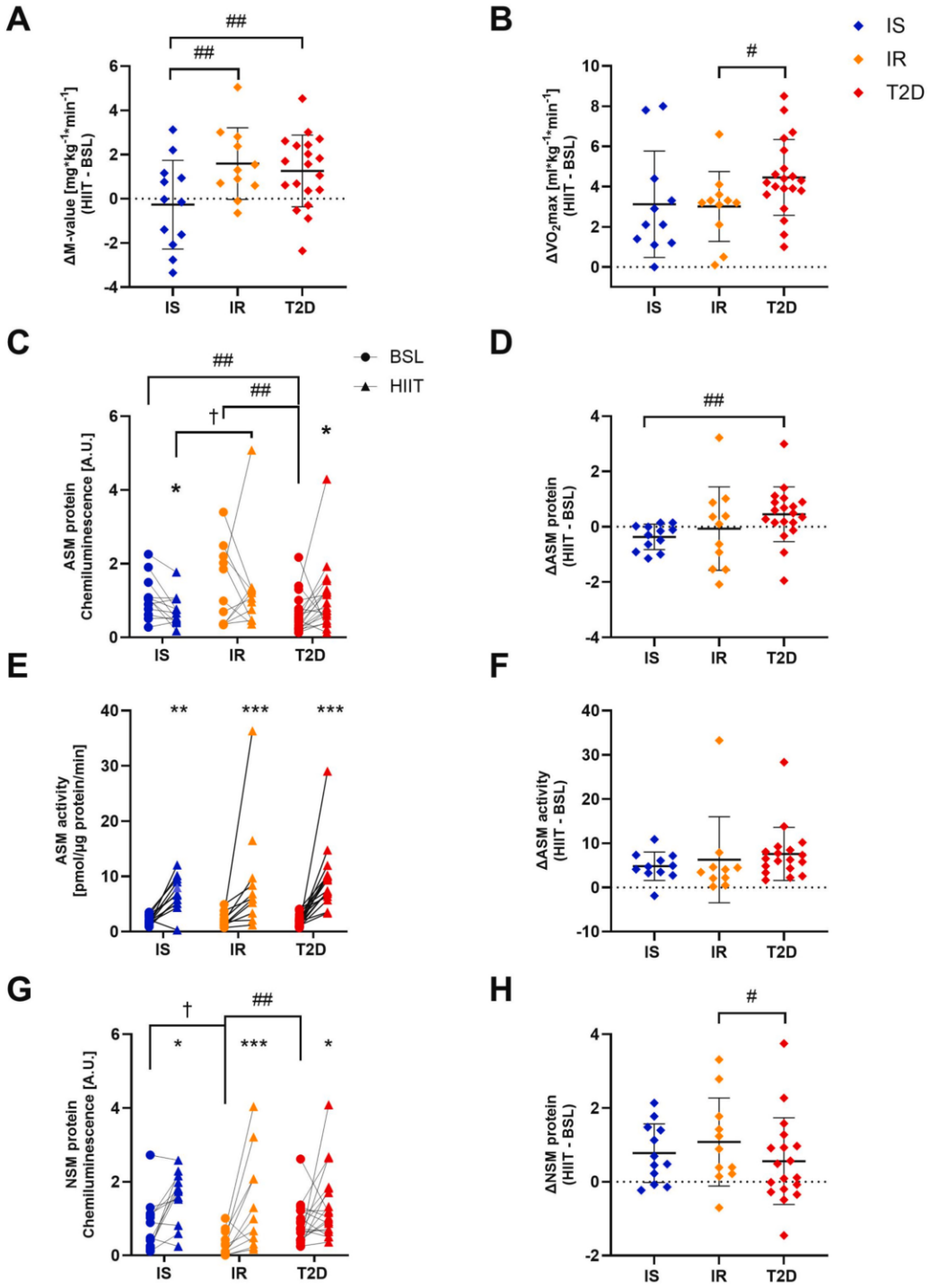

Fig. 1. ASM activity and NSM protein rise after HIIT independently of insulin sensitivity.
(A) Changes in M-value and (B) changes in VO_2max, both expressed as Δ of values after training minus values at baseline (HIIT-BSL) in insulin-sensitive individuals (IS, $n = 12$) as well as in insulin-resistant humans without (IR, $n = 11$) or with type 2 diabetes (T2D, $n = 19$ for M-value and $n = 20$ for VO_2max). (C) Protein levels of acid sphingomyelinase (ASM) in IS (n = 12), IR (n = 11) and T2D (n = 19) at baseline (BSL) and after 12-weeks of HIIT (HIIT). (D) Changes in ASM protein level expressed as Δ (HIIT-BSL). (E) ASM enzymatic activity at BSL and HIIT, (F) changes in ASM enzymatic activity as Δ (HIIT-BSL). (G) Protein level of NSM in IS (n = 12), IR (n = 11) and T2D (n = 19) at BSL and after HIIT. (H) Changes in protein level expressed as Δ (HIIT-BSL).
Data are presented as mean ± standard deviation (SD), A.U., arbitrary units. #$p < 0.05$, ##$p < 0.01$ vs T2D; *p < 0.05, **p < 0.01, ***$p < 0.001$ BSL vs HIIT; †p < 0.05 IS vs IR, based on generalized ANOVA. Comparison of M-values and VO_2max between HIIT and BSL data has been previously published [36,37].

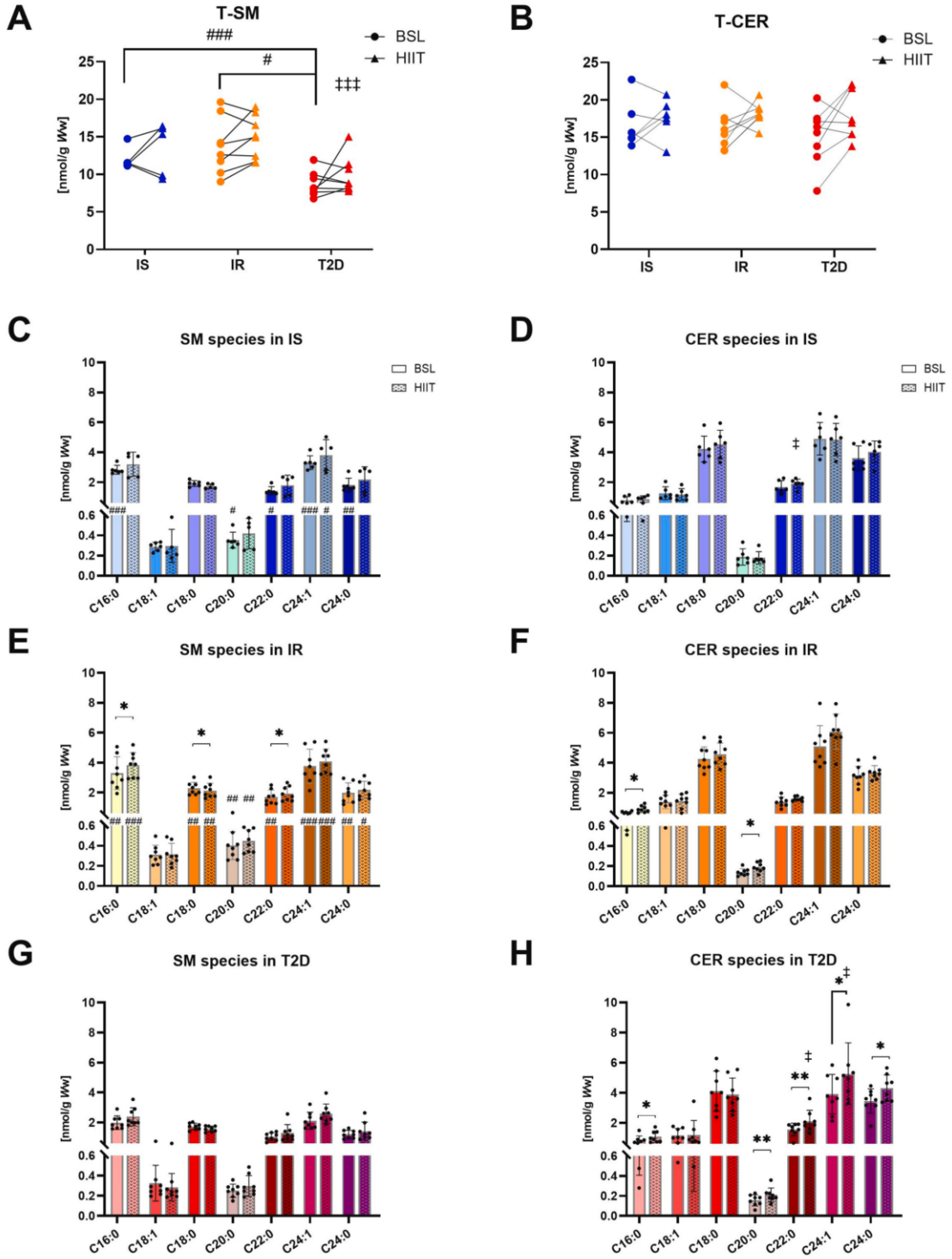

Fig. 2. Despite lower total sphingomyelin at baseline, certain long-chain ceramides increase upon HIIT in T2D.
(A) Total sphingomyelin (T-SM) and (B) total ceramide (T-CER) content in skeletal muscle of IS ($n = 5$ for T-SM and $n = 6$ for T-CER), IR ($n = 8$) and T2D (n = 8) at baseline (BSL) and after HIIT. Sphingomyelin (SM) and ceramide (CER) species in skeletal muscle of IS (C) and (D), IR (E) and (F), as well as T2D (G) and (H), respectively, at BSL and after 12-weeks of HIIT (HIIT).
Data are presented as mean ± SD, *p < 0.05, **p < 0.01 BSL vs HIIT; ‡p < 0.05, ‡‡‡ < 0.001 vs IR; #p < 0.05, ##p < 0.01, ###p < 0.001 vs T2D based on generalized ANOVA.

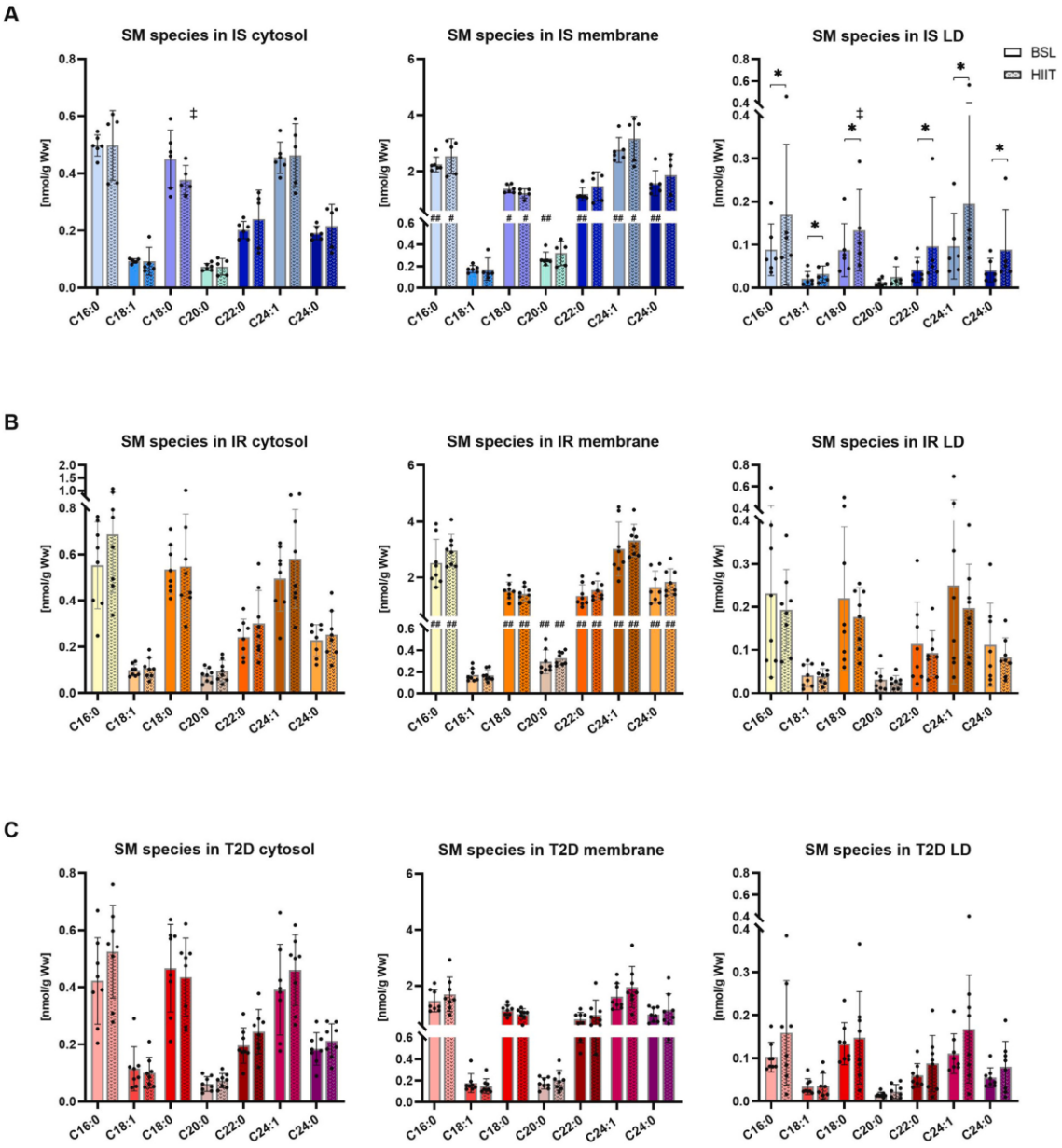

Fig. 3. Membrane sphingomyelin species are reduced in T2D, while HIIT increases specific sphingomyelin species in muscle lipid droplet of IS.
Sphingomyelin (SM) species in cytosol, membrane and lipid droplet (LD) fractions in the skeletal muscle of (A) IS (n = 5–6), (B) IR (n = 8) and (C) T2D (n = 8) at baseline (BSL) and after 12-weeks of HIIT (HIIT).
Data are presented as mean ± SD, *p < 0.05 BSL vs HIIT; ‡p < 0.05 vs IR; #p < 0.05, ##p < 0.01 vs T2D based on generalized ANOVA.

negatively in T2D (Fig. 5B, Table S3). ΔASM protein and ΔASM activity associated negatively with ΔM-value in the T2D group (Fig. 5A,B). Although T-CER were weakly and negatively associated with the M-value in the IR group at BSL ($\beta = -1.45$; $p = 0.051$), there was no association between ΔT-CER and ΔM-value across the whole cohort. ΔNSM protein exhibited distinct group-specific associations; indeed, it associates negatively with ΔT-CER and Δmembrane-CER C18:0 in IS, but positively with different CERs (ΔCER C16:0, C20:0 and Δcytosolic-CER C16:0, C18:1, C22:0, C24:0) in IR (Fig. 5C). ΔT-SM did not correlate with ΔT-CER (data not shown), suggesting that SM- to- CER conversion is not a major regulatory mechanism. Overall, changes in T-CER did not seem to drive changes in mitochondrial dynamics (data not shown), except for the IR group showing a positive association with the mitophagy marker activated PTEN-induced kinase 1, expressed as phos-PINK^{Thr257}/PINK ($\beta = 3.79$; $p = 0.02$). Interestingly, ΔASM protein or ΔASM activity correlated with biomarkers of mitochondrial fusion (mitofusin 2; MFN2), fission (activated form of dynamin-related protein 1 expressed as phos-DRP1^{Ser616}/DRP1), mitophagy (phos-PINK^{Thr257}/PINK, and activated Parkin, expressed as phos-Parkin^{Ser65}/Parkin) as well as exercise-induced mitophagy-related AMP-activated protein kinase (AMPK; phos-AMPKα^{Thr172}/AMPKα).

Across the entire cohort, ΔASM protein positively related to ΔMFN2, Δphos-DRP1 ^{Ser616}/DRP1, Δphos-Parkin^{Ser65}/Parkin and Δphos-AMPKα ^{Thr172}/AMPKα (Fig. 5A, Table S3). Among IR, ΔASM protein associated

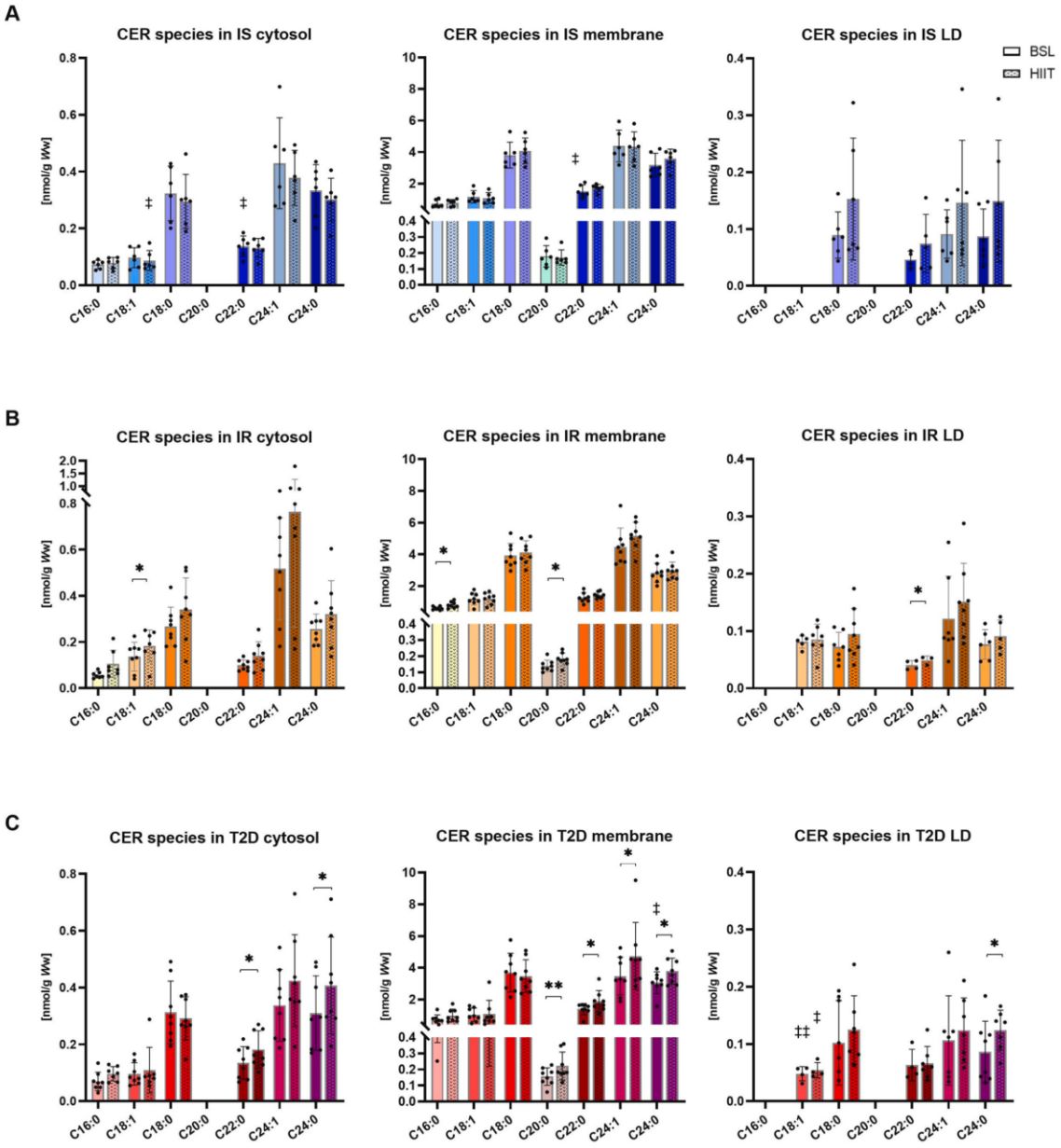

Fig. 4. Membrane long-chain ceramides increase in T2D individuals upon HIIT.
Ceramide (CER) species in cytosol, membrane and lipid droplet (LD) fractions in skeletal muscle of (A) IS (n = 6), (B) IR (n = 8) and (C) T2D (n = 8) at baseline (BSL) and after 12-weeks of HIIT (HIIT).
Data are presented as mean ± SD, *p < 0.05 BSL vs HIIT; ‡p < 0.05, ‡‡p < 0.01 vs IR, based on generalized ANOVA.

positively with ΔVO_2max, ΔMFN2, Δphos-AMPKα ^{Thr172}/AMPKα, while the ΔASM protein tended to correlate negatively with ΔOPA1 (Optic athrophy 1) in IS ($\beta = -0.82$, $p = 0.07$) (Fig. 5A, Table S3). ΔASM activity associated positively with ΔMFN2 across the whole cohort (Fig. 5A). In T2D, ΔASM activity also associated positively with ΔMFN2, but negatively with Δphos-AMPKα ^{Thr172}/AMPKα (Fig. 5B). ΔASM activity further showed a trend towards a positive association with ΔMFN1 in IS ($\beta = 0.15$, $p = 0.06$) and with Δphos-DRP1^{Ser616}/DRP1 ($\beta = 1.09$; $p = 0.05$) and significantly with Δphos-PINK ^{Thr257}/PINK in IR (Fig. 5B, Table S3). ΔNSM protein was negatively associated with ΔMFN2, Δvoltage-dependent anion channel (VDAC) and positively with Δphos-insulin receptor substrate (IRS)1^{Ser1101}/IRS1 across the whole cohort, whereas it positively related to Δphos-AMPKα ^{Thr172}/AMPKα and negatively to ΔMFN2 only in T2D (Fig. 5C). Collectively, the regression analysis revealed group-specific associations of ASM and NSM with lipid species as well as markers of mitochondrial quality control, suggesting that ASM might contribute to the regulation of mitochondrial quality control specifically in insulin-resistant individuals.

4. Discussion

This study shows that reduced skeletal muscle ASM protein levels increase with HIIT only in individuals with T2D, while ASM activity generally rises upon HIIT irrespective of insulin sensitivity at BSL. HIIT-

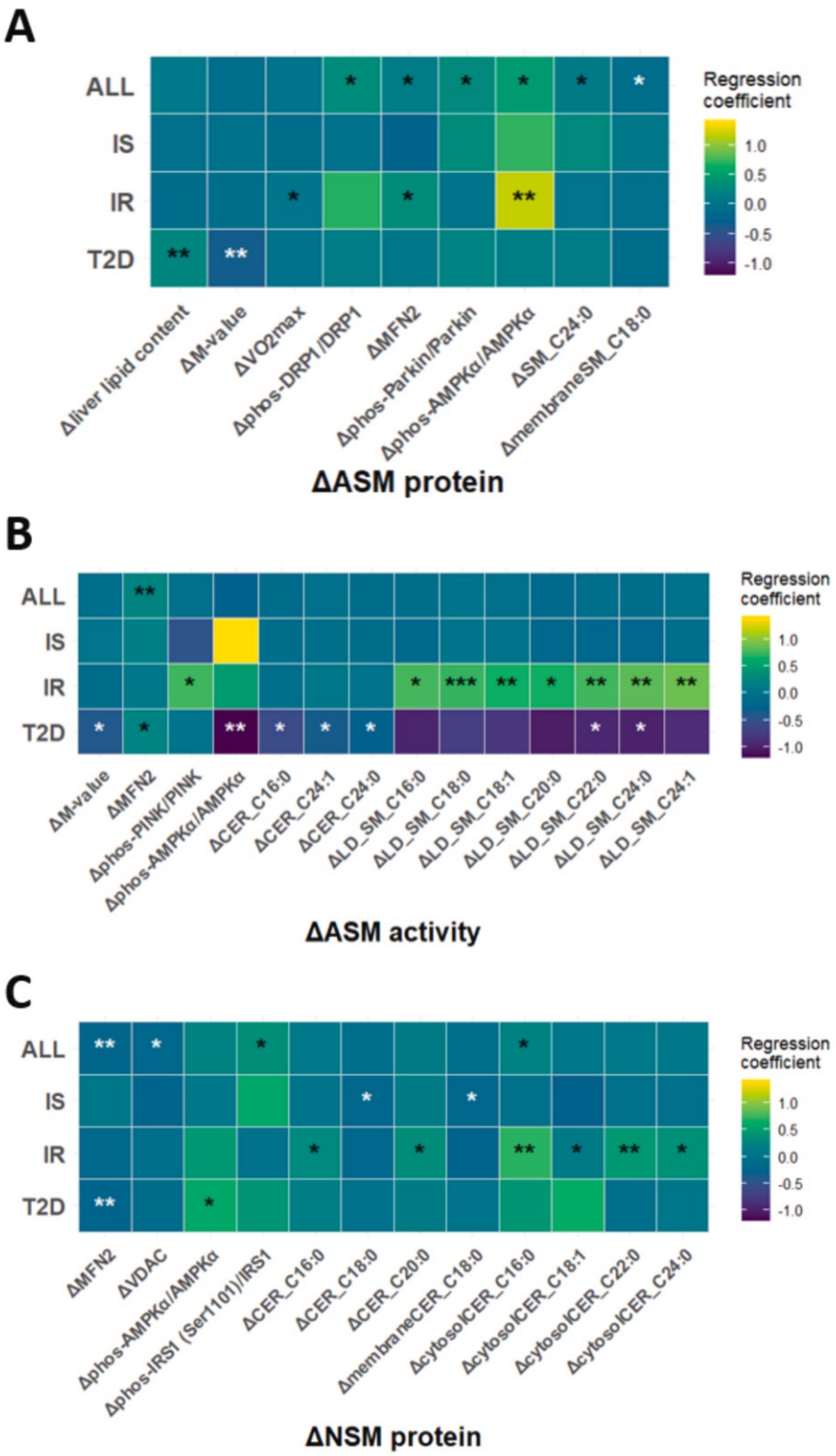

(caption on next page)

Fig. 5. Association of changes in protein expression of muscle sphingomyelinases with changes of mitochondrial dynamics and sphingolipids.
Heatmaps showing regression analysis of changes in markers of mitochondrial dynamics, total (T-) and species of sphingomyelin (SM) and ceramides (CER) with (A) ASM protein and (B) enzymatic activity as well as (C) neutral sphingomyelinase (NSM) protein in the whole study population (ALL), insulin-sensitive (IS), insulin-resistant (IR) and type 2 diabetes (T2D) individuals.
Yellow color denotes positive and purple color denotes negative correlations; each cell with an asterisk refers to a significant linear regression analysis (*$p < 0.05$, **$p < 0.01$). Cells without asterisk indicate that the correlations did not reach statistical significance. Western blot analysis for proteins of the insulin signaling and markers of mitochondrial dynamics at baseline (BSL) and after 12-weeks of HIIT (HIIT) have been previously published [36,37]. (For interpretation of the references to color in this figure legend, the reader is referred to the web version of this article.)

induced changes in ASM activity are more pronounced by trend in T2D and relate to changes in features of mitochondrial dynamics. Indeed, associations between ASM and biomarkers for mitochondrial fusion (MFN2), fission (phos-DRP1^{Ser616}/DRP1) and mitophagy (phos-PINK^{Thr257}/PINK, phos-Parkin^{Ser65}/Parkin, phos-AMPKα ^{Thr172}/AMPKα) were stronger in the insulin-resistant groups than in the insulin-sensitive group, potentially reflecting greater dependency on adaptive remodeling under glucose-intolerance conditions.

Interestingly, skeletal muscle SM content was lower in T2D, whereas CER content was similar among individuals with different insulin sensitivity at BSL and associate with M-values only in the IR group. Notably, only insulin-resistant individuals displayed HIIT-induced changes in SM species and increases in specific CER species upon HIIT, although changes in T-CER were overall modest. These findings indicate a dissociation between SM catabolism and CER generation with no impact of CERs on whole-body – mainly reflecting skeletal muscle – insulin sensitivity.

In the basal resting state, ASM protein levels were lower in individuals with T2D compared to those with normal glucose tolerance (both IR and IS), which is in line with a recent proteomics study reporting higher protein expression of ASM in insulin-sensitive compared to insulin-resistant individuals [9]. However, data on skeletal muscle ASM protein levels in the context of diabetes are only available from experimental models. These models found elevated ASM protein levels in the myocardium of high-fat fed mice [10] and in adipose tissue of Goto-Kakizaki rats as a model of spontaneous T2D [46] compared to control animals. Of note, our study found comparable BSL ASM activity among humans exhibiting different degrees of insulin sensitivity. This aligns with previous animal studies reporting unchanged or even decreased ASM activity in various muscles of streptozotocin (STZ)-induced diabetic rats compared to healthy controls [11]. Conversely, ASM activity increased in mouse myocardium upon high-fat diet [10] and human studies have shown elevated plasma ASM activity in individuals with metabolic dysfunction-associated steatohepatitis (MASH) or T2D [47,48]. It has been suggested that ASM may be implicated in the development of liver steatosis through mechanisms involving endoplasmic reticulum stress, autophagy and lysosomal membrane permeabilization [49]. Taken together, these studies point to tissue-, species- and disease model-specific differences in ASM protein expression and activity. Such variability may differentially impact metabolic pathways and cellular functions in preclinical models and human metabolic diseases.

ASM activity can favor synthesis of CER via the SM pathways, potentially reducing AKT phosphorylation and impairing insulin-stimulated glucose uptake [7,50]. However, increased ASM activity did not raise muscle T-CER levels in aerobic-trained rats [29]. The present lipidomic analysis also revealed neither differences in T-CER levels between the groups nor significant associations with insulin sensitivity across all groups at BSL. Likewise, only some [3,20], but not all [5,6] previous studies reported a negative correlation between muscle CER content and insulin sensitivity in humans. While the different findings may result from study design or altered CER biosynthetic pathways [2,7,51], our data do not support the concept that T-CER play a primary role in skeletal muscle insulin resistance [5].

This study also found lower SM contents and no compartment-specific response in T2D, but a specific increase of SM in the LD fraction in IS individuals upon HIIT, in line with previous studies [4,12]. Given that SM can act as a metabolic "sink" preventing CER formation, the observed sequestration in LD may limit CER production at membrane sites via NSM, thereby maintaining or improving insulin action [52]. The protein level of NSM increased in all groups upon HIIT and ΔNSM positively associated with Δphos-IRS1^{Ser1101}/IRS1 in the whole cohort, supporting the notion that NSM may contribute to insulin resistance through CER-mediated interference with IRS1 function [53].

Conversely ASM protein increased exclusively in T2D and may represent a response to exercise-induced sarcolemmal stress, which is known to be more pronounced in individuals with diabetes after exercising [54]. However, the increases in ASM protein and activity in the T2D group could also exert beneficial effects by facilitating muscle recovery as reported in models of muscle dystrophy [55], possibly by Ca^{2+}-dependent exocytosis of lysosomes and endocytotic removal of membrane lesions [56]. Alternatively, the reduced ASM protein levels mainly observed in the IS group after training may indicate a physiological response to exercise-induced oxidative stress and autophagy [57,58]. Nevertheless, ASM activity uniformly increased across all groups after HIIT, supporting its potential role in the intricate process of repair of skeletal muscle independent of insulin sensitivity [55,59]. Of note, previous studies did not report exercise-induced differences in the levels of ASM and other sphingomyelinases in human skeletal muscle [9]. Surprisingly, the present study observed trend towards an increase in T-CER levels in IR and T2D after HIIT despite enhanced insulin sensitivity [36], underlining that T-CER contents cannot sufficiently explain for insulin resistance in human skeletal muscle, as discussed above [3,5,6,20]. One could speculate that the levels of acide ceramidase (ASAH1), which catalyzes the hydrolysis of CER, are lower in insulin-resistant than in insulin-sensitive individuals [9] and decrease upon HIIT, resulting in higher CER levels. However, this contrast with proteomic studies showing that the expression of ASAH1 remains unchanged at least during short-term HIIT for 2 or 5 weeks [60,61]. The insulin-resistant individuals (IR and T2D) even showed higher muscle CER C20:0 and C16:0 species after HIIT, with the latter known to increase in murine myoblasts upon ASM exposure [62]. People with T2D also had higher CER C24:1 and C24:0 species after HIIT compared to BSL. While some studies have linked these very-long-chain CERs in human plasma to insulin resistance [63,64], their specific role within skeletal muscle remains still unclear. Rodent studies revealed that C24 CERs might support β-oxidation and mitochondrial respiration [7,65]. Whether these results reflect a possible protective effect against obesity, warrants further investigation in humans. However, the increase of specific CER species in IR and T2D after HIIT, did not correspond to reductions in SM species, suggesting that these CER likely arise from other pathways such as *de novo* synthesis, rather than from SM degradation in line with a previous study in trained and untrained healthy individuals [25]. The parallel increase of ASM activity and certain long-chain CER species observed specifically in T2D group might reflect coordinated but independent responses to exercise-related muscle remodeling, rather than a direct enzyme-product relationship.

Finally, HIIT affects mitochondrial quality control to maintain skeletal muscle integrity and function [13,31]. Abnormal mitochondrial dynamics are also frequently observed in skeletal muscle in T2D [13]. As ASM has been linked to mitochondrial fusion and fission in cancer models [66] and ASM-deficient mouse muscle shows reduced expression of the fusion protein OPA1 [67], we examined wheter ASM might also be involved in mitochondrial remodeling in response to exercise. The

observed positive associations of the ΔASM protein level or activity with changes (Δ-values) of markers of mitochondrial fusion (MFN2), fission (phos-DRP1^{Ser616}/DRP1) and mitophagy (phos-Parkin ^{Ser65}/Parkin) across the entire study population, collectively hint at an interplay between ASM, mitochondrial quality control and metabolic function. Indeed, ASM is involved in modulating mitochondrial morphology and function via fusion/fission processes as shown in melanoma cells and ASM-deficient mouse muscle [66,67]. In addition, the positive association between ΔASM and ΔMFN2 in T2D group, suggests that ASM may contribute to enhanced fusion of mitochondria, which are less abundant and morphologically smaller with lower oxidative capacity in T2D [68]. Moreover the present study showed that changes in ASM protein relate positively to changes in phos-AMPKα ^{Thr172}/AMPKα in the IR group, while changes in ASM activity showed an negative association with changes in phos-AMPKα ^{Thr172}/AMPKα in T2D. This could potentially hinder exercise-induced mitophagy and contribute to maintenance of mitochondria integrity. Of note, some T2D individuals were on metformin treatment. Although metformin is not the primary molecular target of AMPK [69,70], chronic metformin treatment has been shown to increase skeletal muscle AMPK activity even after withdrawal [71]. To minimize potential confounding, we focused on exercise-induced changes (Δ-values) in AMPK phosphorylation rather than absolute levels.

Taken together, these findings suggest that ASM may support improvements in mitochondrial function and insulin sensitivity, consistent with previous observations in L6 myoblasts [72]. In contrast, the negative association of ΔNSM protein with ΔMFN2 and positive with phos-AMPKα ^{Thr172}/AMPKα in T2D points to an opposing effect of NSM.

This study comes with specific strengths and limitations. The prospective design with supervised exercise training and comprehensive phenotyping overcomes several limitations of studies on physical activity. However, the relatively small and homogeneous cohort, comprising only overweight, middle-aged Caucasian male participants limits the generalizability of our findings to other populations. Moreover, muscle CER and SM species were analyzed in subgroups of participants, due to limited tissue availability and technical constraints. Although the age and BMI of these subgroups were similar to those of the whole cohort, selection bias cannot be completely excluded and the results should be interpreted cautiously. Moreover, the lack of multiple testing correction may increase the risk of type I error. Due to the biological interrelatedness of the markers and the hypothesis-generating nature of this analysis, the results from the regression analyses should be considered exploratory and are intended to inform future mechanistic studies. This analysis also did not differentiate between the lysosomal and secreted forms of ASM, of which the latter may exert a dominant-negative effect on lysosomal ASM activity or lack activity. While this limits conclusions about isoform-specific roles, such as lysosomal ASM in membrane repair or intracellular signaling, our interpretation is based on total ASM activity, which increased with HIIT regardless of isoform origin and was consistently associated with changes in markers of mitochondrial quality control. Finally, these findings cannot prove causality for the proposed mechanisms, but the data obtained before and after HIIT intervention at least allowed to observe a sequence of events in a clinical study.

In this context, it is noteworthy that although HIIT increased ASM activity in both insulin resistant groups, we observed no consistent rise in CER species, but even a negative relationship between the HIIT-induced increase in ASM activity and specific CER species in T2D, suggesting that ASM may not be the primary driver of CER accumulation post-HIIT. Moreover, our group recently showed that HIIT reduces fission protein DRP1 and increases fusion protein MFN2 in T2D [37]. If ASM-induced CER accumulation were a dominant factor driving mitochondrial fission, we would expect an increase in DRP1 activation rather than the observed reduction. Instead, the observed beneficial adaptations - such as reduced DRP1 activation and increased MFN2 expression – along with the rise of ASM activity point towards alternative pathways. One such mechanism may involve AMPK activation, which is known to enhance mitochondrial quality through mitophagy. Likewise, Mastrototaro et al. reported an increased mitophagy in T2D upon HIIT [37]. Taken together, these finding suggest that ASM may contribute to mitochondrial remodeling independently of CER, possibly via a AMPK-linked mechanism. Thus, our results raise the possibility that ASM may be involved in modulating exercise-induced mitochondrial functionality and thereby representing a possible target for further studies on exercise mimetic drugs.

Supplementary data to this article can be found online at https://doi.org/10.1016/j.metabol.2025.156361.

CRediT authorship contribution statement

Mona Hendlinger: Writing – review & editing, Writing – original draft, Visualization, Resources, Investigation, Conceptualization. **Lucia Mastrototaro:** Writing – review & editing, Investigation, Conceptualization. **Marten Exterkate:** Writing – review & editing, Investigation. **Maria Apostolopoulou:** Writing – review & editing, Investigation. **Yanislava Karusheva:** Writing – review & editing, Investigation. **Geronimo Heilmann:** Writing – review & editing, Investigation. **Polina Lipaeva:** Writing – review & editing, Visualization, Formal analysis. **Klaus Straßburger:** Writing – review & editing, Formal analysis. **Sofiya Gancheva:** Writing – review & editing, Investigation. **Sabine Kahl:** Writing – review & editing, Methodology, Conceptualization. **Michael Roden:** Writing – review & editing, Writing – original draft, Supervision, Resources, Methodology, Funding acquisition.

Declaration of competing interest

M.R. has received honoraria for scientific advisory boards and/or for lectures by Astra-Zeneca, Boehringer Ingelheim, Echosens, Lilly, Madrigal, MSD, Novo Nordisk and Target RWE. The research of M.R. is also supported by a grant from the European Community (HORIZON-HLTH-2022-STAYHLTH-02-01: Panel A) to the INTERCEPT-T2D consortium). All other authors declare no competing interests.

Acknowledgments

This study was supported in part by the Ministry of Culture and Science of the State of Northrhine Westphalia, the German Federal Ministry of Health (BMG) as well as by a grant of the Federal Ministry for Research (BMBF) to the German Center for Diabetes Research (DZD e. V.), German Diabetes Association (DDG), the German Research Foundation (DFG, GRK2576 Vivid), Schmutzler Stiftung and MODS within the programme “Profilbildung 2020”, an initiative of the Ministry of Culture and Science of the State of Northrhine Westphalia. The sole responsibility for the content of this publication lies with the authors.

The authors thank all volunteers for their participation as well as Dr. Julia Szendroedi for contributing to the previously reported clinical parts of this study and Fariba Zivehe, Michelle Reina do Fundo, Jan-Marc Leonhard, Silke Tosenovian, Christina Preuss and Tim te Poel for their technical assistance.

References

[1] IDF. International diabetes federation. IDF diabetes atlas, 11th edn. Brussels. Belgium International Diabetes Federation. https://diabetesatlas.org; 2025.
[2] Roden M, Shulman GI. The integrative biology of type 2 diabetes. Nature 2019; 576:51–60. https://doi.org/10.1038/s41586-019-1797-8.
[3] Adams 2nd JM, Pratipanawatr T, Berria R, Wang E, DeFronzo RA, Sullards MC, et al. Ceramide content is increased in skeletal muscle from obese insulin-resistant humans. Diabetes 2004;53:25–31. https://doi.org/10.2337/diabetes.53.1.25.
[4] Straczkowski M, Kowalska I, Baranowski M, Nikolajuk A, Otziomek E, Zabielski P, et al. Increased skeletal muscle ceramide level in men at risk of developing type 2 diabetes. Diabetologia 2007;50:2366–73. https://doi.org/10.1007/s00125-007-0781-2.
[5] Szendroedi J, Yoshimura T, Phielix E, Koliaki C, Marcucci M, Zhang D, et al. Role of diacylglycerol activation of PKCθ in lipid-induced muscle insulin resistance in

humans. Proc Natl Acad Sci U S A 2014;111:9597–602. https://doi.org/10.1073/pnas.1409229111.
[6] Skovbro M, Baranowski M, Skov-Jensen C, Flint A, Dela F, Gorski J, et al. Human skeletal muscle ceramide content is not a major factor in muscle insulin sensitivity. Diabetologia 2008;51:1253–60. https://doi.org/10.1007/s00125-008-1014-z.
[7] Hammerschmidt P, Brüning JC. Contribution of specific ceramides to obesity-associated metabolic diseases. Cell Mol Life Sci 2022;79:395. https://doi.org/10.1007/s00018-022-04401-3.
[8] Sokolowska E, Blachnio-Zabielska A. The role of ceramides in insulin resistance. Front Endocrinol (Lausanne) 2019;10:577. https://doi.org/10.3389/fendo.2019.00577.
[9] Needham EJ, Hingst JR, Onslev JD, Diaz-Vegas A, Leandersson MR, Huckstep H, et al. Personalized phosphoproteomics of skeletal muscle insulin resistance and exercise links MINDY1 to insulin action. Cell Metab 2024;36:2542–59. e2546, https://doi.org/10.1016/j.cmet.2024.10.020.
[10] Liu R, Duan T, Yu L, Tang Y, Liu S, Wang C, et al. Acid sphingomyelinase promotes diabetic cardiomyopathy via NADPH oxidase 4 mediated apoptosis. Cardiovasc Diabetol 2023;22:25. https://doi.org/10.1186/s12933-023-01747-1.
[11] Błachnio-Zabielska A, Zabielski P, Baranowski M, Gorski J. Effects of streptozotocin-induced diabetes and elevation of plasma FFA on ceramide metabolism in rat skeletal muscle. Horm Metab Res 2010;42:1–7. https://doi.org/10.1055/s-0029-1238322.
[12] Szczerbinski L, Golonko A, Taylor M, Puchta U, Konopka P, Paszko A, et al. Metabolomic profile of skeletal muscle and its change under a mixed-mode exercise intervention in progressively dysglycemic subjects. Front Endocrinol (Lausanne) 2021;12:778442. https://doi.org/10.3389/fendo.2021.778442.
[13] Toledo FG, Goodpaster BH. The role of weight loss and exercise in correcting skeletal muscle mitochondrial abnormalities in obesity, diabetes and aging. Mol Cell Endocrinol 2013;379:30–4. https://doi.org/10.1016/j.mce.2013.06.018.
[14] Kanaley JA, Colberg SR, Corcoran MH, Malin SK, Rodriguez NR, Crespo CJ, et al. Exercise/physical activity in individuals with type 2 diabetes: a consensus statement from the American College of Sports Medicine. Med Sci Sports Exerc 2022;54:353–68. https://doi.org/10.1249/mss.0000000000002800.
[15] Röhling M, Herder C, Roden M, Stemper T, Müssig K. Effects of long-term exercise interventions on glycaemic control in type 1 and type 2 diabetes: a systematic review. Exp Clin Endocrinol Diabetes 2016;124:487–94. https://doi.org/10.1055/s-0042-106293.
[16] Larsen S, Skaaby S, Helge JW, Dela F. Effects of exercise training on mitochondrial function in patients with type 2 diabetes. World J Diabetes 2014;5:482–92. https://doi.org/10.4239/wjd.v5.i4.482.
[17] Cassidy S, Thoma C, Houghton D, Trenell MI. High-intensity interval training: a review of its impact on glucose control and cardiometabolic health. Diabetologia 2017;60:7–23. https://doi.org/10.1007/s00125-016-4106-1.
[18] Ruegsegger GN, Pataky MW, Simha S, Robinson MM, Klaus KA. Nair KS (2023) high-intensity aerobic, but not resistance or combined, exercise training improves both cardiometabolic health and skeletal muscle mitochondrial dynamics. J Appl Physiol 1985;135:763–74. https://doi.org/10.1152/japplphysiol.00405.2023.
[19] Koopman R, Manders RJ, Jonkers RA, Hul GB, Kuipers H, van Loon LJ. Intramyocellular lipid and glycogen content are reduced following resistance exercise in untrained healthy males. Eur J Appl Physiol 2006;96:525–34. https://doi.org/10.1007/s00421-005-0118-0.
[20] Dubé JJ, Amati F, Stefanovic-Racic M, Toledo FG, Sauers SE, Goodpaster BH. Exercise-induced alterations in intramyocellular lipids and insulin resistance: the athlete's paradox revisited. Am J Physiol Endocrinol Metab 2008;294:E882–8. https://doi.org/10.1152/ajpendo.00769.2007.
[21] Bruce CR, Thrush AB, Mertz VA, Bezaire V, Chabowski A, Heigenhauser GJ, et al. Endurance training in obese humans improves glucose tolerance and mitochondrial fatty acid oxidation and alters muscle lipid content. Am J Physiol Endocrinol Metab 2006;291:E99–e107. https://doi.org/10.1152/ajpendo.00587.2005.
[22] Coen PM, Menshikova EV, Distefano G, Zheng D, Tanner CJ, Standley RA, et al. Exercise and weight loss improve muscle mitochondrial respiration, lipid partitioning, and insulin sensitivity after gastric bypass surgery. Diabetes 2015;64:3737–50. https://doi.org/10.2337/db15-0809.
[23] Bergman BC, Goodpaster BH. Exercise and muscle lipid content, composition, and localization: influence on muscle insulin sensitivity. Diabetes 2020;69:848–58. https://doi.org/10.2337/dbi18-0042.
[24] Pesta D, Anadol-Schmitz E, Sarabhai T, Op den Kamp Y, Gancheva S, Trinks N, et al. Determinants of increased muscle insulin sensitivity of exercise-trained versus sedentary normal weight and overweight individuals. Sci Adv 2025;11:eadr8849. https://doi.org/10.1126/sciadv.adr8849.
[25] Helge JW, Dobrzyn A, Saltin B, Gorski J. Exercise and training effects on ceramide metabolism in human skeletal muscle. Exp Physiol 2004;89:119–27. https://doi.org/10.1113/expphysiol.2003.002605.
[26] Pino MF, Stephens NA, Eroshkin AM, Yi F, Hodges A, Cornnell HH, et al. Endurance training remodels skeletal muscle phospholipid composition and increases intrinsic mitochondrial respiration in men with Type 2 diabetes. Physiol Genomics 2019;51:586–95. https://doi.org/10.1152/physiolgenomics.00014.2019.
[27] Lee YI, Leem YH. Acid sphingomyelinase inhibition alleviates muscle damage in gastrocnemius after acute strenuous exercise. J Exerc Nutr Biochem 2019;23:1–6. https://doi.org/10.20463/jenb.2019.0009.
[28] Błachnio-Zabielska A, Baranowski M, Zabielski P, Górski J. Effect of exercise duration on the key pathways of ceramide metabolism in rat skeletal muscles. J Cell Biochem 2008;105:776–84. https://doi.org/10.1002/jcb.21877.
[29] Błachnio-Zabielska A, Zabielski P, Baranowski M, Gorski J. Aerobic training in rats increases skeletal muscle sphingomyelinase and serine palmitoyltransferase activity, while decreasing ceramidase activity. Lipids 2011;46:229–38. https://doi.org/10.1007/s11745-010-3515-z.
[30] Bergman BC, Brozinick JT, Strauss A, Bacon S, Kerege A, Bui HH, et al. Muscle sphingolipids during rest and exercise: a C18:0 signature for insulin resistance in humans. Diabetologia 2016;59:785–98. https://doi.org/10.1007/s00125-015-3850-y.
[31] Hood DA, Memme JM, Oliveira AN, Triolo M. Maintenance of skeletal muscle mitochondria in health, exercise, and aging. Annu Rev Physiol 2019;81:19–41. https://doi.org/10.1146/annurev-physiol-020518-114310.
[32] Fealy CE, Mulya A, Lai N, Kirwan JP. Exercise training decreases activation of the mitochondrial fission protein dynamin-related protein-1 in insulin-resistant human skeletal muscle. J Appl Physiol (1985) 2014;117:239–45. https://doi.org/10.1152/japplphysiol.01064.2013.
[33] Kruse R, Pedersen AJ, Kristensen JM, Petersson SJ, Wojtaszewski JF, Højlund K. Intact initiation of autophagy and mitochondrial fission by acute exercise in skeletal muscle of patients with Type 2 diabetes. Clin Sci (Lond) 2017;131:37–47. https://doi.org/10.1042/cs20160736.
[34] Gibala MJ, Little JP, Macdonald MJ, Hawley JA. Physiological adaptations to low-volume, high-intensity interval training in health and disease. J Physiol 2012;590:1077–84. https://doi.org/10.1113/jphysiol.2011.224725.
[35] Little JP, Gillen JB, Percival ME, Safdar A, Tarnopolsky MA, Punthakee Z, et al. Low-volume high-intensity interval training reduces hyperglycemia and increases muscle mitochondrial capacity in patients with type 2 diabetes. J Appl Physiol (1985) 2011;111:1554–60. https://doi.org/10.1152/japplphysiol.00921.2011.
[36] Apostolopoulou M, Mastrototaro L, Hartwig S, Pesta D, Straßburger K, de Filippo E, et al. Metabolic responsiveness to training depends on insulin sensitivity and protein content of exosomes in insulin-resistant males. Sci Adv 2021;7:eabi9551. https://doi.org/10.1126/sciadv.abi9551.
[37] Mastrototaro L, Apostolopoulou M, Hartwig S, Strassburger K, Lipaeva P, Trinks N, et al. The role of exosomes for sustained specific cardiorespiratory and metabolic improvements in males with type 2 diabetes after detraining. EBioMedicine 2024;110:105471. https://doi.org/10.1016/j.ebiom.2024.105471.
[38] Nowotny B, Zahiragic L, Bierwagen A, Kabisch S, Groener JB, Nowotny PJ, et al. Low-energy diets differing in fibre, red meat and coffee intake equally improve insulin sensitivity in type 2 diabetes: a randomised feasibility trial. Diabetologia 2015;58:255–64. https://doi.org/10.1007/s00125-014-3457-8.
[39] Szendroedi J, Saxena A, Weber KS, Strassburger K, Herder C, Burkart V, et al. Cohort profile: the German diabetes study (GDS). Cardiovasc Diabetol 2016;15:59. https://doi.org/10.1186/s12933-016-0374-9.
[40] Preuss C, Jelenik T, Bodis K, Mussig K, Burkart V, Szendroedi J, et al. A new targeted Lipidomics approach reveals lipid droplets in liver, muscle and heart as a repository for diacylglycerol and ceramide species in non-alcoholic fatty liver. Cells 2019;8(3):277. https://doi.org/10.3390/cells8030277.
[41] de Kok NAW, Exterkate M, Andringa RLH, Minnaard AJ, Driessen AJM. A versatile method to separate complex lipid mixtures using 1-butanol as eluent in a reverse-phase UHPLC-ESI-MS system. Chem Phys Lipids 2021;240:105125. https://doi.org/10.1016/j.chemphyslip.2021.105125.
[42] Pafili K, Kahl S, Mastrototaro L, Strassburger K, Pesta D, Herder C, et al. Mitochondrial respiration is decreased in visceral but not subcutaneous adipose tissue in obese individuals with fatty liver disease. J Hepatol 2022;77:1504–14. https://doi.org/10.1016/j.jhep.2022.08.010.
[43] Parra V, Eisner V, Chiong M, Criollo A, Moraga F, Garcia A, et al. Changes in mitochondrial dynamics during ceramide-induced cardiomyocyte early apoptosis. Cardiovasc Res 2008;77:387–97. https://doi.org/10.1093/cvr/cvm029.
[44] Huffman KM, Koves TR, Hubal MJ, Abouassi H, Beri N, Bateman LA, et al. Metabolite signatures of exercise training in human skeletal muscle relate to mitochondrial remodelling and cardiometabolic fitness. Diabetologia 2014;57:2282–95. https://doi.org/10.1007/s00125-014-3343-4.
[45] Jheng HF, Tsai PJ, Guo SM, Kuo LH, Chang CS, Su IJ, et al. Mitochondrial fission contributes to mitochondrial dysfunction and insulin resistance in skeletal muscle. Mol Cell Biol 2012;32:309–19. https://doi.org/10.1128/mcb.05603-11.
[46] Yang J, Wang M, Yang D, Yan H, Wang Z, Yan D, et al. Integrated lipids biomarker of the prediabetes and type 2 diabetes mellitus Chinese patients. Front Endocrinol (Lausanne) 2022;13:1065665. https://doi.org/10.3389/fendo.2022.1065665.
[47] Grammatikos G, Mühle C, Ferreiros N, Schroeter S, Bogdanou D, Schwalm S, et al. Serum acid sphingomyelinase is upregulated in chronic hepatitis C infection and non alcoholic fatty liver disease. Biochim Biophys Acta 2014;1841:1012–20. https://doi.org/10.1016/j.bbalip.2014.04.007.
[48] Górska M, Barańczuk E, Dobrzyń A. Secretory Zn2+−dependent sphingomyelinase activity in the serum of patients with type 2 diabetes is elevated. Horm Metab Res 2003;35:506–7. https://doi.org/10.1055/s-2003-41810.
[49] Garcia-Ruiz C, Mato JM, Vance D, Kaplowitz N, Fernández-Checa JC. Acid sphingomyelinase-ceramide system in steatohepatitis: a novel target regulating multiple pathways. J Hepatol 2015;62:219–33. https://doi.org/10.1016/j.jhep.2014.09.023.
[50] Chaurasia B, Summers SA. Ceramides in metabolism: key lipotoxic players. Annu Rev Physiol 2021;83:303–30. https://doi.org/10.1146/annurev-physiol-031620-093815.
[51] Sarabhai T, Koliaki C, Mastrototaro L, Kahl S, Pesta D, Apostolopoulou M, et al. Dietary palmitate and oleate differently modulate insulin sensitivity in human skeletal muscle. Diabetologia 2022;65:301–14. https://doi.org/10.1007/s00125-021-05596-z.
[52] Roszczyc-Owsiejczuk K, Zabielski P. Sphingolipids as a culprit of mitochondrial dysfunction in insulin resistance and type 2 diabetes. Front Endocrinol (Lausanne) 2021;12:635175. https://doi.org/10.3389/fendo.2021.635175.

[53] Verma MK, Yateesh AN, Neelima K, Pawar N, Sandhya K, Poornima J, et al. Inhibition of neutral sphingomyelinases in skeletal muscle attenuates fatty-acid induced defects in metabolism and stress. Springerplus 2014;3:255. https://doi.org/10.1186/2193-1801-3-255.
[54] Dial AG, Grafham GK, Monaco CMF, Voth J, Brandt L, Tarnopolsky MA, et al. Alterations in skeletal muscle repair in young adults with type 1 diabetes mellitus. Am J Physiol Cell Physiol 2021;321:C876–c883. https://doi.org/10.1152/ajpcell.00322.2021.
[55] Bittel DC, Sreetama SC, Chandra G, Ziegler R, Nagaraju K, Van der Meulen JH, et al. Secreted acid sphingomyelinase as a potential gene therapy for limb girdle muscular dystrophy 2B. J Clin Invest 2022;132. https://doi.org/10.1172/jci141295.
[56] Tam C, Idone V, Devlin C, Fernandes MC, Flannery A, He X, et al. Exocytosis of acid sphingomyelinase by wounded cells promotes endocytosis and plasma membrane repair. J Cell Biol 2010;189:1027–38. https://doi.org/10.1083/jcb.201003053.
[57] Brandt N, Gunnarsson TP, Bangsbo J, Pilegaard H. Exercise and exercise training-induced increase in autophagy markers in human skeletal muscle. Physiol Rep 2018;6:e13651. https://doi.org/10.14814/phy2.13651.
[58] Torma F, Gombos Z, Jokai M, Takeda M, Mimura T, Radak Z. High intensity interval training and molecular adaptive response of skeletal muscle. Sports Med Health Sci 2019;1:24–32. https://doi.org/10.1016/j.smhs.2019.08.003.
[59] Michailowsky V, Li H, Mittra B, Iyer SR, Mazála DAG, Corrotte M, et al. Defects in sarcolemma repair and skeletal muscle function after injury in a mouse model of Niemann-Pick type A/B disease. Skelet Muscle 2019;9:1. https://doi.org/10.1186/s13395-018-0187-5.
[60] Hostrup M, Lemminger AK, Stocks B, Gonzalez-Franquesa A, Larsen JK, Quesada JP, et al. High-intensity interval training remodels the proteome and acetylome of human skeletal muscle. Elife 2022;11. https://doi.org/10.7554/eLife.69802.
[61] Savikj M, Stocks B, Sato S, Caidahl K, Krook A, Deshmukh AS, et al. Exercise timing influences multi-tissue metabolome and skeletal muscle proteome profiles in type 2 diabetic patients - a randomized crossover trial. Metabolism 2022;135:155268. https://doi.org/10.1016/j.metabol.2022.155268.
[62] Ferreira LF, Moylan JS, Gilliam LA, Smith JD, Nikolova-Karakashian M, Reid MB. Sphingomyelinase stimulates oxidant signaling to weaken skeletal muscle and promote fatigue. Am J Physiol Cell Physiol 2010;299:C552–60. https://doi.org/10.1152/ajpcell.00065.2010.
[63] Haus JM, Kashyap SR, Kasumov T, Zhang R, Kelly KR, Defronzo RA, et al. Plasma ceramides are elevated in obese subjects with type 2 diabetes and correlate with the severity of insulin resistance. Diabetes 2009;58:337–43. https://doi.org/10.2337/db08-1228.
[64] Bergman BC, Brozinick JT, Strauss A, Bacon S, Kerege A, Bui HH, et al. Serum sphingolipids: relationships to insulin sensitivity and changes with exercise in humans. Am J Physiol Endocrinol Metab 2015;309:E398–408. https://doi.org/10.1152/ajpendo.00134.2015.
[65] Turner N, Lim XY, Toop HD, Osborne B, Brandon AE, Taylor EN, et al. A selective inhibitor of ceramide synthase 1 reveals a novel role in fat metabolism. Nat Commun 2018;9:3165. https://doi.org/10.1038/s41467-018-05613-7.
[66] Coazzoli M, Napoli A, Roux-Biejat P, De Palma C, Moscheni C, Catalani E, et al. Acid sphingomyelinase downregulation enhances mitochondrial fusion and promotes oxidative metabolism in a mouse model of melanoma. Cells 2020;9:848.
[67] Michailowsky V, Li H, Mittra B, Iyer SR, Mazala DAG, Corrotte M, et al. Defects in sarcolemma repair and skeletal muscle function after injury in a mouse model of Niemann-Pick type A/B disease. Skelet Muscle 2019;9:1. https://doi.org/10.1186/s13395-018-0187-5.
[68] Bassi-Dibai D, Santos-de-Araújo AD, Dibai-Filho AV, de Azevedo LFS, Goulart CDL, Luz GCP, et al. Rehabilitation of individuals with diabetes mellitus: focus on diabetic myopathy. Front Endocrinol (Lausanne) 2022;13:869921. https://doi.org/10.3389/fendo.2022.869921.
[69] LaMoia TE, Shulman GI. Cellular and molecular mechanisms of metformin action. Endocr Rev 2021;42:77–96. https://doi.org/10.1210/endrev/bnaa023.
[70] Phielix E, Szendroedi J, Roden M. The role of metformin and thiazolidinediones in the regulation of hepatic glucose metabolism and its clinical impact. Trends Pharmacol Sci 2011;32:607–16. https://doi.org/10.1016/j.tips.2011.06.006.
[71] Musi N, Hirshman MF, Nygren J, Svanfeldt M, Bavenholm P, Rooyackers O, et al. Metformin increases AMP-activated protein kinase activity in skeletal muscle of subjects with type 2 diabetes. Diabetes 2002;51:2074–81. https://doi.org/10.2337/diabetes.51.7.2074.
[72] del Campo A, Parra V, Vásquez-Trincado C, Gutiérrez T, Morales PE, López-Crisosto C, et al. Mitochondrial fragmentation impairs insulin-dependent glucose uptake by modulating Akt activity through mitochondrial Ca2+ uptake. Am J Physiol Endocrinol Metab 2014;306:E1–e13. https://doi.org/10.1152/ajpendo.00146.2013.

3.2 Unpublished experimental data on acid sphingomyelinase function in liver and cellular models

Building on the human data presented in the first part of this thesis, the second part focuses on mechanistic studies aimed at elucidating tissue-specific roles of ASM under metabolic stress conditions. To this end, experiments in murine models of diabetes, obesity, and fatty liver disease, as well as in hepatoma cells exposed to high-lipid or high-glucose stimuli, were performed. These studies extend the clinical findings by addressing whether ASM contributes to tissue-specific lipid handling and affects insulin signaling, thereby providing novel insights into its context-dependent role in metabolic regulation.

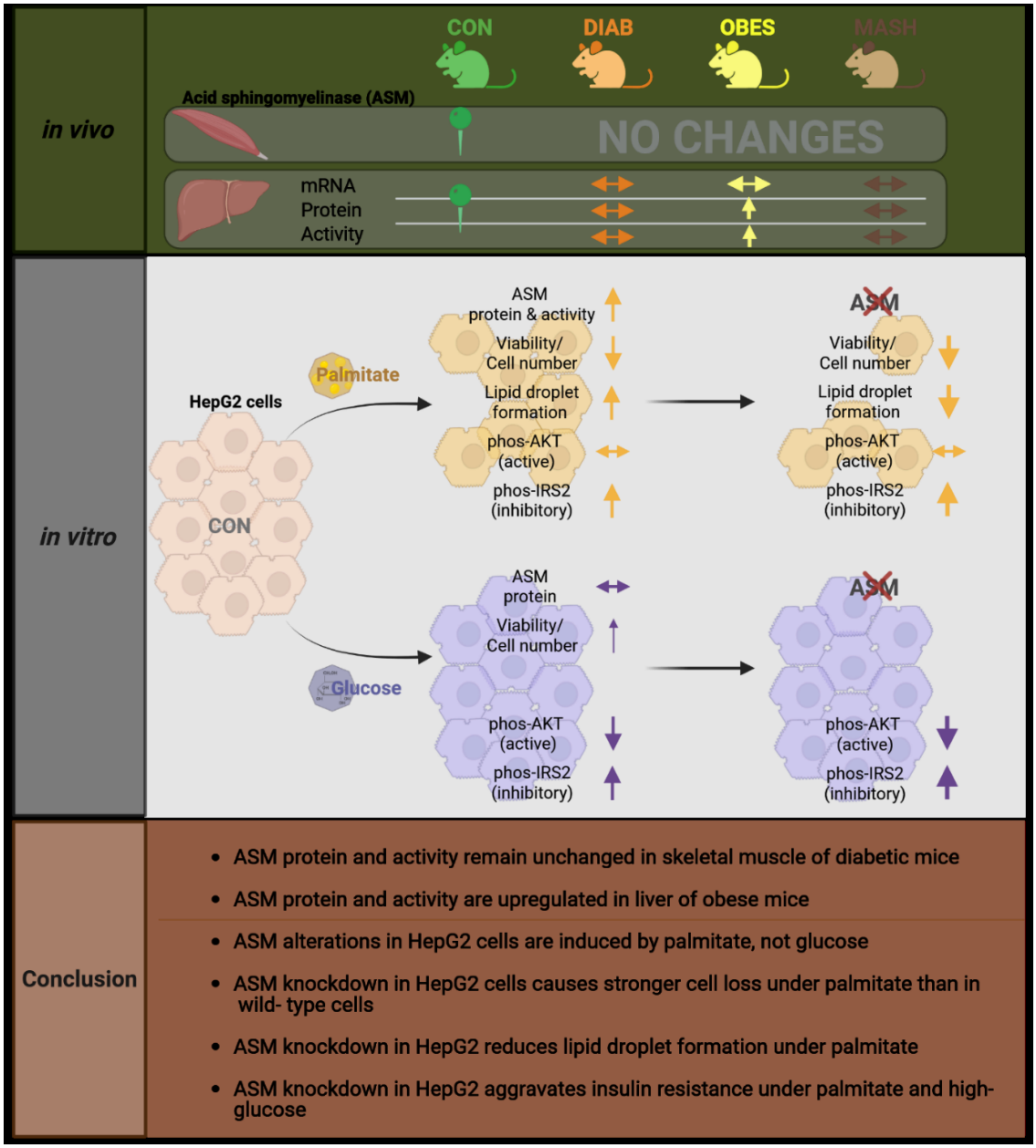

Graphical abstract of unpublished data from the second part of this thesis.

3.2.1 Acid sphingomyelinase protein level is not altered in skeletal muscle of a murine diabetes model

In contrast to human skeletal muscle data, where ASM protein content was decreased in T2D compared to glucose-tolerant individuals, quadriceps of diabetes (DIAB), obesity (OBES) and fatty liver disease (MASH) mouse models showed similar levels of ASM protein in all groups compared to chow-diet (CON) littermates (ASM protein levels in arbitrary units [A.U.] as mean ± SD: DIAB, 0.43 ± 0.2; OBES, 0.57 ± 0.19; MASH, 0.43 ± 0.25; CON, 0.61 ± 0.23). For ASM activity all groups showed similar levels (ASM activity in pmol/µg of protein/min as mean ± SD: DIAB, 0.31 ± 0.12; OBES, 0.41 ± 0.38; MASH, 0.35 ± 0.2; CON, 0.39 ± 0.3).

3.2.2 Hepatic alterations of acid sphingomyelinase protein and activity in a murine diabetes model

3.2.2.1 Acid sphingomyelinase protein level and activity are upregulated in liver tissue of murine obesity model

To further investigate the tissue-specific function of ASM, the levels of ASM mRNA, protein, and activity were assessed in the liver tissue of CON, OBES, DIAB and MASH mice. The levels of ASM mRNA remained similar across the groups, regardless of insulin sensitivity and stages of liver disease progression (Figure 4A). In contrast, ASM protein levels were significantly elevated in the OBES mice compared to all other groups (Figure 4B). ASM activity was also notably higher in the OBES group compared to the CON and DIAB groups (Figure 4C). Interestingly, insulin sensitivity did not impact on ASM protein levels or its activity and no significant differences in ASM protein and activity levels were observed when comparing the DIAB group with the CON group.

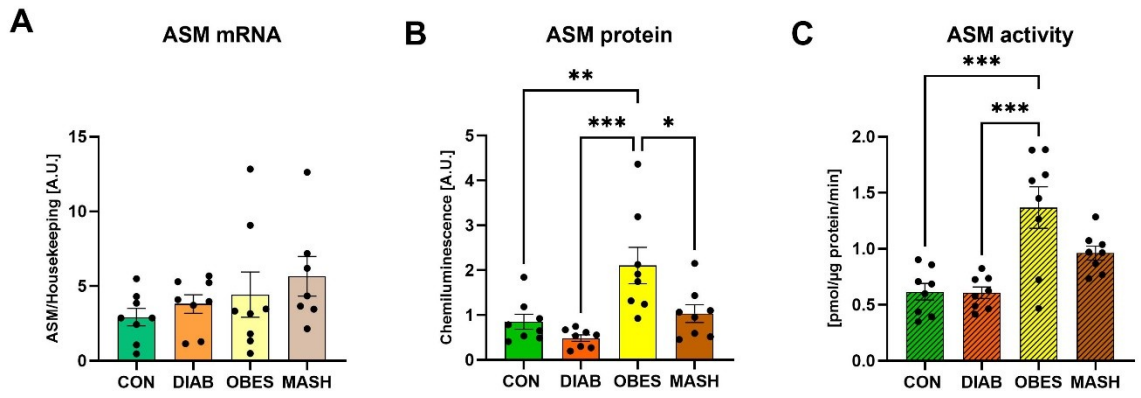

Figure 4: ASM protein level and activity are upregulated in liver tissue of murine obesity model.

(A) ASM mRNA, **(B)** protein and **(C)** enzymatic activity levels in liver tissue from CON (N=8), DIAB (N=8), OBES (N=8) and MASH (N=8) mouse; *p<0.05; **p<0.01; ***p<0.001 based on one-way ANOVA and Tukey`s multiple comparison test, Data represent technical triplicates and the mean absorbance values are presented as one experiment. Data are expressed as mean ± SD.

3.2.2.2 Hepatic acid sphingomyelinase protein and activity correlate with body weight and fat mass.

Next, correlation analyses of liver ASM protein and activity levels with blood glucose, fat mass, and body weight were conducted. ASM protein levels exhibited an inverse correlation with blood glucose levels but showed positive correlations with body weight and fat mass (Figure 5A-C). Similarly, ASM activity did not significantly correlate with blood glucose levels, but displayed positive correlations with body weight and fat mass (Figure 5D-F).

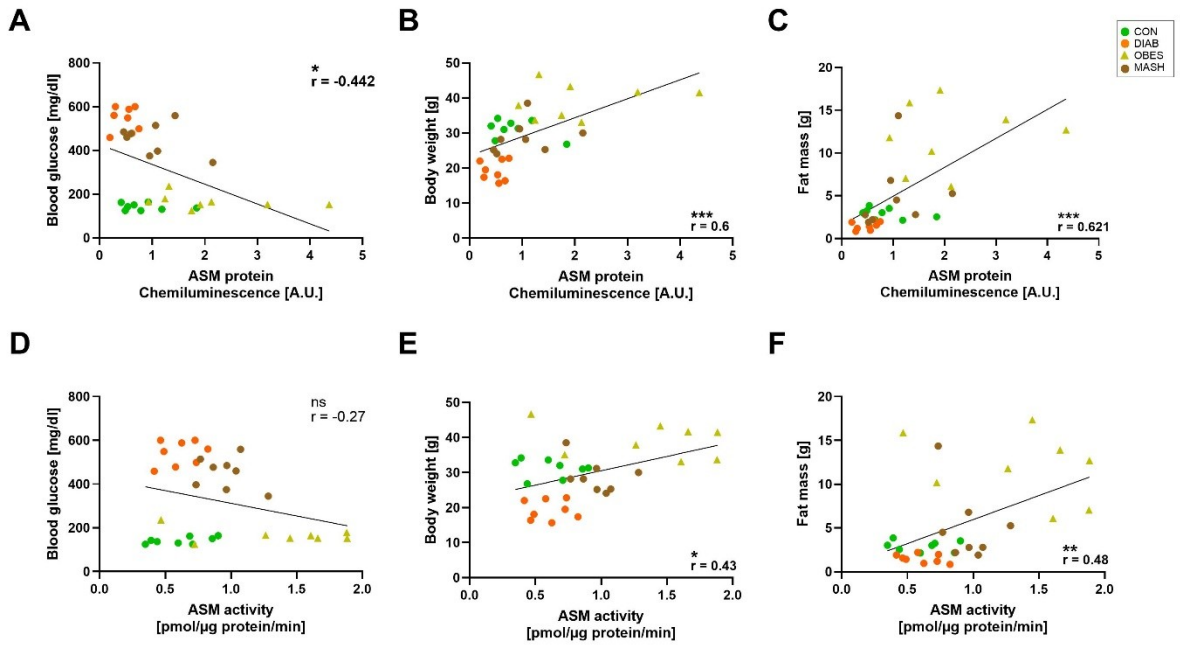

Figure 5: ASM protein level and activity correlate with body weight and fat mass.

Correlation analysis of hepatic ASM protein and enzymatic activity with blood glucose **(A, D)**, body weight **(B, E)** and fat mass **(C, F)** in CON (N=8), DIAB (N=8), OBES (N=8) and MASH (N=8) mice; two-tailed *p<0.05, **p<0.01, ***p<0.001 based on Pearson r-correlation.

Furthermore, as ASM is implicated in inflammatory signaling and apoptosis, correlation analyses were performed of ASM protein and activity with markers of inflammation and fibrosis. These included CD45 (receptor-type tyrosine-protein phosphatase C), F4/80 (EGF-like module-containing mucin-like hormone receptor-like 1 / macrophage marker), monocyte chemoattractant protein-1 (MCP-1), TNF-α, IL-6, collagen type I alpha 1 chain (Col1a1), tissue inhibitor of metalloproteinase 1 (TIMP-1), procollagen type III (PCIII), α- smooth muscle actin (α-SMA), liver collagen level by Sirius Red staining (SR), or hydroxyproline levels none of which showed significant correlation with ASM protein nor activity (Figure S 1A). As abnormalities in mitochondrial have been linked to the progression of MASH (Dewidar et al., 2023), ASM protein and activity were further correlated with FAO-driven mitochondrial respiration, assessed in mechanically permeabilized liver samples with the Oxygraph-2k (Oroboros Instruments, Innsbruck, Austria), as described previously (Dewidar et al., 2023). No significant correlations were observed between ASM protein levels or activity with FAO-driven mitochondrial respiration, plasma NEFA, hepatic TAG content, or distal insulin signaling markers like phos-AKT Thr^{308}/AKT or phos-AKT^{Ser473}/AKT (Figure S 1B).

3.2.3 Acid sphingomyelinase regulation in HepG2 cells under high-glucose or high-lipid conditions

Next, experiments in HepG2 cells were performed under conditions of high-glucose and high-lipid load, in order to elucidate whether the increase in ASM levels observed in the liver of OBES compared to MASH mice, was attributable to the elevated lipid content of the HFD or to alterations in glucose metabolism induced by STZ administration. To ensure that the applied treatments represented suitable *in vitro* conditions, cell viability was first assessed under both glucose and PA exposure. Changes in viability served as a control to confirm that the treatments elicited cellular responses comparable to those described in MASLD. In addition, since PA exposure reflects the progression of MASLD, where hepatic lipid accumulation is characterized by increased LD formation, LD content was also examined.

3.2.3.1 High-glucose does not affect acid sphingomyelinase protein, while high-palmitate increases its expression

High concentrations of glucose lead to glucotoxicity – a key feature of metabolic dysfunction and a hallmark of MASH – and are known to reduce HepG2 cell viability (Chandrasekaran et al., 2010). To assess whether high-glucose exposure affects ASM expression, HepG2 cells were incubated with glucose concentrations ranging from 1 mM to 50 mM, with 5 mM serving as normoglycemic control (CTRL). An osmotic control was included of 5 mM D(+)-glucose with 45 mM D(-)-mannitol. Cells were analyzed after varying timepoints, with detailed data provided in the supplements (Figure S 2). Glucose increased cell viability at 30 mM, 35 mM, and 40 mM compared to CTRL after 48 h of treatment (Figure 6A), whereas higher concentrations reduced viability at later timepoint (Figure S 2B). Western blot analysis demonstrated that ASM protein levels remained unchanged following 48 h of glucose treatment (Figure 6B; Figure S 2 for additional timepoints). To investigate the effects of high-lipid exposure HepG2 cells were treated with PA conjugated to BSA, and cell number and ASM protein expression were analyzed. BSA treatment alone (50-400 µM) had no significant effect on cell number (Figure S 3A/B). Each PA concentration was normalized to the corresponding BSA vehicle control to account for potential vehicle effects. Prolonged exposure significantly reduced cell number at concentrations of 200, 300 and 400 µM after 48 h (Figure 6C), indicating the occurrence of lipotoxicity, although mechanisms

such as caspase activity or fragmented DNA were not assessed. However PA exposure for 48 h gradually increased ASM protein expression at 200 µM and 300 µM compared to CTRL, while with 400 µM PA ASM levels returned to values comparable to CTRL (Figure 6D).

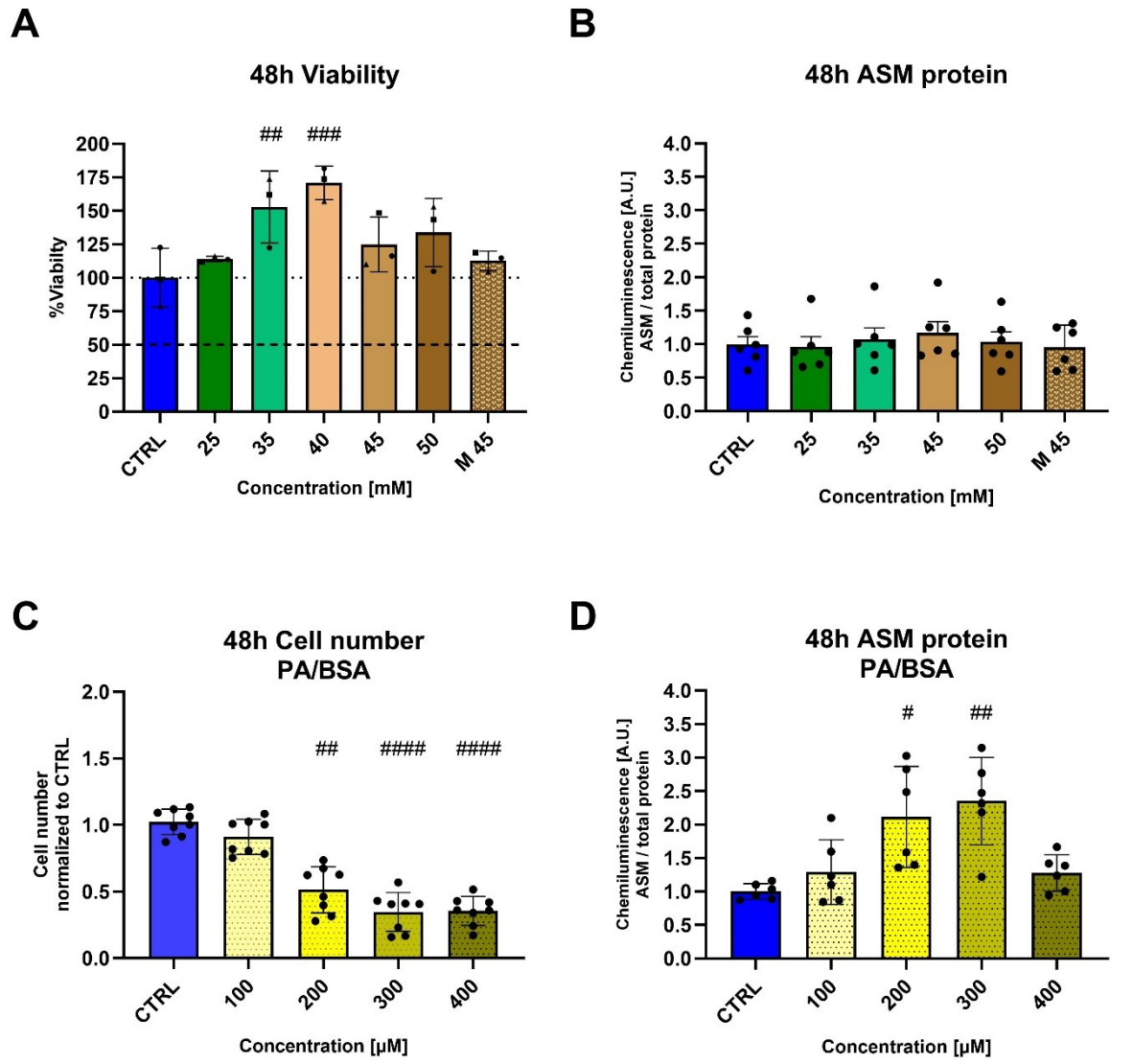

Figure 6: High-glucose does not affect acid sphingomyelinase protein, while high-lipid load increases its expression.

(A) Cell viability assessed via MTT assay with varying glucose concentrations for 48 h. Experiments were conducted with n=3, each containing technical quadruplicates. Values were normalized to the mean of quadruplicates for each biological replicate. **(B)** ASM protein level at varying glucose concentrations for 48 h assessed via Western blot and normalized to total protein (n=6). **(C)** Cell number measured via Hoechst staining after 48 h (n=8) of palmitate (PA) normalized to respective BSA concentration on HepG2 cells and **(D)** respective ASM protein level at varying PA concentrations for 48 h assessed via Western blot and normalized to total protein (n=6). Data expressed as mean ± SD; #p<0.05, ##p<0.01, ###p<0.001, ####p<0.0001 vs untreated control cells (CTRL) based on one-way ANOVA & Dunnett´s multiple comparison test.

3.2.3.2 High-palmitate exposure increases HepG2 lipid droplet formation

To investigate whether the reduction in cell viability observed under PA treatment was preceded by changes in lipid storage, LD formation was analyzed at 24 h and 48 h using BODIPY staining. HepG2 cells were treated with PA conjugated to BSA, with BSA alone serving as vehicle control (data in Figure S 3C/D). After normalization of PA-induced LD formation to the corresponding BSA treatment, a marked increase in LDs was detected after 24 h at concentrations of 50, 100, and 200 µM compared to CTRL (Figure 7A). This increase became more pronounced after 48 h of PA exposure, with elevated LD formation at all concentrations tested HepG2 cells (Figure 7B).

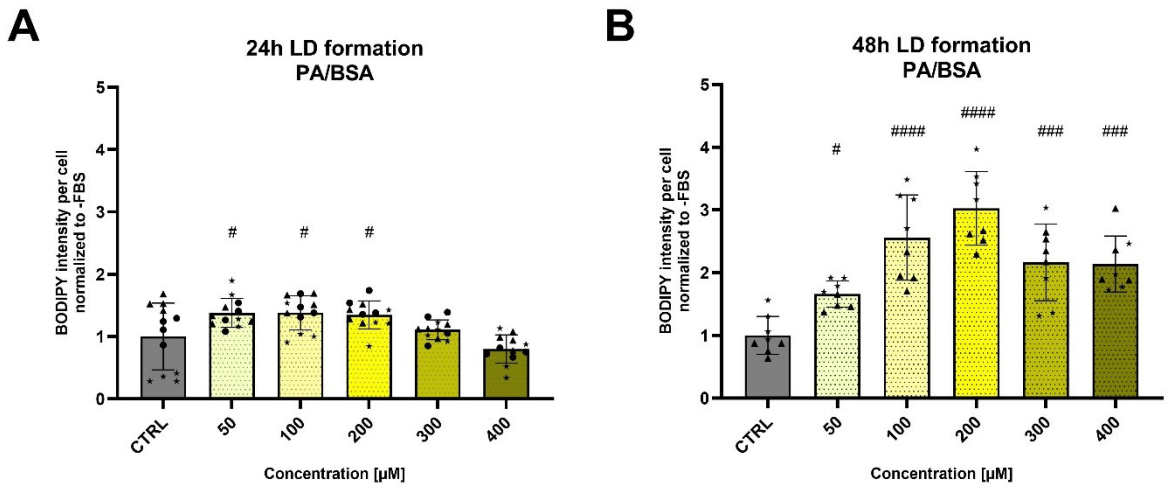

Figure 7: High-palmitate exposure increases HepG2 lipid droplet formation.

Lipid droplet (LD) formation measured via BODIPY staining in HepG2 cells after **(A)** 24 h (n=12) and **(B)** 48 h (n=8) of palmitate (PA) - & BSA-treatment shown as ratios. Values were normalized to the mean of untreated cells (CTRL). Data expressed as mean ± SD; #p<0.05, ###p<0.001, ####p<0.0001 vs CTRL based on one-way ANOVA & Dunnett´s multiple comparison test.

3.2.4 Knockdown of acid sphingomyelinase in HepG2 cells via siRNA

The above findings show that PA decreases cell count and increases the formation of LD as well as ASM protein content in HepG2 cells, suggesting a potential link between ASM protein and the observed lipotoxic effects.

Thus, the impact of ASM downregulation on cell viability and LD formation under PA treatment was investigated. Knockdown (KD) efficiency was assessed by measuring the levels of ASM mRNA, protein, and enzymatic activity at 24 h, 48 h, 72 h, and 96 h post-transfection (Figure S 4). ASM mRNA levels, measured via qRT-PCR, were reduced by ~78 % after 48 h, followed by a decrease in protein expression (~69%) and

enzymatic activity declined by ~66% at 72 h post transfection, as compared to cells treated only with the transfection reagent (vehicle) (Figure S 4).
For all subsequent experiments, only samples with knockdown efficiency ≥65% for both ASM protein and enzymatic activity were considered for the analysis.

3.2.4.1 Knockdown of acid sphingomyelinase aggravates palmitate-driven cell loss and impairs lipid droplet formation

Once the efficiency of ASM KD via siRNA was confirmed, as shown by reduced mRNA, protein and activity levels, the effect of the KD on cell viability was assessed. As expected, treatment with the transfection reagent (vehicle-Metafecten) or siRNA (ASM KD) alone did not affect cell number compared to untreated cells (CTRL) after 24 h and 48 h (Figure S 5A/B). Likewise, BSA treatment had no significant impact on cell number in either ASM KD or wild-type HepG2 cells compared to CTRL (Figure S 5A/B). After normalization of PA to the respective BSA concentrations, a stronger reduction in cell number was observed in ASM KD cells compared to wild-type cells following 24 h of treatment (Figure 8A). Unpaired t-tests confirmed significant differences between KD and wild-type cells at all PA concentrations tested (data not shown). After 48 h, the reduction in cell number became more pronounced, and even lower PA concentrations already caused a detectable decrease compared to wild-type cells (Figure 8B). ASM KD exacerbated the PA-induced reduction in cell number by ~29.5% after 24 h and by ~14.2% after 48 h compared to wild-type cells. This enhanced loss of viability was unexpected and prompted the suggestion that LD formation may also be impaired in ASM KD cells. Thus, LD formation was analyzed by BODIPY staining (Figure S 5C/D). Comparison of PA treatment normalized to the respective BSA control revealed increased LD formation at 24 h and 48 h in wild-type cells, whereas this response was absent or even reduced in ASM KD cells compared to CTRL (Figure 8C/D).

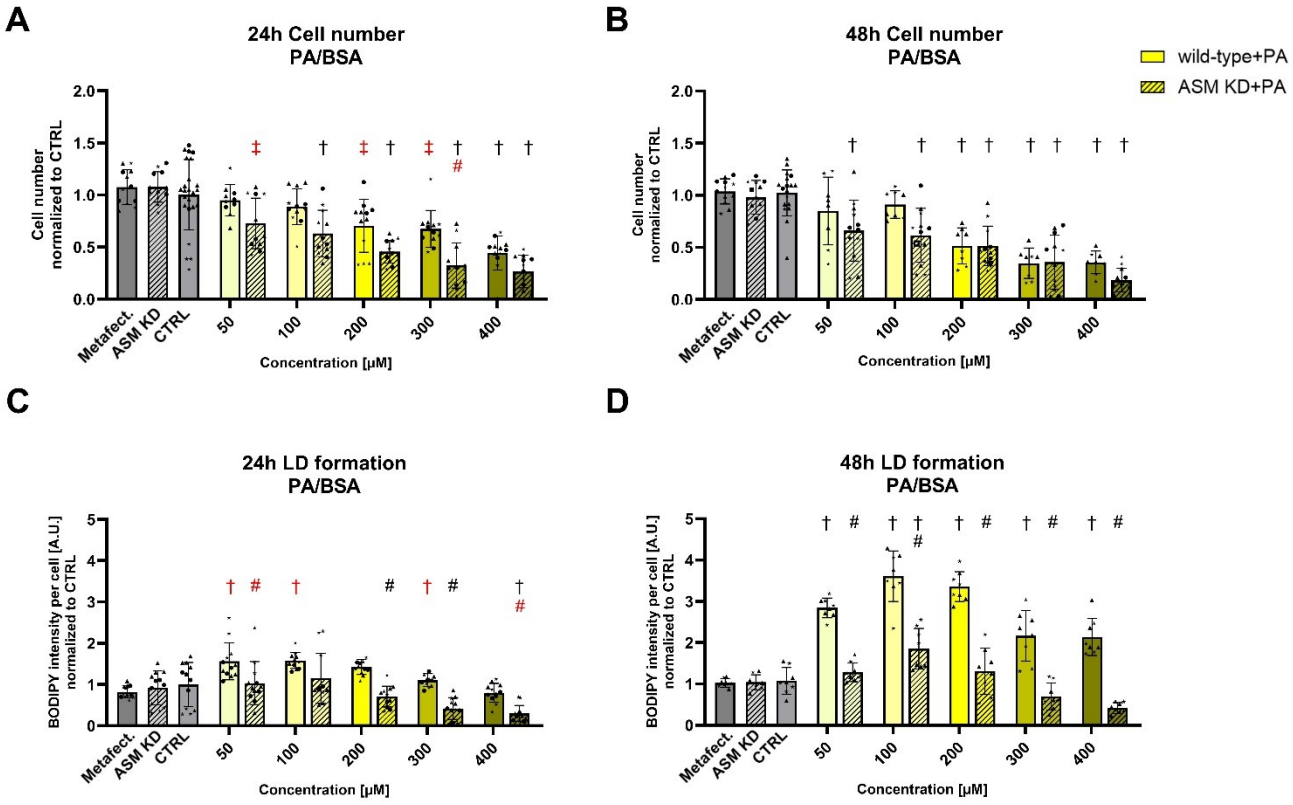

Figure 8: Knockdown of ASM aggravates palmitate-driven cell loss and impairs lipid droplet formation.

Cell number measured via Hoechst staining after **(A)** 24 h (n=12) and **(B)** 48 h (n=8-12) of palmitate (PA) - & BSA-treatment ratios in HepG2 wild-type and ASM knockdown (KD) cells and normalized to mean of untreated cells (CTRL). Lipid droplet (LD) formation measured via BODIPY staining after **(A)** 24 h (n=12) and **(B)** 48 h (n=8) of palmitate (PA) - & BSA-treatment ratios in HepG2 wild-type and ASM knockdown (KD) cells. Data expressed as mean ± SD; ‡<0.05, †<0.01, †p<0.001 vs CTRL; #p<0.05, #p<0.001 vs wild-type based on one-way ANOVA & Tukey´s multiple comparison test, unpaired t-test not shown.

3.2.4.2 Knockdown of acid sphingomyelinase aggravates palmitate- or high-glucose-induced insulin resistance

The previous results demonstrated that PA treatment led to an upregulation of ASM protein in wild-type HepG2 cells (Figure 7D), and that ASM KD results in decreased cell number and LD formation (Figure 8) upon PA treatment. These findings suggest that ASM plays a protective role against lipotoxicity in hepatoma cells in contrast to the initial hypothesis. As no correlations between ASM and distal insulin signaling (phosAKT/AKT) were observed in the MASLD mouse model, but ASM can localize at the plasma membrane and regulate membrane composition, the analysis was extended to proximal insulin signaling. Given that lipotoxicity is implicated in the

development of insulin resistance, only PA concentrations presumed to cause minimal lipotoxicity were selected to specifically investigate the early onset of insulin resistance. Phos-AKT^{Ser473}/AKT levels were reduced not solely by PA but also by respective BSA concentrations compared to untreated CTRL, indicating potential vehicle effects and making it uncertain whether the impairment reflects PA itself or components within the BSA preparation (Figure S 6C). Accordingly, no significant effect of PA treatment was observed on distal insulin signaling (phos-AKT^{Ser473}/AKT), in either wild-type or ASM KD cells, analyzing the ratios PA/BSA (Figure 9A). In contrast, proximal insulin signaling (phos-IRS2^{Ser388}/IRS2) was selectively impaired by PA treatment, with stronger effects in ASM KD cells (Figure 9B), while BSA alone showed no effect (Figure S 6D).

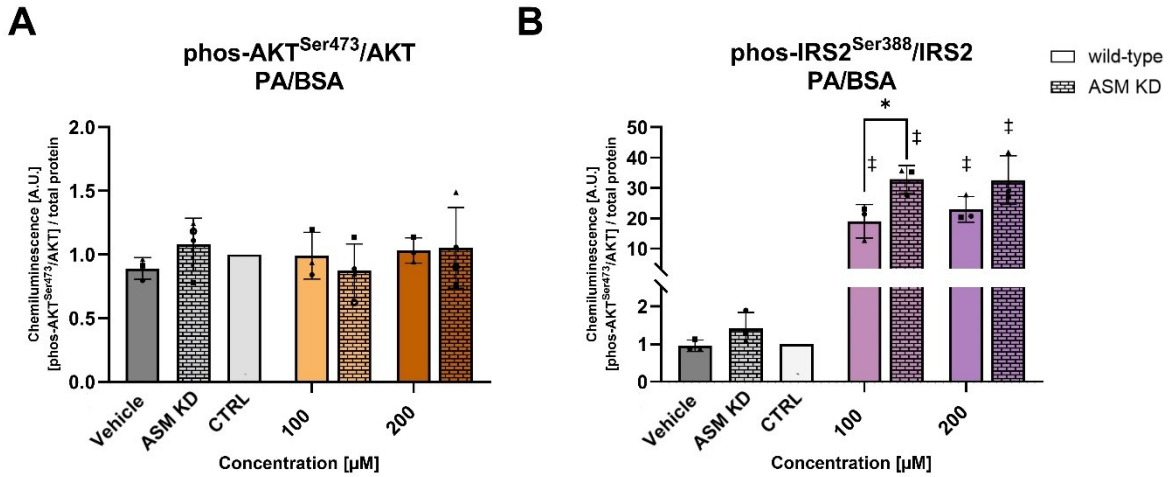

Figure 9: ASM knockdown in HepG2 cells inhibits proximal insulin signaling pathway in response to palmitate treatments compared to wild-type cells.

Western-Blot analysis of HepG2 wild-type and ASM knockdown (KD), following palmitate (PA) treatment for 48 h and 10 nm insulin for 10 min. Ratios of PA/BSA of each condition and treatment concentration, normalization to untreated cells (CTRL) as inter-run calibrator (IRC). **(A)** Ratio phos-AKT^{Ser473}/AKT (n=3-4) and **(B)** ratio phos-IRS2^{Ser388}/IRS2 (n=3). Data expressed as mean ± SD; ‡p<0.001 vs CTRL; *p<0.05 vs wild-type, based on one-way ANOVA & Tukey´s multiple comparison test.

In the MASLD mouse model ASM protein showed a negative correlation with blood glucose levels, despite showing no associations with distal insulin signaling and was not altered by varying glucose concentrations. However, PA treatment in HepG2 cells indicated that ASM acts at the level of proximal insulin signaling, the analysis was extended to high-glucose conditions.

Figure 10A shows that high glucose (35 mM, 45 mM, 50 mM) led to a reduction in distal insulin signaling in wild-type cells, as evidenced by decreased phos-AKT^{Ser473}/AKT

ratios compared to normoglycemic CTRL cells. This impairment was even more pronounced in ASM KD, where a significant reduction in insulin signaling was already observed at 25 mM glucose (Figure 10A). Interestingly, wild-type cells treated with high glucose showed a gradual inhibition of IRS2 with increasing glucose concentrations, although this was not significantly different from normoglycemic CTRL. In contrast, ASM KD cells displayed greater inhibitory effects under high-glucose treatment, as indicated by increased phos-IRS2^{Ser388}/IRS2 levels, with significant differences observed at 45 mM and 50 mM glucose treatments compared to CTRL. Notably, at 50 mM glucose, the inhibitory effect was significantly more pronounced in ASM KD cells than in wild-type cells (Figure 10B).

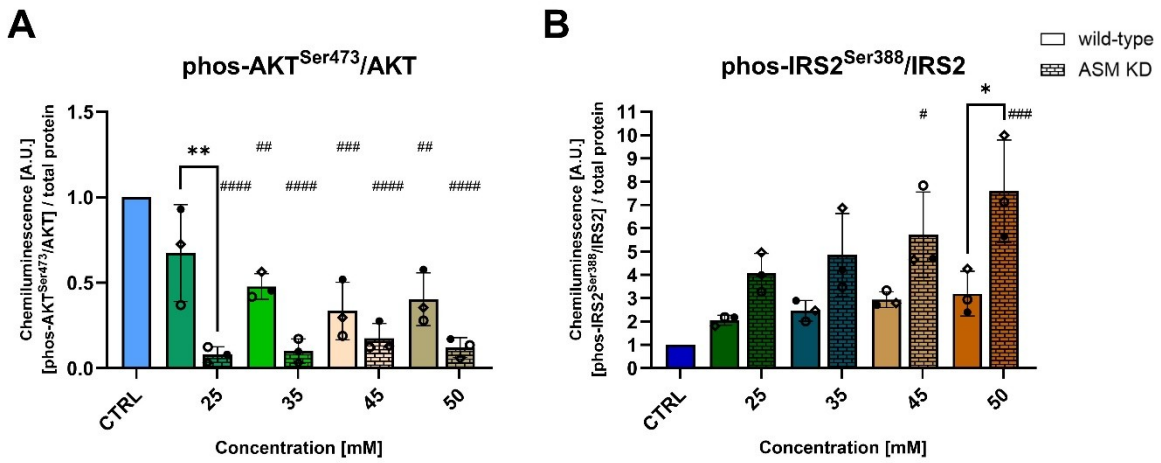

Figure 10: ASM knockdown in HepG2 cells increases insulin resistance in response to high-glucose treatment compared to wild-type.

Western-blot analysis of HepG2 wild-type and ASM knockdown (KD) cells, following glucose treatment for 48 h and 10 nm insulin for 10 min. **(A)** Ratio phos-AKT^{Ser473}/AKT and **(B)** ratio phos-IRS2^{Ser388}/IRS2. Data expressed as mean ± SD; #p<0.05, ##p<0.01, ###p<0.001, ####p<0.0001 vs CTRL; *p<0.05, **p<0.01 vs wild-type, based on one-way ANOVA & Tukey´s multiple comparison test

4 Discussion

This dissertation aimed to advance our understanding on the role and modulation of ASM in lipid-induced insulin resistance, with a particular emphasis on its tissue-specific functions. In the first section of this thesis human studies were conducted to evaluate ASM protein levels and activity in the skeletal muscle of IS, IR, and T2D individuals undergoing a 12-week training intervention. The results revealed that basal ASM protein levels are significantly affected by the metabolic status of individuals. Furthermore, our findings highlighted that ASM plays a crucial role in exercise-induced changes in mitochondrial dynamics, which appear to be independent of ceramide accumulation. This observation underscores the potential of ASM as a modulator of mitochondrial function beyond its established role in ceramide synthesis. In the second section of this thesis, another important aspect was the investigation of the molecular mechanisms through which ASM influences liver lipid metabolism and its implications in T2D-associated comorbidities, including the progression of liver fibrosis. Previous research has shown that the absence of ASM confers protection against hepatic fibrosis, underscoring the pivotal role of ASM in the pathophysiology of liver disease. However, our findings challenge this view by suggesting a more nuanced, context-dependent role of ASM. ASM expression and activity are upregulated in response to PA treatment, which reduces cell viability and increases formation of LD. Furthermore, ASM KD led to a marked reduction in cell number and LD formation under lipotoxic conditions, indicating that ASM may actually support cell viability and lipid storage capacity during metabolic stress. These results point to a potentially protective or adaptive role of ASM in early lipid handling.

Moreover, ASM KD cells exhibited a more pronounced impairment in insulin signaling, particularly at the level of proximal signaling, following both high-lipid and high-glucose exposure. These findings support the notion that ASM modulates insulin sensitivity not only through ceramide accumulation but also via alternative mechanisms, potentially involving plasma membrane integrity.

Overall, this dissertation provides novel insights into the tissue-specific role of ASM in metabolic regulation. By integrating findings from human studies and mechanistic *in vitro* models, this work broadens our understanding of ASM as a complex modulator of lipid metabolism, insulin signaling, and mitochondrial dynamics.

4.1 Extended discussion of published findings

4.1.1 Acid sphingomyelinase is implicated in mitochondrial adaptations and plasma membrane remodeling in skeletal muscle

The first section of this thesis showed that (i) ASM protein is downregulated in skeletal muscle of T2D individuals as compared to glucose-tolerant humans; (ii) exercise training enhances ASM activity along with increases in specific ceramides - particularly the C24:0 and C24:1 species; and (iii) changes in ASM protein and activity are linked to modifications in MFN2 and AMPK-dependent mitochondrial quality control, rather than to whole-body insulin sensitivity.

Based on our data, it can be hypothesized that ASM supports exercise-induced metabolic remodeling primarily through its canonical role in sphingomyelin hydrolysis. Indeed, ceramides can be further metabolized into bioactive lipids, such as S1P, which promotes cell differentiation and proliferation (Maceyka et al., 2002) as well as muscle adaption by regulating fatigue resistance (Cordeiro et al., 2019), repair mechanisms (Calise et al., 2012; Donati et al., 2013) and cytoskeletal remodeling (Cordeiro et al., 2019; Sassoli et al., 2019). Indeed, increased S1P levels have been observed in human and animal skeletal muscle following various exercise regimens (Baranowski et al., 2015; Bergman et al., 2016b; Błachnio-Zabielska et al., 2008), suggesting that exercise stimulates the conversion of ceramide to sphingosine and its subsequent phosphorylation to S1P (Bergman et al., 2016b). Rodent studies further indicate that acute exercise increases ASM protein levels, suggesting that exercise promotes sphingomyelin degradation and subsequent ceramide production (Lee and Leem, 2019). Overexpression of ASM in hepatocytes also activates this pathway, which show higher ceramide levels- but not as high as expected from sphingomyelin breakdown alone - suggesting that some ceramide is further metabolized to S1P. This metabolic pathway may underlie insulin-like effects mediated by S1P through AKT activation (Osawa et al., 2011). Although some studies report that acute exercise elevates both ceramides and S1P (Bergman et al., 2016a; Helge et al., 2004), increases in sphingomyelin levels have been observed in untrained, but not in trained, individuals, suggesting that sphingomyelin degradation is not the sole contributor to exercise-induced ceramide and S1P accumulation (Helge et al., 2004). This aligns with our findings in IR and T2D individuals, where the HIIT-induced increase in specific ceramide species did not coincide with a reduction in sphingomyelin species, indicating

that these ceramides likely originate from alternative pathways such as *de novo* synthesis rather than sphingomyelin hydrolysis.

Beyond sphingolipids, exercise-induced remodeling of plasma membrane phospholipids may further improve insulin sensitivity. Both acute and long-term (12-week) exercise interventions have been shown to increase the absolute levels of PC and PE while concurrently reducing the PC:PE ratio in normoglycemic and prediabetic individuals, (Lee et al., 2018), which is associated with improved membrane integrity, calcium handling, and optimized insulin receptor kinetics (Lee et al., 2018). Another study found that baseline levels of PC and PE were higher in athletes compared to obese and T2D subjects, but their response to exercise varied: levels decreased in athletes, remained unchanged in obese individuals, and increased in those with T2D (Newsom et al., 2016). However, the PC:PE ratio did not change in response to exercise and was inversely correlated with insulin sensitivity across the whole cohort. (Newsom et al., 2016).

ASM may contribute to this membrane remodeling mainly by hydrolyzing sphingomyelin rather than cleaving phosphocholine residues from PC to form sn1,2-DAG. This preference is regulated by lipid metabolites such as DAGs, ceramides, NEFAs, and cholesterol, which enhance sphingomyelin hydrolysis while inhibiting PC cleavage (Breiden and Sandhoff, 2021; Oninla et al., 2014). In fibroblasts and liver, ASM-derived ceramide and sphingosine can also reduce PC biosynthesis through two mechanisms. First, ceramides directly inhibit CTP:phosphocholine cytidylyltransferase (CCT), a key enzyme in the CDP-choline pathway, thereby reducing *de novo* PC synthesis (Bladergroen et al., 1999; Ramos et al., 2002; Ramos et al., 2003). Second, sphingosine, generated from ceramide via CDase, has been shown to further suppresses CCT activity (Sohal and Cornell, 1990). Additionally, ASM-mediated depletion of S-adenosylmethionine (SAM) may impair the PEMT pathway, further limiting PC production through reduced PE methylation (Marí et al., 2004). Thus, decreased hepatic PC levels may result from both impaired methylation and direct inhibition of CCT. This dual mechanism is supported by evidence from ASM knockout mice, which exhibit elevated hepatic PC levels (Prinetti et al., 2011), as well as liver samples from MASH individuals, where increased ASM mRNA goes along with a reduced PC:PE ratio (Li et al., 2006; Moles et al., 2010b). While ASM-mediated PC reduction appears to be beneficial for hepatic metabolism and glucose homeostasis, its effects in skeletal muscle may differ. Despite acting through similar pathways, ASM

may influence muscle membrane integrity via modulation of the PC:PE ratio with opposing physiological outcomes. Two possible mechanisms could explain this: (i) direct hydrolysis of PC, though this is unlikely given that ceramides and DAGs inhibit ASM-driven PC cleavage, or (ii) indirect suppression of PC synthesis due to ceramide- and sphingosine-mediated inhibition of the CDP-choline pathway and PEMT activity. Thus, ASM may contribute to membrane composition remodeling during chronic exercise by lowering PC levels through ceramide generation and consequently enhancing membrane stability in skeletal muscle.

Beyond possible effects on plasma membrane composition, ASM may also act directly at mitochondria. In line with our correlation data, an RNA sequencing localization study has revealed the presence of ASM mRNA on the mitochondrial outer membrane (Fazal et al., 2019). Consistent with these observations, Karunakaran et al. recently demonstrated that inhibition of ASM, and thus reduced ceramide generation, attenuates chemotherapy-induced pancreatic β-cell dysfunction by lowering mitochondrial ROS production through aldehyde dehydrogenase 2 (ALDH2) and casein kinase 2 (CK2) signaling pathways (Karunakaran et al., 2024). Furthermore, ASM expression has been shown to influence mitochondrial fusion and morphology in mouse melanoma cells (Coazzoli et al., 2020), and its mitochondrial localization has been suggested (Matsumoto et al., 2003). Together, these studies support our findings and lead to the hypothesis that the phospholipid-cleaving activity of ASM near or on the mitochondrial membrane might directly modulate mitochondrial fusion and fission events. However, comprehensive studies are still needed to confirm the potential involvement of ASM in plasma membrane modulation and mitochondrial functions.

4.2 Unpublished data on regulation of acid sphingomyelinase in skeletal muscle of murine diabetes model, liver and hepatoma cell models

The second part of this thesis focuses on mechanistic studies aimed at elucidating tissue-specific roles of ASM under metabolic stress conditions. In contrast to human skeletal muscle, where ASM protein were reduced in T2D compared to glucose-tolerant individuals, no alterations were observed in skeletal muscle of murine models of diabetes, obesity, and fatty liver disease diabetes, suggesting that ASM changes are exercise-driven and absent without such a stimulus. In these same models,

however, metabolic stress induced ASM changes in the liver. Because access to human liver tissue was not feasible, hepatoma cells exposed to high-lipid or high-glucose stimuli were used to further elucidate the underlying molecular mechanisms. Hepatic insulin resistance is an early hallmark of MASLD, and lipotoxic conditions such as elevated ceramides are known to impair insulin signaling. Therefore, this section also examined whether ASM contributes to tissue-specific lipid handling and affects insulin signaling, suggesting a context-dependent role in metabolic regulation.

4.2.1 Hepatic acid sphingomyelinase is upregulated in obesity and modulates lipid storage and metabolic flexibility

Elevated ASM gene expression has been documented in individuals with MASLD and shown to correlate with disease severity (Moles et al., 2010a). Experimental whole body inhibition or genetic knockout of ASM has further been shown to prevent HFD- or carbon tetrachloride-induced hepatic fibrosis, positioning ASM as a promising therapeutic target (Fucho et al., 2014; Quillin et al., 2015). Previous studies have also demonstrated that MCD-induced liver injury is associated with increased ASM activity. For instance, Caballero et al. observed a rapid rise in ASM activity and ceramide levels in the liver within two days of MCD or methionine-deficient diet (Caballero et al., 2010). In this study, no differences in hepatic ASM mRNA levels were observed in DIAB and MASH mouse models as compared to control. However, ASM protein levels were significantly upregulated in the OBES mouse group compared to all other groups, while ASM activity was elevated relative to the CON and DIAB groups. Interestingly, this finding contrasts with research by Chocian et al., which reported decreased ASM activity in the livers of HFD-fed rats (Chocian et al., 2010). Furthermore, whole-cohort analysis revealed that ASM protein and activity correlated positively with body weight and fat mass, while ASM protein levels inversely correlated with blood glucose levels. These results suggest that elevated glucose levels may suppress the HFD-induced rise of ASM activity, potentially reflecting the metabolic consequences of hyperglycemia.

It is well-established that mitochondrial adaptions in FAO and altered oxidative phosphorylation play a critical role in the progression of MASLD (Fromenty and Roden, 2023) and that ceramides are implicated in modulating mitochondrial FAO (Fucho et al., 2017). For instance genetically induced shifts in ceramide chain length strongly affect mitochondrial function. Mice with CerS2 deficiency (↓C22:0/C24:0, ↑C16:0) show

reduced PA oxidation capacity and diminished activity of ETC complex II and IV under HFD compared to wild-type littermates (Hajduch et al., 2021), whereas CerS6 deletion (↓C16:0) enhances PA oxidation and mitochondrial respiration (Hajduch et al., 2021). Furthermore, ceramides can directly impair mitochondrial respiration by inhibiting the ubiquinone pool of complex III and affecting NADPH oxidase activity (Holland and Summers, 2008). Moreover, ceramides can specifically target mitochondria for autophagic clearance - a process that may reduce FAO capacity (Scarlatti et al., 2004; Sentelle et al., 2012). Ceramide synthesis can be induced by TNF-α via tumor necrosis factor receptor 1 (TNFR1)-mediated activation of ASM, leading to increased ROS production and subsequent altering mitochondrial function in hepatocytes (Colell et al., 2002; García-Ruiz et al., 2003; Schwabe and Brenner, 2006). Hence, the correlation of FAO-driven mitochondrial respiration with ASM expression was assessed. Although previous evidence links ASM and ceramides to mitochondrial FAO, a whole-cohort analysis revealed no correlations between ASM protein levels or activity and mitochondrial FAO. Collectively, these data do not support the notion that ASM-derived ceramides directly influence mitochondrial FAO in the used MASLD mouse model.

Further analyses also revealed that neither ASM protein levels nor its activity correlated with key markers of inflammation (e.g., TNF-α) or fibrosis (e.g., α-SMA). This finding is unexpected given that previous studies have demonstrated that TNF-α activates ASM and that ASM depletion confers resistance to TNF-α-induced apoptosis in mouse hepatocytes (García-Ruiz et al., 2003; Marí et al., 2004). Additionally, the present results did not support the findings by Moles et al. who reported that ASM activity increased during the *in vitro* activation of hepatic stellate cells (HSCs), characterized by upregulation of α-SMA, and that chemical inhibition of ASM markedly reduced α-SMA protein and mRNA levels. (Moles et al., 2010b). These discrepancies may be explained by differences in experimental models. Indeed, Moles et al. employed isolated HSCs or the LX2 human cell line, whereas our study was based on whole liver homogenates from MASLD mouse model.

4.2.2 Acid sphingomyelinase expression is unaltered under hyperglycemia and does not mediate glucotoxicity

HepG2 cells were exposed to high concentrations of glucose, to investigate whether ASM protein levels are affected by hyperglycemia. Although glucotoxicity is associated with caspases activation, mitochondrial cytochrome c release, and ER stress (Jiang et

al., 2020; Sharma et al., 2011) and ASM-driven ceramide mediated apoptosis (Gulbins et al., 2015), prolonged high-glucose exposure reduced cell viability without changing ASM expression. Therefore, these data indicate that ASM is not involved in the specific mechanisms leading to glucotoxicity and cell death in HepG2 cells.

These results suggest that hyperglycemia does not exert either a stimulatory or inhibitory effect on ASM protein levels in HepG2 cells. It could be further speculated that factors like hyperinsulinemia may underlie the unaltered ASM levels observed in the DIAB and MASH mice model groups.

4.2.3 Palmitate treatment induces acid sphingomyelinase activity and lipid droplet formation and lowers cell viability

The liver becomes susceptible to lipotoxicity when the influx of NEFAs - primarily derived from adipose tissue lipolysis or dietary intake - exceeds its ability to oxidize or export lipids. This imbalance leads to the formation of LDs, which initially serve as a protective mechanism against fatty acid toxicity but may exacerbate steatosis when lipid homeostasis is disrupted (Alsabeeh et al., 2018). Elevated levels of circulating NEFAs, especially PA, are strongly associated with insulin resistance, mitochondrial proton leak, ROS formation, ER stress, inflammation and the progression of metabolic diseases, such as T2D and MASLD (Egnatchik et al., 2014; Gao et al., 2018; Mota et al., 2016; Nakamura et al., 2009; Peng et al., 2011; Shi et al., 2018; Zhang et al., 2012). Studies using HepG2 cells have demonstrated that PA treatment could be used as *in vitro* HFD-induced fatty liver model (Krishnan et al., 2018), and that it induces mitochondrial calcium overload, oxidative stress, and apoptosis through the activation of the JNK cascade and ceramide accumulation (Alsabeeh et al., 2018; Gao et al., 2010; Malhi et al., 2006; Zhang et al., 2012; Zhu et al., 2016). These mechanisms not only impair insulin signaling but also propagate inflammatory responses, contributing to systemic metabolic dysregulation (Pardo et al., 2015).

To investigate the role of ASM in lipid-induced insulin resistance, HepG2 cells were exposed to PA, in order to model lipotoxicity and insulin resistance *in vitro*. In cell culture experiments, the molar ratio of fatty acids to bovine serum albumin (FA:BSA) is critical in determining the extent and nature of lipotoxic effects and influences the fraction of unbound fatty acids available for cellular uptake. (Alsabeeh et al., 2018; Oliveira et al., 2015). Physiological serum FA:BSA ratios typically range from 1:1 to 3:1, but these ratios can rise to 5:1 in disease states such as obesity and MASLD,

further exacerbating lipotoxicity (Kleinfeld et al., 1996; Yamato et al., 2007). Given the importance of this parameter, the molar ratio of 6:1 was used, known to induce lipotoxicity *in vitro* (Alnahdi et al., 2019). Unfortunately, many studies do not explicitly report the FA:BSA ratios used in their PA treatments, complicating the comparison of results and limiting the interpretive strength of such studies. In the present study the used PA-BSA treatment caused a progressive, dose-and time-dependent decline in HepG2 cell viability, as previously shown (de Sousa et al., 2021; Maseko et al., 2024; Zeng et al., 2020). In addition, BSA treatment alone did not result in significant differences in LD formation, as assessed by BODIPY staining. Moreover, a 24 h exposure to PA resulted in a dose-dependent increase in LD formation. These observations are consistent with previous studies utilizing Oil Red O or Nile Red staining, which reported enhanced LD accumulation following 24 h PA treatment at concentrations of 200-250 µM, though the molar ratios in these studies were not specified (Fang et al., 2024; Mayer et al., 2020; Weng et al., 2023) Notably, further increases in PA concentration did not led to additional LD formation at the 24 h time point. However, prolonged PA exposure for 48 h resulted in increased LD accumulation across all treatment groups, with more pronounced effect at intermediate (100-200 µM) concentrations rather than at the highest concentrations. This finding suggests that there may be a saturation threshold for LD formation. Eynaudi et al. (2021) similarly reported maximal LD content, assessed by BODIPY staining, after 6 h of treatment with 200 µM PA, followed by a declining with multiple, smaller mitochondria associated LDs at 18 h exposure (Eynaudi et al., 2021). These mitochondria exhibited a higher membrane potential (Δψ_m) and increased ATP production (Eynaudi et al., 2021). Another study shows that exposing HepG2 cells to 2 mM PA for 12 and 24 h caused less lipid accumulation than 0.5 or 1 mM PA, suggesting cytotoxic effects at high PA concentrations even over short treatment periods (Gómez-Lechón et al., 2007). Collectively, we observed that LD accumulation is reduced at high-PA concentrations over prolonged exposure along with decreased cell viability, supporting the hypothesis that increased LD formation functions as a protective mechanism against lipotoxicity by sequestering excess fatty acids into TAGs, which are less harmful to the cell (Alsabeeh et al., 2018; Mashek, 2021). Nevertheless, once the capacity for LD formation is exceeded, lipotoxic effects become apparent. It is important to note that the protective role of LDs is not solely dependent on their abundance but also on their size, composition, and dynamic interactions with

other cellular compartments, critical for lipid metabolism and signaling (Mashek, 2021). Analysis of ASM protein and activity revealed no significant change within 24 h of PA treatment. However, prolonged PA exposure led to an increase in ASM levels at moderate concentrations (200–300 µM), which then returned to control levels at 400 µM. To the best of current knowledge, these findings appear to be novel. While it is well established that PA treatment increases *de novo* ceramide synthesis in HepG2 cells (Charytoniuk et al., 2019; Deevska et al., 2017; Frandsen et al., 2022), changes in ASM activity under PA exposure have not been reported. The present results suggest that ASM may contribute to ceramide accumulation under conditions of moderate lipotoxic stress (Chaurasia and Summers, 2021; Delcheva et al., 2024). But the absence of further ASM elevation at high PA exposure points to a temporally limited role or association with additional cellular processes.

4.2.4 Acid sphingomyelinase protects from early onset of lipotoxicity

Next, the impact of ASM KD on cell viability and LD formation was assessed, to determine whether ASM contributes specifically to early lipotoxic responses. This study shows that ASM KD did not affect cell viability and that PA exposure resulted in a more pronounced reduction in cell number in ASM KD compared to wild-type cells. This effect was particularly evident after 24 h of PA treatment at lower to mid-range concentrations (50-300 µM), suggesting that reduced ASM activity exacerbates PA-induced lipotoxicity. In parallel, LD formation appears to be impaired in the absence of ASM, which may compromise lipid storage capacity and cellular adaptation to PA-induced stress leading to the suggestion that ASM is required for efficient LD biogenesis during lipotoxic stress. The reduced LD abundance in ASM KD cells is unlikely to result from enhanced LD consumption, as differences were evident only under PA exposure, indicating a failure to induce rather than maintain LD formation. Similarly to these findings, cell-based studies have demonstrated that high-glucose concentrations increase LD accumulation in primary hepatocytes, an effect that is attenuated by pharmacological inhibition or KD of ASM (Osawa et al., 2011), while ASM inhibition with desipramine in PA-treated HepG2 cells likewise reduced intracellular TAG levels compared to untreated controls (Deevska et al., 2009). Together, these observations support a context-dependent function of ASM in lipid metabolism, influenced by both cell type and the nature of the metabolic stressor.

Impaired LD storage may force excess fatty acids toward mitochondrial FAO, increasing ROS production and subsequent lipotoxicity, which is consistent with the observed reduction in cell number. While direct links between ASM and LD biogenesis remain underexplored in literature, it may be speculated that ASM activity at the plasma membrane might influence trafficking of palmitoylated proteins required for LD dynamics (Suzuki et al., 2015; Xiong et al., 2019). Palmitoylation, the covalent attachment of PA (C16:0) to cysteine residues, anchors proteins to membranes and facilitates trafficking, signal transduction, and vesicle fusion (Bijlmakers and Marsh, 2003; Smotrys and Linder, 2004). In glioblastoma cells, it was shown that ASM localizes to the outer leaflet of the plasma membrane even under non-stress conditions and that ASM-generated ceramides traffic to the Golgi apparatus and facilitate the export of palmitoylated proteins. In the absence of ASM, these proteins become trapped in the trans-Golgi network, possibly due to insufficient ceramide levels in the Golgi membrane (Xiong et al., 2019). In support of this concept, Suzuki et al. demonstrated that palmitoylation is required for proper localization of ELMO domain containing 2 (ELMOD2), a GTPase-activating protein involved in targeting ATGL to LDs in adipocytes. (Suzuki et al., 2015). Thus, loss of ASM may impair trafficking of key lipogenic and lipolytic proteins via palmitoylation, resulting in disruption of LD formation and lipid buffering. Thus, the present results suggest a protective function of ASM in HepG2 cells under PA-induced stress, promoting LD biogenesis and limiting lipotoxicity. These findings contrast with existing literature describing ASM as a mediator of lipotoxicity in hepatocytes. For example, García-Ruiz et al. showed that ASM is required for TNF-α and Fas-induced apoptosis via ceramide signaling (Garcia-Ruiz et al., 2015), and Fernandez et al. reported protection from alcohol-induced ER stress and steatosis in ASM-deficient mice. Elevated ASM mRNA levels were also found in individuals with alcoholic hepatitis, supporting its pathological role in liver injury (Fernandez et al., 2013). In contrast, another study described less TAG accumulation and LD formation in liver tissue of ASM knockout mice upon HFD (Deevska et al., 2009). This discrepancy may reflect model-specific differences. HepG2 cells are less responsive to inflammatory signaling due to low TNF-α responsiveness (Hill et al., 1995) and lack the immune and paracrine context present *in vivo*. The HepG2 model used in the present study mimics nutrient-induced lipotoxicity rather than cytokine-driven liver injury, potentially shifting ASM's role from a pro-apoptotic effector to a regulator of lipid storage. Moreover, pro-lipotoxic effects of ASM reported *in vivo* are

often linked to inflammatory stress (Garcia-Ruiz et al., 2015), which may not be fully activated in HepG2 cells under PA treatment.

In summary, this present data uncover a new role of ASM in supporting LD formation during saturated fatty acid overload. In the absence of ASM, the reduced lipid storage capacity likely redirects fatty acids toward oxidative metabolism, thereby enhancing lipotoxicity. Although this contrasts with the established view of ASM as a mediator of hepatic injury, particularly under inflammatory conditions, it is consistent with emerging evidence implicating ASM in intracellular trafficking, membrane remodeling, and lipid homeostasis.

4.2.5 Acid sphingomyelinase preserves hepatic insulin signaling by regulating IRS2 phosphorylation

Given that ASM KD in HepG2 cells reduced LD formation and aggravated lipotoxic stress under PA treatment, these findings suggest a potential protective role of ASM in maintaining lipid and membrane homeostasis during metabolic stress. Since lipotoxicity is closely associated with insulin resistance, we next assessed whether ASM downregulation also alters insulin signaling in hepatocytes under conditions of elevated lipid or glucose exposure. ASM protein expression and enzymatic activity increased following 48 h of PA treatment, indicating that ASM upregulation may represent an adaptive response to counteract membrane stress or to facilitate lipid processing. Despite this, insulin signaling at the level of AKT phosphorylation (Ser473) remained largely unaffected after PA treatment, with only the highest concentration (200 µM) leading to a reduction in phos-AKT^{Ser473}/AKT. Notably, a similar reduction was observed in BSA controls at that dose, suggesting a non-specific effect on AKT activation in HepG2 cells under these conditions. IRS2 is essential for hepatocyte insulin signaling and contains multiple regulatory phosphorylation sites. While tyrosine phosphorylation promotes signal transduction, certain serine/threonine residues such as Ser303 and Ser675 are inhibitory (Park et al., 2013). Although the functional consequences of many IRS2 phospho-sites remain to be fully elucidated, Ser388 is detectable by commercial antibodies and has been linked to inhibitory regulation of IRS2 (Cao et al., 2024; He et al., 2021b). However, PA treatment led to a marked increase in IRS2 phosphorylation at Ser388, which was further enhanced in ASM KD cells, indicating that ASM may limit IRS2 inhibitory phosphorylation under high-lipid

load conditions. One possible explanation is that ASM-generated ceramides modulate plasma membrane microdomain architecture, thereby influencing the localization and activation of insulin signaling components. In other cell types, ASM inhibition disrupts ceramide-enriched membrane domains, resulting in increased sphingomyelin, loss of membrane cholesterol, and mislocalization of key signaling proteins from the plasma membrane like K-Ras (Cho et al., 2016). A similar mechanism may occur in hepatocytes, where ASM KD may stabilizes sphingomyelin-rich rafts and prevents ceramide-driven membrane remodeling. Notably, sphingomyelin enrichment has been associated with impaired InsR function, including its dissociation from caveolin-1 and reduced tyrosine kinase activity, effects that appear independent of ceramide depletion (Li et al., 2011). Thus, persistent sphingomyelin-rich domains may misposition the InsR and IRS2, reducing their interaction and promoting inhibitory phosphorylation events. Furthermore, ASM inhibition leads to sphingomyelin accumulation and may secondarily increase PC levels, either through reduced substrate turnover by sphingomyelin synthase or via compensatory activation of glycerophospholipid synthesis, as observed in ASM-deficient livers (Deevska et al., 2009). This lipid shift toward excess PC and sphingomyelin, can modify membrane fluidity and receptor organization. In hepatocytes, PC is sensed by phosphatidylcholine transfer protein (PC-TP, also known as StARD2), which forms a complex with the mitochondrial thioesterase (THEM2) to regulate insulin signaling. Elevated PC availability stabilizes the PC-TP–THEM2 complex in an inhibitory configuration that represses IRS2 function (Ersoy et al., 2013). In line with the present findings, this mechanism may contribute to the enhanced IRS2 Ser388 phosphorylation observed in ASM-deficient cells under PA treatment.

Under high-glucose conditions, a similarly dose-dependent decrease in AKT phosphorylation was observed, with a more pronounced effect in ASM KD cells. A modest but reproducible increase in IRS2 Ser388 phosphorylation was also detected, which again intensified with ASM KD. These data suggest that ASM helps maintain insulin responsiveness not only under lipotoxic but also glucotoxic stress, possibly by preserving a membrane environment that shields IRS2 from premature inhibitory modification. In line with these results, Osawa et al. (2011) demonstrated that ASM overexpression in primary hepatocytes enhanced AKT activation and improved glucose tolerance in wild-type and diabetic *db/db* mice. They proposed that ASM-derived ceramides are rapidly converted to S1P, a metabolite that activates pro-

survival and insulin-sensitizing pathways via S1P receptor signaling. (Osawa et al., 2011). However, not all data support a protective role for ASM; Fucho et al. (2014) reported that pharmacological ASM inhibition normalized HFD-induced hyperglycemia and improved insulin sensitivity (Fucho et al., 2014), while Deevska et al. (2009) found that ASM deletion in LDL receptor-deficient mice prevented HFD-induced obesity, hyperglycemia, and hepatic steatosis (Deevska et al., 2009). These contrasting findings underline the context-dependent function of ASM and ceramide signaling.

Taken together, the present results suggest that ASM exerts a protective role during the early stages of lipid- and glucose-induced insulin resistance in hepatocytes, likely by maintaining membrane composition and microdomain architecture that support proper IRS2 function. However, the role of ASM appears to depend on the metabolic state, the duration of stress exposure, and the downstream lipid metabolites generated. In the cellular model used in this thesis, the absence of ASM exacerbated proximal insulin signaling defects, which points to a membrane-based mechanism by which ASM may regulate IRS2 phosphorylation and preserve hepatic insulin sensitivity.

4.3 Limitations

While this thesis provides novel insights and robust findings on the role of ASM in metabolic regulation, it is important to acknowledge several methodological and conceptual limitations that should be considered when interpreting the results.

The limitations of the human study are already described in the publication (Section 3.1)

The murine models of diabetes and MASLD used in this work only partially recapitulate human pathophysiology. Diabetes was induced via STZ and diet: high-dose STZ ablates β-cells and mimics insulin-deficient diabetes (T1D or SIDD), whereas low-dose STZ combined with HFD models insulin resistance with moderate hyperglycemia (closer to SIRD) (Dewidar et al., 2023). Such chemically induced models cannot fully capture the gradual, polygenic nature of human T2D or other subtypes. Likewise, the diet-induced obese mouse model of MASLD manifests steatosis and mild inflammation but does not progress to the advanced stages of human liver disease within the 12-week timeframe. This may also explain why no differences were observed between STZ-treated mice and controls in ASM expression, a finding not necessarily reflecting human phenotypes.

The *in vitro* findings were obtained in HepG2 hepatoma cells, which, as carcinoma-derived lines, differ substantially from healthy primary hepatocytes and cannot replicate the multicellular architecture of the liver. While these cells provided a controlled system to study ASM function, their metabolic and signaling responses may not fully represent those in liver tissue. Moreover, although changes in viability, LD accumulation, and insulin signaling were observed with PA and ASM KD, ceramide and S1P levels as well as downstream metabolic or organelle stress markers were not measured. This leaves the biochemical mechanism inferred rather than proven and limits clarification of how ASM deficiency exacerbates lipotoxic injury.

Across all experimental arms, certain technical limitations should be acknowledged. Total ASM activity was measured without distinguishing between L-ASM and S-ASM isoforms or resolving subcellular localization, preventing assignment of effects to a specific isoform or compartment.

In summary, these limitations mean that the human exercise results should be viewed as proof-of-concept for a narrow demographic, and that the roles of ASM observed in cell and animal models require confirmation in more physiologically integrated systems. While these data suggest that ASM may buffer lipotoxic stress in the liver and support mitochondrial adaptation in muscle, these interpretations remain provisional. They should be considered as hypothesis-generating evidence, providing a foundation for the mechanistic and translational studies outlined in the following section.

4.4 Conclusion and outlook

ASM protein expression was reduced in skeletal muscle of individuals with T2D at baseline compared to glucose-tolerant humans but significantly rose following HIIT, accompanied by elevated enzymatic activity in all groups. ASM activity correlated with markers of mitochondrial remodeling such as MFN2 and AMPK-driven mitophagy, suggesting a role for ASM in mitochondrial quality control rather than in ceramide-driven lipotoxicity. These findings propose a model in which ASM contributes to exercise-induced mitochondrial maintenance, possibly via effects on membrane architecture or organelle cross-talk.

In hepatic cells and tissue, ASM activity increased following PA exposure or HFD conditions, accompanied by enhanced LD formation and moderately reduced cell viability. Surprisingly, KD of ASM further aggravated the detrimental effects of PA, markedly reducing cell viability and LD accumulation, suggesting a protective role of

ASM in buffering lipotoxic stress by promoting lipid sequestration into LD. In the absence of ASM, the reduced capacity for lipid storage may increase cellular exposure to toxic lipid species, potentially due to impaired palmitoylation or dysregulation of proteins required for LD biogenesis. Moreover, ASM appears to support hepatic insulin signaling under conditions of metabolic stress. Indeed, ASM KD enhanced inhibitory IRS2 phosphorylation in PA-treated HepG2 cells, indicating a disruption of proximal insulin signaling possibly through disruption of membrane microdomain structure. Thus, it could be speculated that ASM help maintain lipid compartmentalization and insulin sensitivity in hepatocytes under moderate nutrient challenge, while chronic or excessive ASM activation may contribute to inflammation and steatosis.

Altogether, this PhD thesis identifies ASM as a dual-function enzyme, supporting mitochondrial adaptation in skeletal muscle during physiological stress while maintaining lipid and membrane homeostasis in liver under early metabolic challenge. These context-specific effects underscore the complexity of ASM signaling and prompt several avenues for future investigation.

Future work should focus on determining the effect of ASM on mitochondrial morphology, autophagic flux or organelle interactions in human primary myotubes undergoing electric pulse stimulation (EPS), which reassemble contraction-like stimuli *in vitro*. Additionally, high-resolution microscopy techniques could further clarify whether ASM translocates to mitochondria and other organelles or modulates their function indirectly via membrane remodeling.

In the liver, more physiologically representative models such as hepatic organoids, could clarify the spatial and temporal roles of ASM in lipid accumulation, inflammation, and fibrogenesis under glucotoxic, lipotoxic or cytokine-rich conditions.

In conclusion, this work provides novel insights into the dualistic and context-sensitive roles of ASM in metabolic regulation. By combining clinical, biochemical and mechanistic approaches, it lays the foundation for future studies to define whether and how ASM represents a modifiable node for the prevention or treatment of metabolic diseases such as T2D and MASLD.

5 Supplements

5.1 Abbreviations

ACC	acetyl-CoA carboxylase
AKT	protein kinase B
ALDH2	aldehyde dehydrogenase 2
AMPK	AMP-activated protein kinase
APSa	dapter protein with PH and SH2 domains
ASM	acid sphingomyelinase
ATF6	activating transcription factor 6
Atg5	autophagy protein 5
ATGL	adipose triglyceride lipase
ATP	adenosine triphosphate
BAX	Bcl-2-associated X protein
Bid	BH3 interacting domain death agonist
BSA	bovine serum albumin
CaMK	calcium/calmodulin-dependent protein kinase
Cbl	casitas B-lineage lymphoma
CCT	CTP:phosphocholine cytidylyltransferase
CD45	receptor-type tyrosine-protein phosphatase C
CDase	ceramidase
cDNA	complementary DNA
CEPT1	choline/ethanolamine phosphotransferase 1
CerK	ceramide kinase
CerS	ceramide synthase
CGI-58	comparative gene identification 58
CHOP	C/EBP homologous protein
CK2	casein kinase 2
CLEC16A	C-type lectin domain family 16 member A
Col1a1	collagen type I alpha 1 chain
CSA	citrate synthase activity
CTSD	cathepsin D
DAGs	diacylglycerols
DES1	dihydroceramide desaturase
DGAT2	diacylglycerol-O-acyltransferase 2
DM	Diabetes Mellitus
DMSO	dimethylsulfoxid
DNL	*de novo* lipogenesis
DRP1	dynamin related protein 1
EDTA	ethylenediaminetetraacetic acid
ELMOD2	ELMO domain containing 2
EMEM	Eagle's Minimum Essential Medium
ER	endoplasmic reticulum
ETC	electron transport chain
F4/80	EGF-like module-containing mucin-like hormone receptor-like 1
FAO	fatty acid oxidation
FAS	fatty acid synthase
Fas or Apo-1	CD95 or apoptosis antigen 1
FBS	fetal bovine serum
FOXO1	forkhead box O1
FUNDC1	FUN14 domain-containing protein 1
G-6-P	glucose-6-phosphate
GBA	glucocerebrosidase
GCS	glucosylceramide synthase
GLUT4	glucosetransporter typ 4
GPAT1	glycerol-3-phosphate acyltransferase 1
GPR41	G protein-coupled receptor 41
GPX4	glutathione peroxidase 4
GRP78 or BiP	78-kDa glucose-regulated protein
GSK3	glycogen synthase kinase 3
GSV	GLUT4 storage vesicles
GYS	glycogen synthase
H_2O_2	hydrogen peroxide
HFD	high-fat-diet
HIIT	High-intensity interval training

HSC	hepatic stellate cell
HSL	hormone-sensitive lipase
HSP	heat-shock protein
IKK	inhibitor of κB kinase
IL-6	interleukin-6
IMCL	intramyocellular lipid
IMTG	intramyocellular triglycerides
InsR	insulin receptor
IRC	inter-run calibrator
IRE1	inositol-requiring enzyme 1
IRS	insulin receptor substrate
JNK	c-Jun N-terminal kinase
KD	knockdown
KDSR	3-ketodihydrosphingosine reductase
L-ASM	lysosomal ASM
LC3l	microtubule-associated protein 1A/1B-light chain
LC50	lethal concentration 50
LD	lipid droplet
LDL	low-density lipoprotein
LMP	lysosomal membrane permeabilization
MARD	mild age-related diabetes
MASH	metabolic dysfunction-associated steatohepatitis
MASL	metabolic dysfunction-associated steatotic liver
MASLD	metabolic dysfunction-associated steatotic liver disease
MCD	methionine-choline-deficient
MCP-1	monocyte chemoattractant protein-1
MFF	mitochondrial fission factor
MFN	mitofusin
mNSM	mitochondrial-associated neutral sphingomyelinase
MOD	mild obesity-related diabetes
mRNA	messenger RNA
MST1	macrophage stimulating 1
mTORC2	mechanistic target of rapamycin complex 2
NAFLD	non-alcoholic fatty liver disease
NEFAs	non-esterified fatty acids
NF-κB	nuclear factor kappa B
NIX	BNIP3-like protein X
NPD	Niemann-Pick disease
NRF-1	nuclear respiratory factor 1
NSM	neutral sphingomyelinase
$O_2^{\bullet -}$	superoxide
OH•	hydroxyl radicals
OPA1	optic atrophy 1
p38 MAPK	p38 mitogen-activated protein kinase
PA	palmitic acid/palmitate
Parkin	E3 ubiquitin protein ligase
PBS	phosphate buffered saline
PC	phosphatidylcholine
PCIII	procollagen type III
PC-TP, or StARD2	phosphatidylcholine transfer protein
PCYT2	phosphatidylcholine cytidylyltransferase
PDIA4	protein disulfide isomerase A4
PDK1	phosphoinositide-dependent kinase 1
PDX1	Pancreatic and duodenal homeobox 1
PE	phosphatidylethanolamine
PEMT	phosphatidylethanolamine N-methyltransferase
PGC-1α	proliferator-activated receptor γ coactivator 1α
PI3K	phosphoinositide 3-kinase
PINK	PTEN-induced kinase 1
PIP2	phosphatidylinositol-4,5-bisphosphate
PIP3	phosphatidylinositol-3,4,5-trisphosphate
PKA	protein kinase A
PKCs	protein kinase Cs
PKR	protein kinase R
PERK	PKR--like endoplasmic reticulum kinase
PLIN5	perilipin 5
PP2A	protein phosphatase 2A
PPAR-γ	peroxisome proliferator-activated receptor γ
PTEN	phosphatase and tensin homolog
PTPs	protein tyrosine phosphatases
qRT-PCR	Real-Time Polymerase Chain Reaction
ROS	reactive oxygen species
RT	room temperature

S1P	sphingosine-1-phosphate
SAID	severe autoimmune diabetes
SAM	S-adenosylmethionine
S-ASM	secretory ASM
Ser	serin
SERCA	sarcoplasmic/endoplasmic reticulum calcium ATPase
SIDD	severe insulin-deficient diabetes
SIRD	severe insulin-resistant diabetes
siRNA	small interfering RNA
SOCS3	suppressor of cytokine signaling 3
SphK	sphingosine kinase
SPP	S1P phosphatase
SPT	serine palmitoyltransferase
SQSTM1	sequestosome 1
SR	sarcoplasmic reticulum
SRs	Sirius Red staining
SREBP-1c	sterol regulatory element-binding protein 1c
STZ	streptozotocin
T1D	Type 1 diabetes mellitus
T2D	Type 2 diabetes mellitus
TAG	triglycerides
TFAM	mitochondrial transcription factor A
THEM2	thioesterase 2
Thr	threonine
TIMP-1	tissue inhibitor of metalloproteinase 1
TNFR1	tumor necrosis factor receptor 1
TNF-α	tumor necrosis factor-α
TRAIL	TNF-related apoptosis-inducing ligand
RB3	tribbles pseudokinase-3
Tyr	tyrosine
ULK1	unc-51 like autophagy activating kinase1
UPR	unfolded protein response
VLDL	very low-density lipoprotein
WAT	white adipose tissue
XBP1	spliced X-box binding protein 1
α-SMA	α- smooth muscle actin
ψ_m	membrane potential

5.2 Supplements of published data

Supplemental Figure 1

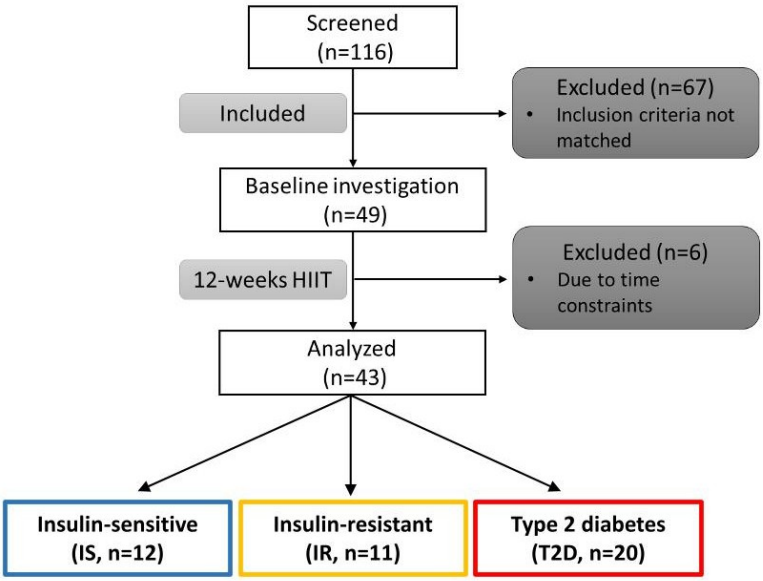

Fig. S1: Flow chart of study design

Supplemental Figure 2

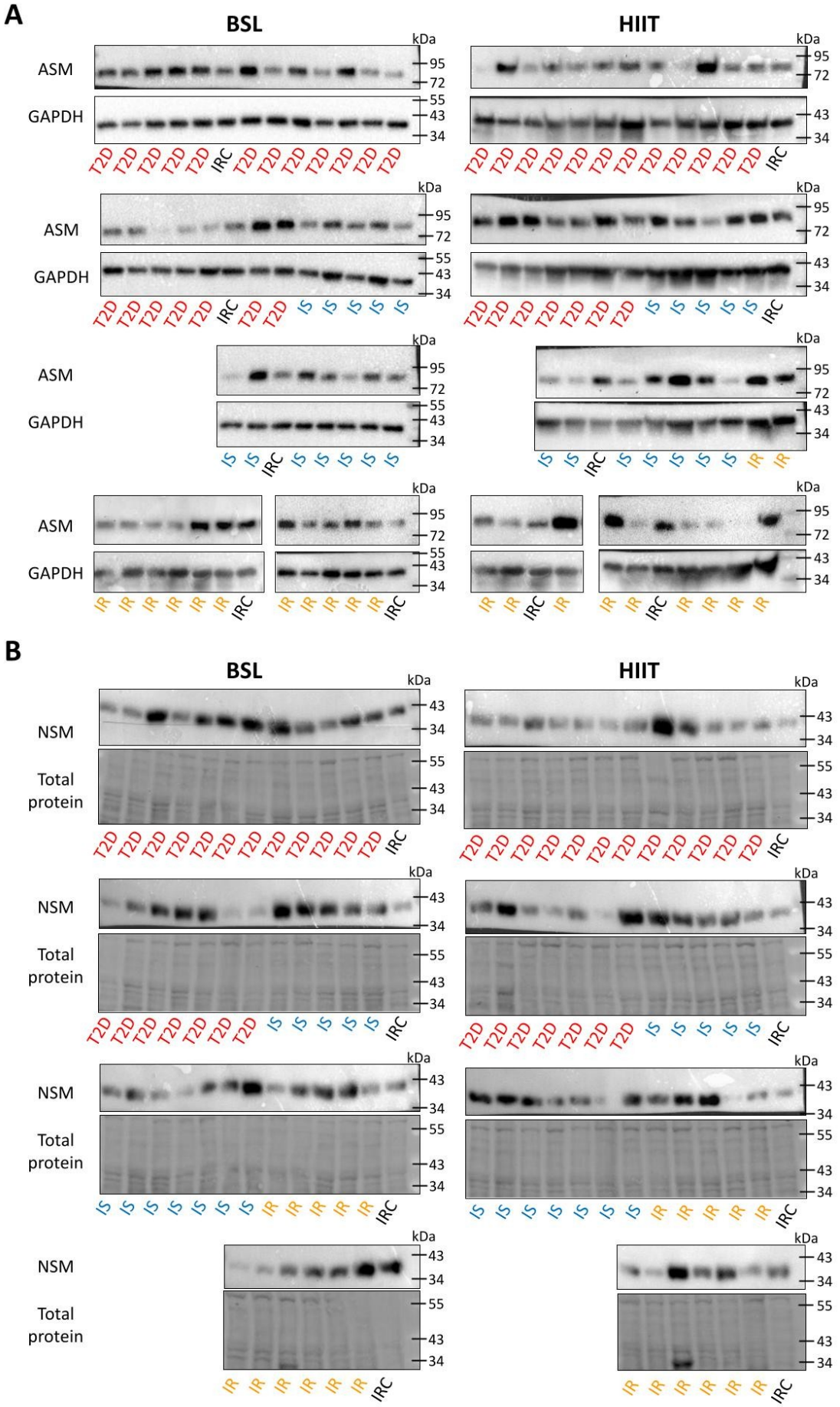

Fig. S2: Representative Western-blots of ASM, GAPDH **(A)** and NSM, total protein (B) baseline (BSL) and after HIIT

Supplemental Figure 3

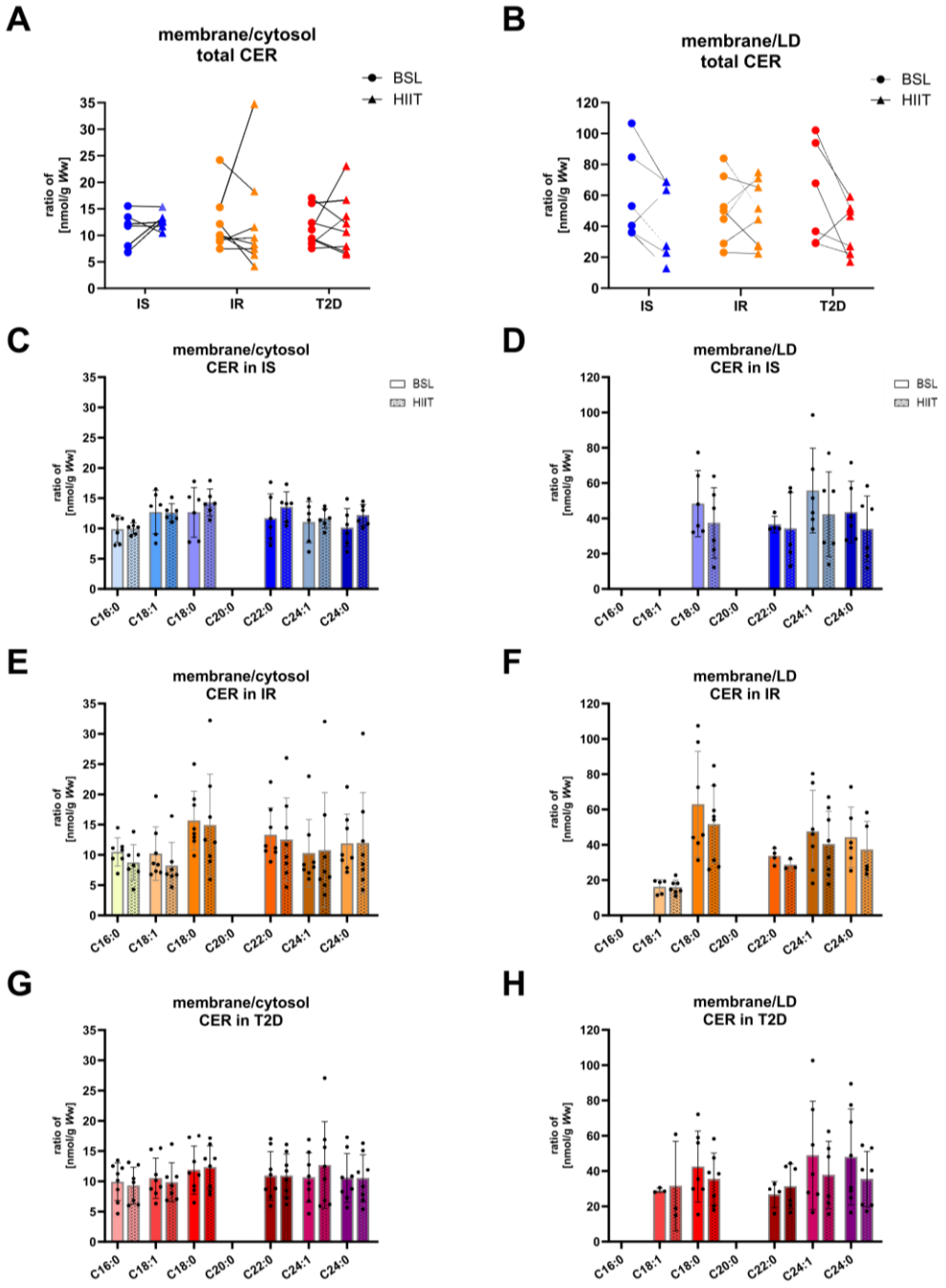

Fig. S3: Ceramide ratios of membrane/cytosol and membrane/LD are not effected by HIIT

Total ceramide (CER) ratios of membrane/cytosol fraction **(A)** and ratios of membrane/lipid droplets (LD) **(B)** in skeletal muscle of IS (n=6), IR (n=8) and T2D (n=8) at baseline (BSL) and after 12-weeks of HIIT (HIIT). Ratios of membrane/cytosol and membrane/LD ceramide species in skeletal muscle of IS **(C/D)**, IR **(E/F)** and T2D **(G/H)** individuals at BSL and after 12-weeks of HIIT. Data are presented as mean ± SD, Statistics based on mixed model ANOVA.

Table S1: Anthropometric and metabolic parameters at baseline (BSL) and after 12-weeks of HIIT (HIIT) in IS, IR and T2D individuals.

Parameter	IS (n=12)		IR (n=11)		T2D (n=20)	
	BSL	HIIT	BSL	HIIT	BSL	HIIT
Age (years)	58 ± 4		56 ± 4		57 ± 6	
BMI (kg/m²)	29.3 ± 1.8	29.1 ± 1.4	32.2 ± 2.2$^{\#\#}$	32.1 ± 2.4	31.2 ± 2.8$^{\#}$	30.8 ± 2.8
HbA1c (%)	5.4 ± 0.3	5.5 ± 0.3	5.4 ± 0.3	5.4 ± 0.4	7.2 ± 1.1$^{\#\#\#\dagger\dagger\dagger}$	6.9 ± 0.8
M-value ($mg*kg^{-1}*min^{-1}$)	7.2 (6.5, 7.8)	7.6 (5.5, 8.5)	4.6 (3.2, 5.2)$^{\#\#\#}$	5.2 (4.8, 6.4)**	2.5 (1.8,4.5)$^{\#\#\#\dagger}$	3.1 (2.7, 5.9)**
VO_2max ($ml*kg^{-1}*min^{-1}$)	26.2 (24.9, 29)	30.9 (27.5, 33.8)*	24.7 (24.1, 25.8)	27.9 (26.4, 29.6)$^{\#}$***	23.2 (21.2, 26.1)$^{\#}$	27 (25.3, 30.4)***

Data are shown as means ± SD or median (q1, q3). #p<0.05, ##p<0.01, ###p<0.001 vs IS; †p<0.05, and †††p<0.001 vs IR; *p<0.05, **p<0.01, ***p<0.001 HIIT vs BSL. Anthropometric and metabolic parameters have been previously published [36].

Abbreviations: BMI, body mass index; HbA1c, hemoglobin A1c.

Table S2: List of primary and secondary antibodies used for protein detection.

Target protein	Dilution	Supplier	Catalog ID
Acid Sphingomyelinase	1/1000	Abcam	ab272729
AMPKα	1/1000	Cell Signaling Technology	#2532
DRP1	1/1000	Cell Signaling Technology	#5391
GAPDH	1/20000	Cell Signaling Technology	#2118
IRS1	1/1000	Millipore	06-248
MFN1	1/1000	Abcam	ab57602
MFN2	1/1000	Abcam	ab56889
Neutral Sphingomyelinase	1/1000	Abcam	ab131330
OPA1	1/1000	BD Biosciences	612607
Parkin	1/1000	Cell Signaling Technology	#4211
PINK1	1/1000	Abcam	ab23707
VDAC	1/1000	Abcam	ab14734
phos-AMPKα (Thr172)	1/1000 in TBST + 5% BSA	Cell Signaling Technology	#2535
phos-DRP1(Ser616)	1/1000 in TBST + 5% BSA	Cell Signaling Technology	#3455
phos-IRS1(Ser1101)	1/1000 in TBST + 5% BSA	Cell Signaling Technology	#2385
phos-PARKIN(Ser65)	1/1000 in TBST + 5% BSA	Ubiquigent	68-0056-100
phos-PINK1(Thr257)	1/1000 in TBST + 5% BSA	Ubiquigent	68-0057-100
Anti-rabbit IgG HRP-conjugated	1/20000	Cell Signaling Technology	#7074
Anti-mouse IgG HRP-conjugated	1/10000	Cell Signaling Technology	#7076

Table S3: Regression analysis of Δ-values ASM protein and activity as well as NSM protein with variables.

Regression coefficient β and p-value are given for each association. P-values < 0.05 are shown in bolt.

Association	with	ALL	IS	IR	T2D
ΔASM protein	ΔASM activity	β=0,215 p=0,1306	β=-0,169 p=0,76773	β=0,304 p=0,23773	β=0,104 p=0,6054
ΔASM protein	ΔPKCθ	β=-0,215 p=0,21369	β=0,271 p=0,63897	β=-0,178 p=0,34006	β=-0,156 p=0,66657
ΔASM protein	ΔPKCε	β=-0,018 p=0,91084	β=0,49 p=0,55	β=-0,037 p=0,75245	β=0,086 p=0,77829
ΔASM protein	ΔOPA	β=-0,018 p=0,88681	β=-0,818 p=0,0663	β=0,281 p=0,18717	β=0,139 p=0,43042
ΔASM protein	ΔDRP1	β=-0,09 p=0,28575	β=0,059 p=0,80684	β=-0,174 p=0,33776	β=-0,008 p=0,94884
ΔASM protein	ΔDRP^{Ser616}	β=0,241 p=0,07965	β=0,048 p=0,82303	β=0,524 p=0,2003	β=0,15 p=0,4308
ΔASM protein	ΔDRP^{Ser616}/DRP1	**β=0,33** **p=0,01557**	β=-0,012 p=0,97497	β=0,698 p=0,05027	β=0,159 p=0,38948
ΔASM protein	ΔMFN1	β=0,013 p=0,83147	β=-0,209 p=0,11374	β=0,167 p=0,18795	β=-0,014 p=0,88557
ΔASM protein	ΔMFN2	**β=0,154** **p=0,02896**	β=-0,244 p=0,24903	**β=0,34** **p=0,03729**	β=0,063 p=0,40268
ΔASM protein	ΔPINK	β=-0,06 p=0,55398	β=-0,561 p=0,12382	β=-0,18 p=0,51588	β=-0,015 p=0,86495
ΔASM protein	$\Delta phosPINK^{Thr257}$	β=0,11 p=0,15526	β=0,21 p=0,48061	β=0,306 p=0,06259	β=-0,036 p=0,72103
ΔASM protein	$\Delta phosPINK^{Thr257}$/PINK	β=0,176 p=0,20596	β=0,771 p=0,14412	β=0,486 p=0,12428	β=-0,017 p=0,91496
ΔASM protein	ΔParkin	β=-0,213 p=0,05153	β=-0,26 p=0,4242	β=-0,045 p=0,79599	β=-0,141 p=0,3891
ΔASM protein	$\Delta Parkin^{Ser65}$	**β=0,094** **p=0,03856**	β=0,07 p=0,63653	β=-0,021 p=0,84285	β=0,097 p=0,10339
ΔASM protein	$\Delta phosParkin^{Ser65}$/Parkin	**β=0,307** **p=0,01587**	β=0,331 p=0,3045	β=0,024 p=0,91403	β=0,238 p=0,20446
ΔASM protein	ΔVDAC	β=0,031 p=0,72841	β=-0,161 p=0,54704	β=-0,131 p=0,49084	β=0,139 p=0,23999
ΔASM protein	ΔAMPKα	β=-0,063 p=0,52861	β=-0,224 p=0,58361	β=0,04 p=0,87154	β=-0,027 p=0,82897
ΔASM protein	$\Delta phosAMPK\alpha^{Thr172}$	**β=0,353** **p=0,02454**	β=0,516 p=0,22826	**β=0,909** **p=0,04424**	β=0,139 p=0,49383
ΔASM protein	$\Delta phosAMPK\alpha^{Thr172}$/AMPKα	**β=0,482** **p=0,01421**	β=0,725 p=0,37146	**β=1,182** **p=0,00377**	β=0,166 p=0,4949
ΔASM protein	ΔIRS1	β=0,071 p=0,56754	β=-0,336 p=0,3736	β=-0,212 p=0,41484	β=0,188 p=0,2371
ΔASM protein	$\Delta phosIRS1^{Ser1101}$	β=0,141 p=0,38456	β=0,446 p=0,6553	β=-0,41 p=0,49204	β=-0,002 p=0,98921
ΔASM protein	$\Delta phosIRS1^{Ser1101}$/IRS1	β=-0,096 p=0,58307	β=0,034 p=0,9809	β=0,38 p=0,77088	β=-0,153 p=0,36464

		β=0,098	β=-0,037	β=-0,122	**β=0,262**
ΔASM protein	Δliver_lipid_content	p=0,16451	p=0,92476	p=0,29242	**p=0,00108**
		β=-0,1	β=-0,024	β=-0,079	**β=-0,341**
ΔASM protein	ΔM-value	p=0,17941	p=0,88138	p=0,42731	**p=0,00314**
		β=0,008	β=-0,079	**β=0,039**	β=-0,001
ΔASM protein	ΔVO_2max	p=0,60543	p=0,27083	**p=0,04511**	p=0,9485
		β=-0,022	β=-0,197	β=0,098	β=-0,07
ΔASM protein	ΔT-CER	p=0,64544	p=0,36853	p=0,26778	p=0,34811
		β=-0,075	β=-0,412	β=-0,011	β=-0,105
ΔASM protein	ΔCER_C16:0	p=0,42389	p=0,5033	p=0,9403	p=0,43829
		β=-0,083	β=-0,07	β=0,157	β=-0,183
ΔASM protein	ΔCER_C18:1	p=0,37472	p=0,84646	p=0,11277	p=0,30958
		β=0,021	β=-0,105	β=0,181	β=-0,018
ΔASM protein	ΔCER_C18:0	p=0,70499	p=0,71038	p=0,08576	p=0,81017
		β=-0,056	β=-0,682	β=-0,021	β=-0,056
ΔASM protein	ΔCER_C20:0	p=0,54493	p=0,34925	p=0,90664	p=0,46827
		β=0,055	β=-0,16	β=0,095	β=0,045
ΔASM protein	ΔCER_C22:0	p=0,34956	p=0,62845	p=0,46414	p=0,55816
		β=-0,044	β=-0,276	β=0,077	β=-0,105
ΔASM protein	ΔCER_C24:1	p=0,48911	p=0,44083	p=0,49255	p=0,21782
		β=0,017	β=-0,197	β=0,063	β=0,006
ΔASM protein	ΔCER_C24:0	p=0,74868	p=0,53463	p=0,54716	p=0,9325
		ß=0,095	ß=0,158	ß=0,138	ß=0,069
ΔASM protein	ΔT-SM	p=0,1365	p=0,6863	p=0,3749	p=0,4102
		ß=0,059	ß=0,120	ß=-0,011	ß=0,070
ΔASM protein	ΔSM_C16:0	p=0,3018	p=0,7804	p=0,9130	p=0,4461
		ß=-0,052	ß=0,082	ß=-0,042	ß=-0,062
ΔASM protein	ΔSM_C18:0	p=0,0867	p=0,7386	p=0,2449	p=0,2517
		ß=-0,043	ß=0,213	ß=-0,132	ß=-0,009
ΔASM protein	ΔSM_C18:1	p=0,4568	p=0,7784	p=0,1635	p=0,8783
		ß=0,020	ß=0,238	ß=-0,037	ß=0,017
ΔASM protein	ΔSM_C20:0	p=0,7405	p=0,7235	p=0,6809	p=0,8465
		ß=0,088	ß=0,268	ß=0,026	ß=0,099
ΔASM protein	ΔSM_C22:0	p=0,1157	p=0,6439	p=0,7501	p=0,2567
		ß=0,128	ß=0,303	ß=0,040	ß=0,150
ΔASM protein	ΔSM_C24:0	**p=0,0408**	p=0,6133	p=0,6707	p=0,1292
		ß=0,100	ß=0,096	ß=0,016	ß=0,116
ΔASM protein	Δmembrane_SM_C16:0	p=0,0858	p=0,7734	p=0,8674	p=0,2374
		ß=-0,095	ß=0,090	ß=-0,044	ß=-0,121
ΔASM protein	Δmembrane_SM_C18:0	**p=0,0444**	p=0,6060	p=0,4487	p=0,1885
		ß=-0,054	ß=0,325	ß=-0,119	ß=-0,030
ΔASM protein	Δmembrane_SM_C18:1	p=0,4440	p=0,6772	p=0,3117	p=0,7349
		ß=0,013	ß=0,288	ß=-0,006	ß=0,002
ΔASM protein	Δmembrane_SM_C20:0	p=0,8512	p=0,6553	p=0,9594	p=0,9851
		ß=0,077	ß=0,271	ß=0,038	ß=0,083
ΔASM protein	Δmembrane_SM_C22:0	p=0,2572	p=0,6168	p=0,7245	p=0,4686
		ß=0,129	ß=0,327	ß=0,056	ß=0,147
ΔASM protein	Δmembrane_SM_C24:0	p=0,0802	p=0,5828	p=0,6421	p=0,2245
		ß=0,104	ß=0,122	ß=0,039	ß=0,118
ΔASM protein	Δmembrane_SM_C24:1	p=0,1389	p=0,7053	p=0,7519	p=0,3495

		ß=0,024	ß=0,103	ß=-0,134	ß=0,045
ΔASM protein	Δcytosol_SM_C16:0	p=0,7414	p=0,8515	p=0,3399	p=0,6437
		ß=0,002	ß=0,184	ß=-0,079	ß=0,015
ΔASM protein	Δcytosol_SM_C18:0	p=0,9709	p=0,7480	p=0,5582	p=0,8433
		ß=-0,036	ß=0,218	ß=-0,196	ß=0,014
ΔASM protein	Δcytosol_SM_C18:1	p=0,6013	p=0,8009	p=0,0872	p=0,8345
		ß=0,019	ß=0,189	ß=-0,119	ß=0,022
ΔASM protein	Δcytosol_SM_C20:0	p=0,8459	p=0,8328	p=0,5770	p=0,8523
		ß=0,093	ß=0,395	ß=-0,045	ß=0,109
ΔASM protein	Δcytosol_SM_C22:0	p=0,3089	p=0,6719	p=0,8058	p=0,3374
		ß=0,088	ß=0,286	ß=-0,075	ß=0,125
ΔASM protein	Δcytosol_SM_C24:0	p=0,2659	p=0,7030	p=0,6089	p=0,2501
		ß=0,049	ß=0,097	ß=-0,108	ß=0,074
ΔASM protein	Δcytosol_SM__C24:1	p=0,4994	p=0,8536	p=0,4803	p=0,4210
		ß=-0,066	ß=-0,398	ß=0,107	ß=-0,097
ΔASM protein	ΔLD_SM_C16:0	p=0,6831	p=0,4707	p=0,7601	p=0,7164
		ß=-0,058	ß=-0,438	ß=0,216	ß=-0,105
ΔASM protein	ΔLD_SM_C18:0	p=0,6566	p=0,0690	p=0,4356	p=0,6073
		ß=-0,137	ß=-0,409	ß=0,098	ß=-0,149
ΔASM protein	ΔLD_SM_C18:1	p=0,3397	p=0,2020	p=0,7217	p=0,5136
		ß=-0,093	ß=-0,324	ß=0,086	ß=-0,134
ΔASM protein	ΔLD_SM_C20:0	p=0,5677	p=0,5875	p=0,7797	p=0,6378
		ß=-0,010	ß=-0,179	ß=0,176	ß=-0,045
ΔASM protein	ΔLD_SM_C22:0	p=0,9488	p=0,7431	p=0,5887	p=0,8591
		ß=0,012	ß=-0,175	ß=0,200	ß=-0,017
ΔASM protein	ΔLD_SM_C24:0	p=0,9375	p=0,7582	p=0,5679	p=0,9444
		ß=-0,017	ß=-0,382	ß=0,183	ß=-0,050
ΔASM protein	ΔLD_SM_C24:1	p=0,9181	p=0,4244	p=0,6284	p=0,8414
		β=0,283	β=-0,06	β=0,556	β=0,163
ΔASM activity	ΔASM protein	p=0,1306	p=0,76773	p=0,23773	p=0,6054
		β=0,018	β=-0,053	β=-0,372	β=0,769
ΔASM activity	ΔPKCθ	p=0,92929	p=0,81778	p=0,20013	p=0,14231
		β=0,151	β=0,186	β=-0,036	β=0,462
ΔASM activity	ΔPKCε	p=0,4236	p=0,56893	p=0,84485	p=0,30546
		β=-0,07	β=-0,188	β=0,107	β=0,144
ΔASM activity	ΔOPA	p=0,64211	p=0,53107	p=0,76441	p=0,51516
		β=0,037	β=0,103	β=0,164	β=0,079
ΔASM activity	ΔDRP1	p=0,72186	p=0,4836	p=0,56051	p=0,66003
		β=0,204	β=0,152	**β=1,252**	β=-0,231
ΔASM activity	ΔDRP^{Ser616}	p=0,21464	p=0,22342	**p=0,03645**	p=0,34171
		β=0,168	β=0,049	β=1,087	β=-0,31
ΔASM activity	ΔDRP^{Ser616}/DRP1	p=0,3084	p=0,82839	p=0,05248	p=0,14182
		β=0,1	β=0,148	β=-0,078	β=0,169
ΔASM activity	ΔMFN1	p=0,15679	p=0,05924	p=0,69632	p=0,21425
		β=0,243	β=0,179	β=0,087	**β=0,23**
ΔASM activity	ΔMFN2	**p=0,00265**	p=0,15813	p=0,70611	**p=0,01148**
		β=-0,001	β=0,109	β=-0,467	β=0,001
ΔASM activity	ΔPINK	p=0,99149	p=0,64965	p=0,23421	p=0,99017
		β=-0,038	**β=-0,37**	β=0,294	β=0,007
ΔASM activity	$\Delta phosPINK^{Thr257}$	p=0,68477	**p=0,01724**	p=0,22716	p=0,96211

		β=-0,037	β=-0,479	**β=0,761**	β=0,001
ΔASM activity	ΔphosPINK^{Thr257}/PINK	p=0,81775	p=0,13797	**p=0,04872**	p=0,9959
		β=-0,062	β=0,149	β=-0,032	β=-0,017
ΔASM activity	ΔParkin	p=0,64168	p=0,45746	p=0,90725	p=0,94154
		β=0,088	β=-0,018	β=0,148	β=0,085
ΔASM activity	ΔParkin^{Ser65}	p=0,10914	p=0,843	p=0,31852	p=0,32063
		β=0,15	β=-0,167	β=0,181	β=0,101
ΔASM activity	ΔphosParkin^{Ser65}/Parkin	p=0,34012	p=0,40306	p=0,60156	p=0,70605
		β=-0,109	β=0,026	β=-0,327	β=-0,242
ΔASM activity	ΔVDAC	p=0,30624	p=0,87488	p=0,26886	p=0,13164
		β=0,169	β=0,007	β=0,338	**β=0,599**
ΔASM activity	ΔAMPKα	p=0,20473	p=0,97947	p=0,29311	**p=0,01315**
		β=-0,011	β=0,884	β=0,577	β=-0,604
ΔASM activity	ΔphosAMPKα^{Thr172}	p=0,97318	p=0,4183	p=0,43011	p=0,15301
		β=-0,269	β=1,931	β=0,466	**β=-1,203**
ΔASM activity	ΔphosAMPKα^{Thr172}/AMPKα	p=0,51328	p=0,30217	p=0,56478	**p=0,00887**
		β=0,169	β=0,225	β=-0,197	β=0,148
ΔASM activity	ΔIRS1	p=0,27649	p=0,33457	p=0,58452	p=0,63401
		β=0,132	β=-0,007	β=-0,359	β=0,19
ΔASM activity	ΔphosIRS1^{Ser1101}	p=0,42229	p=0,98394	p=0,15707	p=0,48989
		β=-0,127	β=-0,166	β=-0,244	β=-0,065
ΔASM activity	ΔphosIRS1^{Ser1101}/IRS1	p=0,47156	p=0,74143	p=0,72104	p=0,84377
		β=-0,002	β=-0,132	β=-0,114	β=0,152
ΔASM activity	Δliver_lipid_content	p=0,97742	p=0,53482	p=0,49911	p=0,17239
		β=-0,102	β=0,041	β=-0,116	**β=-0,399**
ΔASM activity	ΔM-value	p=0,24861	p=0,66971	p=0,36022	**p=0,015**
		β=0,022	β=0,013	β=0,017	β=0,02
ΔASM activity	ΔVO_2max	p=0,21244	p=0,76186	p=0,62929	p=0,39243
		β=-0,029	β=-0,021	β=0,053	β=-0,259
ΔASM activity	ΔT_CER	p=0,59243	p=0,79524	p=0,62724	p=0,08645
		β=-0,123	β=-0,082	β=-0,059	**β=-0,581**
ΔASM activity	ΔCER_C16:0	p=0,23421	p=0,71262	p=0,7351	**p=0,01734**
		β=0,036	β=0,119	β=0,039	β=-0,219
ΔASM activity	ΔCER_C18:1	p=0,73621	p=0,29066	p=0,76765	p=0,59668
		β=0,062	β=0,094	β=0,138	β=-0,034
ΔASM activity	ΔCER_C18:0	p=0,30684	p=0,2951	p=0,30788	p=0,83607
		β=-0,122	β=-0,153	β=-0,144	β=-0,262
ΔASM activity	ΔCER_C20:0	p=0,23592	p=0,56764	p=0,47783	p=0,09412
		β=-0,06	β=-0,079	β=0,01	β=-0,211
ΔASM activity	ΔCER_C22:0	p=0,36795	p=0,48218	p=0,94931	p=0,18918
		β=-0,043	β=-0,058	β=0,069	**β=-0,356**
ΔASM activity	ΔCER_C24:1	p=0,55139	p=0,65399	p=0,6036	**p=0,03363**
		β=-0,079	β=-0,082	β=0,002	**β=-0,278**
ΔASM activity	ΔCER_C24:0	p=0,17209	p=0,45228	p=0,98483	**p=0,02169**
		ß=-0,039	ß=-0,116	ß=-0,110	ß=0,193
ΔASM activity	ΔT-SM	p=0,5928	p=0,1584	p=0,5579	p=0,2917
		ß=-0,019	ß=-0,135	ß=0,014	ß=0,169
ΔASM activity	ΔSM_C16:0	p=0,7727	p=0,1030	p=0,9031	p=0,4013
		ß=0,024	ß=0,040	ß=-0,056	ß=0,119
ΔASM activity	ΔSM_C18:0	p=0,4964	p=0,5333	p=0,1715	p=0,3320

		ß=0,001	ß=0,014	ß=-0,032	ß=0,083
ΔASM activity	ΔSM_C18:1	p=0,9925	p=0,9459	p=0,7933	p=0,5000
		ß=-0,094	ß=-0,206	ß=-0,068	ß=0,059
ΔASM activity	ΔSM_C20:0	p=0,1522	p=0,1285	p=0,5242	p=0,7585
		ß=-0,059	ß=-0,173	ß=-0,038	ß=0,158
ΔASM activity	ΔSM_C22:0	p=0,3610	p=0,1635	p=0,6849	p=0,4283
		ß=-0,053	ß=-0,193	ß=-0,055	ß=0,261
ΔASM activity	ΔSM_C24:0	p=0,4683	p=0,1011	p=0,6190	p=0,2526
		ß=0,024	ß=-0,106	ß=0,044	ß=0,265
ΔASM activity	ΔSM_C24:1	p=0,7281	p=0,0827	p=0,7044	p=0,2236
		ß=-0,009	ß=-0,133	ß=-0,012	ß=0,300
ΔASM activity	Δmembrane_SM_C16:0	p=0,9060	p=0,1065	p=0,9314	p=0,2070
		ß=0,017	ß=0,036	ß=-0,099	ß=0,189
ΔASM activity	Δmembrane_SM_C18:0	p=0,7606	p=0,4312	p=0,1183	p=0,3756
		ß=-0,016	ß=-0,001	ß=-0,088	ß=0,140
ΔASM activity	Δmembrane_SM_C18:1	p=0,8429	p=0,9968	p=0,5392	p=0,4745
		ß=-0,088	ß=-0,199	ß=-0,085	ß=0,159
ΔASM activity	Δmembrane_SM_C20:0	p=0,2544	p=0,1310	p=0,5465	p=0,4994
		ß=-0,047	ß=-0,163	ß=-0,067	ß=0,273
ΔASM activity	Δmembrane_SM_C22:0	p=0,5368	p=0,1574	p=0,5935	p=0,2683
		ß=-0,045	ß=-0,192	ß=-0,094	ß=0,380
ΔASM activity	Δmembrane_SM_C24:0	p=0,5980	p=0,1086	p=0,5079	p=0,1476
		ß=0,033	ß=-0,105	ß=0,013	ß=0,387
ΔASM activity	Δmembrane_SM_C24:1	p=0,6815	p=0,0791	p=0,9281	p=0,1422
		ß=-0,061	ß=-0,149	ß=-0,114	ß=0,015
ΔASM activity	Δcytosol_SM_C16:0	p=0,4540	p=0,2211	p=0,5000	p=0,9443
		ß=0,016	ß=0,053	ß=-0,216	ß=0,170
ΔASM activity	Δcytosol_SM_C18:0	p=0,8103	p=0,7357	p=0,1405	p=0,2748
		ß=0,009	ß=0,033	ß=-0,171	ß=0,195
ΔASM activity	Δcytosol_SM_C18:1	p=0,9098	p=0,8899	p=0,2350	p=0,1674
		ß=-0,139	ß=-0,244	ß=-0,278	ß=0,032
ΔASM activity	Δcytosol_SM_C20:0	p=0,2015	p=0,2129	p=0,2474	p=0,9003
		ß=-0,134	ß=-0,241	ß=-0,215	ß=0,044
ΔASM activity	Δcytosol_SM_C22:0	p=0,1846	p=0,2698	p=0,2948	p=0,8661
		ß=-0,116	ß=-0,217	ß=-0,166	ß=0,055
ΔASM activity	Δcytosol_SM_C24:0	p=0,1839	p=0,1797	p=0,3196	p=0,8286
		ß=-0,038	ß=-0,125	ß=-0,127	ß=0,113
ΔASM activity	Δcytosol_SM__C24:1	p=0,6396	p=0,3106	p=0,4787	p=0,5838
		ß=-0,080	ß=-0,139	**ß=0,779**	ß=-0,973
ΔASM activity	ΔLD_SM_C16:0	p=0,6617	p=0,3290	**p=0,0171**	p=0,0550
		ß=0,014	ß=0,023	**ß=0,733**	ß=-0,736
ΔASM activity	ΔLD_SM_C18:0	p=0,9255	p=0,8192	**p=0,0010**	p=0,0632
		ß=-0,051	ß=0,004	**ß=0,670**	ß=-0,807
ΔASM activity	ΔLD_SM_C18:1	p=0,7528	p=0,9684	**p=0,0049**	p=0,0715
		ß=-0,134	ß=-0,180	**ß=0,673**	ß=-1,036
ΔASM activity	ΔLD_SM_C20:0	p=0,4579	p=0,1630	**p=0,0219**	p=0,0576
		ß=-0,098	ß=-0,170	**ß=0,764**	**ß=-0,943**
ΔASM activity	ΔLD_SM_C22:0	p=0,5739	p=0,1126	**p=0,0099**	**p=0,0492**
		ß=-0,090	ß=-0,169	**ß=0,841**	**ß=-0,989**
ΔASM activity	ΔLD_SM_C24:0	p=0,6101	p=0,1499	**p=0,0073**	**p=0,0269**

		ß=-0,020	ß=-0,094	**ß=0,897**	ß=-0,906
ΔASM activity	ΔLD_SM_C24:1	p=0,9120	p=0,4828	**p=0,0078**	p=0,0570
		ß=0,103	ß=0,097	ß=0,212	ß=-0,307
ΔNSM protein	ΔOPA	p=0,3659	p=0,7438	p=0,2599	p=0,0982
		ß=-0,003	ß=0,322	ß=0,005	ß=-0,082
ΔNSM protein	ΔDRP^{Ser616}/DRP1	p=0,9816	p=0,1218	p=0,9895	p=0,6879
		ß=-0,082	ß=-0,030	ß=-0,093	ß=-0,144
ΔNSM protein	ΔMFN1	p=0,1299	p=0,7278	p=0,4132	p=0,1830
		ß=-0,186	ß=0,064	ß=-0,160	**ß=-0,208**
ΔNSM protein	ΔMFN2	**p=0,0038**	p=0,6550	p=0,3058	**p=0,0050**
		ß=-0,170	ß=-0,062	ß=-0,483	ß=0,113
ΔNSM protein	$\Delta phosPINK^{Thr257}$/PINK	p=0,1786	p=0,8548	p=0,0714	p=0,5541
		ß=-0,089	ß=0,182	ß=0,235	ß=-0,177
ΔNSM protein	$\Delta phosParkin^{Ser65}$/Parkin	p=0,4971	p=0,4400	p=0,2173	p=0,3978
		ß=-0,169	ß=-0,209	ß=-0,072	ß=-0,116
ΔNSM protein	ΔVDAC	**p=0,0330**	p=0,1939	p=0,6664	p=0,3745
		ß=0,220	ß=0,084	ß=0,448	**ß=0,608**
ΔNSM protein	$\Delta phosAMPK\alpha^{Thr172}$/AMPKα	p=0,2802	p=0,8697	p=0,5659	**p=0,0206**
		ß=0,351	ß=0,582	ß=-0,015	ß=0,417
ΔNSM protein	$\Delta phosIRS1^{Ser1101}$/IRS1	**p=0,0391**	p=0,2775	p=0,9923	p=0,0734
		ß=-0,011	ß=-0,242	ß=0,128	ß=-0,056
ΔNSM protein	Δliver lipid content	p=0,8700	p=0,3094	p=0,1982	p=0,6228
		ß=0,049	ß=-0,075	ß=0,149	ß=0,104
ΔNSM protein	ΔM-value	p=0,4851	p=0,3984	p=0,0608	p=0,4965
		ß=-0,010	ß=0,010	ß=-0,002	ß=-0,013
ΔNSM protein	ΔVO2max	p=0,4334	p=0,8073	p=0,9348	p=0,4826
		ß=0,096	ß=0,018	**ß=0,285**	ß=0,173
ΔNSM protein	ΔCER_C16:0	p=0,2730	p=0,9443	**p=0,0271**	p=0,5101
		ß=-0,004	ß=-0,209	ß=-0,068	ß=0,144
ΔNSM protein	ΔCER_C18:1	p=0,9604	p=0,0564	p=0,5605	p=0,6875
		ß=-0,055	ß=-0,181	ß=-0,184	ß=-0,016
ΔNSM protein	ΔCER_C18:0	p=0,2727	p=0,0243	p=0,1113	p=0,9129
		ß=0,140	ß=0,119	ß=0,341	ß=0,120
ΔNSM protein	ΔCER_C20:0	p=0,1099	p=0,7021	p=0,0265	p=0,4173
		ß=-0,012	ß=-0,002	ß=0,141	ß=-0,066
ΔNSM protein	ΔCER_C22:0	p=0,8403	p=0,9906	p=0,3002	p=0,6552
		ß=0,051	ß=0,001	ß=0,113	ß=0,197
ΔNSM protein	ΔCER_C24:1	p=0,4217	p=0,9973	p=0,3391	p=0,2313
		ß=-0,014	ß=-0,016	ß=0,084	ß=0,074
ΔNSM protein	ΔCER_C24:0	p=0,7794	p=0,9031	p=0,4545	p=0,5655
		ß=0,089	ß=0,023	ß=0,263	ß=0,195
ΔNSM protein	Δmembrane_CER_C16:0	p=0,3280	p=0,9321	p=0,0599	p=0,4716
		ß=-0,009	**ß=-0,192**	ß=-0,109	ß=0,189
ΔNSM protein	Δmembrane_CER_C18:1	p=0,9215	**p=0,0646**	p=0,4309	p=0,5847
		ß=-0,060	ß=-0,173	**ß=-0,217**	ß=0,012
ΔNSM protein	Δmembrane_CER_C18:0	p=0,2309	p=0,0393	**p=0,0975**	p=0,9267
		ß=0,090	ß=0,108	**ß=0,260**	ß=0,055
ΔNSM protein	Δmembrane_CER_C20:0	p=0,2961	p=0,6925	**p=0,0980**	p=0,7670
		ß=-0,019	ß=0,007	ß=0,092	ß=-0,047
ΔNSM protein	Δmembrane_CER_C22:0	p=0,7492	p=0,9644	p=0,5499	p=0,7518

		ß=0,041	ß=0,020	ß=0,061	ß=0,225
ΔNSM protein	Δmembrane_CER_C24:1	p=0,5553	p=0,9084	p=0,6609	p=0,2121
		ß=-0,022	ß=-0,004	ß=0,034	ß=0,096
ΔNSM protein	Δmembrane_CER_C24:0	p=0,6795	p=0,9764	p=0,7954	p=0,4704
		ß=0,222	ß=-0,027	**ß=0,714**	ß=0,426
ΔNSM protein	Δcytosol_CER_C16:0	**p=0,0495**	p=0,8687	**p=0,0096**	p=0,3969
		ß=0,048	ß=-0,295	**ß=0,133**	ß=0,655
ΔNSM protein	Δcytosol_CER_C18:1	p=0,6755	p=0,1884	**p=0,0138**	p=0,3649
		ß=0,035	ß=-0,217	ß=0,058	ß=-0,032
ΔNSM protein	Δcytosol_CER_C18:0	p=0,6786	p=0,2476	p=0,7181	p=0,9010
		ß=0,097	ß=-0,021	**ß=0,451**	ß=-0,062
ΔNSM protein	Δcytosol_CER_C22:0	p=0,2209	p=0,8876	**p=0,0087**	p=0,7352
		ß=0,075	ß=-0,111	ß=0,279	ß=0,008
ΔNSM protein	Δcytosol_CER_C24:1	p=0,3607	p=0,3496	p=0,1211	p=0,9733
		ß=0,074	ß=-0,036	**ß=0,377**	ß=0,053
ΔNSM protein	Δcytosol_CER_C24:0	p=0,3275	p=0,7699	**p=0,0412**	p=0,7580
		ß=-0,149	ß=-1,719	ß=-0,091	ß=0,962
ΔNSM protein	ΔLD_CER_C18:1	p=0,2625	p=0,0000	p=0,7408	p=0,0000
		ß=-0,105	ß=-0,145	ß=-0,210	ß=0,861
ΔNSM protein	ΔLD_CER_C18:0	p=0,3881	p=0,5397	p=0,3640	p=0,2588
		ß=-0,190	ß=0,327	ß=0,042	ß=0,333
ΔNSM protein	ΔLD_CER_C22:0	p=0,5607	p=0,8852	p=0,0000	p=0,7326
		ß=-0,057	ß=-0,064	ß=0,061	ß=0,925
ΔNSM protein	ΔLD_CER_C24:1	p=0,7070	p=0,8535	p=0,8413	p=0,2370
		ß=-0,171	ß=-0,065	ß=-0,016	ß=0,298
ΔNSM protein	ΔLD_CER_C24:0	p=0,3360	p=0,8590	p=0,9554	p=0,5664
		ß=0,026	ß=0,182	ß=0,033	ß=-0,173
ΔNSM protein	ΔT-SM	p=0,6850	p=0,2949	p=0,8471	p=0,2711
		ß=0,019	ß=0,215	ß=0,034	ß=-0,154
ΔNSM protein	ΔSM_C16:0	p=0,7412	p=0,2263	p=0,7522	p=0,3757
		ß=0,013	ß=-0,091	ß=0,061	ß=0,018
ΔNSM protein	ΔSM_C18:0	p=0,6671	p=0,3848	p=0,0863	p=0,8712
		ß=-0,017	ß=-0,105	ß=-0,079	ß=-0,099
ΔNSM protein	ΔSM_C18:1	p=0,7601	p=0,7227	p=0,4638	p=0,3432
		ß=0,038	ß=0,327	ß=0,075	ß=-0,101
ΔNSM protein	ΔSM_C20:0	p=0,5244	p=0,2026	p=0,4326	p=0,5344
		ß=0,014	ß=0,272	ß=0,085	ß=-0,181
ΔNSM protein	ΔSM_C22:0	p=0,8169	p=0,2719	p=0,3033	p=0,2836
		ß=0,002	ß=0,319	ß=0,074	ß=-0,276
ΔNSM protein	ΔSM_C24:0	p=0,9780	p=0,2546	p=0,4588	p=0,1468
		ß=-0,030	ß=0,171	ß=0,042	ß=-0,262
ΔNSM protein	ΔSM_C24:1	p=0,6081	p=0,3349	p=0,6923	p=0,1538
		ß=0,028	ß=0,214	ß=0,033	ß=-0,181
ΔNSM protein	Δmembrane_SM_C16:0	p=0,6724	p=0,2044	p=0,8019	p=0,3965
		ß=0,029	ß=-0,074	ß=0,055	ß=0,055
ΔNSM protein	Δmembrane_SM_C18:0	p=0,5440	p=0,4658	p=0,3723	p=0,7736
		ß=-0,006	ß=-0,078	ß=-0,069	ß=-0,110
ΔNSM protein	Δmembrane_SM_C18:1	p=0,9330	p=0,8028	p=0,5994	p=0,5151
		ß=0,047	ß=0,320	ß=0,054	ß=-0,083
ΔNSM protein	Δmembrane_SM_C20:0	p=0,4883	p=0,1813	p=0,6783	p=0,6871

Group	BSL ASM protein	HIIT ASM protein	ΔASM protein	BSL ASM activity	HIIT ASM activity	ΔASM activity	BSL NSM protein	HIIT NSM protein	ΔNSM protein	BSL PKCθ	HIIT PKCθ	ΔPKCθ	BSL PKCε	HIIT PKCε
IS	0,894844419	1,043854361	0,149009942	0,159102492	1,046608568	0,887506076	2,724886714	2,584357148	-0,140529567	0,60340096	0,920558903	0,317157944	0,494224543	0,972385345
IS	1,902155901	0,756501719	-1,145654182	0,478502133	1,220678853	0,74217672	1,028230209	2,155621744	1,127391535	0,493339459	0,730669454	0,237329994	1,408322672	0,477975309
IS	0,615691097	0,462249105	-0,153441991	0,559614677	1,186503141	0,626888463	1,301514432	1,528765856	0,227251424	2,394619672	0,718418615	-1,676201058	1,131399028	0,630355358
IS	1,038157198	0,40467112	-0,633486078	0,335446041	0,918353201	0,58290716	1,130205507	1,581829768	0,451624262	1,329524754	0,734595033	-0,594929721	0,625193527	0,441648272
IS	2,256404808	1,768808507	-0,4875963	0,536811516	1,829143497	1,292331981	0,891981242	0,814527196	-0,077454046	0,525164407	0,883520981	0,358356574	0,256187565	0,864809319
IS	0,278498462	0,427754857	0,149256395	0,635870359	1,723642441	1,087772083	0,208922236	1,982731902	1,773809666	0,614138892	0,760973661	0,146834769	1,296302011	0,886587934
IS	1,072609974	1,069564919	-0,003045056	0,197061491	1,046330763	0,849269272	0,412014307	1,810147998	1,398133692	1,787648262	1,009259229	-0,778389033	0,430691333	0,17143141
IS	1,08456081	0,173229623	-0,911331186	0,296227684	0,786561938	0,490334255	0,154933228	2,290810312	2,135877084		0,611576284			0,426996967
IS	1,065241327	0,771613066	-0,29362826	0,301026524	1,622627626	1,321601101	0,114463288	0,595772431	0,481309143	2,719570363	0,892551085	-1,827019278	1,846710068	0,261760907
IS	0,770595711	0,662902864	-0,107692847	0,391928384	0,057235982	-0,334692401	0,25484885	1,737739744	1,482890893	1,071867997	1,07126373	-0,000604268	0,826402911	0,279964413
IS	1,494013077	0,503106907	-0,990906169	0,211409685	2,169399121	1,957989435	0,476376098	0,248075035	-0,228301063	0,339032806			0,421543069	
IS	0,509294889			0,264772457			1,091608297	1,787766142	0,696157846	1,01115081	0,895053076	-0,116097734	0,619073623	1,448097393
IR	2,018381963	0,472739957	-1,545642006	0,685178138	1,076713156	0,391535018	0,426294301	3,211981176	2,785686875	0,607816568	0,464606795	-0,143209773	0,560806182	0,663033126
IR	0,362257829	0,463436967	0,101179138	0,424280709	1,230904434	0,806623725	0,651310463	2,073267685	1,421957222	0,71398086	0,462698185	-0,251282675	0,68038401	0,735461356
IR	0,366277891	0,752866493	0,386588602	0,235183599	1,065978839	0,83079524	0,723948198	4,038147365	3,314199167	1,02080357	0,61454489	-0,40625868	1,346380093	1,544535699
IR	0,338506682	1,356223408	1,017716726		2,970324562		1,009762672	0,308606096	-0,701156576	1,081734415	1,082176431	0,000442016	1,105168379	1,446967966
IR	0,342208047	1,216075313	0,873867267	0,131646631	0,220096506	0,088449876	0,305300137	2,078707119	1,773406982	1,04276455	1,300625557	0,257861007	0,767004478	0,735910553
IR	3,399050808	1,31565272	-2,083398088	0,889878836	1,510794511	0,620915676	0,009756709	0,226988024	0,217231315	0,593608586	0,777477724	0,183869138	0,661587831	0,471098826
IR	1,854915211	5,077360049	3,222444838	0,551086935	6,538478335	5,9873914	0,023145444	0,169211601	0,146066157	3,110149811	0,733685	-2,376464811	1,022161037	0,600071482
IR	0,69832253	1,063089674	0,364767144	0,231459865	0,607926833	0,376466968	0,056853238	1,295585244	1,238732006	1,285414957	1,282133443	-0,003281514	0,791220771	1,00838241
IR	2,489728785	0,957776974	-1,531951811	0,32916621	1,747369038	1,418202828	0,090269649	0,482980058	0,392710409	0,785673558	0,892788299	0,10711474	0,657908286	0,700227246
IR	0,989223128	0,359509279	-0,629713849	0,339969088	0,376417532	0,036448444	0,106469017	0,995868636	0,889399619	0,784516762	0,647440242	-0,137076519	0,568569969	0,539596694
IR	2,202469595	1,278723437	-0,923746159	0,211190118	0,944121719	0,732931601	0,278614776	0,665065189	0,386450413	0,687060797	1,573366904	0,886306108	0,422411858	0,977024667
T2D	0,208864869	0,939168412	0,730303543	0,265869482	1,790247133	1,52437765	0,420462491	0,988911236	0,568448745	2,286939902	0,642167543	-1,644772359	0,977214774	0,526485124
T2D	0,553474954	1,242183158	0,688708204	0,551704667	1,724856406	1,173151739	0,414748941	1,327083951	0,91233501	0,695345044	0,488508167	-0,206836876	4,994056531	0,692473352
T2D	0,328665117	1,222302719	0,893637602	0,186778312	1,315855322	1,12907701	1,221037156	1,206872317	-0,014164839	0,664285051	1,586281503	0,921996453	3,839515028	2,071280742
T2D	0,717336348	1,598328174	0,880991826	0,736624499	1,810831229	1,074206729	0,622627395	0,71379067	0,091163276	0,457590067	1,251366919	0,793776851	2,771961278	1,3163103
T2D	0,423817339	1,54250097	1,118683631	0,41802252	1,80952032	1,3914978	1,221080105	0,872879156	-0,348200949	0,428674329	0,901458078	0,472783749	0,790304755	1,979852507
T2D	0,224453805	0,377511006	0,153057201	0,331486145	2,15996609	1,828479946	0,702691369	0,501069693	-0,201621675	0,591998111	1,153343541	0,56134543	0,531503659	0,738689614
T2D	1,006593032	1,161679252	0,15508622	0,396012887	1,842848275	1,446835388	2,618184345	1,163390721	-1,454793624	1,520915532	0,172755885	-1,348159646	2,50563177	0,660191832
T2D	0,467489747	0,136080232	-0,331409514	0,15472285			0,882642897	7,488039488	6,605396591	2,006748585	0,362628102	-1,644120483	4,340591161	1,027617638
T2D	0,133084809	0,407718164	0,274633355	0,33744235	0,637907763	0,300465413	0,738444466	1,704264503	0,965820037	2,086287161	0,162064278	-1,924222883	4,854260584	0,67559389
T2D	0,510641151	1,921409356	1,410768204	0,6907111	1,148245289	0,45753419	0,432540153	0,92394497	0,491404817	2,470249733	0,320374505	-2,149875228	2,694415164	0,821969827
T2D	0,625977259	0,811186522	0,185209263	0,161071737	1,035061892	0,873990156	1,002977599	0,513983943	-0,488993655	0,701242003	0,519379629	-0,181862374	1,703949648	1,187700656
T2D	0,779728827	0,651378703	-0,128350124	0,17088454	1,834043136	1,663158596	0,724858648	0,647291516	-0,077567133	1,982587684	1,047769301	-0,934818384	2,459884604	0,44783446
T2D	2,173600673	0,228792999	-1,944807674	0,73266979	1,333381627	0,600711838	0,244836456	1,826173632	1,581337176	0,42477822			1,226411246	
T2D	1,300642839	4,292899703	2,992256864	0,127539273	5,224753925	5,097214652	0,405028005	2,675915054	2,27088705	0,431422651			0,311808792	
T2D	1,393558786	0,466668292	-0,926890493	0,362754209	1,679903571	1,317149362	0,925680947	1,853143493	0,927462547	0,704012701	1,537222674	0,833209973	0,253678807	0,706700227
T2D	0,249294526	0,742506001	0,493211475	0,173275454	2,657958301	2,484682847	1,319688157	1,040396405	-0,279291752	1,425282202	1,162723528	-0,262558674	0,751885175	0,934451945
T2D	0,244354107	0,592066861	0,347712754	0,25687582	1,296201939	1,03932612	1,371780379	2,64660442	1,274824041	1,487827659	1,172168799	-0,31565886	0,742806231	0,977774289
T2D	0,253251814	1,290265853	1,037014039	0,469324184	1,247523231	0,778199047	0,250669255	0,363397232	0,112727977	0,907096653	0,398724008	-0,508372645	1,090606605	0,308190972
T2D	0,129950653	0,725674213	0,59572356	0,203103875	0,607797312	0,404693436	0,338432612	4,086556486	3,748123874	1,16039092	0,110234263	-1,050156657	0,514308051	1,370423529
T2D										1,174440759			0,940575112	

ΔPKCε	BSL OPA	HIIT OPA	ΔOPA	BSL DRP1	HIIT DRP1	ΔDRP1	BSL DRP^{Ser616}	HIIT DRP^{Ser616}	ΔDRP^{Ser616}	BSL DRP^{Ser616}/DRP1	HIIT DRP^{Ser616}/DRP1	ΔDRP^{Ser616}/DRP1	BSL MFN1	HIIT MFN1
0,478160802	1,675630259	0,273806786	-1,401823472	1,458229427	2,220346781	0,762117354	0,432829191	1,117526386	0,684697194	0,296818308	0,503311643	0,206493335	1,726238806	2,014946109
-0,930347363	0,836148825	3,821682635	2,98553381	1,305230416	1,118097494	-0,187132922	1,300531109	1,871207675	0,570676566	0,996399634	1,673563965	0,67716433	1,581319434	2,559966319
-0,50104367	1,006484436	1,332511523	0,326027087	1,945861011	2,51405171	0,568190698	1,314235977	1,008791877	-0,305444099	0,675400745	0,401261388	-0,274139358	1,238537595	1,43642586
-0,183545255	1,573982178	2,536419742	0,962437564	0,742174131	2,597828	1,85565387	1,478775667	1,154111288	-0,324664379	1,992491527	0,444260085	-1,548231442	0,946853007	0,92195587
0,608621754	2,024595936	2,299889134	0,275293199	0,897847501	2,062768756	1,164921255	1,18718153	1,48240767	0,29522614	1,322252976	0,718649469	-0,603603507	1,108201013	1,028620315
-0,409714077	3,699077436	1,566889087	-2,13218835	1,326834137	1,58483958	0,258005442	0,926255825	1,588790423	0,662534597	0,698094659	1,002492898	0,304398238	1,349179292	1,216873239
-0,259259923	1,170385761	2,071206535	0,900820774	0,586280747	0,898535058	0,312254311	0,975056268	1,213659723	0,238603455	1,663121761	1,350709371	-0,312412389	0,945214625	0,967392087
	0,794144748	1,351890218	0,557745471	0,999223702	0,947754156	-0,051469546	0,790403997	1,426990886	0,636586889	0,791018062	1,505655107	0,714637045	1,087997621	1,529773571
-1,584949161	1,01125804	1,075233143	0,063975103	1,347246579	1,397173289	0,04992671	1,202672531	1,393603021	0,19093049	0,892689245	0,997444649	0,104755405	1,26936942	1,424175876
-0,546438498	0,78388805	0,999486622	0,215598573	0,878071922	0,884450587	0,006378665	1,31612906	1,225076031	-0,091053029	1,498885259	1,385126596	-0,113758663	1,718251529	1,088527768
	0,640594494			1,278624311			2,039179638			1,594823139			1,224482501	
0,82902377	0,805549506	1,134387611	0,328838105	1,531504012	2,728448285	1,196944273	1,421635807	1,711360857	0,28972505	0,928261236	0,627228622	-0,301032615	1,323362124	1,459632846
0,102226944	1,246251575	1,080081553	-0,166170023	1,116686463	2,280636492	1,163950029	2,109785839	2,152323459	0,04253762	1,889326958	0,94373806	-0,945588898	1,235097358	1,335569564
0,055077346	1,115748332	0,848720428	-0,267027904	0,79589505	1,747283775	0,951388725	1,50921546	1,753182775	0,243967315	1,896249335	1,003376097	-0,892873238	1,572595298	0,951981175
0,198155606	0,84242714	1,148221125	0,305793986	0,972373801	0,915857639	-0,056516162	1,090302327	1,630777155	0,540474828	1,121279004	1,780601139	0,659322135	1,041970579	1,911569358
0,341799586	1,290900704	2,047291146	0,756390442	1,41835041	1,109100555	-0,309249855	1,270029773	1,910510697	0,640480924	0,895427367	1,72257663	0,827149263	1,284721309	2,024355168
-0,031093926	0,258263895	1,43931093	1,181047035	1,845421963	0,946576519	-0,898845444	1,525743872	1,336045031	-0,189698841	0,82677236	1,411449581	0,58467722	1,017340495	1,812162725
-0,190489005	0,189874375	0,67717288	0,487298505	1,766676147	1,179137969	-0,587538179	2,008842332	0,69944715	-1,309395182	1,137074463	0,593185165	-0,543889298	1,240811083	1,350082049
-0,422089555	0,251323053	0,781391333	0,53006828	0,982917295	1,841902935	0,85898564	0,260524855	2,382233498	2,121708643	0,265052672	1,293354527	1,028301855	1,106938799	0,844181845
0,217161639	0,237872213	0,802509812	0,564637599	0,843940569	1,749790815	0,905850246	0,236863251	4,718530509	4,481667257	0,280663426	2,696625486	2,415962061	1,147427456	1,090506301
0,042318959	0,539618971	1,036281306	0,496662335	1,175371889	1,150840347	-0,024531542	0,650200018	1,289141375	0,638941357	0,553186633	1,120173948	0,566987315	1,892831714	1,22298622
-0,028973275	0,852334028	0,787955135	-0,064378893	0,932256028	1,611019218	0,67876319	3,431474766	0,760505052	-2,670969713	3,680828724	0,472064544	-3,20876418	1,204461204	0,88474166
0,554612809	1,003816011	1,074643309	0,070827297	0,612417818	1,585492415	0,973074597	0,631536769	1,50271125	0,871174481	1,031218803	0,947788357	-0,083430446	1,045967224	1,389324427
-0,45072965	0,548691783	0,497711891	-0,050979892	1,26988142	1,06022095	-0,20966047	0,545477733	0,407330229	-0,138147504	0,429550133	0,384193718	-0,045356415	1,327289873	1,619464917
-4,301583179	0,654710723	0,5927972	-0,061913522	4,785222041	1,676757038	-3,108465002	0,774139633	0,861420818	0,087281185	0,16177716	0,513742181	0,351965021	1,921732553	3,108208457
-1,768234286	0,544889985	0,935177754	0,390287769	0,692419335	0,418718905	-0,27370043	0,871380128	0,745434178	-0,12594595	1,258457244	1,780273519	0,521816275	2,016085886	2,139180102
-1,455650978	1,360642418	1,990881479	0,630239061	1,80880047	1,344380762	-0,464419708	1,081417305	0,656228945	-0,42518836	0,597864343	0,488127295	-0,109737048	2,21674331	1,24424844
1,189547752	2,176248621	1,831140108	-0,345108513	2,696712754	3,742563178	1,045850424	1,062447453	0,733752712	-0,328694741	0,393978725	0,196056199	-0,197922526	1,558607936	1,717890877
0,207185955	1,249971735	1,707939424	0,457967689	3,056336484	1,583163567	-1,473172917	0,805683315	1,076651575	0,27096826	0,263610803	0,680063385	0,416452582	1,055799372	1,554215377
-1,845439939	1,632683505	1,780087822	0,147404317	0,49395927	0,556950372	0,062991102	0,988765784	1,224307325	0,23554154	2,00171521	2,198234143	0,196518933	1,144946837	1,010590429
-3,312973523		0,827235566		0,316435966	0,494516647	0,178080681	4,484534839	1,612315565	-2,872219274	14,17201369	3,260386837	-10,91162685	0,878679627	1,307799642
-4,178666693	1,701755259	1,092368756	-0,609386503	0,958012256	0,531379369	-0,426632887	0,354245563	0,889682912	0,535437349	0,369771431	1,674289528	1,304518097	0,992667298	0,841376959
-1,872445337	0,568514959	0,292230511	-0,276284448	0,693452929	0,656725685	-0,036727244	0,255878537	0,711387374	0,455508837	0,368991933	1,08323367	0,714241736	1,29186941	0,719764255
-0,516248992	0,162399767	0,893727532	0,731327765	0,739071056	1,62427651	0,885205454	0,144992032	1,315639743	1,170647711	0,196181451	0,809985082	0,613803632	1,121652598	1,143889072
-2,012050144	1,11660035	0,98346544	-0,13313491	1,119294778	1,355718304	0,236423526	0,348544378	0,849403265	0,500858887	0,311396412	0,626533745	0,315137332	0,766967521	0,890213175
	1,555213997	0,493310875	-1,061903122	1,845462398	1,836071041	-0,009391357	0,486357599	0,936605972	0,450248374	0,263542405	0,510114234	0,246571829	1,119655512	0,720023757
	1,534166645	0,742670781	-0,791495864	4,865203436	3,89184048	-0,973362956	1,544226185	1,238299932	-0,305926253	0,317402182	0,318178491	0,00077631	1,09503769	0,827829438
0,45302142	1,968657986	1,119527606	-0,849130381	1,840388399	1,46481572	-0,375572679	1,525445482	1,771150722	0,245705239	0,828871494	1,209128696	0,380257202	1,635850845	2,070352561
0,182566771	0,600194972	0,709219925	0,109024953	0,703830056	1,20602	0,502189944	0,900610942	1,794420603	0,893809661	1,279585795	1,487886273	0,208300478	0,768148316	1,331976641
0,234968059	2,300638194	0,842274093	-1,458364102	0,68149622	2,446312759	1,76481654	1,05607915	2,082588195	1,026509045	1,549647847	0,851317227	-0,69833062	0,802998281	1,749494444
-0,782415633	1,229968498	0,435814377	-0,794154121	0,952988612	1,166884372	0,21389576	0,192737346	1,042197598	0,849460252	0,202245172	0,893145562	0,690900389	0,94477494	1,543541953
0,856115479	1,267225819	2,548080297	1,280854478	0,743054697	1,590313876	0,847259179	0,232682074	1,462976087	1,230294013	0,313142592	0,919929146	0,606786555	2,123519113	0,905056136
	2,981595754	4,444375901	1,462780147	0,632169045	0,603567945	-0,0286011		1,172517809			1,942644269		1,195604265	2,158842395

ΔMFN1	BSL MFN2	HIIT MFN2	ΔMFN2	BSL PINK	HIIT PINK	ΔPINK	BSL phosPINK^{Thr257}	HIIT phosPINK^{Thr257}	ΔphosPINK^{Thr257}	BSL phosPINK^{Thr257}/PINK	HIIT phosPINK^{Thr257}/PINK	ΔphosPINK^{Thr257}/PINK	BSL Parkin	HIIT Parkin
0,288707303	1,092404259	1,119256781	0,026852522	0,76608542	0,154268842	-0,611816579	0,805852882	1,025167989	0,219315107	1,051909957	6,645334071	5,593424113	3,674140764	0,955044429
0,978646885	1,075130541	2,425097496	1,349966955	1,204578551	1,349382574	0,144804023	0,617391969	1,248244115	0,630852146	0,51253774	0,925048344	0,412510603	0,821531452	1,141540612
0,197888265	0,91792147	1,191221815	0,273300345	1,051214276	1,517846981	0,466632705	0,743769912	0,943043674	0,199273761	0,707534067	0,621303521	-0,086230546	0,236017558	0,19790452
-0,024897137	1,074784295	0,88088873	-0,193895565	1,123411402	0,812415663	-0,310995739	0,797988205	1,337233877	0,539245672	0,710325891	1,645997164	0,935671273	1,017602207	0,554295032
-0,079580698	0,790204187	1,367322318	0,577118131	2,171470003	1,49135311	-0,680116892	0,950325568	0,741316351	-0,209009217	0,437641582	0,497076343	0,059434761	0,632467988	1,117631955
-0,132306053	1,012769886	1,446082534	0,433312648	2,677504889	0,729317384	-1,948187505	0,77562413	0,986212237	0,210588108	0,289681686	1,352240135	1,062558449	1,110096264	0,721575403
0,022177462	0,99362469	1,177133382	0,183508692	1,147064032	1,548504219	0,401440187	1,629003325	1,417625706	-0,211377618	1,420150297	0,915480687	-0,50466961	0,465097575	0,57767044
0,44177595	0,763235458	1,590281404	0,827045946	1,379415558	1,570336553	0,190920995	1,583733713	0,905646345	-0,678087368	1,148119364	0,576721177	-0,571398187	0,811098998	0,817132187
0,154806456	1,04490048	1,335108572	0,290208092	1,181138508	1,536606778	0,35546827	0,977704376	1,162728428	0,185024052	0,827764373	0,756685734	-0,071078639	0,629884309	0,822468353
-0,629723762	1,32559035	0,833143489	-0,492446861	1,661772124	0,681524756	-0,980247368	0,731560112	2,988288415	2,256728303	0,440228899	4,384710002	3,944481103	1,19227314	0,523297122
	1,279526117			1,461712617			2,399759177			1,641744861			0,552860761	
0,136270723	1,585031513	1,176833888	-0,408197625	1,269377937	0,641331284	-0,628046654	2,620860523	1,92443527	-0,696425252	2,064681011	3,000688285	0,936007274	0,196204697	0,668423771
0,100472206	1,455915404	0,732663696	-0,723251708	0,851479805	0,826447424	-0,025032381	2,09140274	1,453511466	-0,637891274	2,456197701	1,758746442	-0,697451259	0,717945004	0,841455904
-0,620614123	1,531600343	0,801707258	-0,729893085	1,385469831	1,625036271	0,23956644	1,889992936	1,153073638	-0,736919298	1,364153079	0,709567939	-0,65458514	0,385817476	0,978859391
0,869598779	1,978356753	1,20743851	-0,770918243	1,062977022	0,357899933	-0,705077089	1,476951694	0,871967912	-0,604983781	1,389448373	2,436345556	1,046897184	1,378170879	1,826055785
0,739633859	0,892110539	2,555569056	1,663458517	1,308848994	0,466787701	-0,842061294	0,37893632	0,893462286	0,514525967	0,289518746	1,914065613	1,624546867	0,97401103	0,778842324
0,794822231	1,007941906	1,824446976	0,816505069	0,295182908	0,918248544	0,623065636	0,695007842	1,039485337	0,344477495	2,354498934	1,132030476	-1,222468458	0,986491035	0,639660639
0,109270966	1,408794803	1,134103847	-0,274690956	0,27850106	1,494138638	1,215637577	0,844887859	0,771614656	-0,073273203	3,0336971	0,516427751	-2,517269349	0,789292287	
-0,262756954	1,075359155	1,756317149	0,680957994	0,451754634	0,287151116	-0,164603518	0,501201742	1,243027867	0,741826125	1,109455674	4,328828263	3,219372588	1,140457389	0,589075185
-0,056921155	0,926282512	1,247942733	0,321660221	0,521440981	0,71696838	0,195527399	1,248406645	2,197156136	0,948749491	2,394147545	3,064509116	0,670361571	1,243245564	0,727771078
-0,669845494	0,889061372	0,860789507	-0,028271865	1,203079754	1,083213805	-0,119865949	0,535703379	0,703020424	0,167317045	0,445276697	0,649013538	0,203736841	0,949484484	0,756151674
-0,319719544	0,903584961	1,01491154	0,11132658	1,771761045	0,972385983	-0,799375062	1,177673252	0,847530271	-0,330142981	0,664690792	0,87159861	0,206907818	1,189219337	0,639250551
0,343357203	1,220027136	0,911623704	-0,308403432	0,893267459	0,884548826	-0,008718633	1,15955836	0,811338908	-0,348219452	1,298108812	0,917234735	-0,380874077	0,936405172	0,767765782
0,292175044	0,59689465	1,069679232	0,472784582	0,975909175	0,794882131	-0,181027044	0,762347453	1,490133394	0,727785941	0,781166396	1,874659571	1,093493175	2,020871773	0,543245604
1,186475903	1,417661066	2,368472886	0,95081182	0,872065147	0,588140031	-0,283925116	0,706687684	0,798105692	0,091418009	0,810361114	1,356999439	0,546638326	2,103453112	0,993882663
0,123094216	0,910768087	2,417053656	1,506285569	1,531798849	1,127536562	-0,404262287	0,59749108	1,754538895	1,157047814	0,390058447	1,556081598	1,166023151	3,039377351	0,383537599
-0,97249487	1,329671611	1,694939155	0,365267544	1,011765103	0,65779247	-0,353972633	0,75590078	1,303527755	0,547626975	0,747110942	1,981670229	1,234559287	2,593600284	0,327302924
0,159282941	1,10087673	1,849838234	0,748961504	1,612409449	1,492928981	-0,119480468	0,784340409	0,355924237	-0,428416172	0,486439973	0,238406676	-0,248033297	1,970316623	0,527380982
0,498416005	0,686866951	0,952590976	0,265724025	0,958831937	0,927937691	-0,030894247	0,830792463	0,980028337	0,149235874	0,866463069	1,056135932	0,189672863	1,574749727	0,632567121
-0,134356408	1,061363325	1,945927037	0,884563712	0,767279052	1,300920824	0,533641771	0,843136349	1,006541599	0,16340525	1,098865329	0,773714726	-0,325150603	2,163381655	0,574100076
0,429120016	0,921152727	0,989329238	0,068176511	0,442048263	0,715172901	0,273124639	1,090195044	1,693073404	0,60287836	2,466235333	2,367362356	-0,098872977	2,324369927	0,582725685
-0,15129034	0,630201538	0,862781864	0,232580326	0,463991589	1,015564349	0,55157276	1,129773437	2,056940202	0,927166764	2,434900682	2,025415921	-0,409484762	0,988267763	0,724836156
-0,572105155	0,661831746	0,744269808	0,082438062	0,929883974	1,219410204	0,289526229	0,771495484	0,925190753	0,153695268	0,829668545	0,758719871	-0,070948674	0,484502711	0,62899491
0,022236474	0,539635361	1,816664056	1,277028695	0,751939261	0,995276167	0,243336907	0,878038833	1,006013464	0,127974631	1,167699147	1,010788259	-0,156910888	1,138791781	0,833082141
0,123245654	0,563907766	1,441982331	0,878074565	1,110082455	0,645305114	-0,464777341	0,779701847	2,204631072	1,424929225	0,702381921	3,416416552	2,714034631	2,787497333	0,713850773
-0,399631755	0,522269093	0,575692697	0,053423604	0,77775988	0,590676563	-0,187083318	1,248282629	2,907548819	1,65926619	1,60497174	4,922404242	3,317432502	0,611739099	0,688405996
-0,267208252	0,870200188	1,530302008	0,660101819	0,675209594	0,891800812	0,216591218	1,639057234	2,600445589	0,961388355	2,427479184	2,915948891	0,488469707	0,714452303	0,510742687
0,434501715	1,616501757	2,666991848	1,050490091	0,86218444	1,139216956	0,277032517	1,545105413	1,501676928	-0,043428486	1,79208223	1,318165885	-0,473916344	0,641360511	0,677001168
0,563828326	0,616996403	1,475732993	0,85873659	0,834238647	1,068815027	0,23457638	1,471649194	1,677747268	0,206098074	1,764062597	1,569726496	-0,194336101	0,588110732	0,771636793
0,946496163	0,977436301	2,356186547	1,378750247	1,493965804	1,033321805	-0,460643999	0,757260536	1,267440532	0,510179996	0,506879431	1,226569037	0,719689606	1,567542224	0,936436687
0,598767013	0,685745044	1,182999388	0,497254344	0,534379249	0,521739536	-0,012639712	0,462321003	1,140783031	0,678462028	0,865155233	2,186499108	1,321343876	2,221006493	1,006572974
-1,218462977	1,49577584	1,726851904	0,231076064	3,223813803			1,06460292	1,437715335	0,373112414	0,330230896			2,736366608	0,843543085
0,96323813	1,148505153	0,818170008	-0,330335145	1,773884722			0,566243227	1,87255489	1,306311663	0,319210837			1,704828046	1,100807983

ΔParkin	BSL phosParkin^{Ser65}	HIIT phosParkin^{Ser65}	ΔphosParkin^{Ser65}	BSL phosParkin^{Ser65}/Parkin	HIIT phosParkin^{Ser65}/Parkin	ΔphosParkin^{Ser65}/Parkin	BSL VDAC	HIIT VDAC	ΔVDAC	BSL AMPKα	HIIT AMPKα	ΔAMPKα	BSL phosAMPKα^{Thr172}	HIIT phosAMPKα^{Thr172}
-2,719096336	1,157752966	0,930661477	-0,22709149	0,315108495	0,974469301	0,659360806	1,011829615	1,950018789	0,938189174	0,333385724	0,175904556	-0,157481168	0,507048046	0,788606759
0,32000916	0,9251093	1,157213814	0,232104514	1,12607898	1,013729868	-0,112349112	0,944922867	1,5801249	0,635202033					
-0,038113039	1,511310451	1,008057526	-0,503252925	6,403381432	5,093655913	-1,309725519	0,829916143	2,08777959	1,257863447					
-0,463307175	1,661061326	1,137317726	-0,5237436	1,632328738	2,051827387	0,419498648	0,756789043	0,490819672	-0,265969371	0,165714972	0,41347209	0,247757118	0,274702536	0,243468384
0,485163967	1,273537993	1,047197917	-0,226340076	2,013600715	0,936979219	-1,076621496	0,448852437	0,823718795	0,374866357	0,187322437	0,560909442	0,373587005	0,488936931	0,16566144
-0,388520861	0,731313789	1,051993485	0,320679695	0,658784119	1,457912064	0,799127945	1,586645365	1,074767615	-0,51187775	0,281660864	0,273287971	-0,008372892	0,214100334	0,263638436
0,112572865	1,294760978	1,140155942	-0,154605036	2,783848053	1,973713493	-0,81013456	1,291429737	0,923554162	-0,367875575					
0,006033189	1,215131084	1,128732986	-0,086398098	1,498129189	1,381334628	-0,116794561	0,577837241	0,98632891	0,408491669	0,051977113	0,056299262	0,004322149	0,38259225	0,129815445
0,192584044	0,810002321	1,07525135	0,265249028	1,285954118	1,307346775	0,021392657	0,677705017	0,834184124	0,156479107					
-0,668976018	1,13206002	1,173232886	0,041172866	0,94949721	2,242001412	1,292504202	0,566243275	0,622565022	0,056321747	0,409953716	0,4199035	0,009949784	0,377949454	
	1,076382319			1,946932021			0,618832914							
0,472219074	1,641237088	1,785430964	0,144193875	8,364922505	2,671106326	-5,693816179	0,471404512	0,958875201	0,487470689	0,209979115	0,619605634	0,409626519	0,363444281	0,310847392
0,1235109	1,566566343	1,465196702	-0,101369641	2,182014409	1,741263797	-0,440750613	1,131636975	0,879948115	-0,25168886	0,343834816	0,642260006	0,29842519	0,314278034	0,120127352
0,593041915	0,961284538	1,367341419	0,406056881	2,491552608	1,396872147	-1,094680461	1,184604212	0,621990867	-0,562613345	0,969269077	0,882848654	-0,086420423	0,260513234	0,129025996
0,447884907	0,870535256	0,689114223	-0,181421034	0,631659883	0,377378516	-0,254281367	0,864159566	1,226790911	0,362631346	0,574634208	0,766767217	0,192133009	0,081748978	0,154178452
-0,195168705	0,96123319	0,749849607	-0,211383583	0,986881216	0,962774599	-0,024106617	1,737023067	1,204954984	-0,532068083					
-0,346830397	0,861479764	0,718475466	-0,143004299	0,87327683	1,123213502	0,249936671	1,795280715	1,40795254	-0,387328175	0,980999793	0,793063895	-0,187935898	0,105645895	0,3452894
		0,769021412					1,661899845	0,747299341	-0,914600505	0,697150479	0,175245873	-0,521904606	0,507048046	
-0,551382204	0,664943588	1,230360556	0,565416968	0,583049919	2,08863077	1,505580851	1,65000221	0,513326518	-1,136675692	0,584043832	0,71414351	0,130099679	0,190474981	0,659931436
-0,515474486	1,143302838	1,800712398	0,657409559	0,919611436	2,474284086	1,554672651	0,98154806	0,571010386	-0,410537674	0,642560213	0,334727367	-0,307832846	0,394335001	0,125825152
-0,19333281	0,982875841	1,073193118	0,090317276	1,035167881	1,419282869	0,384114988	1,191404706	0,659824784	-0,531579922					
-0,549968786	0,911010938	1,12788703	0,216876092	0,766057959	1,764389608	0,998331649	0,544860717	1,107592628	0,562731911	0,420299069	0,295802246	-0,124496823		0,871244151
-0,16863939	1,055745339	1,128578866	0,072833527	1,127445011	1,469952026	0,342507015	0,831217141	1,340839797	0,509622656	0,343595341	0,551336244	0,207740903	0,508675743	0,141445959
-1,477626168	0,821902922	1,202321269	0,380418347	0,406707112	2,213218587	1,806511476	0,556003959	0,972853703	0,416849744	0,340627289	0,562740998	0,222113709	0,482232975	1,317711702
-1,109570449	0,787687906	1,014302729	0,226614823	0,374473717	1,020545751	0,646072034	1,263095504	1,566077316	0,302981812					
-2,655839752	0,801188294	1,150858902	0,349670608	0,263602772	3,000641672	2,7370389	1,023705983	1,315194156	0,291488173	1,250085614	1,043558288	-0,206527326	0,43278421	0,94045883
-2,26629736	0,770242975	1,33253899	0,562296015	0,296978289	4,071271269	3,77429298	1,413553777	1,637777026	0,224223249	1,432297506	0,525671037	-0,906626469	1,4189195	0,979686714
-1,442935641	0,85204661	0,970801873	0,118755264	0,432441466	1,84079803	1,408356564	1,141679963	0,842353096	-0,299326867	0,814528955	0,725883912	-0,088645043	0,341153395	0,902605388
-0,942182606	0,964746062	1,101882559	0,137136496	0,612634532	1,741921959	1,129287427	0,626873314	0,768292183	0,141418869	0,320950919	0,371288023	0,050337104	0,622619262	0,739822498
-1,589281579	0,867577742	1,205054008	0,337476266	0,401028519	2,099031264	1,698002744	0,727158262	0,854948431	0,12779017	0,309433361	0,441587203	0,132153842	0,725499147	0,521335847
-1,741644243	1,146630513	1,203007215	0,056376702	0,4933081	2,064448586	1,571140485	1,123873788	0,856521596	-0,267352191	0,246567871	0,177166884	-0,069400987	0,16777657	0,367881077
-0,263431607	0,726247765	1,412994122	0,686746357	0,734869427	1,949397957	1,21452853	0,564376323	0,750292304	0,185915982	0,291751409	0,319901751	0,028150342	0,467581256	3,208060744
0,144492199	1,120224437	1,406049946	0,28582551	2,312111805	2,235391613	-0,076720192	0,52323209	0,590036375	0,066804285	0,334689038	0,14824841	-0,186440627	0,640246645	0,718268809
-0,30570964	0,86701993	1,499005592	0,631985662	0,761350709	1,79934909	1,037998381	0,588562245	1,27927337	0,690711125	0,18207294	0,313142751	0,131069811	0,802733202	0,421272725
-2,07364656	0,630121319	0,824617692	0,194496373	0,226052708	1,155168172	0,929115465	1,026340297	0,585417818	-0,440922479	0,124058925	0,162703462	0,038644537	0,592001558	0,080032315
0,076666897	1,331975719	1,127141225	-0,204834493	2,17735914	1,637320465	-0,540038675	0,515463181	0,757528742	0,242065561	0,171216234	0,116110169	-0,055106065	0,341081804	0,52356255
-0,203709616	0,758886598	1,509437253	0,750550654	1,062193508	2,955377122	1,893183614	0,983418432	0,357457758	-0,625960674					
0,035640657	0,838315335	0,663321589	-0,174993747	1,307089103	0,979793861	-0,327295242	1,622645623	0,871715047	-0,750930575	0,332814195	0,283467171	-0,049347024	0,661173614	0,742778458
0,183526061	0,747235604	0,723671072	-0,023564532	1,270569576	0,937838992	-0,332730584	0,332375116	0,811511495	0,47913638					
-0,631105536	0,976703557	1,03794396	0,061240403	0,623079584	1,108397369	0,485317785	1,344690887	2,439436883	1,094745996	0,160535049	0,288667973	0,128132923	1,558925067	2,558717394
-1,214433519	0,780079184	0,716237264	-0,06384192	0,351227782	0,711560197	0,360332415	0,311003674	0,841490042	0,530486368	0,304192181	0,270640766	-0,033551415	0,239717858	0,186390691
-1,892823523	1,046675603	1,042105238	-0,004570365	0,382505619	1,235390647	0,852885028	1,49711157	2,254293357	0,757181787	0,341251885	0,106595592	-0,234656294	0,456233017	0,602472866
-0,604020063	0,752932836	0,836405463	0,083472628	0,441647378	0,7598105	0,318163122	1,751170001	1,657416412	-0,093753589					

ΔphosAMPKα^{Thr172}/AMPKα	BSL IRS1	HIIT IRS1	ΔIRS1	BSL phosIRS1^{Ser1101}	HIIT phosIRS1^{Ser1101}	ΔphosIRS1^{Ser1101}	BSL phosIRS1^{Ser1101}/IRS1	HIIT phosIRS1^{Ser1101}/IRS1	ΔphosIRS1^{Ser1101}/IRS1
2,962246314	2,229748616	2,519165348	0,289416732	4,823562456	1,210529943	-3,613032514	2,163276354	0,480528181	-1,682748173
-1,06884212	0,398909409	0,161873769	-0,237035639	6,492590227	3,130479046	-3,362111181	16,27585131	19,33901371	3,063162392
-2,314791077	1,838837246	1,934986751	0,096149505		0,218581585			0,112962833	
0,204555772	0,247340631	0,130892785	-0,116447845	0,590042042	0,916804373	0,32676233	2,385544343	7,004239156	4,618694813
-5,054972242	0,235705347	0,453727796	0,218022449						
	0,638626789	0,286472121	-0,352154668	1,009136331	0,437687592	-0,57144874	1,580165987	1,527854053	-0,052311935
-1,229173315	0,457324774	0,214659937	-0,242664837	1,131323426	1,033893723	-0,097429703	2,473785567	4,816426099	2,342640532
-0,726999337	0,51991649	1,354156504	0,834240014		1,261961143	1,261961143		0,931916761	0,931916761
-0,122625516	0,367990706	0,670657454	0,302666748	0,735494324	1,866357516	1,130863193	1,998676359	2,782877466	0,784201107
0,05881332	0,200229666	0,904394067	0,704164401	0,276158652	0,44060643	0,164447778	1,379209472	0,487184123	-0,892025349
0,327694543	0,59481266	0,656379359	0,061566699	0,093642519	0,185451595	0,091809076	0,157431953	0,282537213	0,12510526
-0,727315065									
0,597956671	0,772793996	0,681789475	-0,091004522	1,896843818	2,092909312	0,196065494	2,454527114	3,06972957	0,615202457
-0,237790071	0,465663838	0,725967599	0,260303762	1,308021567			2,808939543		
2,94536016	0,299982515								
-1,223898889	0,830470288	1,284177841	0,453707553		2,889352567			2,249962952	
0,925875023	0,523786742	0,388672056	-0,135114686	0,274021674			0,523155041		
0,555000274	0,474871662	0,602224295	0,127352632	0,506153814	0,819092925	0,31293911	1,065874961	1,360112722	0,294237761
0,873028071	0,459154971	0,330867338	-0,128287633						
0,824621742	0,71708085	0,243013984	-0,474066866	0,62335259			0,869291922		
0,052663307		0,676136611	0,676136611	1,485287419					
-1,164009995	0,352261747	0,474968276	0,122706528	0,9204165	0,765179081	-0,155237418	2,612876664	1,611010926	-1,001865739
1,396018555	0,973859485	0,240613097	-0,733246388	1,236108761			1,269288619		
8,425598706	1,000336692	0,968918138	-0,031418554	2,600461102	2,338672401	-0,261788701	2,599585843	2,413694522	-0,185891321
2,932075774	0,440184038	0,643950076	0,203766038	1,241027391	0,745417449	-0,495609942	2,819337559	1,157570248	-1,661767312
-3,063549355	0,635888584	2,539496956	1,903608372	1,526995128	2,033083442	0,506088314	2,401356413	0,800585107	-1,600771306
-4,280047799	0,576664738	0,761725983	0,185061245	0,504284511	0,772951998	0,268667487	0,874484736	1,014737603	0,140252867
2,517076372	1,189640127	0,929735101	-0,259905026	0,873246709	1,576352933	0,703106225	0,734042748	1,695486092	0,961443344
0,63371844	1,403232595	0,635291147	-0,767941448	6,911836896	2,612364397	-4,299472499	4,92565304	4,112074299	-0,813578742
-0,846931185	0,880112148	0,928207963	0,048095814	1,980672365	2,583551643	0,602879278	2,250477247	2,783375867	0,53289862
-0,099345941	0,429648637	0,409682413	-0,019966224	1,000469537	1,239877189	0,239407652	2,328576078	3,02643499	0,697858912
4,315009976	0,761830723	1,556217562	0,794386839	1,589846132			2,086875843		

5.3 Supplements of unpublished data

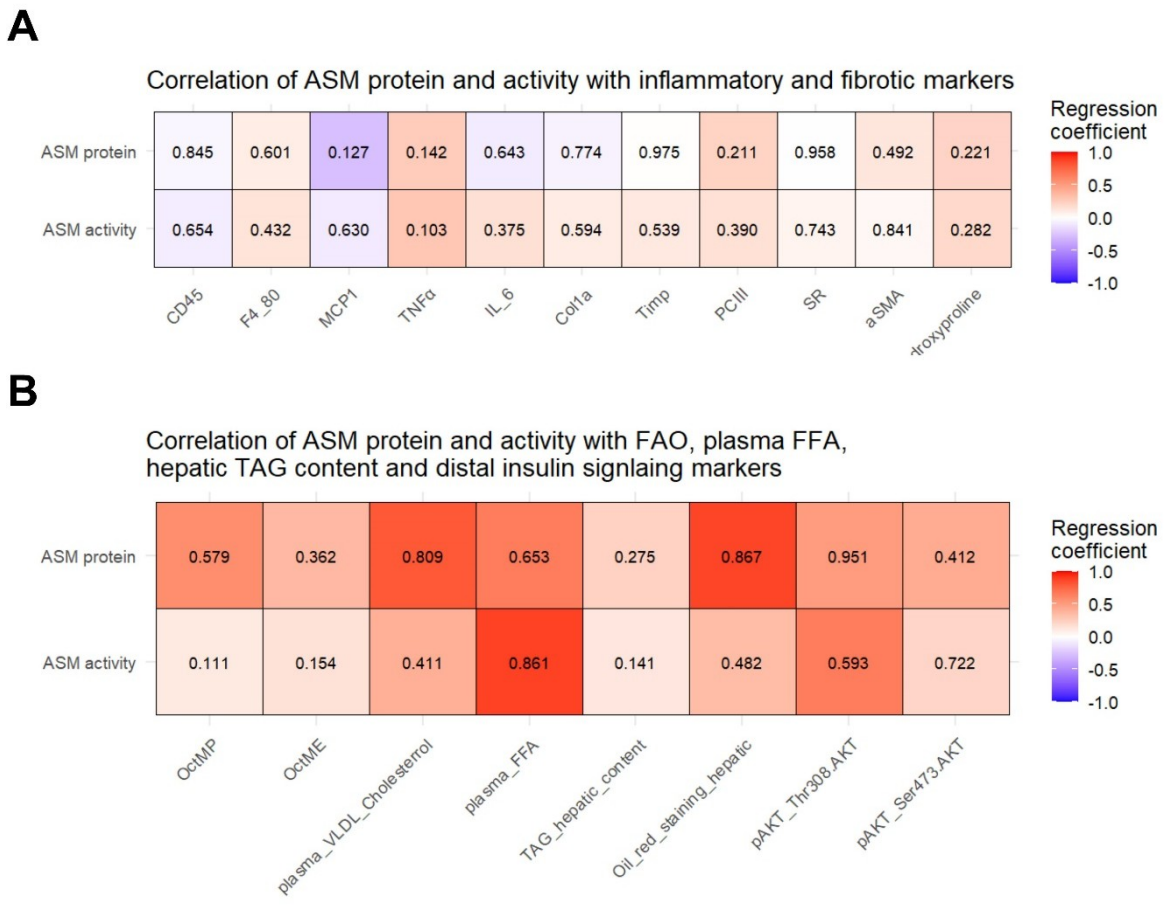

Figure S 1: Heatmap of correlation of ASM protein and activity with metabolic, inflammatory, and fibrotic markers in murine models of metabolic disease.

Heatmap showing Pearson correlation coefficients (Regression coefficient) between ASM protein/activity and various markers of **(A)** inflammation and fibrosis in liver of the whole cohort (n=32), including CD45 (receptor-type tyrosine-protein phosphatase C), F4/80 (EGF-like module-containing mucin-like hormone receptor-like 1), monocyte chemoattractant protein-1 (MCP-1), tumor necrosis factor-α (TNF-α), interleukin-6 (IL-6), collagen type I alpha 1 chain (Col1a1), tissue inhibitor of metalloproteinase 1 (TIMP-1), procollagen type III (PCIII), α- smooth muscle actin (α-SMA), liver collagen level by Sirius Red staining (SRs), or hydroxyproline levels. **(B)** Pearson correlation coefficients (Regression coefficient) between ASM protein/activity coupled mitochondrial respiration $[OctM]_P$ and uncoupled mitochondrial respiration as electron transport chain (ETC) capacity $[OctM]_E$.as well as plasma and hepatic fat content and distal insulin signaling markers. The colors represent the correlation coefficient (r), with red indicating positive and blue indicating negative correlations. The numerical values inside each tile denote the two-tailed p-values, indicating no statistical significance of the correlations.

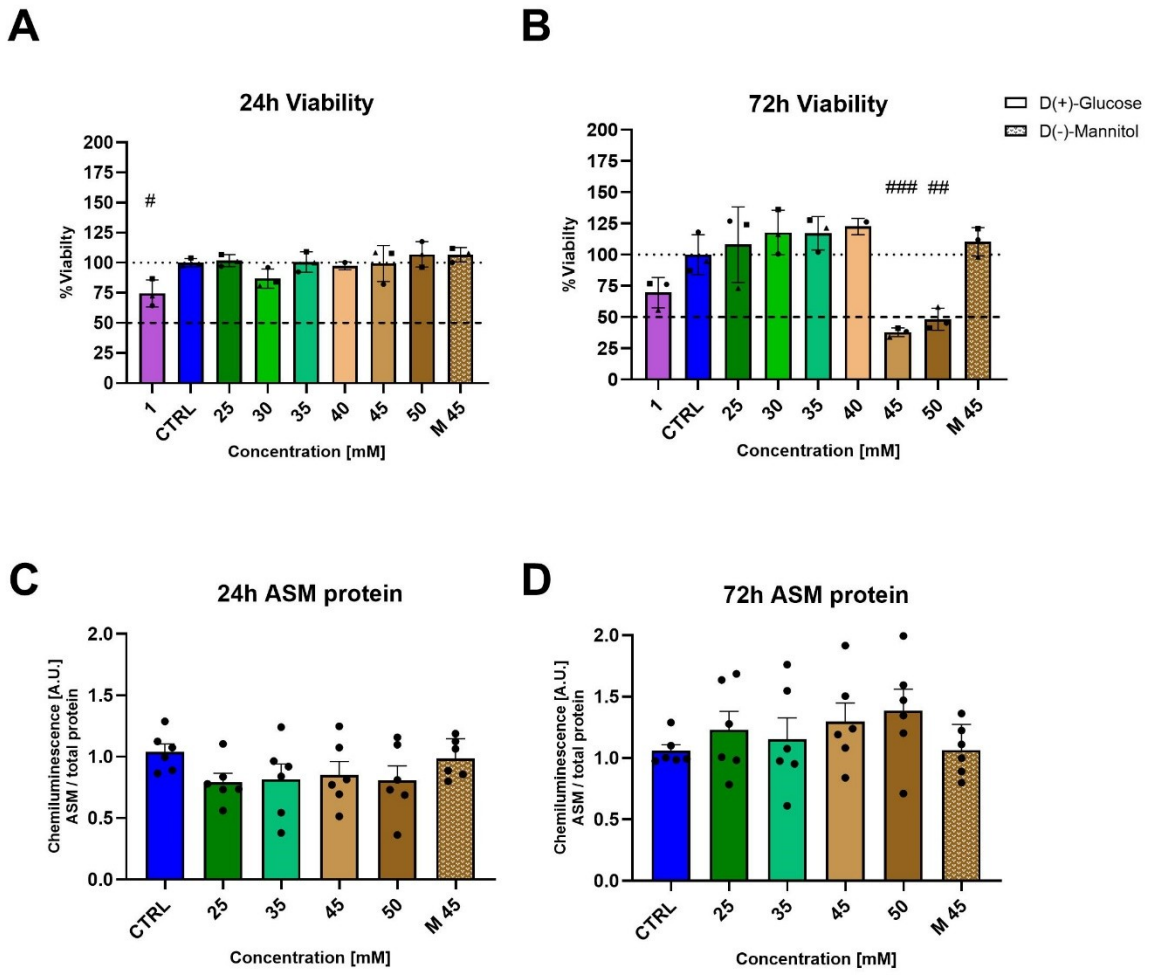

Figure S 2: High-glucose treatment leads to reduced cell viability in HepG2 cells with no alterations in ASM protein over time.

Cell viability assessed via MTT assay with varying glucose concentrations for **(A)** 24 h, 48 h shown in Figure 6A and **(B)** 72 h. Experiments were conducted with n=3, each containing technical quadruplicates. Values were normalized to the mean of quadruplicates for each biological replicate. Data expressed as mean ± SD; #p<0.05, ##p<0.01, ###p<0.001 vs 5 mM normoglycemic control (CTRL) based on one-way ANOVA & Dunnett´s multiple comparison test. ASM protein level at varying glucose concentrations for **(C)** 24 h, 48 h shown in Figure 6B and **(D)** 72 h assessed via Western blot and normalized to total protein (n=6). Statistics based on one-way ANOVA & Dunnett´s multiple comparison test.

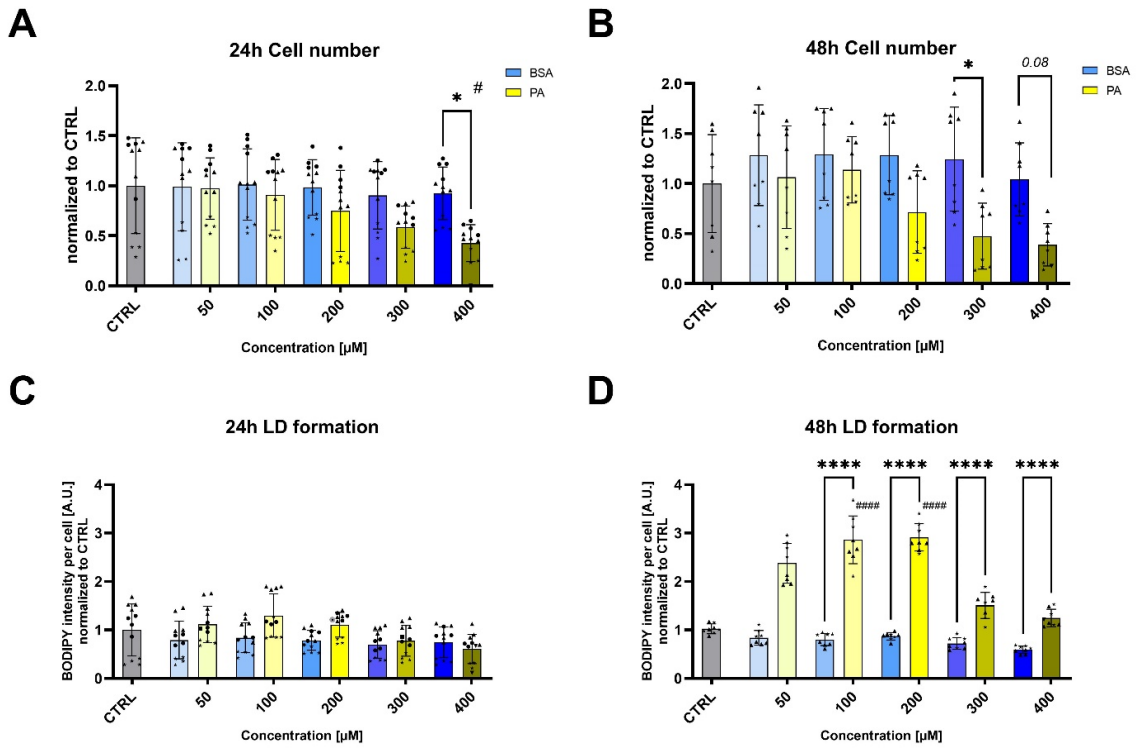

Figure S 3: High-palmitate exposure leads to reduced cell number and increased lipid droplet formation in HepG2 cells.

Cell number measured via Hoechst staining after **(A)** 24 h (n=12) and **(B)** 48 h (n=8) of palmitate (PA) - & BSA-treatment on HepG2 cells**.** Lipid droplet (LD) formation measured via BODIPY staining after **(C)** 24 h (n=12) and **(D)** 48 h (n=8) of palmitate (PA) - & BSA-treatment on HepG2 cells. Values were normalized to the mean of untreated cells (CTRL). Data expressed as mean ± SD; *p<0.05; #p<0.05, ##p<0.01, ####p<0.0001 vs CTRL based on one-way ANOVA & Tukey´s multiple comparison test.

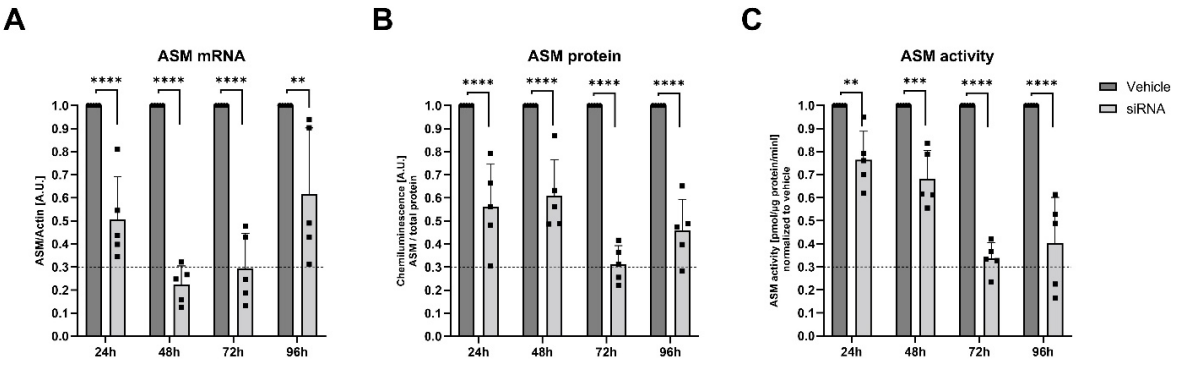

Figure S 4: Knockdown of ASM in HepG2 cells via siRNA.

ASM **(A)** mRNA, **(B)** protein **(C)** activity at different time points after siRNA transfection (n=5). Data expressed as mean ± SD; **p<0.01, ***p<0.001, ****p<0.0001 vs vehicle, based on two-way ANOVA and Šídák's multiple comparison test.

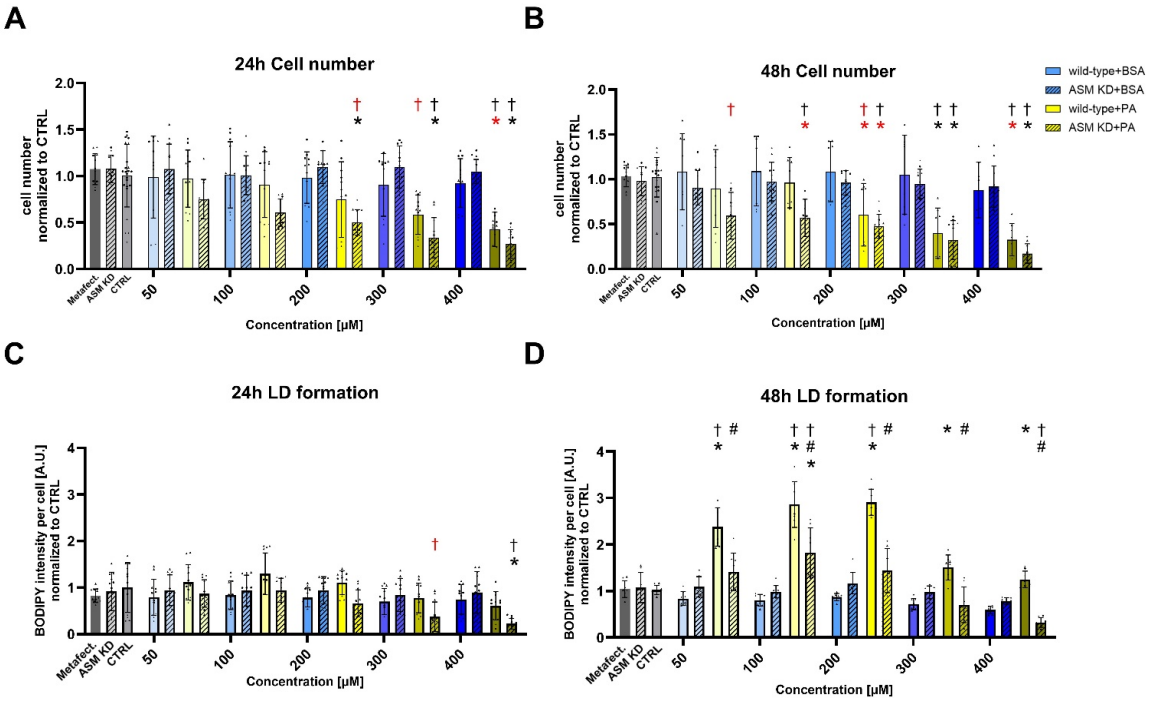

Figure S 5: ASM knockdown in HepG2 cells did not affect cell number or lipid droplet formation under BSA treatment.

Cell number measured via Hoechst staining after **(A)** 24 h (n=12) and **(B)** 48 h (n=8-12) of palmitate (PA) - & BSA-treatment in HepG2 wild-type and ASM knockdown (KD) cells. Lipid droplet (LD) formation measured via BODIPY staining after **(C)** 24 h (n=12) and **(D)** 48 h (n=8) of palmitate (PA) - & BSA-treatment in HepG2 wild-type and ASM knockdown (KD) cells. Values normalized to mean of untreated cells (CTRL). Data expressed as mean ± SD; *p<0.05, *p<0.001 vs respective BSA concentration; †<0.05, †p<0.001 vs CTRL; #p<0.001 vs wild-type based on two-way ANOVA & Tukey´s multiple comparison test.

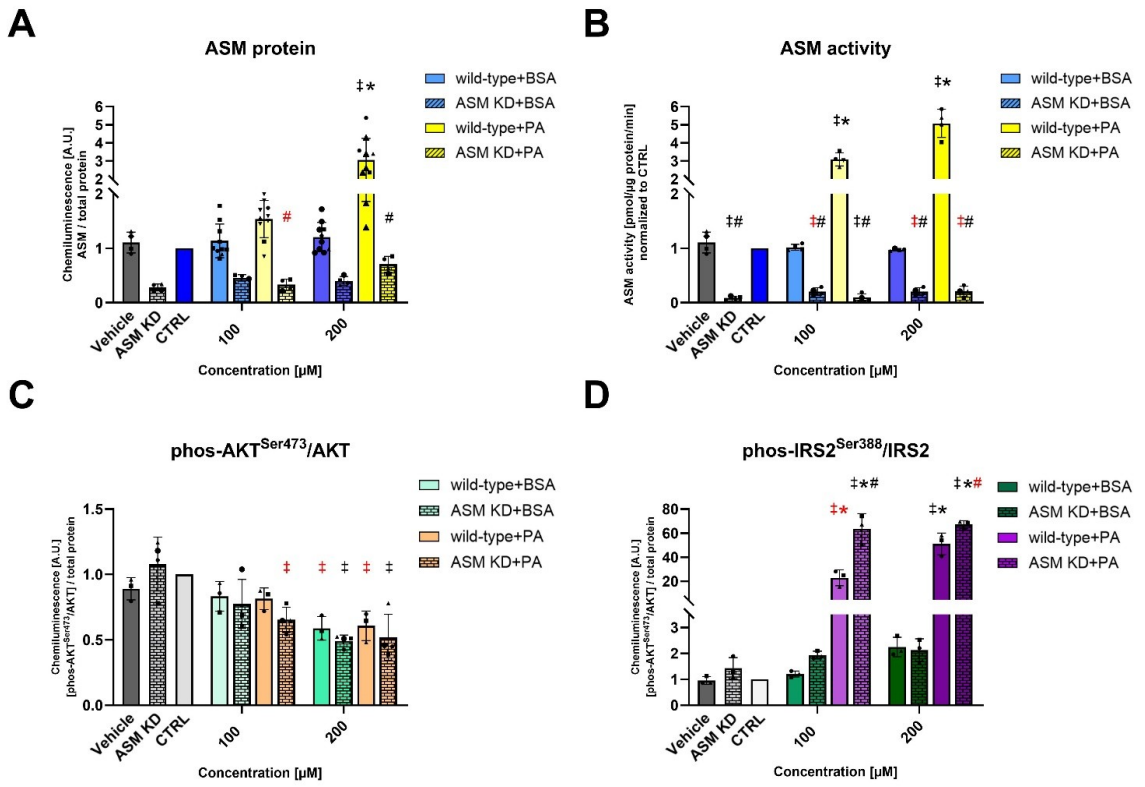

Figure S 6: ASM knockdown in HepG2 cells inhibits proximal insulin signaling pathway in response to palmitate treatments compared to wild-type cells.

Western-Blot analysis of HepG2 wild-type and ASM knockdown (KD), following palmitate (PA) treatment for 48 h and 10 nm insulin for 10 min. **(A)** ASM protein level of wild-type (n=10) and ASM KD (n=4) cells, and **(B)** ASM enzymatic activity (n=4). **(C)** Ratio phos-AKT^{Ser473}/AKT (n=3-4) and **(D)** ratio phos-IRS2^{Ser388}/IRS2 (n=3). Data normalized to untreated cells (CTRL) as inter-run calibrator (IRC). Data expressed as mean ± SD; *p<0.05, *p<0.001 vs respective BSA concentration; ‡<0.05, ‡p<0.001 vs CTRL; #p<0.05, #p<0.001 vs wild-type, based on two-way ANOVA & Tukey´s multiple comparison test.

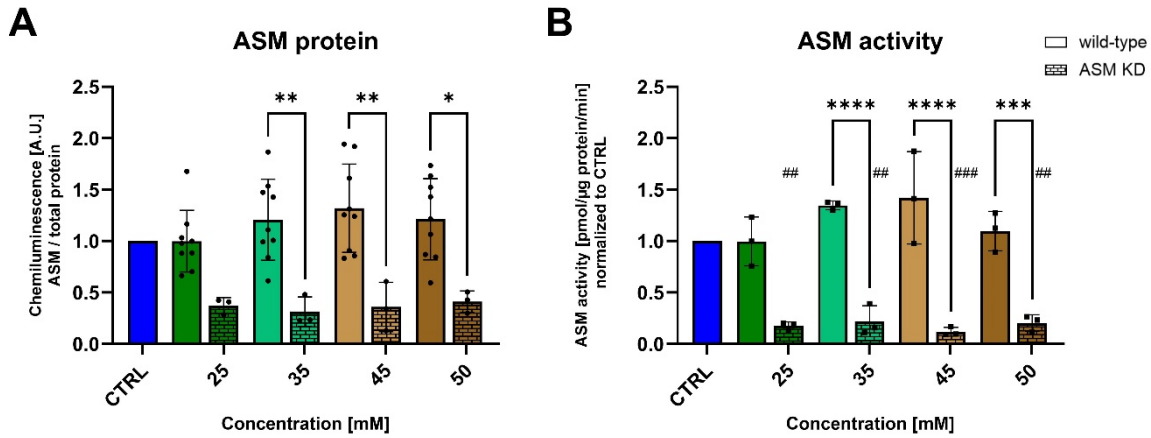

Figure S 7: ASM knockdown in HepG2 cells in response to high-glucose treatment compared to wild-type.

Western-blot analysis of HepG2 wild-type and ASM knockdown (KD) cells, following glucose treatment for 48 h and 10 nm insulin for 10 min. **(A)** ASM protein level of wild-type (n=9) and ASM KD (n=3) cells,

(B) ASM activity (n=3). Data expressed as mean ± SD; *p<0.05, **p<0.01, ***p<0.001, ****p<0.0001; ##p<0.01, ###p<0.001 vs CTRL, based on one-way ANOVA & Tukey´s multiple comparison test

5.4 List of Figures

5.5 List of Tables

6 References

ADA. 2022. Standards of Medical Care in Diabetes-2022 Abridged for Primary Care Providers. *Clin Diabetes*. 40:10-38. https://doi.org/10.2337/cd22-as01

ADA. 2024. 2. Diagnosis and Classification of Diabetes: Standards of Care in Diabetes-2024. *Diabetes Care*. 47:S20-s42. https://doi.org/10.2337/dc24-S002

Adams, J.M., 2nd, T. Pratipanawatr, R. Berria, et al. 2004. Ceramide content is increased in skeletal muscle from obese insulin-resistant humans. *Diabetes*. 53:25-31. https://doi.org/10.2337/diabetes.53.1.25

Aerts, J.M., R. Ottenhoff, A.S. Powlson, et al. 2007. Pharmacological inhibition of glucosylceramide synthase enhances insulin sensitivity. *Diabetes*. 56:1341-1349. https://doi.org/10.2337/db06-1619

Ahlqvist, E., P. Storm, A. Käräjämäki, et al. 2018. Novel subgroups of adult-onset diabetes and their association with outcomes: a data-driven cluster analysis of six variables. *Lancet Diabetes Endocrinol*. 6:361-369. https://doi.org/10.1016/s2213-8587(18)30051-2

Ahmed, B., R. Sultana, and M.W. Greene. 2021. Adipose tissue and insulin resistance in obese. *Biomed Pharmacother*. 137:111315. https://doi.org/10.1016/j.biopha.2021.111315

Ajoolabady, A., H. Aslkhodapasandhokmabad, P. Libby, et al. 2021. Ferritinophagy and ferroptosis in the management of metabolic diseases. *Trends Endocrinol Metab*. 32:444-462. https://doi.org/10.1016/j.tem.2021.04.010

Akl, M.G., E. Fawzy, M. Deif, et al. 2017. Perturbed adipose tissue hydrogen peroxide metabolism in centrally obese men: Association with insulin resistance. *PLoS One*. 12:e0177268. https://doi.org/10.1371/journal.pone.0177268

Alnahdi, A., A. John, and H. Raza. 2019. Augmentation of Glucotoxicity, Oxidative Stress, Apoptosis and Mitochondrial Dysfunction in HepG2 Cells by Palmitic Acid. *Nutrients*. 11. https://doi.org/10.3390/nu11091979

Alsabeeh, N., B. Chausse, P.A. Kakimoto, et al. 2018. Cell culture models of fatty acid overload: Problems and solutions. *Biochim Biophys Acta Mol Cell Biol Lipids*. 1863:143-151. https://doi.org/10.1016/j.bbalip.2017.11.006

Anderson, E.J., M.E. Lustig, K.E. Boyle, et al. 2009. Mitochondrial H2O2 emission and cellular redox state link excess fat intake to insulin resistance in both rodents and humans. *J Clin Invest*. 119:573-581. https://doi.org/10.1172/jci37048

Andrews, N.W., P.E. Almeida, and M. Corrotte. 2014. Damage control: cellular mechanisms of plasma membrane repair. *Trends Cell Biol*. 24:734-742. https://doi.org/10.1016/j.tcb.2014.07.008

Apostolopoulou, M., R. Gordillo, C. Koliaki, et al. 2018. Specific Hepatic Sphingolipids Relate to Insulin Resistance, Oxidative Stress, and Inflammation in Nonalcoholic Steatohepatitis. *Diabetes Care*. 41:1235-1243. https://doi.org/10.2337/dc17-1318

Arab, J.P., M. Arrese, and M. Trauner. 2018. Recent Insights into the Pathogenesis of Nonalcoholic Fatty Liver Disease. *Annu Rev Pathol*. 13:321-350. https://doi.org/10.1146/annurev-pathol-020117-043617

Arendt, B.M., D.W. Ma, B. Simons, et al. 2013. Nonalcoholic fatty liver disease is associated with lower hepatic and erythrocyte ratios of phosphatidylcholine to phosphatidylethanolamine. *Appl Physiol Nutr Metab*. 38:334-340. https://doi.org/10.1139/apnm-2012-0261

Arribat, Y., N.T. Broskey, C. Greggio, et al. 2019. Distinct patterns of skeletal muscle mitochondria fusion, fission and mitophagy upon duration of exercise training. *Acta Physiol (Oxf)*. 225:e13179. https://doi.org/10.1111/apha.13179

Ashcroft, S.P., B. Stocks, B. Egan, et al. 2024. Exercise induces tissue-specific adaptations to enhance cardiometabolic health. *Cell Metab*. 36:278-300. https://doi.org/10.1016/j.cmet.2023.12.008

Axelrod, C.L., C.E. Fealy, A. Mulya, et al. 2019. Exercise training remodels human skeletal muscle mitochondrial fission and fusion machinery towards a pro-elongation phenotype. *Acta Physiol (Oxf)*. 225:e13216. https://doi.org/10.1111/apha.13216

Bach, D., D. Naon, S. Pich, et al. 2005. Expression of Mfn2, the Charcot-Marie-Tooth neuropathy type 2A gene, in human skeletal muscle: effects of type 2 diabetes, obesity, weight loss, and the regulatory role of tumor necrosis factor alpha and interleukin-6. *Diabetes*. 54:2685-2693. https://doi.org/10.2337/diabetes.54.9.2685

Baiceanu, A., P. Mesdom, M. Lagouge, et al. 2016. Endoplasmic reticulum proteostasis in hepatic steatosis. *Nat Rev Endocrinol*. 12:710-722. https://doi.org/10.1038/nrendo.2016.124

Balan, E., C. Schwalm, D. Naslain, et al. 2019. Regular Endurance Exercise Promotes Fission, Mitophagy, and Oxidative Phosphorylation in Human Skeletal Muscle Independently of Age. *Front Physiol*. 10:1088. https://doi.org/10.3389/fphys.2019.01088

Baranowski, M., A.U. Błachnio-Zabielska, M. Charmas, et al. 2015. Exercise increases sphingoid base-1-phosphate levels in human blood and skeletal muscle in a time- and intensity-dependent manner. *Eur J Appl Physiol*. 115:993-1003. https://doi.org/10.1007/s00421-014-3080-x

Barrera, F., J. Uribe, N. Olvares, et al. 2024. The Janus of a disease: Diabetes and metabolic dysfunction-associated fatty liver disease. *Ann Hepatol*. 29:101501. https://doi.org/10.1016/j.aohep.2024.101501

Bergman, B.C., J.T. Brozinick, A. Strauss, et al. 2016a. Muscle sphingolipids during rest and exercise: a C18:0 signature for insulin resistance in humans. *Diabetologia*. 59:785-798. https://doi.org/10.1007/s00125-015-3850-y

Bergman, B.C., J.T. Brozinick, A. Strauss, et al. 2016b. Muscle sphingolipids during rest and exercise: a C18:0 signature for insulin resistance in humans. *Diabetologia*. 59:785-798. https://doi.org/10.1007/s00125-015-3850-y

Bergman, B.C., G.E. Butterfield, E.E. Wolfel, et al. 1999. Evaluation of exercise and training on muscle lipid metabolism. *Am J Physiol*. 276:E106-117. https://doi.org/10.1152/ajpendo.1999.276.1.E106

Bergman, B.C., D.M. Hunerdosse, A. Kerege, et al. 2012. Localisation and composition of skeletal muscle diacylglycerol predicts insulin resistance in humans. *Diabetologia*. 55:1140-1150. https://doi.org/10.1007/s00125-011-2419-7

Bergman, B.C., L. Perreault, A. Strauss, et al. 2018. Intramuscular triglyceride synthesis: importance in muscle lipid partitioning in humans. *Am J Physiol Endocrinol Metab*. 314:E152-e164. https://doi.org/10.1152/ajpendo.00142.2017

Bhansali, S., A. Bhansali, R. Walia, et al. 2017. Alterations in Mitochondrial Oxidative Stress and Mitophagy in Subjects with Prediabetes and Type 2 Diabetes Mellitus. *Front Endocrinol (Lausanne)*. 8:347. https://doi.org/10.3389/fendo.2017.00347

Bittel, D.C., S.C. Sreetama, G. Chandra, et al. 2022. Secreted acid sphingomyelinase as a potential gene therapy for limb girdle muscular dystrophy 2B. *J Clin Invest*. 132. https://doi.org/10.1172/jci141295

Błachnio-Zabielska, A., M. Baranowski, P. Zabielski, et al. 2008. Effect of exercise duration on the key pathways of ceramide metabolism in rat skeletal muscles. *J Cell Biochem*. 105:776-784. https://doi.org/10.1002/jcb.21877

Błachnio-Zabielska, A., P. Zabielski, M. Baranowski, et al. 2010. Effects of streptozotocin-induced diabetes and elevation of plasma FFA on ceramide metabolism in rat skeletal muscle. *Horm Metab Res*. 42:1-7. https://doi.org/10.1055/s-0029-1238322

Błachnio-Zabielska, A., P. Zabielski, M. Baranowski, et al. 2011. Aerobic training in rats increases skeletal muscle sphingomyelinase and serine palmitoyltransferase activity, while decreasing ceramidase activity. *Lipids*. 46:229-238. https://doi.org/10.1007/s11745-010-3515-z

Bladergroen, B.A., M. Bussière, W. Klein, et al. 1999. Inhibition of phosphatidylcholine and phosphatidylethanolamine biosynthesis in rat-2 fibroblasts by cell-permeable ceramides. *Eur J Biochem*. 264:152-160. https://doi.org/10.1046/j.1432-1327.1999.00589.x

Blazev, R., C.S. Carl, Y.K. Ng, et al. 2022. Phosphoproteomics of three exercise modalities identifies canonical signaling and C18ORF25 as an AMPK substrate regulating skeletal muscle function. *Cell Metab*. 34:1561-1577.e1569. https://doi.org/10.1016/j.cmet.2022.07.003

Blouin, C.M., C. Prado, K.K. Takane, et al. 2010. Plasma membrane subdomain compartmentalization contributes to distinct mechanisms of ceramide action on insulin signaling. *Diabetes*. 59:600-610. https://doi.org/10.2337/db09-0897

Bocca, C., F. Protopapa, B. Foglia, et al. 2022. Hepatic Myofibroblasts: A Heterogeneous and Redox-Modulated Cell Population in Liver Fibrogenesis. *Antioxidants (Basel)*. 11. https://doi.org/10.3390/antiox11071278

Boden, G., X. Chen, J. Ruiz, et al. 1994. Mechanisms of fatty acid-induced inhibition of glucose uptake. *J Clin Invest*. 93:2438-2446. https://doi.org/10.1172/jci117252

Bogacka, I., B. Ukropcova, M. McNeil, et al. 2005. Structural and functional consequences of mitochondrial biogenesis in human adipocytes in vitro. *J Clin Endocrinol Metab*. 90:6650-6656. https://doi.org/10.1210/jc.2005-1024

Bonen, A. 2009. PGC-1alpha-induced improvements in skeletal muscle metabolism and insulin sensitivity. *Appl Physiol Nutr Metab*. 34:307-314. https://doi.org/10.1139/h09-008

Boucher, J., A. Kleinridders, and C.R. Kahn. 2014. Insulin receptor signaling in normal and insulin-resistant states. *Cold Spring Harb Perspect Biol*. 6. https://doi.org/10.1101/cshperspect.a009191

Breiden, B., and K. Sandhoff. 2021. Acid Sphingomyelinase, a Lysosomal and Secretory Phospholipase C, Is Key for Cellular Phospholipid Catabolism. *Int J Mol Sci*. 22. https://doi.org/10.3390/ijms22169001

Brinkmann, C., A. Przyklenk, A. Metten, et al. 2017. Influence of endurance training on skeletal muscle mitophagy regulatory proteins in type 2 diabetic men. *Endocr Res*. 42:325-330. https://doi.org/10.1080/07435800.2017.1323914

Brown, M., S. Dainty, N. Strudwick, et al. 2020. Endoplasmic reticulum stress causes insulin resistance by inhibiting delivery of newly synthesized insulin receptors to the cell surface. *Mol Biol Cell*. 31:2597-2629. https://doi.org/10.1091/mbc.E18-01-0013

Bruce, C.R., A.D. Kriketos, G.J. Cooney, et al. 2004. Disassociation of muscle triglyceride content and insulin sensitivity after exercise training in patients with Type 2 diabetes. *Diabetologia*. 47:23-30. https://doi.org/10.1007/s00125-003-1265-7

Bruce, C.R., A.B. Thrush, V.A. Mertz, et al. 2006. Endurance training in obese humans improves glucose tolerance and mitochondrial fatty acid oxidation and alters muscle lipid content. *Am J Physiol Endocrinol Metab*. 291:E99-e107. https://doi.org/10.1152/ajpendo.00587.2005

Burlingame, B., C. Nishida, R. Uauy, et al. 2009. Fats and fatty acids in human nutrition: introduction. *Ann Nutr Metab*. 55:5-7. https://doi.org/10.1159/000228993

Butt, M.D., S.C. Ong, A. Rafiq, et al. 2024. A systematic review of the economic burden of diabetes mellitus: contrasting perspectives from high and low middle-income countries. *J Pharm Policy Pract*. 17:2322107. https://doi.org/10.1080/20523211.2024.2322107

Caballero, F., A. Fernández, N. Matías, et al. 2010. Specific contribution of methionine and choline in nutritional nonalcoholic steatohepatitis: impact on mitochondrial S-adenosyl-L-methionine and glutathione. *J Biol Chem*. 285:18528-18536. https://doi.org/10.1074/jbc.M109.099333

Calise, S., S. Blescia, F. Cencetti, et al. 2012. Sphingosine 1-phosphate stimulates proliferation and migration of satellite cells: role of S1P receptors. *Biochim Biophys Acta*. 1823:439-450. https://doi.org/10.1016/j.bbamcr.2011.11.016

Cantley, J.L., T. Yoshimura, J.P. Camporez, et al. 2013. CGI-58 knockdown sequesters diacylglycerols in lipid droplets/ER-preventing diacylglycerol-mediated hepatic insulin resistance. *Proc Natl Acad Sci U S A*. 110:1869-1874. https://doi.org/10.1073/pnas.1219456110

Cao, Z., X. Wang, Z. Zeng, et al. 2024. The improvement of modified Si-Miao granule on hepatic insulin resistance and glycogen synthesis in type 2 diabetes mellitus involves the inhibition of TNF-α/JNK1/IRS-2 pathway: network pharmacology, molecular docking, and experimental validation. *Chin Med*. 19:128. https://doi.org/10.1186/s13020-024-00997-9

Cartoni, R., B. Léger, M.B. Hock, et al. 2005. Mitofusins 1/2 and ERRalpha expression are increased in human skeletal muscle after physical exercise. *J Physiol*. 567:349-358. https://doi.org/10.1113/jphysiol.2005.092031

Chadt, A., and H. Al-Hasani. 2020. Glucose transporters in adipose tissue, liver, and skeletal muscle in metabolic health and disease. *Pflugers Arch*. 472:1273-1298. https://doi.org/10.1007/s00424-020-02417-x

Chan, D.C. 2020. Mitochondrial Dynamics and Its Involvement in Disease. *Annu Rev Pathol*. 15:235-259. https://doi.org/10.1146/annurev-pathmechdis-012419-032711

Chan, W.K., K.H. Chuah, R.B. Rajaram, et al. 2023. Metabolic Dysfunction-Associated Steatotic Liver Disease (MASLD): A State-of-the-Art Review. *J Obes Metab Syndr*. 32:197-213. https://doi.org/10.7570/jomes23052

Chandrasekaran, K., K. Swaminathan, S. Chatterjee, et al. 2010. Apoptosis in HepG2 cells exposed to high glucose. *Toxicol In Vitro*. 24:387-396. https://doi.org/10.1016/j.tiv.2009.10.020

Chang, W., G.M. Hatch, Y. Wang, et al. 2019. The relationship between phospholipids and insulin resistance: From clinical to experimental studies. *J Cell Mol Med*. 23:702-710. https://doi.org/10.1111/jcmm.13984

Charruyer, A., S. Grazide, C. Bezombes, et al. 2005. UV-C light induces raft-associated acid sphingomyelinase and JNK activation and translocation independently on a nuclear signal. *J Biol Chem*. 280:19196-19204. https://doi.org/10.1074/jbc.M412867200

Charruyer, A., C. Jean, A. Colomba, et al. 2007. PKCzeta protects against UV-C-induced apoptosis by inhibiting acid sphingomyelinase-dependent ceramide production. *Biochem J*. 405:77-83. https://doi.org/10.1042/bj20061528

Charytoniuk, T., N. Iłowska, K. Berk, et al. 2019. The effect of enterolactone on sphingolipid pathway and hepatic insulin resistance development in HepG2 cells. *Life Sci*. 217:1-7. https://doi.org/10.1016/j.lfs.2018.11.044

Chaurasia, B., and S.A. Summers. 2021. Ceramides in Metabolism: Key Lipotoxic Players. *Annu Rev Physiol*. 83:303-330. https://doi.org/10.1146/annurev-physiol-031620-093815

Chavez, J.A., and S.A. Summers. 2010. Lipid oversupply, selective insulin resistance, and lipotoxicity: molecular mechanisms. *Biochim Biophys Acta*. 1801:252-265. https://doi.org/10.1016/j.bbalip.2009.09.015

Chen, W., H. Zhao, and Y. Li. 2023. Mitochondrial dynamics in health and disease: mechanisms and potential targets. *Signal Transduct Target Ther*. 8:333. https://doi.org/10.1038/s41392-023-01547-9

Chen, Z., R. Tian, Z. She, et al. 2020. Role of oxidative stress in the pathogenesis of nonalcoholic fatty liver disease. *Free Radic Biol Med*. 152:116-141. https://doi.org/10.1016/j.freeradbiomed.2020.02.025

Cheon, H.G., and Y.S. Cho. 2014. Protection of palmitic acid-mediated lipotoxicity by arachidonic acid via channeling of palmitic acid into triglycerides in C2C12. *J Biomed Sci*. 21:13. https://doi.org/10.1186/1423-0127-21-13

Cho, K.J., D. van der Hoeven, Y. Zhou, et al. 2016. Inhibition of Acid Sphingomyelinase Depletes Cellular Phosphatidylserine and Mislocalizes K-Ras from the Plasma Membrane. *Mol Cell Biol*. 36:363-374. https://doi.org/10.1128/mcb.00719-15

Chocian, G., A. Chabowski, M. Zendzian-Piotrowska, et al. 2010. High fat diet induces ceramide and sphingomyelin formation in rat's liver nuclei. *Mol Cell Biochem*. 340:125-131. https://doi.org/10.1007/s11010-010-0409-6

Christe, M., E. Hirzel, A. Lindinger, et al. 2013. Obesity affects mitochondrial citrate synthase in human omental adipose tissue. *ISRN Obes*. 2013:826027. https://doi.org/10.1155/2013/826027

Chung, J.O., C. Koutsari, A.U. Blachnio-Zabielska, et al. 2017. Intramyocellular Ceramides: Subcellular Concentrations and Fractional De Novo Synthesis in Postabsorptive Humans. *Diabetes*. 66:2082-2091. https://doi.org/10.2337/db17-0082

Coazzoli, M., A. Napoli, P. Roux-Biejat, et al. 2020. Acid Sphingomyelinase Downregulation Enhances Mitochondrial Fusion and Promotes Oxidative Metabolism in a Mouse Model of Melanoma. *Cells*. 9. https://doi.org/10.3390/cells9040848

Coen, P.M., J.J. Dube, F. Amati, et al. 2010. Insulin resistance is associated with higher intramyocellular triglycerides in type I but not type II myocytes concomitant with higher ceramide content. *Diabetes*. 59:80-88. https://doi.org/10.2337/db09-0988

Coen, P.M., K.C. Hames, E.M. Leachman, et al. 2013. Reduced skeletal muscle oxidative capacity and elevated ceramide but not diacylglycerol content in severe obesity. *Obesity (Silver Spring)*. 21:2362-2371. https://doi.org/10.1002/oby.20381

Coen, P.M., E.V. Menshikova, G. Distefano, et al. 2015. Exercise and Weight Loss Improve Muscle Mitochondrial Respiration, Lipid Partitioning, and Insulin Sensitivity After Gastric Bypass Surgery. *Diabetes*. 64:3737-3750. https://doi.org/10.2337/db15-0809

Colell, A., A. Morales, J.C. Fernández-Checa, et al. 2002. Ceramide generated by acidic sphingomyelinase contributes to tumor necrosis factor-alpha-mediated apoptosis in human colon HT-29 cells through glycosphingolipids formation. Possible role of ganglioside GD3. *FEBS Lett*. 526:135-141. https://doi.org/10.1016/s0014-5793(02)03140-x

Cordeiro, A.V., V.R.R. Silva, J.R. Pauli, et al. 2019. The role of sphingosine-1-phosphate in skeletal muscle: Physiology, mechanisms, and clinical perspectives. *J Cell Physiol*. 234:10047-10059. https://doi.org/10.1002/jcp.27870

Crawford, A.L., and N. Laiteerapong. 2024. Type 2 Diabetes. *Ann Intern Med*. 177:Itc81-itc96. https://doi.org/10.7326/aitc202406180

Creer, A., P. Gallagher, D. Slivka, et al. 2005. Influence of muscle glycogen availability on ERK1/2 and Akt signaling after resistance exercise in human skeletal muscle. *J Appl Physiol (1985)*. 99:950-956. https://doi.org/10.1152/japplphysiol.00110.2005

Cusi, K., Z. Younossi, and M. Roden. 2024. From NAFLD to MASLD: Promise and pitfalls of a new definition. *Ann Hepatol*. 29:101179. https://doi.org/10.1016/j.aohep.2023.101179

D'Alessandris, C., R. Lauro, I. Presta, et al. 2007. C-reactive protein induces phosphorylation of insulin receptor substrate-1 on Ser307 and Ser 612 in L6 myocytes, thereby impairing the insulin signalling pathway that promotes glucose transport. *Diabetologia*. 50:840-849. https://doi.org/10.1007/s00125-006-0522-y

Dahlman, I., M. Forsgren, A. Sjögren, et al. 2006. Downregulation of electron transport chain genes in visceral adipose tissue in type 2 diabetes independent of obesity and possibly involving tumor necrosis factor-alpha. *Diabetes*. 55:1792-1799. https://doi.org/10.2337/db05-1421

Davies, M.J., V.R. Aroda, B.S. Collins, et al. 2022. Management of Hyperglycemia in Type 2 Diabetes, 2022. A Consensus Report by the American Diabetes Association (ADA) and the European Association for the Study of Diabetes (EASD). *Diabetes Care*. 45:2753-2786. https://doi.org/10.2337/dci22-0034

de Sousa, I.F., V. Migliaccio, M. Lepretti, et al. 2021. Dose- and Time-Dependent Effects of Oleate on Mitochondrial Fusion/Fission Proteins and Cell Viability in HepG2 Cells: Comparison with Palmitate Effects. *Int J Mol Sci*. 22. https://doi.org/10.3390/ijms22189812

Deevska, G.M., P.P. Dotson, 2nd, A.A. Karakashian, et al. 2017. Novel Interconnections in Lipid Metabolism Revealed by Overexpression of Sphingomyelin Synthase-1. *J Biol Chem*. 292:5110-5122. https://doi.org/10.1074/jbc.M116.751602

Deevska, G.M., K.A. Rozenova, N.V. Giltiay, et al. 2009. Acid Sphingomyelinase Deficiency Prevents Diet-induced Hepatic Triacylglycerol Accumulation and Hyperglycemia in Mice. *J Biol Chem*. 284:8359-8368. https://doi.org/10.1074/jbc.M807800200

Defour, A., J.H. Van der Meulen, R. Bhat, et al. 2014. Dysferlin regulates cell membrane repair by facilitating injury-triggered acid sphingomyelinase secretion. *Cell Death Dis*. 5:e1306. https://doi.org/10.1038/cddis.2014.272

Delcheva, G., K. Stefanova, and T. Stankova. 2024. Ceramides-Emerging Biomarkers of Lipotoxicity in Obesity, Diabetes, Cardiovascular Diseases, and Inflammation. *Diseases*. 12. https://doi.org/10.3390/diseases12090195

Desjardins, E.M., and G.R. Steinberg. 2018. Emerging Role of AMPK in Brown and Beige Adipose Tissue (BAT): Implications for Obesity, Insulin Resistance, and Type 2 Diabetes. *Curr Diab Rep*. 18:80. https://doi.org/10.1007/s11892-018-1049-6

Devaux, P.F. 1991. Static and dynamic lipid asymmetry in cell membranes. *Biochemistry*. 30:1163-1173. https://doi.org/10.1021/bi00219a001

Dewidar, B., S. Kahl, K. Pafili, et al. 2020. Metabolic liver disease in diabetes - From mechanisms to clinical trials. *Metabolism*. 111s:154299. https://doi.org/10.1016/j.metabol.2020.154299

Dewidar, B., L. Mastrototaro, C. Englisch, et al. 2023. Alterations of hepatic energy metabolism in murine models of obesity, diabetes and fatty liver diseases. *EBioMedicine*. 94:104714. https://doi.org/10.1016/j.ebiom.2023.104714

Djalalvandi, A., and L. Scorrano. 2022. Mitochondrial dynamics: roles in exercise physiology and muscle mass regulation. *Current Opinion in Physiology*. 27. https://doi.org/10.1016/j.cophys.2022.100550

Donati, C., F. Cencetti, and P. Bruni. 2013. Sphingosine 1-phosphate axis: a new leader actor in skeletal muscle biology. *Front Physiol*. 4:338. https://doi.org/10.3389/fphys.2013.00338

Draeger, A., R. Schoenauer, A.P. Atanassoff, et al. 2014. Dealing with damage: plasma membrane repair mechanisms. *Biochimie*. 107 Pt A:66-72. https://doi.org/10.1016/j.biochi.2014.08.008

Drake, J.C., R.J. Wilson, and Z. Yan. 2016. Molecular mechanisms for mitochondrial adaptation to exercise training in skeletal muscle. *Faseb j*. 30:13-22. https://doi.org/10.1096/fj.15-276337

Drew, B.G., V. Ribas, J.A. Le, et al. 2014. HSP72 is a mitochondrial stress sensor critical for Parkin action, oxidative metabolism, and insulin sensitivity in skeletal muscle. *Diabetes*. 63:1488-1505. https://doi.org/10.2337/db13-0665

Du, Y.X., Y.T. Zhao, Y.X. Sun, et al. 2023. Acid sphingomyelinase mediates ferroptosis induced by high glucose via autophagic degradation of GPX4 in type 2 diabetic osteoporosis. *Mol Med*. 29:125. https://doi.org/10.1186/s10020-023-00724-4

Dubé, J.J., F. Amati, M. Stefanovic-Racic, et al. 2008. Exercise-induced alterations in intramyocellular lipids and insulin resistance: the athlete's paradox revisited. *Am J Physiol Endocrinol Metab*. 294:E882-888. https://doi.org/10.1152/ajpendo.00769.2007

Dubé, J.J., F. Amati, F.G. Toledo, et al. 2011. Effects of weight loss and exercise on insulin resistance, and intramyocellular triacylglycerol, diacylglycerol and ceramide. *Diabetologia*. 54:1147-1156. https://doi.org/10.1007/s00125-011-2065-0

Edmunds, L.R., A. Mills, and M.J. Jurczak. 2019. 1882-P: Liver-Specific Deletion of the Mitochondrial Quality Control E3 Ligase Parkin Is Associated with Increased Hepatic Steatosis and Markers of NAFLD in Diet-Induced Obese Mice. *Diabetes*. 68. https://doi.org/10.2337/db19-1882-P

Egnatchik, R.A., A.K. Leamy, D.A. Jacobson, et al. 2014. ER calcium release promotes mitochondrial dysfunction and hepatic cell lipotoxicity in response to palmitate overload. *Mol Metab*. 3:544-553. https://doi.org/10.1016/j.molmet.2014.05.004

Eilat-Tsanani, S., A. Margalit, and L.N. Golan. 2021. Occurrence of comorbidities in newly diagnosed type 2 diabetes patients and their impact after 11 years' follow-up. *Sci Rep*. 11:11071. https://doi.org/10.1038/s41598-021-90379-0

En Li Cho, E., C.Z. Ang, J. Quek, et al. 2023. Global prevalence of non-alcoholic fatty liver disease in type 2 diabetes mellitus: an updated systematic review and meta-analysis. *Gut*. 72:2138-2148. https://doi.org/10.1136/gutjnl-2023-330110

Ersoy, B.A., A. Tarun, K. D'Aquino, et al. 2013. Phosphatidylcholine transfer protein interacts with thioesterase superfamily member 2 to attenuate insulin signaling. *Sci Signal*. 6:ra64. https://doi.org/10.1126/scisignal.2004111

Espino-Gonzalez, E., E. Dalbram, R. Mounier, et al. 2024. Impaired skeletal muscle regeneration in diabetes: From cellular and molecular mechanisms to novel treatments. *Cell Metab*. 36:1204-1236. https://doi.org/10.1016/j.cmet.2024.02.014

Eynaudi, A., F. Díaz-Castro, J.C. Bórquez, et al. 2021. Differential Effects of Oleic and Palmitic Acids on Lipid Droplet-Mitochondria Interaction in the Hepatic Cell Line HepG2. *Front Nutr*. 8:775382. https://doi.org/10.3389/fnut.2021.775382

Fang, C., S. Liu, W. Yang, et al. 2024. Exercise ameliorates lipid droplet metabolism disorder by the PLIN2-LIPA axis-mediated lipophagy in mouse model of non-alcoholic fatty liver disease. *Biochim Biophys Acta Mol Basis Dis*. 1870:167045. https://doi.org/10.1016/j.bbadis.2024.167045

Fazakerley, D.J., A.Y. Minard, J.R. Krycer, et al. 2018. Mitochondrial oxidative stress causes insulin resistance without disrupting oxidative phosphorylation. *J Biol Chem*. 293:7315-7328. https://doi.org/10.1074/jbc.RA117.001254

Fazal, F.M., S. Han, K.R. Parker, et al. 2019. Atlas of Subcellular RNA Localization Revealed by APEX-Seq. *Cell*. 178:473-490.e426. https://doi.org/10.1016/j.cell.2019.05.027

Fealy, C.E., A. Mulya, N. Lai, et al. 2014. Exercise training decreases activation of the mitochondrial fission protein dynamin-related protein-1 in insulin-resistant human skeletal muscle. *J Appl Physiol (1985)*. 117:239-245. https://doi.org/10.1152/japplphysiol.01064.2013

Feng, J., S. Lu, B. Ou, et al. 2020. The Role of JNk Signaling Pathway in Obesity-Driven Insulin Resistance. *Diabetes Metab Syndr Obes*. 13:1399-1406. https://doi.org/10.2147/dmso.S236127

Fernandez, A., N. Matias, R. Fucho, et al. 2013. ASMase is required for chronic alcohol induced hepatic endoplasmic reticulum stress and mitochondrial cholesterol loading. *J Hepatol*. 59:805-813. https://doi.org/10.1016/j.jhep.2013.05.023

Ferré, P., and F. Foufelle. 2010. Hepatic steatosis: a role for de novo lipogenesis and the transcription factor SREBP-1c. *Diabetes Obes Metab*. 12 Suppl 2:83-92. https://doi.org/10.1111/j.1463-1326.2010.01275.x

Ferreira, L.F., J.S. Moylan, L.A. Gilliam, et al. 2010. Sphingomyelinase stimulates oxidant signaling to weaken skeletal muscle and promote fatigue. *Am J Physiol Cell Physiol*. 299:C552-560. https://doi.org/10.1152/ajpcell.00065.2010

Fox, T.E., M.C. Bewley, K.A. Unrath, et al. 2011. Circulating sphingolipid biomarkers in models of type 1 diabetes. *J Lipid Res*. 52:509-517. https://doi.org/10.1194/jlr.M010595

Francois, M.E., and J.P. Little. 2015. Effectiveness and safety of high-intensity interval training in patients with type 2 diabetes. *Diabetes Spectr*. 28:39-44. https://doi.org/10.2337/diaspect.28.1.39

Frandsen, H.S., J.M. Vej-Nielsen, L.E. Smith, et al. 2022. Mapping Proteome and Lipidome Changes in Early-Onset Non-Alcoholic Fatty Liver Disease Using Hepatic 3D Spheroids. *Cells*. 11. https://doi.org/10.3390/cells11203216

Frangioudakis, G., J. Garrard, K. Raddatz, et al. 2010. Saturated- and n-6 polyunsaturated-fat diets each induce ceramide accumulation in mouse skeletal muscle: reversal and improvement of glucose tolerance by lipid metabolism inhibitors. *Endocrinology*. 151:4187-4196. https://doi.org/10.1210/en.2010-0250

Friedman, S.L., B.A. Neuschwander-Tetri, M. Rinella, et al. 2018. Mechanisms of NAFLD development and therapeutic strategies. *Nat Med*. 24:908-922. https://doi.org/10.1038/s41591-018-0104-9

Fromenty, B., and M. Roden. 2023. Mitochondrial alterations in fatty liver diseases. *J Hepatol*. 78:415-429. https://doi.org/10.1016/j.jhep.2022.09.020

Fu, S., L. Yang, P. Li, et al. 2011. Aberrant lipid metabolism disrupts calcium homeostasis causing liver endoplasmic reticulum stress in obesity. *Nature*. 473:528-531. https://doi.org/10.1038/nature09968

Fucho, R., N. Casals, D. Serra, et al. 2017. Ceramides and mitochondrial fatty acid oxidation in obesity. *Faseb j*. 31:1263-1272. https://doi.org/10.1096/fj.201601156R

Fucho, R., L. Martinez, A. Baulies, et al. 2014. ASMase regulates autophagy and lysosomal membrane permeabilization and its inhibition prevents early stage non-alcoholic steatohepatitis. *J Hepatol*. 61:1126-1134. https://doi.org/10.1016/j.jhep.2014.06.009

Funai, K., I.J. Lodhi, L.D. Spears, et al. 2016. Skeletal Muscle Phospholipid Metabolism Regulates Insulin Sensitivity and Contractile Function. *Diabetes*. 65:358-370. https://doi.org/10.2337/db15-0659

Funai, K., H. Song, L. Yin, et al. 2013. Muscle lipogenesis balances insulin sensitivity and strength through calcium signaling. *J Clin Invest*. 123:1229-1240. https://doi.org/10.1172/jci65726

Gakis, A.G., T. Nomikos, A. Philippou, et al. 2023. The Involvement of Lipid Mediators in the Mechanisms of Exercise-Induced Muscle Damage. *Physiologia*. 3:305-328. https://doi.org/10.3390/physiologia3020022

Galloway, C.A., H. Lee, P.S. Brookes, et al. 2014. Decreasing mitochondrial fission alleviates hepatic steatosis in a murine model of nonalcoholic fatty liver disease. *Am J Physiol Gastrointest Liver Physiol*. 307:G632-641. https://doi.org/10.1152/ajpgi.00182.2014

Gan, K.X., C. Wang, J.H. Chen, et al. 2013. Mitofusin-2 ameliorates high-fat diet-induced insulin resistance in liver of rats. *World J Gastroenterol*. 19:1572-1581. https://doi.org/10.3748/wjg.v19.i10.1572

Gancheva, S., S. Kahl, D. Pesta, et al. 2022. Impaired Hepatic Mitochondrial Capacity in Nonalcoholic Steatohepatitis Associated With Type 2 Diabetes. *Diabetes Care*. 45:928-937. https://doi.org/10.2337/dc21-1758

Gao, D., S. Nong, X. Huang, et al. 2010. The effects of palmitate on hepatic insulin resistance are mediated by NADPH Oxidase 3-derived reactive oxygen species through JNK and

p38MAPK pathways. *J Biol Chem*. 285:29965-29973. https://doi.org/10.1074/jbc.M110.128694

Gao, W., X. Du, L. Lei, et al. 2018. NEFA-induced ROS impaired insulin signalling through the JNK and p38MAPK pathways in non-alcoholic steatohepatitis. *J Cell Mol Med*. 22:3408-3422. https://doi.org/10.1111/jcmm.13617

García-Peña, L.M., E.D. Abel, and R.O. Pereira. 2024. Mitochondrial Dynamics, Diabetes, and Cardiovascular Disease. *Diabetes*. 73:151-161. https://doi.org/10.2337/dbi23-0003

García-Ruiz, C., A. Colell, M. Marí, et al. 2003. Defective TNF-alpha-mediated hepatocellular apoptosis and liver damage in acidic sphingomyelinase knockout mice. *J Clin Invest*. 111:197-208. https://doi.org/10.1172/jci16010

Garcia-Ruiz, C., J.M. Mato, D. Vance, et al. 2015. Acid sphingomyelinase-ceramide system in steatohepatitis: A novel target regulating multiple pathways. *Journal of Hepatology*. 62:219-233. https://doi.org/10.1016/j.jhep.2014.09.023

Gemmink, A., P. Schrauwen, and M.K.C. Hesselink. 2020. Exercising your fat (metabolism) into shape: a muscle-centred view. *Diabetologia*. 63:1453-1463. https://doi.org/10.1007/s00125-020-05170-z

Genders, A.J., G.P. Holloway, and D.J. Bishop. 2020. Are Alterations in Skeletal Muscle Mitochondria a Cause or Consequence of Insulin Resistance? *International Journal of Molecular Sciences*. 21:6948.

Gibala, M.J., J.P. Little, M.J. Macdonald, et al. 2012. Physiological adaptations to low-volume, high-intensity interval training in health and disease. *J Physiol*. 590:1077-1084. https://doi.org/10.1113/jphysiol.2011.224725

Gómez-Lechón, M.J., M.T. Donato, A. Martínez-Romero, et al. 2007. A human hepatocellular in vitro model to investigate steatosis. *Chem Biol Interact*. 165:106-116. https://doi.org/10.1016/j.cbi.2006.11.004

Gong, Z., S. Han, C. Li, et al. 2023. Rhinacanthin C Ameliorates Insulin Resistance and Lipid Accumulation in NAFLD Mice via the AMPK/SIRT1 and SREBP-1c/FAS/ACC Signaling Pathways. *Evid Based Complement Alternat Med*. 2023:6603522. https://doi.org/10.1155/2023/6603522

Goodpaster, B.H., J. He, S. Watkins, et al. 2001. Skeletal muscle lipid content and insulin resistance: evidence for a paradox in endurance-trained athletes. *J Clin Endocrinol Metab*. 86:5755-5761. https://doi.org/10.1210/jcem.86.12.8075

Goodpaster, B.H., R. Theriault, S.C. Watkins, et al. 2000. Intramuscular lipid content is increased in obesity and decreased by weight loss. *Metabolism*. 49:467-472. https://doi.org/10.1016/s0026-0495(00)80010-4

Gorden, D.L., D.S. Myers, P.T. Ivanova, et al. 2015. Biomarkers of NAFLD progression: a lipidomics approach to an epidemic. *J Lipid Res*. 56:722-736. https://doi.org/10.1194/jlr.P056002

Görlach, A., K. Bertram, S. Hudecova, et al. 2015. Calcium and ROS: A mutual interplay. *Redox Biol*. 6:260-271. https://doi.org/10.1016/j.redox.2015.08.010

Górska, M., A. Dobrzyń, M. Zendzian-Piotrowska, et al. 2004. Effect of streptozotocin-diabetes on the functioning of the sphingomyelin-signalling pathway in skeletal muscles of the rat. *Horm Metab Res*. 36:14-21. https://doi.org/10.1055/s-2004-814197

Grassmé, H., E. Gulbins, B. Brenner, et al. 1997. Acidic sphingomyelinase mediates entry of N. gonorrhoeae into nonphagocytic cells. *Cell*. 91:605-615. https://doi.org/10.1016/s0092-8674(00)80448-1

Gregor, M.F., L. Yang, E. Fabbrini, et al. 2009. Endoplasmic reticulum stress is reduced in tissues of obese subjects after weight loss. *Diabetes*. 58:693-700. https://doi.org/10.2337/db08-1220

Gustavsson, M., N.J. Traaseth, and G. Veglia. 2011. Activating and deactivating roles of lipid bilayers on the Ca(2+)-ATPase/phospholamban complex. *Biochemistry*. 50:10367-10374. https://doi.org/10.1021/bi200759y

Haberl, E.M., R. Pohl, L. Rein-Fischboeck, et al. 2020. Hepatic lipid profile in mice fed a choline-deficient, low-methionine diet resembles human non-alcoholic fatty liver disease. *Lipids Health Dis*. 19:250. https://doi.org/10.1186/s12944-020-01425-1

Hage Hassan, R., A.C. Pacheco de Sousa, R. Mahfouz, et al. 2016. Sustained Action of Ceramide on the Insulin Signaling Pathway in Muscle Cells: IMPLICATION OF THE DOUBLE-STRANDED RNA-ACTIVATED PROTEIN KINASE. *J Biol Chem*. 291:3019-3029. https://doi.org/10.1074/jbc.M115.686949

Hajduch, E., F. Lachkar, P. Ferré, et al. 2021. Roles of Ceramides in Non-Alcoholic Fatty Liver Disease. *J Clin Med*. 10. https://doi.org/10.3390/jcm10040792

Hammerschmidt, P., and J.C. Brüning. 2022. Contribution of specific ceramides to obesity-associated metabolic diseases. *Cell Mol Life Sci*. 79:395. https://doi.org/10.1007/s00018-022-04401-3

Hammerschmidt, P., D. Ostkotte, H. Nolte, et al. 2019. CerS6-Derived Sphingolipids Interact with Mff and Promote Mitochondrial Fragmentation in Obesity. *Cell*. 177:1536-1552.e1523. https://doi.org/10.1016/j.cell.2019.05.008

Handschin, C., and B.M. Spiegelman. 2008. The role of exercise and PGC1alpha in inflammation and chronic disease. *Nature*. 454:463-469. https://doi.org/10.1038/nature07206

Hanke, S., and M. Mann. 2009. The phosphotyrosine interactome of the insulin receptor family and its substrates IRS-1 and IRS-2. *Mol Cell Proteomics*. 8:519-534. https://doi.org/10.1074/mcp.M800407-MCP200

Harber, M.P., J.D. Crane, M.D. Douglass, et al. 2008. Resistance exercise reduces muscular substrates in women. *Int J Sports Med*. 29:719-725. https://doi.org/10.1055/s-2007-989442

Harman-Boehm, I., M. Blüher, H. Redel, et al. 2007. Macrophage infiltration into omental versus subcutaneous fat across different populations: effect of regional adiposity and the comorbidities of obesity. *J Clin Endocrinol Metab*. 92:2240-2247. https://doi.org/10.1210/jc.2006-1811

Haus, J.M., S.R. Kashyap, T. Kasumov, et al. 2009. Plasma ceramides are elevated in obese subjects with type 2 diabetes and correlate with the severity of insulin resistance. *Diabetes*. 58:337-343. https://doi.org/10.2337/db08-1228

Hawley, J.A., and S.J. Lessard. 2008. Exercise training-induced improvements in insulin action. *Acta Physiol (Oxf)*. 192:127-135. https://doi.org/10.1111/j.1748-1716.2007.01783.x

He, F., Y. Huang, Z. Song, et al. 2021a. Mitophagy-mediated adipose inflammation contributes to type 2 diabetes with hepatic insulin resistance. *J Exp Med*. 218. https://doi.org/10.1084/jem.20201416

He, L., J.H. Jhong, Q. Chen, et al. 2021b. Global characterization of macrophage polarization mechanisms and identification of M2-type polarization inhibitors. *Cell Rep*. 37:109955. https://doi.org/10.1016/j.celrep.2021.109955

Heinrich, M., J. Neumeyer, M. Jakob, et al. 2004. Cathepsin D links TNF-induced acid sphingomyelinase to Bid-mediated caspase-9 and -3 activation. *Cell Death Differ*. 11:550-563. https://doi.org/10.1038/sj.cdd.4401382

Helge, J.W., A. Dobrzyn, B. Saltin, et al. 2004. Exercise and training effects on ceramide metabolism in human skeletal muscle. *Exp Physiol*. 89:119-127. https://doi.org/10.1113/expphysiol.2003.002605

Hendlinger, M., L. Mastrototaro, M. Exterkate, et al. 2025. Exercise training increases skeletal muscle sphingomyelinases and affects mitochondrial quality control in men with type 2 diabetes. *Metabolism*. 172:156361. https://doi.org/10.1016/j.metabol.2025.156361

Henstridge, D.C., C.R. Bruce, B.G. Drew, et al. 2014. Activating HSP72 in rodent skeletal muscle increases mitochondrial number and oxidative capacity and decreases insulin resistance. *Diabetes*. 63:1881-1894. https://doi.org/10.2337/db13-0967

Hernández-Alvarez, M.I., H. Thabit, N. Burns, et al. 2010. Subjects with early-onset type 2 diabetes show defective activation of the skeletal muscle PGC-1{alpha}/Mitofusin-2 regulatory pathway in response to physical activity. *Diabetes Care*. 33:645-651. https://doi.org/10.2337/dc09-1305

Hernández, E., S. Kahl, A. Seelig, et al. 2017. Acute dietary fat intake initiates alterations in energy metabolism and insulin resistance. *J Clin Invest*. 127:695-708. https://doi.org/10.1172/jci89444

Hill, D.B., J. Schmidt, S.I. Shedlofsky, et al. 1995. In vitro tumor necrosis factor cytotoxicity in Hep G2 liver cells. *Hepatology*. 21:1114-1119.

Hodson, L., and P.J. Gunn. 2019. The regulation of hepatic fatty acid synthesis and partitioning: the effect of nutritional state. *Nat Rev Endocrinol*. 15:689-700. https://doi.org/10.1038/s41574-019-0256-9

Holland, W.L., and S.A. Summers. 2008. Sphingolipids, insulin resistance, and metabolic disease: new insights from in vivo manipulation of sphingolipid metabolism. *Endocr Rev*. 29:381-402. https://doi.org/10.1210/er.2007-0025

Hood, D.A., J.M. Memme, A.N. Oliveira, et al. 2019. Maintenance of Skeletal Muscle Mitochondria in Health, Exercise, and Aging. *Annu Rev Physiol*. 81:19-41. https://doi.org/10.1146/annurev-physiol-020518-114310

Houzelle, A., J.A. Jörgensen, G. Schaart, et al. 2021. Human skeletal muscle mitochondrial dynamics in relation to oxidative capacity and insulin sensitivity. *Diabetologia*. 64:424-436. https://doi.org/10.1007/s00125-020-05335-w

IDF. 2025. International Diabetes Federation. IDF Diabetes Atlas, 11th edn. Brussels. Belgium International Diabetes Federation https://diabetesatlas.org.

Irrcher, I., V. Ljubicic, and D.A. Hood. 2009. Interactions between ROS and AMP kinase activity in the regulation of PGC-1alpha transcription in skeletal muscle cells. *Am J Physiol Cell Physiol*. 296:C116-123. https://doi.org/10.1152/ajpcell.00267.2007

Islam, H., J.T. Bonafiglia, P.C. Turnbull, et al. 2020. The impact of acute and chronic exercise on Nrf2 expression in relation to markers of mitochondrial biogenesis in human skeletal muscle. *Eur J Appl Physiol*. 120:149-160. https://doi.org/10.1007/s00421-019-04259-7

Jacob, S., J. Machann, K. Rett, et al. 1999. Association of increased intramyocellular lipid content with insulin resistance in lean nondiabetic offspring of type 2 diabetic subjects. *Diabetes*. 48:1113-1119. https://doi.org/10.2337/diabetes.48.5.1113

Jelenik, T., K. Kaul, G. Séquaris, et al. 2017. Mechanisms of Insulin Resistance in Primary and Secondary Nonalcoholic Fatty Liver. *Diabetes*. 66:2241-2253. https://doi.org/10.2337/db16-1147

Jelleyman, C., T. Yates, G. O'Donovan, et al. 2015. The effects of high-intensity interval training on glucose regulation and insulin resistance: a meta-analysis. *Obes Rev*. 16:942-961. https://doi.org/10.1111/obr.12317

Jenkins, R.W., D. Canals, J. Idkowiak-Baldys, et al. 2010. Regulated secretion of acid sphingomyelinase: implications for selectivity of ceramide formation. *J Biol Chem*. 285:35706-35718. https://doi.org/10.1074/jbc.M110.125609

Jheng, H.F., P.J. Tsai, S.M. Guo, et al. 2012. Mitochondrial fission contributes to mitochondrial dysfunction and insulin resistance in skeletal muscle. *Mol Cell Biol*. 32:309-319. https://doi.org/10.1128/mcb.05603-11

Jin, H.S., J. Kim, S.J. Lee, et al. 2014. The PARK2 gene is involved in the maintenance of pancreatic β-cell functions related to insulin production and secretion. *Mol Cell Endocrinol*. 382:178-189. https://doi.org/10.1016/j.mce.2013.09.031

Jornayvaz, F.R., A.L. Birkenfeld, M.J. Jurczak, et al. 2011. Hepatic insulin resistance in mice with hepatic overexpression of diacylglycerol acyltransferase 2. *Proc Natl Acad Sci U S A*. 108:5748-5752. https://doi.org/10.1073/pnas.1103451108

Justice, M.J., I. Bronova, K.S. Schweitzer, et al. 2018. Inhibition of acid sphingomyelinase disrupts LYNUS signaling and triggers autophagy. *J Lipid Res*. 59:596-606. https://doi.org/10.1194/jlr.M080242

Kahn, B.B. 2019. Adipose Tissue, Inter-Organ Communication, and the Path to Type 2 Diabetes: The 2016 Banting Medal for Scientific Achievement Lecture. *Diabetes*. 68:3-14. https://doi.org/10.2337/dbi18-0035

Kanaley, J.A., S.R. Colberg, M.H. Corcoran, et al. 2022. Exercise/Physical Activity in Individuals with Type 2 Diabetes: A Consensus Statement from the American College of Sports Medicine. *Med Sci Sports Exerc*. 54:353-368. https://doi.org/10.1249/mss.0000000000002800

Karunakaran, U., E.Y. Ha, S. Elumalai, et al. 2024. Mitochondrial ALDH2 improves ß-cell survival and function against doxorubicin-induced apoptosis by targeting CK2 signaling. *J Diabetes Investig*. 15:684-692. https://doi.org/10.1111/jdi.14230

Kashkar, H., K. Wiegmann, B. Yazdanpanah, et al. 2005. Acid sphingomyelinase is indispensable for UV light-induced Bax conformational change at the mitochondrial membrane. *J Biol Chem*. 280:20804-20813. https://doi.org/10.1074/jbc.M410869200

Kelley, D.E., J. He, E.V. Menshikova, et al. 2002. Dysfunction of Mitochondria in Human Skeletal Muscle in Type 2 Diabetes. *Diabetes*. 51:2944-2950. https://doi.org/10.2337/diabetes.51.10.2944

Keppley, L.J.W., S.J. Walker, A.N. Gademsey, et al. 2020. Nervonic acid limits weight gain in a mouse model of diet-induced obesity. *Faseb j*. 34:15314-15326. https://doi.org/10.1096/fj.202000525R

Kern, P.A., S. Ranganathan, C. Li, et al. 2001. Adipose tissue tumor necrosis factor and interleukin-6 expression in human obesity and insulin resistance. *Am J Physiol Endocrinol Metab*. 280:E745-751. https://doi.org/10.1152/ajpendo.2001.280.5.E745

Kiens, B., and E.A. Richter. 1998. Utilization of skeletal muscle triacylglycerol during postexercise recovery in humans. *Am J Physiol*. 275:E332-337. https://doi.org/10.1152/ajpendo.1998.275.2.E332

Kjøbsted, R., J.R. Hingst, J. Fentz, et al. 2018. AMPK in skeletal muscle function and metabolism. *Faseb j*. 32:1741-1777. https://doi.org/10.1096/fj.201700442R

Kleinfeld, A.M., D. Prothro, D.L. Brown, et al. 1996. Increases in serum unbound free fatty acid levels following coronary angioplasty. *Am J Cardiol*. 78:1350-1354. https://doi.org/10.1016/s0002-9149(96)00651-0

Koh, H.J., T. Toyoda, M.M. Didesch, et al. 2013. Tribbles 3 mediates endoplasmic reticulum stress-induced insulin resistance in skeletal muscle. *Nat Commun*. 4:1871. https://doi.org/10.1038/ncomms2851

Koliaki, C., J. Szendroedi, K. Kaul, et al. 2015. Adaptation of hepatic mitochondrial function in humans with non-alcoholic fatty liver is lost in steatohepatitis. *Cell Metab*. 21:739-746. https://doi.org/10.1016/j.cmet.2015.04.004

Kong, D., G. Song, C. Wang, et al. 2013. Overexpression of mitofusin 2 improves translocation of glucose transporter 4 in skeletal muscle of high-fat diet-fed rats through AMP-activated protein kinase signaling. *Mol Med Rep*. 8:205-210. https://doi.org/10.3892/mmr.2013.1457

Koopman, R., R.J. Manders, R.A. Jonkers, et al. 2006. Intramyocellular lipid and glycogen content are reduced following resistance exercise in untrained healthy males. *Eur J Appl Physiol*. 96:525-534. https://doi.org/10.1007/s00421-005-0118-0

Kornhuber, J., C. Rhein, C.P. Müller, et al. 2015. Secretory sphingomyelinase in health and disease. *Biol Chem*. 396:707-736. https://doi.org/10.1515/hsz-2015-0109

Krishnan, J., C. Danzer, T. Simka, et al. 2012. Dietary obesity-associated Hif1α activation in adipocytes restricts fatty acid oxidation and energy expenditure via suppression of the Sirt2-NAD+ system. *Genes Dev*. 26:259-270. https://doi.org/10.1101/gad.180406.111

Krishnan, S., Y. Ding, N. Saedi, et al. 2018. Gut Microbiota-Derived Tryptophan Metabolites Modulate Inflammatory Response in Hepatocytes and Macrophages. *Cell Rep*. 23:1099-1111. https://doi.org/10.1016/j.celrep.2018.03.109

Krssak, M., K. Falk Petersen, A. Dresner, et al. 1999. Intramyocellular lipid concentrations are correlated with insulin sensitivity in humans: a 1H NMR spectroscopy study. *Diabetologia*. 42:113-116. https://doi.org/10.1007/s001250051123

Krssak, M., K.F. Petersen, R. Bergeron, et al. 2000. Intramuscular glycogen and intramyocellular lipid utilization during prolonged exercise and recovery in man: a 13C and 1H nuclear magnetic resonance spectroscopy study. *J Clin Endocrinol Metab*. 85:748-754. https://doi.org/10.1210/jcem.85.2.6354

Kruse, R., A.J. Pedersen, J.M. Kristensen, et al. 2017. Intact initiation of autophagy and mitochondrial fission by acute exercise in skeletal muscle of patients with Type 2 diabetes. *Clin Sci (Lond)*. 131:37-47. https://doi.org/10.1042/cs20160736

Kumashiro, N., D.M. Erion, D. Zhang, et al. 2011. Cellular mechanism of insulin resistance in nonalcoholic fatty liver disease. *Proc Natl Acad Sci U S A*. 108:16381-16385. https://doi.org/10.1073/pnas.1113359108

Laker, R.C., J.C. Drake, R.J. Wilson, et al. 2017. Ampk phosphorylation of Ulk1 is required for targeting of mitochondria to lysosomes in exercise-induced mitophagy. *Nat Commun*. 8:548. https://doi.org/10.1038/s41467-017-00520-9

Larsen, S., S. Skaaby, J.W. Helge, et al. 2014. Effects of exercise training on mitochondrial function in patients with type 2 diabetes. *World J Diabetes*. 5:482-492. https://doi.org/10.4239/wjd.v5.i4.482

Lee, A.H., and L.H. Glimcher. 2009. Intersection of the unfolded protein response and hepatic lipid metabolism. *Cell Mol Life Sci*. 66:2835-2850. https://doi.org/10.1007/s00018-009-0049-8

Lee, C.H., C.F. Chiang, F.H. Lin, et al. 2022. PDIA4, a new endoplasmic reticulum stress protein, modulates insulin resistance and inflammation in skeletal muscle. *Front Endocrinol (Lausanne)*. 13:1053882. https://doi.org/10.3389/fendo.2022.1053882

Lee, S., F. Norheim, H.L. Gulseth, et al. 2018. Skeletal muscle phosphatidylcholine and phosphatidylethanolamine respond to exercise and influence insulin sensitivity in men. *Sci Rep*. 8:6531. https://doi.org/10.1038/s41598-018-24976-x

Lee, Y.I., and Y.H. Leem. 2019. Acid sphingomyelinase inhibition alleviates muscle damage in gastrocnemius after acute strenuous exercise. *J Exerc Nutrition Biochem*. 23:1-6. https://doi.org/10.20463/jenb.2019.0009

Lennicke, C., and H.M. Cochemé. 2021. Redox metabolism: ROS as specific molecular regulators of cell signaling and function. *Mol Cell*. 81:3691-3707. https://doi.org/10.1016/j.molcel.2021.08.018

Li, X., E. Gulbins, and Y. Zhang. 2012. Oxidative stress triggers Ca-dependent lysosome trafficking and activation of acid sphingomyelinase. *Cell Physiol Biochem*. 30:815-826. https://doi.org/10.1159/000341460

Li, X., M. Xu, A.L. Pitzer, et al. 2014. Control of autophagy maturation by acid sphingomyelinase in mouse coronary arterial smooth muscle cells: protective role in atherosclerosis. *J Mol Med (Berl)*. 92:473-485. https://doi.org/10.1007/s00109-014-1120-y

Li, Z., L.B. Agellon, T.M. Allen, et al. 2006. The ratio of phosphatidylcholine to phosphatidylethanolamine influences membrane integrity and steatohepatitis. *Cell Metab*. 3:321-331. https://doi.org/10.1016/j.cmet.2006.03.007

Li, Z., M. Berk, T.M. McIntyre, et al. 2008. The lysosomal-mitochondrial axis in free fatty acid-induced hepatic lipotoxicity. *Hepatology*. 47:1495-1503. https://doi.org/10.1002/hep.22183

Li, Z., H. Zhang, J. Liu, et al. 2011. Reducing plasma membrane sphingomyelin increases insulin sensitivity. *Mol Cell Biol*. 31:4205-4218. https://doi.org/10.1128/mcb.05893-11

Liu, R., T. Duan, L. Yu, et al. 2023. Acid sphingomyelinase promotes diabetic cardiomyopathy via NADPH oxidase 4 mediated apoptosis. *Cardiovasc Diabetol*. 22:25. https://doi.org/10.1186/s12933-023-01747-1

Livak, K.J., and T.D. Schmittgen. 2001. Analysis of relative gene expression data using real-time quantitative PCR and the 2(-Delta Delta C(T)) Method. *Methods*. 25:402-408. https://doi.org/10.1006/meth.2001.1262

Longato, L., M. Tong, J.R. Wands, et al. 2012. High fat diet induced hepatic steatosis and insulin resistance: Role of dysregulated ceramide metabolism. *Hepatol Res*. 42:412-427. https://doi.org/10.1111/j.1872-034X.2011.00934.x

Lopez-Pedrosa, J.M., M. Camprubi-Robles, G. Guzman-Rolo, et al. 2024. The Vicious Cycle of Type 2 Diabetes Mellitus and Skeletal Muscle Atrophy: Clinical, Biochemical, and Nutritional Bases. *Nutrients*. 16. https://doi.org/10.3390/nu16010172

Lund, M.T., M. Kristensen, M. Hansen, et al. 2016. Hepatic mitochondrial oxidative phosphorylation is normal in obese patients with and without type 2 diabetes. *J Physiol*. 594:4351-4358. https://doi.org/10.1113/jp272105

Luukkonen, P.K., Y. Zhou, S. Sädevirta, et al. 2016. Hepatic ceramides dissociate steatosis and insulin resistance in patients with non-alcoholic fatty liver disease. *J Hepatol*. 64:1167-1175. https://doi.org/10.1016/j.jhep.2016.01.002

Ma, K., Y. Zhang, J. Zhao, et al. 2024. Endoplasmic reticulum stress: bridging inflammation and obesity-associated adipose tissue. *Front Immunol*. 15:1381227. https://doi.org/10.3389/fimmu.2024.1381227

Maceyka, M., S.G. Payne, S. Milstien, et al. 2002. Sphingosine kinase, sphingosine-1-phosphate, and apoptosis. *Biochim Biophys Acta*. 1585:193-201. https://doi.org/10.1016/s1388-1981(02)00341-4

Magkos, F., X. Su, D. Bradley, et al. 2012. Intrahepatic diacylglycerol content is associated with hepatic insulin resistance in obese subjects. *Gastroenterology*. 142:1444-1446.e1442. https://doi.org/10.1053/j.gastro.2012.03.003

Malhi, H., S.F. Bronk, N.W. Werneburg, et al. 2006. Free fatty acids induce JNK-dependent hepatocyte lipoapoptosis. *J Biol Chem*. 281:12093-12101. https://doi.org/10.1074/jbc.M510660200

Mancini, G., K. Pirruccio, X. Yang, et al. 2019. Mitofusin 2 in Mature Adipocytes Controls Adiposity and Body Weight. *Cell Rep*. 26:2849-2858.e2844. https://doi.org/10.1016/j.celrep.2019.02.039

Mansour, S.Z., E.M. Moustafa, and F.S.M. Moawed. 2022. Modulation of endoplasmic reticulum stress via sulforaphane-mediated AMPK upregulation against nonalcoholic fatty liver disease in rats. *Cell Stress Chaperones*. 27:499-511. https://doi.org/10.1007/s12192-022-01286-w

Mantzaris, M.D., E.V. Tsianos, and D. Galaris. 2011. Interruption of triacylglycerol synthesis in the endoplasmic reticulum is the initiating event for saturated fatty acid-induced lipotoxicity in liver cells. *Febs j*. 278:519-530. https://doi.org/10.1111/j.1742-4658.2010.07972.x

Marí, M., A. Colell, A. Morales, et al. 2004. Acidic sphingomyelinase downregulates the liver-specific methionine adenosyltransferase 1A, contributing to tumor necrosis factor-induced lethal hepatitis. *J Clin Invest*. 113:895-904. https://doi.org/10.1172/jci19852

Maseko, T.E., E. Peterová, M. Elkalaf, et al. 2024. Collagen I Increases Palmitate-Induced Lipotoxicity in HepG2 Cells via Integrin-Mediated Death. *Biomolecules*. 14. https://doi.org/10.3390/biom14091179

Mashek, D.G. 2021. Hepatic lipid droplets: A balancing act between energy storage and metabolic dysfunction in NAFLD. *Mol Metab*. 50:101115. https://doi.org/10.1016/j.molmet.2020.101115

Matsumoto, A., K.E. Comatas, L. Liu, et al. 2003. Screening for nitric oxide-dependent protein-protein interactions. *Science*. 301:657-661. https://doi.org/10.1126/science.1079319

Mayer, C., M. Côme, V. Blanckaert, et al. 2020. Effect of Carotenoids from Phaeodactylum tricornutum on Palmitate-Treated HepG2 Cells. *Molecules*. 25. https://doi.org/10.3390/molecules25122845

Meng, T.C., T. Fukada, and N.K. Tonks. 2002. Reversible oxidation and inactivation of protein tyrosine phosphatases in vivo. *Mol Cell*. 9:387-399. https://doi.org/10.1016/s1097-2765(02)00445-8

Michailowsky, V., H. Li, B. Mittra, et al. 2019a. Defects in sarcolemma repair and skeletal muscle function after injury in a mouse model of Niemann-Pick type A/B disease. *Skelet Muscle*. 9:1. https://doi.org/10.1186/s13395-018-0187-5

Michailowsky, V., H. Li, B. Mittra, et al. 2019b. Defects in sarcolemma repair and skeletal muscle function after injury in a mouse model of Niemann-Pick type A/B disease. *Skelet Muscle*. 9:1. https://doi.org/10.1186/s13395-018-0187-5

Misu, H., T. Takamura, N. Matsuzawa, et al. 2007. Genes involved in oxidative phosphorylation are coordinately upregulated with fasting hyperglycaemia in livers of patients with type 2 diabetes. *Diabetologia*. 50:268-277. https://doi.org/10.1007/s00125-006-0489-8

Moles, A., N. Tarrats, A. Morales, et al. 2010a. Acidic sphingomyelinase controls hepatic stellate cell activation and in vivo liver fibrogenesis. *Am J Pathol*. 177:1214-1224. https://doi.org/10.2353/ajpath.2010.091257

Moles, A., N. Tarrats, A. Morales, et al. 2010b. Acidic sphingomyelinase controls hepatic stellate cell activation and in vivo liver fibrogenesis. *Am J Pathol*. 177:1214-1224. https://doi.org/10.2353/ajpath.2010.091257

Møller, A.B., M.H. Vendelbo, B. Christensen, et al. 2015. Physical exercise increases autophagic signaling through ULK1 in human skeletal muscle. *J Appl Physiol (1985)*. 118:971-979. https://doi.org/10.1152/japplphysiol.01116.2014

Moore, M.P., R.P. Cunningham, G.M. Meers, et al. 2022. Compromised hepatic mitochondrial fatty acid oxidation and reduced markers of mitochondrial turnover in human NAFLD. *Hepatology*. 76:1452-1465. https://doi.org/10.1002/hep.32324

Mootha, V.K., C.M. Lindgren, K.F. Eriksson, et al. 2003. PGC-1alpha-responsive genes involved in oxidative phosphorylation are coordinately downregulated in human diabetes. *Nat Genet*. 34:267-273. https://doi.org/10.1038/ng1180

Mota, M., B.A. Banini, S.C. Cazanave, et al. 2016. Molecular mechanisms of lipotoxicity and glucotoxicity in nonalcoholic fatty liver disease. *Metabolism*. 65:1049-1061. https://doi.org/10.1016/j.metabol.2016.02.014

Mozaffaritabar, S., E. Koltai, L. Zhou, et al. 2024. PGC-1α activation boosts exercise-dependent cellular response in the skeletal muscle. *J Physiol Biochem*. 80:329-335. https://doi.org/10.1007/s13105-024-01006-1

Mukhopadhyay, A., S.A. Saddoughi, P. Song, et al. 2009. Direct interaction between the inhibitor 2 and ceramide via sphingolipid-protein binding is involved in the regulation of protein phosphatase 2A activity and signaling. *Faseb j*. 23:751-763. https://doi.org/10.1096/fj.08-120550

Nakamura, S., T. Takamura, N. Matsuzawa-Nagata, et al. 2009. Palmitate induces insulin resistance in H4IIEC3 hepatocytes through reactive oxygen species produced by mitochondria. *J Biol Chem*. 284:14809-14818. https://doi.org/10.1074/jbc.M901488200

Nasiri-Ansari, N., C. Nikolopoulou, K. Papoutsi, et al. 2021. Empagliflozin Attenuates Non-Alcoholic Fatty Liver Disease (NAFLD) in High Fat Diet Fed ApoE((-/-)) Mice by Activating Autophagy and Reducing ER Stress and Apoptosis. *Int J Mol Sci*. 22. https://doi.org/10.3390/ijms22020818

Newsom, S.A., J.T. Brozinick, K. Kiseljak-Vassiliades, et al. 2016. Skeletal muscle phosphatidylcholine and phosphatidylethanolamine are related to insulin sensitivity and respond to acute exercise in humans. *J Appl Physiol (1985)*. 120:1355-1363. https://doi.org/10.1152/japplphysiol.00664.2015

Ngo, J., D.W. Choi, I.A. Stanley, et al. 2023. Mitochondrial morphology controls fatty acid utilization by changing CPT1 sensitivity to malonyl-CoA. *Embo j*. 42:e111901. https://doi.org/10.15252/embj.2022111901

Ning, P., X. Jiang, J. Yang, et al. 2022. Mitophagy: A potential therapeutic target for insulin resistance. *Front Physiol*. 13:957968. https://doi.org/10.3389/fphys.2022.957968

Nishida, Y., A. Nawaz, T. Kado, et al. 2020. Astaxanthin stimulates mitochondrial biogenesis in insulin resistant muscle via activation of AMPK pathway. *J Cachexia Sarcopenia Muscle*. 11:241-258. https://doi.org/10.1002/jcsm.12530

Nishikawa, T., and E. Araki. 2007. Impact of mitochondrial ROS production in the pathogenesis of diabetes mellitus and its complications. *Antioxid Redox Signal*. 9:343-353. https://doi.org/10.1089/ars.2006.1458

Ojuka, E.O., T.E. Jones, D.H. Han, et al. 2003. Raising Ca2+ in L6 myotubes mimics effects of exercise on mitochondrial biogenesis in muscle. *Faseb j*. 17:675-681. https://doi.org/10.1096/fj.02-0951com

Okamoto, Y., H. Higashiyama, J.X. Rong, et al. 2007. Comparison of mitochondrial and macrophage content between subcutaneous and visceral fat in db/db mice. *Exp Mol Pathol*. 83:73-83. https://doi.org/10.1016/j.yexmp.2007.02.007

Oliveira, A.F., D.A. Cunha, L. Ladriere, et al. 2015. In vitro use of free fatty acids bound to albumin: A comparison of protocols. *Biotechniques*. 58:228-233. https://doi.org/10.2144/000114285

Oliveira, A.N., and D.A. Hood. 2019. Exercise is mitochondrial medicine for muscle. *Sports Med Health Sci*. 1:11-18. https://doi.org/10.1016/j.smhs.2019.08.008

Oninla, V.O., B. Breiden, J.O. Babalola, et al. 2014. Acid sphingomyelinase activity is regulated by membrane lipids and facilitates cholesterol transfer by NPC2. *J Lipid Res*. 55:2606-2619. https://doi.org/10.1194/jlr.M054528

Osawa, Y., E. Seki, Y. Kodama, et al. 2011. Acid sphingomyelinase regulates glucose and lipid metabolism in hepatocytes through AKT activation and AMP-activated protein kinase suppression. *FASEB J*. 25:1133-1144. https://doi.org/10.1096/fj.10-168351

Pafili, K., S. Kahl, L. Mastrototaro, et al. 2022a. Mitochondrial respiration is decreased in visceral but not subcutaneous adipose tissue in obese individuals with fatty liver disease. *J Hepatol*. 77:1504-1514. https://doi.org/10.1016/j.jhep.2022.08.010

Pafili, K., S. Kahl, L. Mastrototaro, et al. 2022b. Mitochondrial respiration is decreased in visceral but not subcutaneous adipose tissue in obese individuals with fatty liver disease. *J Hepatol*. 77:1504-1514. https://doi.org/10.1016/j.jhep.2022.08.010

Pardo, V., Á. González-Rodríguez, J. Muntané, et al. 2015. Role of hepatocyte S6K1 in palmitic acid-induced endoplasmic reticulum stress, lipotoxicity, insulin resistance and in oleic acid-induced protection. *Food Chem Toxicol*. 80:298-309. https://doi.org/10.1016/j.fct.2015.03.029

Park, K., Q. Li, C. Rask-Madsen, et al. 2013. Serine phosphorylation sites on IRS2 activated by angiotensin II and protein kinase C to induce selective insulin resistance in endothelial cells. *Mol Cell Biol*. 33:3227-3241. https://doi.org/10.1128/mcb.00506-13

Park, M., V. Kaddai, J. Ching, et al. 2016. A Role for Ceramides, but Not Sphingomyelins, as Antagonists of Insulin Signaling and Mitochondrial Metabolism in C2C12 Myotubes. *J Biol Chem*. 291:23978-23988. https://doi.org/10.1074/jbc.M116.737684

Park, M.A., G. Zhang, A.P. Martin, et al. 2008. Vorinostat and sorafenib increase ER stress, autophagy and apoptosis via ceramide-dependent CD95 and PERK activation. *Cancer Biol Ther*. 7:1648-1662. https://doi.org/10.4161/cbt.7.10.6623

Patti, M.E., A.J. Butte, S. Crunkhorn, et al. 2003. Coordinated reduction of genes of oxidative metabolism in humans with insulin resistance and diabetes: Potential role of PGC1 and NRF1. *Proc Natl Acad Sci U S A*. 100:8466-8471. https://doi.org/10.1073/pnas.1032913100

Pearson-Stuttard, J., S. Holloway, R. Polya, et al. 2022. Variations in comorbidity burden in people with type 2 diabetes over disease duration: A population-based analysis of real world evidence. *EClinicalMedicine*. 52:101584. https://doi.org/10.1016/j.eclinm.2022.101584

Pedersen, J.S., M.O. Rygg, K. Chrøis, et al. 2022. Influence of NAFLD and bariatric surgery on hepatic and adipose tissue mitochondrial biogenesis and respiration. *Nat Commun*. 13:2931. https://doi.org/10.1038/s41467-022-30629-5

Peng, G., L. Li, Y. Liu, et al. 2011. Oleate blocks palmitate-induced abnormal lipid distribution, endoplasmic reticulum expansion and stress, and insulin resistance in skeletal muscle. *Endocrinology*. 152:2206-2218. https://doi.org/10.1210/en.2010-1369

Pereira, M.J., S. Skrtic, P. Katsogiannos, et al. 2016. Impaired adipose tissue lipid storage, but not altered lipolysis, contributes to elevated levels of NEFA in type 2 diabetes. Degree of hyperglycemia and adiposity are important factors. *Metabolism*. 65:1768-1780. https://doi.org/10.1016/j.metabol.2016.09.008

Perreault, L., S.A. Newsom, A. Strauss, et al. 2018. Intracellular localization of diacylglycerols and sphingolipids influences insulin sensitivity and mitochondrial function in human skeletal muscle. *JCI Insight*. 3. https://doi.org/10.1172/jci.insight.96805

Perrotta, C., L. Bizzozero, D. Cazzato, et al. 2010. Syntaxin 4 is required for acid sphingomyelinase activity and apoptotic function. *J Biol Chem*. 285:40240-40251. https://doi.org/10.1074/jbc.M110.139287

Perry, C.G., J. Lally, G.P. Holloway, et al. 2010. Repeated transient mRNA bursts precede increases in transcriptional and mitochondrial proteins during training in human skeletal muscle. *J Physiol*. 588:4795-4810. https://doi.org/10.1113/jphysiol.2010.199448

Perseghin, G., T.B. Price, K.F. Petersen, et al. 1996. Increased glucose transport-phosphorylation and muscle glycogen synthesis after exercise training in insulin-resistant subjects. *N Engl J Med*. 335:1357-1362. https://doi.org/10.1056/nejm199610313351804

Perseghin, G., P. Scifo, F. De Cobelli, et al. 1999. Intramyocellular triglyceride content is a determinant of in vivo insulin resistance in humans: a 1H-13C nuclear magnetic resonance spectroscopy assessment in offspring of type 2 diabetic parents. *Diabetes*. 48:1600-1606. https://doi.org/10.2337/diabetes.48.8.1600

Petersen, K.F., D.E. Befroy, S. Dufour, et al. 2016a. Assessment of Hepatic Mitochondrial Oxidation and Pyruvate Cycling in NAFLD by (13)C Magnetic Resonance Spectroscopy. *Cell Metab*. 24:167-171. https://doi.org/10.1016/j.cmet.2016.06.005

Petersen, M.C., and M.J. Jurczak. 2016. CrossTalk opposing view: Intramyocellular ceramide accumulation does not modulate insulin resistance. *J Physiol*. 594:3171-3174. https://doi.org/10.1113/jp271677

Petersen, M.C., A.K. Madiraju, B.M. Gassaway, et al. 2016b. Insulin receptor Thr1160 phosphorylation mediates lipid-induced hepatic insulin resistance. *J Clin Invest*. 126:4361-4371. https://doi.org/10.1172/jci86013

Petersen, M.C., and G.I. Shulman. 2018. Mechanisms of Insulin Action and Insulin Resistance. *Physiol Rev*. 98:2133-2223. https://doi.org/10.1152/physrev.00063.2017

Phielix, E., R. Meex, E. Moonen-Kornips, et al. 2010. Exercise training increases mitochondrial content and ex vivo mitochondrial function similarly in patients with type 2 diabetes and in control individuals. *Diabetologia*. 53:1714-1721. https://doi.org/10.1007/s00125-010-1764-2

Phielix, E., V.B. Schrauwen-Hinderling, M. Mensink, et al. 2008. Lower intrinsic ADP-stimulated mitochondrial respiration underlies in vivo mitochondrial dysfunction in muscle of male type 2 diabetic patients. *Diabetes*. 57:2943-2949. https://doi.org/10.2337/db08-0391

Pickles, S., P. Vigié, and R.J. Youle. 2018. Mitophagy and Quality Control Mechanisms in Mitochondrial Maintenance. *Curr Biol*. 28:R170-r185. https://doi.org/10.1016/j.cub.2018.01.004

Pinti, M.V., G.K. Fink, Q.A. Hathaway, et al. 2019. Mitochondrial dysfunction in type 2 diabetes mellitus: an organ-based analysis. *Am J Physiol Endocrinol Metab*. 316:E268-e285. https://doi.org/10.1152/ajpendo.00314.2018

Politis-Barber, V., H.S. Brunetta, S. Paglialunga, et al. 2020. Long-term, high-fat feeding exacerbates short-term increases in adipose mitochondrial reactive oxygen species, without impairing mitochondrial respiration. *Am J Physiol Endocrinol Metab*. 319:E376-e387. https://doi.org/10.1152/ajpendo.00028.2020

Poulain-Godefroy, O., C. Lecoeur, F. Pattou, et al. 2008. Inflammation is associated with a decrease of lipogenic factors in omental fat in women. *Am J Physiol Regul Integr Comp Physiol*. 295:R1-7. https://doi.org/10.1152/ajpregu.00926.2007

Previs, S.F., D.J. Withers, J.M. Ren, et al. 2000. Contrasting effects of IRS-1 versus IRS-2 gene disruption on carbohydrate and lipid metabolism in vivo. *J Biol Chem*. 275:38990-38994. https://doi.org/10.1074/jbc.M006490200

Prinetti, A., S. Prioni, E. Chiricozzi, et al. 2011. Secondary alterations of sphingolipid metabolism in lysosomal storage diseases. *Neurochem Res*. 36:1654-1668. https://doi.org/10.1007/s11064-010-0380-3

Puigserver, P., J. Rhee, J. Lin, et al. 2001. Cytokine stimulation of energy expenditure through p38 MAP kinase activation of PPARgamma coactivator-1. *Mol Cell*. 8:971-982. https://doi.org/10.1016/s1097-2765(01)00390-2

Puigserver, P., and B.M. Spiegelman. 2003. Peroxisome proliferator-activated receptor-gamma coactivator 1 alpha (PGC-1 alpha): transcriptional coactivator and metabolic regulator. *Endocr Rev*. 24:78-90. https://doi.org/10.1210/er.2002-0012

Qu, Y., L. Sun, Z. Yang, et al. 2011. Variation in the PTEN-induced putative kinase 1 gene associated with the increase risk of type 2 diabetes in northern Chinese. *J Genet*. 90:125-128. https://doi.org/10.1007/s12041-011-0020-y

Quillin, R.C., 3rd, G.C. Wilson, H. Nojima, et al. 2015. Inhibition of acidic sphingomyelinase reduces established hepatic fibrosis in mice. *Hepatol Res*. 45:305-314. https://doi.org/10.1111/hepr.12352

Raichur, S., B. Brunner, M. Bielohuby, et al. 2019. The role of C16:0 ceramide in the development of obesity and type 2 diabetes: CerS6 inhibition as a novel therapeutic approach. *Mol Metab*. 21:36-50. https://doi.org/10.1016/j.molmet.2018.12.008

Ramos, B., M. El Mouedden, E. Claro, et al. 2002. Inhibition of CTP:phosphocholine cytidylyltransferase by C(2)-ceramide and its relationship to apoptosis. *Mol Pharmacol*. 62:1068-1075. https://doi.org/10.1124/mol.62.5.1068

Ramos, B., J.M. Lahti, E. Claro, et al. 2003. Prevalence of necrosis in C2-ceramide-induced cytotoxicity in NB16 neuroblastoma cells. *Mol Pharmacol*. 64:502-511. https://doi.org/10.1124/mol.64.2.502

Razquin, C., E. Toledo, C.B. Clish, et al. 2018. Plasma Lipidomic Profiling and Risk of Type 2 Diabetes in the PREDIMED Trial. *Diabetes Care*. 41:2617-2624. https://doi.org/10.2337/dc18-0840

Reidy, P.T., A.I. McKenzie, Z. Mahmassani, et al. 2018. Skeletal muscle ceramides and relationship with insulin sensitivity after 2 weeks of simulated sedentary behaviour and recovery in healthy older adults. *J Physiol*. 596:5217-5236. https://doi.org/10.1113/jp276798

Rhein, C., P. Tripal, A. Seebahn, et al. 2012. Functional implications of novel human acid sphingomyelinase splice variants. *PLoS One*. 7:e35467. https://doi.org/10.1371/journal.pone.0035467

Richter, E.A., and M. Hargreaves. 2013. Exercise, GLUT4, and skeletal muscle glucose uptake. *Physiol Rev*. 93:993-1017. https://doi.org/10.1152/physrev.00038.2012

Rico-Sanz, J., M. Moosavi, E.L. Thomas, et al. 2000. In vivo evaluation of the effects of continuous exercise on skeletal muscle triglycerides in trained humans. *Lipids*. 35:1313-1318. https://doi.org/10.1007/s11745-000-0647-2

Rinella, M.E., J.V. Lazarus, V. Ratziu, et al. 2023. A multisociety Delphi consensus statement on new fatty liver disease nomenclature. *Hepatology*. 78:1966-1986. https://doi.org/10.1097/hep.0000000000000520

Ritov, V.B., E.V. Menshikova, J. He, et al. 2005. Deficiency of subsarcolemmal mitochondria in obesity and type 2 diabetes. *Diabetes*. 54:8-14. https://doi.org/10.2337/diabetes.54.1.8

Roden, M., M. Krssak, H. Stingl, et al. 1999. Rapid impairment of skeletal muscle glucose transport/phosphorylation by free fatty acids in humans. *Diabetes*. 48:358-364. https://doi.org/10.2337/diabetes.48.2.358

Roden, M., T.B. Price, G. Perseghin, et al. 1996. Mechanism of free fatty acid-induced insulin resistance in humans. *J Clin Invest*. 97:2859-2865. https://doi.org/10.1172/jci118742

Roden, M., and G.I. Shulman. 2019. The integrative biology of type 2 diabetes. *Nature*. 576:51-60. https://doi.org/10.1038/s41586-019-1797-8

Rodriguez-Lafrasse, C., R. Rousson, P.G. Pentchev, et al. 1994. Free sphingoid bases in tissues from patients with type C Niemann-Pick disease and other lysosomal storage disorders. *Biochim Biophys Acta*. 1226:138-144. https://doi.org/10.1016/0925-4439(94)90021-3

Roeb, E., A. Canbay, H. Bantel, et al. 2024. [Not Available]. *Z Gastroenterol*. 62:1077-1087. https://doi.org/10.1055/a-2309-6052

Röhling, M., C. Herder, M. Roden, et al. 2016. Effects of Long-Term Exercise Interventions on Glycaemic Control in Type 1 and Type 2 Diabetes: a Systematic Review. *Exp Clin Endocrinol Diabetes*. 124:487-494. https://doi.org/10.1055/s-0042-106293

Rotolo, J.A., J. Zhang, M. Donepudi, et al. 2005. Caspase-dependent and -independent activation of acid sphingomyelinase signaling. *J Biol Chem*. 280:26425-26434. https://doi.org/10.1074/jbc.M414569200

Roux-Biejat, P., M. Coazzoli, P. Marrazzo, et al. 2021. Acid Sphingomyelinase Controls Early Phases of Skeletal Muscle Regeneration by Shaping the Macrophage Phenotype. *Cells*. 10. https://doi.org/10.3390/cells10113028

Rozpedek, W., D. Pytel, B. Mucha, et al. 2016. The Role of the PERK/eIF2α/ATF4/CHOP Signaling Pathway in Tumor Progression During Endoplasmic Reticulum Stress. *Curr Mol Med*. 16:533-544. https://doi.org/10.2174/1566524016666160523143937

Rui, L., M. Yuan, D. Frantz, et al. 2002. SOCS-1 and SOCS-3 block insulin signaling by ubiquitin-mediated degradation of IRS1 and IRS2. *J Biol Chem*. 277:42394-42398. https://doi.org/10.1074/jbc.C200444200

Ryu, D., K.J. Oh, H.Y. Jo, et al. 2009. TORC2 regulates hepatic insulin signaling via a mammalian phosphatidic acid phosphatase, LIPIN1. *Cell Metab*. 9:240-251. https://doi.org/10.1016/j.cmet.2009.01.007

Ryu, D., W.Y. Seo, Y.S. Yoon, et al. 2011. Endoplasmic reticulum stress promotes LIPIN2-dependent hepatic insulin resistance. *Diabetes*. 60:1072-1081. https://doi.org/10.2337/db10-1046

Samuel, V.T., Z.X. Liu, A. Wang, et al. 2007. Inhibition of protein kinase Cepsilon prevents hepatic insulin resistance in nonalcoholic fatty liver disease. *J Clin Invest*. 117:739-745. https://doi.org/10.1172/jci30400

Sangwung, P., K.F. Petersen, G.I. Shulman, et al. 2020. Mitochondrial Dysfunction, Insulin Resistance, and Potential Genetic Implications. *Endocrinology*. 161. https://doi.org/10.1210/endocr/bqaa017

Sassano, M.L., A.R. van Vliet, and P. Agostinis. 2017. Mitochondria-Associated Membranes As Networking Platforms and Regulators of Cancer Cell Fate. *Front Oncol*. 7:174. https://doi.org/10.3389/fonc.2017.00174

Sassoli, C., F. Pierucci, S. Zecchi-Orlandini, et al. 2019. Sphingosine 1-Phosphate (S1P)/ S1P Receptor Signaling and Mechanotransduction: Implications for Intrinsic Tissue Repair/Regeneration. *Int J Mol Sci*. 20. https://doi.org/10.3390/ijms20225545

Scarlatti, F., C. Bauvy, A. Ventruti, et al. 2004. Ceramide-mediated macroautophagy involves inhibition of protein kinase B and up-regulation of beclin 1. *J Biol Chem*. 279:18384-18391. https://doi.org/10.1074/jbc.M313561200

Schmid, A.I., J. Szendroedi, M. Chmelik, et al. 2011. Liver ATP synthesis is lower and relates to insulin sensitivity in patients with type 2 diabetes. *Diabetes Care*. 34:448-453. https://doi.org/10.2337/dc10-1076

Schmittgen, T.D., and K.J. Livak. 2008. Analyzing real-time PCR data by the comparative C(T) method. *Nat Protoc*. 3:1101-1108. https://doi.org/10.1038/nprot.2008.73

Schuchman, E.H. 2010. Acid sphingomyelinase, cell membranes and human disease: lessons from Niemann-Pick disease. *FEBS Lett*. 584:1895-1900. https://doi.org/10.1016/j.febslet.2009.11.083

Schwabe, R.F., and D.A. Brenner. 2006. Mechanisms of Liver Injury. I. TNF-alpha-induced liver injury: role of IKK, JNK, and ROS pathways. *Am J Physiol Gastrointest Liver Physiol*. 290:G583-589. https://doi.org/10.1152/ajpgi.00422.2005

Schwalm, C., C. Jamart, N. Benoit, et al. 2015. Activation of autophagy in human skeletal muscle is dependent on exercise intensity and AMPK activation. *Faseb j*. 29:3515-3526. https://doi.org/10.1096/fj.14-267187

Schwingshackl, L., B. Missbach, S. Dias, et al. 2014. Impact of different training modalities on glycaemic control and blood lipids in patients with type 2 diabetes: a systematic review and network meta-analysis. *Diabetologia*. 57:1789-1797. https://doi.org/10.1007/s00125-014-3303-z

Sebastián, D., M.I. Hernández-Alvarez, J. Segalés, et al. 2012. Mitofusin 2 (Mfn2) links mitochondrial and endoplasmic reticulum function with insulin signaling and is essential for normal glucose homeostasis. *Proc Natl Acad Sci U S A*. 109:5523-5528. https://doi.org/10.1073/pnas.1108220109

Sentelle, R.D., C.E. Senkal, W. Jiang, et al. 2012. Ceramide targets autophagosomes to mitochondria and induces lethal mitophagy. *Nat Chem Biol*. 8:831-838. https://doi.org/10.1038/nchembio.1059

Sharma, N.K., S.K. Das, A.K. Mondal, et al. 2008. Endoplasmic reticulum stress markers are associated with obesity in nondiabetic subjects. *J Clin Endocrinol Metab*. 93:4532-4541. https://doi.org/10.1210/jc.2008-1001

Shepherd, S.O., M. Cocks, P.J. Meikle, et al. 2017. Lipid droplet remodelling and reduced muscle ceramides following sprint interval and moderate-intensity continuous exercise training in obese males. *Int J Obes (Lond)*. 41:1745-1754. https://doi.org/10.1038/ijo.2017.170

Shepherd, S.O., M. Cocks, K.D. Tipton, et al. 2014. Resistance training increases skeletal muscle oxidative capacity and net intramuscular triglyceride breakdown in type I and II fibres of sedentary males. *Exp Physiol*. 99:894-908. https://doi.org/10.1113/expphysiol.2014.078014

Shi, Z., X.B. Li, Z.C. Peng, et al. 2018. Berberine Protects against NEFA-Induced Impairment of Mitochondrial Respiratory Chain Function and Insulin Signaling in Bovine Hepatocytes. *Int J Mol Sci*. 19. https://doi.org/10.3390/ijms19061691

Singh, A., R. Kukreti, L. Saso, et al. 2022. Mechanistic Insight into Oxidative Stress-Triggered Signaling Pathways and Type 2 Diabetes. *Molecules*. 27. https://doi.org/10.3390/molecules27030950

Skovbro, M., M. Baranowski, C. Skov-Jensen, et al. 2008. Human skeletal muscle ceramide content is not a major factor in muscle insulin sensitivity. *Diabetologia*. 51:1253-1260. https://doi.org/10.1007/s00125-008-1014-z

Sohal, P.S., and R.B. Cornell. 1990. Sphingosine inhibits the activity of rat liver CTP:phosphocholine cytidylyltransferase. *J Biol Chem*. 265:11746-11750.

Soleimanpour, S.A., A.M. Ferrari, J.C. Raum, et al. 2015. Diabetes Susceptibility Genes Pdx1 and Clec16a Function in a Pathway Regulating Mitophagy in β-Cells. *Diabetes*. 64:3475-3484. https://doi.org/10.2337/db15-0376

Soleimanpour, S.A., A. Gupta, M. Bakay, et al. 2014. The diabetes susceptibility gene Clec16a regulates mitophagy. *Cell*. 157:1577-1590. https://doi.org/10.1016/j.cell.2014.05.016

Sparks, L.M., N.M. Johannsen, T.S. Church, et al. 2013. Nine months of combined training improves ex vivo skeletal muscle metabolism in individuals with type 2 diabetes. *J Clin Endocrinol Metab*. 98:1694-1702. https://doi.org/10.1210/jc.2012-3874

Sprenger, H.G., and T. Langer. 2019. The Good and the Bad of Mitochondrial Breakups. *Trends Cell Biol*. 29:888-900. https://doi.org/10.1016/j.tcb.2019.08.003

Steffensen, C.H., C. Roepstorff, M. Madsen, et al. 2002. Myocellular triacylglycerol breakdown in females but not in males during exercise. *Am J Physiol Endocrinol Metab*. 282:E634-642. https://doi.org/10.1152/ajpendo.00078.2001

Stephan, M., B. Edelmann, S. Winoto-Morbach, et al. 2017. Role of caspases in CD95-induced biphasic activation of acid sphingomyelinase. *Oncotarget*. 8:20067-20085. https://doi.org/10.18632/oncotarget.15379

Stratford, S., K.L. Hoehn, F. Liu, et al. 2004. Regulation of insulin action by ceramide: dual mechanisms linking ceramide accumulation to the inhibition of Akt/protein kinase B. *J Biol Chem*. 279:36608-36615. https://doi.org/10.1074/jbc.M406499200

Summers, S.A., and B.H. Goodpaster. 2016. CrossTalk proposal: Intramyocellular ceramide accumulation does modulate insulin resistance. *J Physiol*. 594:3167-3170. https://doi.org/10.1113/jp271676

Sun, X.J., D.L. Crimmins, M.G. Myers, Jr., et al. 1993. Pleiotropic insulin signals are engaged by multisite phosphorylation of IRS-1. *Mol Cell Biol*. 13:7418-7428. https://doi.org/10.1128/mcb.13.12.7418-7428.1993

Sunny, N.E., E.J. Parks, J.D. Browning, et al. 2011. Excessive hepatic mitochondrial TCA cycle and gluconeogenesis in humans with nonalcoholic fatty liver disease. *Cell Metab*. 14:804-810. https://doi.org/10.1016/j.cmet.2011.11.004

Suzuki, M., T. Murakami, J. Cheng, et al. 2015. ELMOD2 is anchored to lipid droplets by palmitoylation and regulates adipocyte triglyceride lipase recruitment. *Mol Biol Cell*. 26:2333-2342. https://doi.org/10.1091/mbc.E14-11-1504

Syed-Abdul, M.M. 2023. Lipid Metabolism in Metabolic-Associated Steatotic Liver Disease (MASLD). *Metabolites*. 14. https://doi.org/10.3390/metabo14010012

Szendroedi, J., M. Chmelik, A.I. Schmid, et al. 2009. Abnormal hepatic energy homeostasis in type 2 diabetes. *Hepatology*. 50:1079-1086. https://doi.org/10.1002/hep.23093

Szendroedi, J., E. Phielix, and M. Roden. 2011. The role of mitochondria in insulin resistance and type 2 diabetes mellitus. *Nat Rev Endocrinol*. 8:92-103. https://doi.org/10.1038/nrendo.2011.138

Szendroedi, J., T. Yoshimura, E. Phielix, et al. 2014. Role of diacylglycerol activation of PKCθ in lipid-induced muscle insulin resistance in humans. *Proc Natl Acad Sci U S A*. 111:9597-9602. https://doi.org/10.1073/pnas.1409229111

Tam, C., V. Idone, C. Devlin, et al. 2010. Exocytosis of acid sphingomyelinase by wounded cells promotes endocytosis and plasma membrane repair. *J Cell Biol*. 189:1027-1038. https://doi.org/10.1083/jcb.201003053

Taniguchi, M., K. Kitatani, T. Kondo, et al. 2012. Regulation of autophagy and its associated cell death by "sphingolipid rheostat": reciprocal role of ceramide and sphingosine 1-phosphate in the mammalian target of rapamycin pathway. *J Biol Chem*. 287:39898-39910. https://doi.org/10.1074/jbc.M112.416552

Thayyullathil, F., A.R. Cheratta, A. Alakkal, et al. 2021. Acid sphingomyelinase-dependent autophagic degradation of GPX4 is critical for the execution of ferroptosis. *Cell Death Dis*. 12:26. https://doi.org/10.1038/s41419-020-03297-w

Thomas, D.E., E.J. Elliott, and G.A. Naughton. 2006. Exercise for type 2 diabetes mellitus. *Cochrane Database Syst Rev*. 2006:Cd002968. https://doi.org/10.1002/14651858.CD002968.pub2

Tian, T., X.C. Liao, M. Zhang, et al. 2022. [Effects of celastrol on autophagy and endoplasmic reticulum stress-mediated apoptosis in a mouse model of nonalcoholic fatty liver disease]. *Zhonghua Gan Zang Bing Za Zhi*. 30:656-662. https://doi.org/10.3760/cma.j.cn501113-20210817-00408

Tidball, J.G. 2011. Mechanisms of muscle injury, repair, and regeneration. *Compr Physiol*. 1:2029-2062. https://doi.org/10.1002/cphy.c100092

Tonks, K.T., A.C. Coster, M.J. Christopher, et al. 2016. Skeletal muscle and plasma lipidomic signatures of insulin resistance and overweight/obesity in humans. *Obesity (Silver Spring)*. 24:908-916. https://doi.org/10.1002/oby.21448

Trayhurn, P. 2013. Hypoxia and adipose tissue function and dysfunction in obesity. *Physiol Rev*. 93:1-21. https://doi.org/10.1152/physrev.00017.2012

Tsai, K.H., W.J. Wang, C.W. Lin, et al. 2012. NADPH oxidase-derived superoxide anion-induced apoptosis is mediated via the JNK-dependent activation of NF-κB in cardiomyocytes exposed to high glucose. *J Cell Physiol*. 227:1347-1357. https://doi.org/10.1002/jcp.22847

Turner, N., X.Y. Lim, H.D. Toop, et al. 2018. A selective inhibitor of ceramide synthase 1 reveals a novel role in fat metabolism. *Nat Commun*. 9:3165. https://doi.org/10.1038/s41467-018-05613-7

Turpin-Nolan, S.M., P. Hammerschmidt, W. Chen, et al. 2019. CerS1-Derived C(18:0) Ceramide in Skeletal Muscle Promotes Obesity-Induced Insulin Resistance. *Cell Rep*. 26:1-10.e17. https://doi.org/10.1016/j.celrep.2018.12.031

Turpin, S.M., H.T. Nicholls, D.M. Willmes, et al. 2014. Obesity-induced CerS6-dependent C16:0 ceramide production promotes weight gain and glucose intolerance. *Cell Metab*. 20:678-686. https://doi.org/10.1016/j.cmet.2014.08.002

Undamatla, R., O.G. Fagunloye, J. Chen, et al. 2023. Reduced hepatocyte mitophagy is an early feature of NAFLD pathogenesis and hastens the onset of steatosis, inflammation and fibrosis. *Res Sq*. https://doi.org/10.21203/rs.3.rs-2469234/v1

van der Veen, J.N., J.P. Kennelly, S. Wan, et al. 2017. The critical role of phosphatidylcholine and phosphatidylethanolamine metabolism in health and disease. *Biochim Biophys Acta Biomembr*. 1859:1558-1572. https://doi.org/10.1016/j.bbamem.2017.04.006

Van Huynh, T., L. Rethi, L. Rethi, et al. 2023. The Complex Interplay between Imbalanced Mitochondrial Dynamics and Metabolic Disorders in Type 2 Diabetes. *Cells*. 12. https://doi.org/10.3390/cells12091223

Vanier, M.T. 2013. Niemann-Pick diseases. *Handb Clin Neurol*. 113:1717-1721. https://doi.org/10.1016/b978-0-444-59565-2.00041-1

Varela, Y.R., M.N. Iriondo, F.M. Goñi, et al. 2024. Ceramide regulation of autophagy: A biophysical approach. *Biochim Biophys Acta Mol Cell Biol Lipids*. 1869:159444. https://doi.org/10.1016/j.bbalip.2023.159444

Verdurmen, W.P., M. Thanos, I.R. Ruttekolk, et al. 2010. Cationic cell-penetrating peptides induce ceramide formation via acid sphingomyelinase: implications for uptake. *J Control Release*. 147:171-179. https://doi.org/10.1016/j.jconrel.2010.06.030

Vesković, M., N. Šutulović, D. Hrnčić, et al. 2023. The Interconnection between Hepatic Insulin Resistance and Metabolic Dysfunction-Associated Steatotic Liver Disease-The Transition from an Adipocentric to Liver-Centric Approach. *Curr Issues Mol Biol*. 45:9084-9102. https://doi.org/10.3390/cimb45110570

Viollet, B., L. Lantier, J. Devin-Leclerc, et al. 2009. Targeting the AMPK pathway for the treatment of Type 2 diabetes. *Front Biosci (Landmark Ed)*. 14:3380-3400. https://doi.org/10.2741/3460

Walker, A.K., R.L. Jacobs, J.L. Watts, et al. 2011. A conserved SREBP-1/phosphatidylcholine feedback circuit regulates lipogenesis in metazoans. *Cell*. 147:840-852. https://doi.org/10.1016/j.cell.2011.09.045

Walkey, C.J., L. Yu, L.B. Agellon, et al. 1998. Biochemical and evolutionary significance of phospholipid methylation. *J Biol Chem*. 273:27043-27046. https://doi.org/10.1074/jbc.273.42.27043

Wang, J.M., Y. Qiu, Z. Yang, et al. 2018. IRE1α prevents hepatic steatosis by processing and promoting the degradation of select microRNAs. *Sci Signal*. 11. https://doi.org/10.1126/scisignal.aao4617

Wang, K., C. Li, X. Lin, et al. 2020. Targeting alkaline ceramidase 3 alleviates the severity of nonalcoholic steatohepatitis by reducing oxidative stress. *Cell Death Dis*. 11:28. https://doi.org/10.1038/s41419-019-2214-9

Weng, S.W., J.C. Wu, F.C. Shen, et al. 2023. Chaperonin counteracts diet-induced non-alcoholic fatty liver disease by aiding sirtuin 3 in the control of fatty acid oxidation. *Diabetologia*. 66:913-930. https://doi.org/10.1007/s00125-023-05869-9

Willy, J.A., S.K. Young, J.L. Stevens, et al. 2015. CHOP links endoplasmic reticulum stress to NF-κB activation in the pathogenesis of nonalcoholic steatohepatitis. *Mol Biol Cell*. 26:2190-2204. https://doi.org/10.1091/mbc.E15-01-0036

Winder, W.W., B.F. Holmes, D.S. Rubink, et al. 2000. Activation of AMP-activated protein kinase increases mitochondrial enzymes in skeletal muscle. *J Appl Physiol (1985)*. 88:2219-2226. https://doi.org/10.1152/jappl.2000.88.6.2219

Wolfe, R.R. 2006. The underappreciated role of muscle in health and disease. *Am J Clin Nutr*. 84:475-482. https://doi.org/10.1093/ajcn/84.3.475

Wondmkun, Y.T. 2020. Obesity, Insulin Resistance, and Type 2 Diabetes: Associations and Therapeutic Implications. *Diabetes Metab Syndr Obes*. 13:3611-3616. https://doi.org/10.2147/dmso.S275898

Wu, H., Y. Wang, W. Li, et al. 2019a. Deficiency of mitophagy receptor FUNDC1 impairs mitochondrial quality and aggravates dietary-induced obesity and metabolic syndrome. *Autophagy*. 15:1882-1898. https://doi.org/10.1080/15548627.2019.1596482

Wu, J., Y.D. Tseng, C.F. Xu, et al. 2008. Structural and biochemical characterization of the KRLB region in insulin receptor substrate-2. *Nat Struct Mol Biol*. 15:251-258. https://doi.org/10.1038/nsmb.1388

Wu, X., N. Xu, M. Li, et al. 2019b. Protective Effect of Patchouli Alcohol Against High-Fat Diet Induced Hepatic Steatosis by Alleviating Endoplasmic Reticulum Stress and Regulating VLDL Metabolism in Rats. *Front Pharmacol*. 10:1134. https://doi.org/10.3389/fphar.2019.01134

Xiong, X., C.F. Lee, W. Li, et al. 2019. Acid Sphingomyelinase regulates the localization and trafficking of palmitoylated proteins. *Biol Open*. 8. https://doi.org/10.1242/bio.040311

Xu, S., J. Xi, T. Wu, et al. 2023. The Role of Adipocyte Endoplasmic Reticulum Stress in Obese Adipose Tissue Dysfunction: A Review. *Int J Gen Med*. 16:4405-4418. https://doi.org/10.2147/ijgm.S428482

Yamada, T., D. Murata, Y. Adachi, et al. 2018. Mitochondrial Stasis Reveals p62-Mediated Ubiquitination in Parkin-Independent Mitophagy and Mitigates Nonalcoholic Fatty Liver Disease. *Cell Metab*. 28:588-604.e585. https://doi.org/10.1016/j.cmet.2018.06.014

Yamato, M., T. Shiba, M. Yoshida, et al. 2007. Fatty acids increase the circulating levels of oxidative stress factors in mice with diet-induced obesity via redox changes of albumin. *Febs j*. 274:3855-3863. https://doi.org/10.1111/j.1742-4658.2007.05914.x

Yoo, S.Z., M.H. No, J.W. Heo, et al. 2019. Effects of Acute Exercise on Mitochondrial Function, Dynamics, and Mitophagy in Rat Cardiac and Skeletal Muscles. *Int Neurourol J*. 23:S22-31. https://doi.org/10.5213/inj.1938038.019

Yoon, Y., C.A. Galloway, B.S. Jhun, et al. 2011. Mitochondrial dynamics in diabetes. *Antioxid Redox Signal*. 14:439-457. https://doi.org/10.1089/ars.2010.3286

Younossi, Z.M., P. Golabi, L. de Avila, et al. 2019. The global epidemiology of NAFLD and NASH in patients with type 2 diabetes: A systematic review and meta-analysis. *J Hepatol*. 71:793-801. https://doi.org/10.1016/j.jhep.2019.06.021

Zaharia, O.P., K. Strassburger, A. Strom, et al. 2019. Risk of diabetes-associated diseases in subgroups of patients with recent-onset diabetes: a 5-year follow-up study. *Lancet Diabetes Endocrinol*. 7:684-694. https://doi.org/10.1016/s2213-8587(19)30187-1

Zatterale, F., M. Longo, J. Naderi, et al. 2019. Chronic Adipose Tissue Inflammation Linking Obesity to Insulin Resistance and Type 2 Diabetes. *Front Physiol*. 10:1607. https://doi.org/10.3389/fphys.2019.01607

Zeng, X., M. Zhu, X. Liu, et al. 2020. Oleic acid ameliorates palmitic acid induced hepatocellular lipotoxicity by inhibition of ER stress and pyroptosis. *Nutr Metab (Lond)*. 17:11. https://doi.org/10.1186/s12986-020-0434-8

Zhang, Y., P. Mattjus, P.C. Schmid, et al. 2001. Involvement of the acid sphingomyelinase pathway in uva-induced apoptosis. *J Biol Chem*. 276:11775-11782. https://doi.org/10.1074/jbc.M006000200

Zhang, Y., R. Xue, Z. Zhang, et al. 2012. Palmitic and linoleic acids induce ER stress and apoptosis in hepatoma cells. *Lipids Health Dis*. 11:1. https://doi.org/10.1186/1476-511x-11-1

Zhou, T., L. Chang, Y. Luo, et al. 2019. Mst1 inhibition attenuates non-alcoholic fatty liver disease via reversing Parkin-related mitophagy. *Redox Biol*. 21:101120. https://doi.org/10.1016/j.redox.2019.101120

Zhu, C., Q. Huai, X. Zhang, et al. 2023. Insights into the roles and pathomechanisms of ceramide and sphigosine-1-phosphate in nonalcoholic fatty liver disease. *Int J Biol Sci*. 19:311-330. https://doi.org/10.7150/ijbs.78525

Zhu, Q., J. Yang, R. Zhu, et al. 2016. Dihydroceramide-desaturase-1-mediated caspase 9 activation through ceramide plays a pivotal role in palmitic acid-induced HepG2 cell apoptosis. *Apoptosis*. 21:1033-1044. https://doi.org/10.1007/s10495-016-1267-9

Zorzano, A., M.I. Hernández-Alvarez, M. Palacín, et al. 2010. Alterations in the mitochondrial regulatory pathways constituted by the nuclear co-factors PGC-1alpha or PGC-1beta and mitofusin 2 in skeletal muscle in type 2 diabetes. *Biochim Biophys Acta*. 1797:1028-1033. https://doi.org/10.1016/j.bbabio.2010.02.017

III Acknowledgment

First and foremost, I would like to sincerely thank Prof. Dr. Michael Roden for the opportunity to work in the fascinating field of clinical diabetology. I learned a great deal about human studies – from study design and conduct to how each component is evaluated in top-tier clinical research. I am deeply grateful for the many insightful and sometimes challenging discussions, for allowing me to voice my own perspective, and for letting me actively participate in each step leading up to a publication. Thank you for your patience, your continuous support, and your authentic humanity – as well as for your wonderful anecdotes about how things are done in Austria, especially how you always manage to bring in the perfect proverb at just the right moment.

I would also like to thank Prof. Dr. Hadi Al-Hasani for allowing me to be part of the VIVID graduate school and, somewhat involuntarily, to act as spokesperson. I am thankful for the chance to grow through organizational challenges and leadership tasks.

From the bottom of my heart, I want to thank Dr. Lucia Mastrototaro for her consistent support, guidance, and trust throughout this journey. Thank you for all the time spent together: working, discussing, laughing, and sharing. I truly value not only your scientific mentorship but also your friendship beyond the lab. My heartfelt thanks go out to all the "Mädels 6.OG" which include Michelle Reina do Fundo, Fariba Zivehe, Olga Dürrschmidt, Alexandra Stein, and our recent member Sevgican Yilmaz. Thank you for your help, your encouragement, both technical and emotional, and for all the laughter and warmth. I feel incredibly grateful to have worked alongside such extraordinarily hard-working, kind, and generous people. You have been inspiring role models and a true source of motivation. I'm especially happy that what grew out of our time together are not just colleagues, but real friendships that will last well beyond this thesis. To all other members of the RG Energy Metabolism and of the German Diabetes Center: thank you! I truly cannot imagine my PhD time without you.

Last but not least, I would like to thank my family.

Danke Mutti, danke Vati! Für euren emotionalen Support, der so oft dringend nötig war. Ihr seid meine Wurzeln, mein Halt, und ihr gebt mir das sichere Gefühl zu wissen, wer ich bin und wo ich hingehöre. Danke, dass ihr mir zugehört habt und mich immer wieder motiviert habt, durchzuhalten. Spezieller Dank an meinen Bruder Marco, dass du mich immer wieder an das Ziel erinnert hast: wie es wohl sein wird, wenn es endlich geschafft ist und ich als „Dr. Stoppel" ein Bierchen trinken kann.

IV Eidesstattliche Versicherung

Ich versichere an Eides Statt, dass die Dissertation von mir selbständig und ohne unzulässige fremde Hilfe unter Beachtung der „Grundsätze zur Sicherung guter wissenschaftlicher Praxis an der Heinrich-Heine-Universität Düsseldorf“ erstellt worden ist. Alle aus anderen Quellen direkt oder indirekt übernommenen Gedanken, Inhalte oder Texte sind als solche kenntlich gemacht. Die Dissertation wurde weder in gleicher noch in ähnlicher Form bereits in einem anderen Prüfungsverfahren eingereicht. Ich habe bisher keine erfolglosen Promotionsversuche unternommen.
Ich erkläre zudem, dass die vorliegende elektronische Fassung mit der eingereichten Druckfassung übereinstimmt.

Düsseldorf, den

Mona Hendlinger